

CMOS – Based Peptide Arrays

Dissertation

submitted to the

*Combined Faculties for the Natural Sciences and for Mathematics
of the Ruperto-Carola University of Heidelberg, Germany*

for the degree of

Doctor of Natural Sciences

put forward by

Dipl. Phys. Kai König

born in Heidelberg

May 2010

Dissertation
submitted to the
Combined Faculties for the Natural Sciences and for Mathematics
of the Ruperto-Carola University of Heidelberg, Germany
for the degree of
Doctor of Natural Sciences

Put forward by

Diplom-Physiker:

Born in:

Kai Lars König

Heidelberg

Oral examination: 21.07.2010

CMOS – Based Peptide Arrays

Referees:

Prof. Dr.

Volker Lindenstruth

PD Dr.

Ralf Bischoff

Peptidbibliotheken auf CMOS - Basis

Peptidarrays sind ein wichtiges Werkzeug für die Proteomik und Peptidomik, da auf ihnen eine große Zahl Peptide parallel auf einem gemeinsamen Träger synthetisiert und Zielmolekülen in Lösung ausgesetzt werden können. Bei partikelbasierter Synthese werden die Aminosäuren für die in-situ-Synthese in festen Partikeln zu ihren Syntheseloki transportiert und durch Schmelzen freigesetzt. Dies erlaubt eine Vergrößerung der Dichte verglichen mit flüssigkeitsbasierten Systemen.

Diese Arbeit konzentriert sich auf die Entwicklung anwendungsspezifischer Hochspannungsschaltungen für die elektrostatische Ablagerung geladener Aminosäurepartikel und deren Einbettung in ein kombinatorisches Peptidsynthesesystem.

Der Übertrag von Aminosäurepartikeln aus dem Aerosol zu Syntheseloki auf der Chipoberfläche wurde für Pixelmittelpunktabstände von 45 μm bis 100 μm untersucht. Die Kompatibilität zwischen Chips, Partikelübertrag und poly-(ethylenglykol)methacrylat-basierten Oberflächenmodifikationen wurde erarbeitet. Die ersten kombinatorischen Synthesen auf CMOS-Chips mit über 16.000 individuellen Syntheseorten pro Chip, bei einer Dichte von 10.000 Spots pro cm^2 , wurden durchgeführt. Dies ist eine 25-fache Verbesserung im Vergleich zu den 400 Spots pro cm^2 , die momentan auf laser-bedruckten Glaträgern verfügbar sind. Für FLAG- und HA-Peptidepitope zeigte ein Immunassay regelmäßige Spots mit vergleichbarer Signalintensität über den gesamten Chip.

CMOS - Based Peptide Arrays

Peptide arrays are an important tool in proteomics and peptidomics, allowing a large number of peptides to be synthesized on a common support and exposed to a solution of target molecules in parallel. In particle-based synthesis, the amino acids for in situ synthesis of peptides are transported to synthesis loci in solid particles and released upon melting, allowing an increase in density over liquid-based systems.

This thesis focuses on the development of application-specific high voltage integrated circuits for electrostatic deposition of charged amino acid particles and their integration into a combinatorial peptide synthesis system.

Transfer of amino acid particles from the aerosol to synthesis loci on the chip surface was investigated for a pixel pitch between 45 μm and 100 μm , and compatibility between the chips, particle transfer and the poly(ethylene glycol)methacrylate - based surface modifications was established. The first combinatorial syntheses on CMOS chips were performed with over 16,000 distinct synthesis sites per chip, at a density of 10,000 spots per cm^2 , which is a 25-fold increase over the 400 spots per cm^2 currently available on laser-printed glass slides. For FLAG and HA peptide epitopes, immunostaining showed regular spots of comparable signal intensity over the whole chip area.

Content Overview

Introduction	1
PART I: FUNDAMENTALS	
1 Peptide Arrays: Generation and Applications	7
2 Application Specific Integrated Circuits	19
3 Microparticle Technology and Particle Transfer	35
PART II: NEW MATERIALS AND METHODS	
4 Particle-Based Peptide Synthesis – Related Works	59
5 Microchip Development.	67
PART III: RESULTS AND DISCUSSION	
6 Transfer of Amino Acid Particles	93
7 On-Chip Synthesis	133
8 Conclusion and Outlook	155
References.	159
Acknowledgements	167
APPENDICES	
A1 Introduction to Amino Acids, Peptides and Proteins	171
A2 Bond Pad Lists and Bond Diagrams	179
A3 Pressure Tolerance of Peptidchip 3.1	185
A4 Peptidchip 5 Main PCB Schematics	187

Table of Contents

Introduction	1
PART I: FUNDAMENTALS	
1 Peptide Arrays: Generation and Applications	7
1.1. Laboratory Peptide Synthesis	7
1.1.1. Applications	7
1.1.2. Solid-phase Peptide Synthesis	8
1.1.3. Peptide Libraries	11
1.2. Peptide Array State of the Art	13
1.2.1. Challenges in Peptide Arrays	13
1.2.1.1. Maximizing Spot Density and Minimizing Cost per Peptide Spot	13
1.2.1.2. Maximizing Peptide Chain Length	14
1.2.1.3. Optimizing Detection Specificity and Sensitivity	14
1.2.1.4. Handling and Usability	15
1.2.1.5. Use of Non-standard Amino Acids	15
1.2.1.6. Synthesis in the User's Lab vs. Synthesis at the Provider	15
1.2.2. Peptide Array Technology	16
1.3. Detection of Bound Molecules	17
1.3.1. Labeled Molecules	17
1.3.2. Detection of Bound Molecules in Bioarray Experiments	17
2 Application Specific Integrated Circuits	19
2.1. Introduction	19
2.2. High Voltage CMOS	20
2.2.1. HV CMOS Technology State of the Art	20
2.2.2. Voltage Limiting Effects in CMOS Processes	21
2.2.2.1. Gate Oxide Breakdown	21
2.2.2.2. Channel Hot Carrier Effects (HCE)	21
2.2.2.3. Drain-induced Barrier Lowering (DIBL) and Punchthrough	23
2.2.3. HV-CMOS Solutions.	23
2.2.3.1. HV-CMOS Structures	23
2.2.3.2. HV Interconnect	27
2.2.4. Commercially Available HV Processes and Extended LV Processes	28
2.3. CMOS Photosensors	30
2.3.1. Physical Introduction	30
2.3.2. CMOS Photosensor Devices	30
2.3.2.1. Characteristics of Photosensor Devices.	30
2.3.2.2. Photodiodes	31
2.3.2.3. Phototransistors	32
2.3.2.4. Photogate	33
2.3.3. Parasitic Effects	34

2.3.3.1. Parasitic Effects of Light on MOSFETs	34
2.3.3.2. Passivation, Oxide and Metal Effects	34
3 Microparticle Technology and Particle Transfer	35
3.1. Introduction	35
3.2. Particle-Based Peptide Synthesis	35
3.3. Peptide Laser Printing	36
3.3.1. Motivation	36
3.3.2. Laser Printers and LED Printers	36
3.3.3. The Peptide Laser Printer	38
3.3.4. Limitations of Peptide Laser Printing	38
3.4. Particle Properties and Manufacture	38
3.4.1. Commercial Laser Printer Toner	38
3.4.2. Amino Acid Particles	39
3.4.2.1. Manufacture and Composition	39
3.4.2.2. Properties	40
3.5. Triboelectric Charging of Particles.	42
3.5.1. Motivation	42
3.5.2. Theory of Triboelectric Charging	42
3.5.3. Measurement of q / m -values	43
3.5.3.1. Faraday Cell	43
3.5.3.2. Induced Charges Measurement Method	43
3.5.4. Triboelectric Properties of Amino Acid Particles	45
3.6. Forces Acting Upon Microparticles	46
3.6.1. Approach	46
3.6.2. Mass-dependent Forces	47
3.6.2.1. Gravitational Force	47
3.6.2.2. Inertial Force	47
3.6.3. Surface-dependent Forces	48
3.6.3.1. Dynamic Lift	48
3.6.3.2. Drag Force	48
3.6.4. Electromagnetic Forces	49
3.6.4.1. Electrostatic Force	49
3.6.4.2. Dielectrophoretic Force	50
3.6.4.3. Other Electromagnetic Forces	50
3.6.5. Particle Adsorption and Desorption on Surfaces.	50
3.6.6. Comparison of Forces Acting Upon Particles in an Aerosol	51
3.6.6.1. Scaling with Airstream Velocity and Particle Size	51
3.6.6.2. Comparison of Forces for Typical Particles	51
3.7. Direct Particle Transfer	53
3.8. Selective Desorption into an Airstream	54
3.9. Selective Adsorption from an Aerosol	54

PART II: NEW MATERIALS AND METHODS

4	Particle-Based Peptide Synthesis – Related Works	59
4.1.	Preparation of Support with PEGMA Films	59
4.2.	Aerosol Generation	60
4.3.	Fixed-Pattern Chips	61
4.3.1.	Structure and Function of Fixed-Pattern Chips	61
4.3.2.	Particle Deposition on Fixed-Pattern Chips Using Color Toner Particles	62
4.4.	Peptidchip 3	62
4.4.1.	Objectives	62
4.4.2.	Microchip Design	63
4.4.3.	Particle Transfer Results	64
5	Microchip Development	67
5.1.	Introduction	67
5.2.	Microchip Versions	67
5.2.1.	Overview	67
5.2.2.	Fixed-pattern Chips	68
5.2.3.	Fully Combinatorial Synthesis Chips	68
5.2.3.1.	Peptidchip 3	68
5.2.3.2.	Peptidchip 3.1	69
5.2.3.3.	Peptidchip 5	69
5.2.3.4.	Peptidchip 5.1	69
5.2.4.	Fully Combinatorial Synthesis and Detection Chips	69
5.2.4.1.	Peptidchip 4	69
5.2.4.2.	Peptidchip 6	70
5.3.	Peptidchip 3.1	70
5.3.1.	Objectives	70
5.3.2.	Microelectronics	71
5.3.2.1.	Changes from Peptidchip 3 to Peptidchip 3.1	71
5.3.2.2.	Description of Pixel Arrays	72
5.3.3.	Packaging, Electronic and Mechanical Supports	74
5.3.3.1.	Support PCB	74
5.3.3.2.	Chip Covering	75
5.4.	Peptidchip 5	76
5.4.1.	Design Requirements	76
5.4.2.	Microelectronics	77
5.4.2.1.	Overview and Top Level Design	77
5.4.2.2.	Pixel Area	78
5.4.2.3.	Supply and Control	81
5.4.2.4.	Mechanical Considerations	83
5.4.3.	Packaging, Electronic and Mechanical Supports	85
5.4.3.1.	Support PCB and Bonding	85
5.4.3.2.	Main PCB	86
5.4.4.	Control Software	89

PART III: RESULTS AND DISCUSSION

6	Transfer of Amino Acid Particles	93
6.1.	Introduction	93
6.2.	Aerosol Chambers	93
6.2.1.	Aerosol Chamber Concept	93
6.2.2.	First Generation Aerosol Chambers in Experiments	95
6.2.3.	Regulating Aerosol Parameters	96
6.2.3.1.	State of the Art and Objectives	96
6.2.3.2.	An Aerosol Chamber with Monitored Aerosol	97
6.2.3.3.	Alternatives to the Aerosol Chamber Concept	102
6.2.3.4.	Conclusions and Outlook	103
6.3.	Transfer of Amino Acid Particles onto CMOS Chips.	104
6.3.1.	Prerequisites	104
6.3.2.	Amino Acid Particle Deposition on Peptidchip 3.1 and 5.	104
6.3.2.1.	Peptidchip 3.1	104
6.3.2.2.	Peptidchip 5.	105
6.3.2.3.	Minimum Voltage for Particle Transfer on Peptidchip 5 with and without Covering	107
6.3.3.	Sequential Deposition of Different Sorts of Particles	108
6.3.4.	Influence of Deposition Patterns and Particle Properties on Transfer Quality	110
6.3.4.1.	Coarse Fraction Particles	110
6.3.4.2.	Sparse Deposition Patterns	112
6.3.4.3.	Fine Fraction Particles	113
6.4.	Metal-Oxide Layers on the Chip Surface.	115
6.4.1.	Motivation	115
6.4.2.	Results	115
6.4.2.1.	Effects of Film Generation on Electronic Functionality	115
6.4.2.2.	Particle Deposition	115
6.4.3.	Discussion	116
6.4.4.	Conclusions.	118
6.5.	Compatibility of PEGMA Films with Particle Deposition	118
6.5.1.	Approach	118
6.5.2.	Step-by-step Testing of Surface Modification Procedure	119
6.5.3.	Integrity of Bond Contacts and Electronics after Surface Modification	120
6.5.4.	Blocking of Electric Fields.	121
6.5.4.1.	Introduction and Theory.	121
6.5.4.2.	Experimental Verification using Fixed-Pattern Chips	122
6.5.5.	Thin Polymer Layers.	123
6.5.6.	Heteropolymers	125
6.5.7.	Effects of Water and Ions on Heteropolymer Layers	127
6.5.8.	Conclusions.	129
6.6.	Selective Deposition from Liquids	129
6.6.1.	Objectives	129
6.6.2.	Particle Transfer in Hexane	130
6.6.3.	Conclusions.	131
6.7.	Summary and Outlook	132

7 On-Chip Synthesis	133
7.1. Introduction	133
7.2. Synthesis on Peptidchip 3.1	134
7.2.1. Objectives and Preparation.	134
7.2.2. Amino Acid Particle Deposition and Peptide Synthesis	135
7.2.3. Removing of Side-Chain Protection Groups, Staining and Detection of Epitopes	139
7.2.4. Discussion	141
7.3. Synthesis on Peptidchip 5.	142
7.3.1. Objectives and Preparation.	142
7.3.2. Amino Acid Particle Deposition and Peptide Synthesis	143
7.3.3. Removing of Side-Chain Protection Groups, Staining and Detection of Epitopes	147
7.3.4. Discussion	152
8 Conclusion and Outlook	155
8.1. Discussion of Results	155
8.1.1. Microelectronics and Materials	155
8.1.2. Particle Transfer	155
8.1.3. Synthesis	156
8.2. From Prototype to Application	156
8.3. Future Chip Generations	157
References.	159
Acknowledgements	167
APPENDICES	
A1 Introduction to Amino Acids, Peptides and Proteins	171
A1.1 Biochemical Classification	171
A1.2 Amino Acids and the Peptide Bond	172
A1.2.1 The Peptide Backbone	172
A1.2.2 Side Groups of Amino Acids and Peptides	176
A1.3 Protein Structure	176
A1.4 Protein Biosynthesis	178
A2 Bond Pad Lists and Bond Diagrams	179
A2.1 Peptidchip 3.1	179
A2.2 Peptidchip 5	182
A3 Pressure Tolerance of Peptidchip 3.1	185
A4 Peptidchip 5 Main PCB Schematics	187

Introduction

Science enables engineering. Understanding the principles of nature leads to applied research and to the development of novel tools that eventually find their way into everyday use. Furthermore, if their underlying principles are understood, existing tools can be adapted and recombined to overcome challenges even in fields of technology they were not originally developed for. One example are CMOS camera chips which, using semiconductor technology originally developed for purely electronic applications, nowadays replace the less convenient chemical film in most modern cameras.

Engineering enables science, as well. Testing hypotheses and gathering data requires sophisticated tools. The enormous machine of the LHC collider and its detectors, which were built in order to test hypotheses of modern particle physics, is but one example. Constructing it would have been impossible without both established and specially-developed parts, such as vacuum pumps, superconducting magnets or cutting-edge readout electronics.

This thesis describes the development of such a tool for use in the life sciences built in collaboration between the German Cancer Research Center (DKFZ) and the Kirchhoff Institute for Physics (KIP) at Heidelberg University, namely a microelectronic chip designed as an active support for particle-based combinatorial synthesis of linear polymers in general and peptides in particular. Such peptide arrays are used e.g.

- to detect antibodies, in medical diagnosis or immunological research,
- to study interactions between peptides and proteins or other biologically relevant molecules (e.g. DNA or metal ions), which can result in an increased understanding of biochemical processes or reveal novel starting points for drug development, or
- to find catalysts based on peptides (or metallo peptides) mimicking the function of catalytic proteins or to discover peptides catalyzing “non-natural” reactions.

Arrays of molecules on a single support allow for comparative screening of a complex molecule library within one experiment at minimal consumption of reagents and greatly reduced effort compared to traditional formats. Binding events detected can easily be correlated to the molecule synthesized in that position, as the position of each sort of molecule on the support is known.

In combinatorial synthesis, linear heteropolymer molecules (such as DNA or peptides) are created by subsequently adding monomers to the polymer chain. Chemical protection groups ensure stepwise addition of single monomers. Solid-phase synthesis can be performed on a common substrate, resulting in an ordered library of molecules. The substrate is divided into synthesis loci, with a distinct heteropolymer being synthesized in each of them. E.g. using a microtiter plate for solid-phase synthesis, each well on the plate is a synthesis site for one specific polymer. The monomers are transported to their synthesis sites in many systems by spotting, that is by transfer in solution within small liquid drops generated by a miniaturized device similar to a pipette or an inkjet printing-head. Alternatively, arrays can be generated using lithographic methods, in which the whole support is exposed to a solution of monomers, but coupling can occur only in areas previously illuminated, or electrochemical methods.

After the array is produced, it can be experimentally used as follows: The support and synthesized molecules are exposed to a solution containing target molecules after synthesis. Thus, these molecules interact with all the different polymers on the surface in parallel. Experimental results are obtained by using labeled molecules of interest, e.g. by attaching fluorescent or radioactive groups and using suitable scanners or films.

Highly complex microarray systems based on combinatorial synthesis techniques are in widespread use in biological, medical and pharmaceutical research. Those devices can display thousands of different nucleotides or peptides. Density and size of the synthesis sites are the critical parameter for such systems, since they limit the number of molecule sorts synthesized per array. Additionally, per sort of peptide tested, smaller amounts of target molecules (i.e. proteins or antibodies), which may be expensive or hard to obtain, are required as synthesis site size decreases.

Miniaturization of peptide arrays is lagging behind that of nucleic acid arrays, both in terms of synthesis sites per cm^2 and in terms of cost per synthesis site. One reason is that, for each layer, there are four standard nucleic acids, but twenty standard amino acids from which the polymer can be formed. In liquid transfer systems, each monomer sort is coupled subsequently upon contact of the liquid with the surface. Here, peptide synthesis with its twenty different standard monomers is at a disadvantage compared to nucleic acid synthesis. Lithographic methods similarly suffer from this difficulty: In mask-based approaches, the mask costs are multiplied by the number of monomers used, while both mask-based and mask-less systems for peptide synthesis would have the whole chip exposed to twenty monomer solutions per synthesis layer.

Liquid transfer systems are furthermore limited in how far they can be miniaturized by two effects: First, liquid droplets can not be reduced in volume indefinitely, as liquid evaporation is proportional to the surface of the droplet. Small droplets tend to evaporate rapidly, reducing the maximum distance they can travel to the support, which may result in insufficient coupling. Second, liquids spread on the support, and synthesis sites must be spaced far enough to avoid the merging of deposited liquid drops, which could cause mixtures of peptides to be synthesized on both synthesis sites.

Particle-based combinatorial synthesis replaces the liquid drops with solid particles. They can be transferred by a laser printer that prints but monomer particles instead of toners containing dyes onto i.e. glass substrates. As a color laser printer uses one toner per color, one sort of particles is used for each sort of monomer. In this method, all particle sorts of one layer are deposited, and remain inert unless heated. Upon heating they become viscous (similar to a gel). The liquefied particle matrix serves as a solvent which both allows the amino acids to diffuse towards the support and to chemically couple to it. Until this step, the monomers are packaged inside the particles, protecting them from decaying in the environment. The remains of the particle matrix and excess monomers are then washed away, and the support can be prepared (by removal of the protecting groups) for the next layer of particles to be deposited.

Chip based combinatorial synthesis takes this concept one step further, replacing the glass substrate with an active support in the form of a specially-designed microelectronic (CMOS) chip that electrostatically attracts monomer particles to their respective synthesis areas on its surface. The pattern of attraction is arbitrarily programmable. On this chip, each synthesis site corresponds to one pixel, which is an electrostatic actuator including a control circuit, which can be programmed to attract or repel charged particles onto its associated synthesis site. By subsequent programming of patterns and exposure to particles of each monomer sort (e.g. in

an aerosol), layers of monomer particles can be generated. The polymer chains are elongated upon heating the particles. As with other combinatorial synthesis methods, washing away the excess particles and removing protecting groups prepares the support for the next layer of particles to be deposited.

A chip-based combinatorial synthesis system consists of numerous components from different disciplines of science and engineering. E.g. combinatorial synthesis chemistry, functionalization of the support, particle technology and the physics of particle transport, and biological methods for the detection of binding events must be combined. Each component depends on the availability of other components in order to allow for it to be tested under realistic conditions, improved and adapted. Eventually, the system must be taken from the proof-of-principle stage to being fully automated in an integrated machine, including bioinformatics tools, to be used routinely in actual research applications like the ones described above.

This thesis can only focus on few specific components of this complex a system. Nevertheless, both a broad understanding of all the aspects and tight cooperation between experts from all the relevant fields of science and engineering are required to integrate these components into a peptide synthesis system.

The development and use of the microelectronic chips and their integration into both the particle deposition and the synthesis system are the primary aspects of the Peptidchip project covered in this work. This thesis presents:

- An overview of the relevant biological methods (chapter 1) and an introduction to the microelectronic technology used (chapter 2). For readers without previous knowledge in the biochemistry of amino acids, appendix A1 offers an introduction.
- Remarks on microparticles and microparticle transfer in electric fields (chapter 3).
- Previous and related works directly relevant to this thesis (chapter 4).
- The materials and methods developed as part of this thesis, especially the different chips that were designed and the electronic and mechanic components required for their use (chapter 5).
- The experiments performed in order to improve particle deposition from the aerosol and to ensure compatibility between the chip, the aerosol and surface modifications for synthesis, which were required to generate peptide arrays (chapter 6).
- Results from peptide syntheses on the microchips developed during this thesis. In particular, successful combinatorial synthesis on more than 16,000 synthesis locations, at 10,000 sites per cm^2 , is shown (chapter 7).
- An outlook on how these results could be developed further and on possible future applications completes the thesis (chapter 8).

PART I

FUNDAMENTALS

1. Peptide Arrays: Generation and Applications

1.1 Laboratory Peptide Synthesis

1.1.1 Applications

In the living organism, thousands of molecules composed of amino acids play critical roles. Numerous research approaches aim at studying those molecules with regards to their function and their regulative interactions, and various techniques exist. A selection of these objectives and methods is highlighted in this chapter.

Many biological and medical approaches aim at the investigation and identification of e.g. protein-protein, protein-peptide, protein-metal, protein-DNA or protein-RNA interactions. Especially the identification of specific interacting regions of a given protein is of great interest. In some cases, subfunctions of a protein can be represented by short peptide chains (starting at around 8 amino acids) equal to a continuous linear sequence representing part of its primary structure (*epitopes*) [ALB08, KNO99]. In other cases, a binding site of a protein formed from amino acids discontinuously distributed over its peptide chain can be mimicked by an equivalent peptide sequence (*mimetopes*) [EIC04]. These studies are regularly performed with synthetic peptides [UTT08].

Furthermore highly complex protein networks exist, which allow survival of the organism even under varying circumstances. They are regulated by the interactions of the proteins with each other by stimulation or inhibition. Shorter peptides can stimulate or activate biological activity of proteins, as well [EIC05, BIA03]. Malfunction of the regulating interactions potentially leads to severe diseases or dysfunctions within the organism, such that studying these interactions is a main focus of medical and pharmaceutical research.

One class of proteins, called enzymes, plays a critical role in organisms in catalyzing chemical reactions required for survival. Peptides can also be efficient catalysts, facilitating chemical syntheses, e.g. mimicking the function of known enzymes. Peptides could also be designed to catalyze novel reactions [REV07].

Finally, peptides are capable of very specific binding, as can be seen in the variable domains of antibodies. If such specific capture groups are found, they can be used to detect the presence of target molecules in serum or other solutions [REI02]. Even vaccinations using synthetic peptides have been shown [SCH90]. Numerous peptide-based drugs have been developed to date making use of this specific binding [VLI10]. Peptidic HIV fusion inhibitors like *T20* inhibit the entry of HI viruses into its host cells, slowing the progress of the disease [QAD10]. Peptidic medications for cancer treatment by arresting the cell cycle or inducing apoptosis are currently being developed [RAU09, SHR09]. Other diseases against which synthetic therapeutic peptides are already available are, among others, hypertension, type 1 and 2 diabetes, severe chronic pain, prostate and breast cancer, and other tumors [VLI10].

Besides the applications of peptides in diagnosis and treatment of diseases, even material science can benefit from methods of sorting materials that are difficult to sort with conventional means. For example, specific peptide binding to sorts of carbon nanotubes has been demonstrated, allowing to separate conducting from semiconducting tubes, which may

turn out helpful e.g. in building future carbon-nanotube based field effect transistors [WAN03].

1.1.2 Solid-phase Peptide Synthesis

It is possible to synthesize peptides or proteins by using genetically modified cells, breaking them up and sorting the components. However, for each peptide, a specific clone has to be generated, and purification e.g. via chromatographic methods is laborious and expensive. Cell-free synthesis of peptides would be less laborious and thus preferable for many applications. In situ biosynthesis methods have been developed, such as phage display or ribosome display, that use cell extracts containing all essential elements to synthesize proteins from mRNA or DNA outside of living cells. Array formats of such methods exist, and can be used to synthesize peptides or even complete proteins [HE08]. They are, however, hard to expand to non-standard amino acids. Chemical synthesis, in contrast, allows for the use of arbitrary amino acids (such as synthetic amino acids that do not occur in natural organisms, non-proteinogenic amino acids, D-amino acids, amino acids mimicking post-translational modifications, β or γ amino acids or PNAs [POR08]) that require massive effort or are impossible to synthesize using ribosomes. Peptides from non-standard amino acids are of particular pharmaceutical interest because, compared to peptides from standard amino acids which are quickly degenerated by *peptidases* inside organisms, they have an increased half-life within organisms, making them more suitable for pharmaceutical use [OTV08, NES09].

Today's chemical peptide synthesis techniques are based on *solid-phase peptide synthesis* or *Merrifield synthesis* [MER63, MER64-1, MER64-2], allowing step-by-step synthesis of peptides from the C- to the N-terminus. To improve handling, especially the separation of the peptides being synthesized from the different reagents they need to be exposed to, the peptides are covalently bound to a *solid support*, such as a glass slide or polystyrene beads. The surface of the support is functionalized in such a way that carboxyl groups can bind onto it. Between reaction steps, reagents, including excess amino acids from the previous step, can be easily washed off the surface. This allows using an excess of amino acids (compared to synthesis on the surface) in order to increase synthesis yield.

Protecting groups are used to ensure that in each reaction step, the peptide chain is elongated by exactly one monomer, and that no branching of the polypeptide occurs (fig. 1.1). Protecting groups serve two different purposes: first, to protect the N-terminal amino group of the newly added amino acid, and second, to block side-chains onto which amino acids could couple. The protecting group for the N-terminal amino group is removed after each synthesis step, while the side-chain protecting groups are removed after the completion of the synthesis. Depending on the sort of side-chain to be protected, a variety of different protecting groups exist [ISI09]. These protecting groups must be *orthogonal*, that is the N-terminal and side-chain protecting groups must be removable by exposure to different conditions. Protecting groups are covalently bound, and may be released depending on e.g. pH, presence of specific reagents or exposure to light.

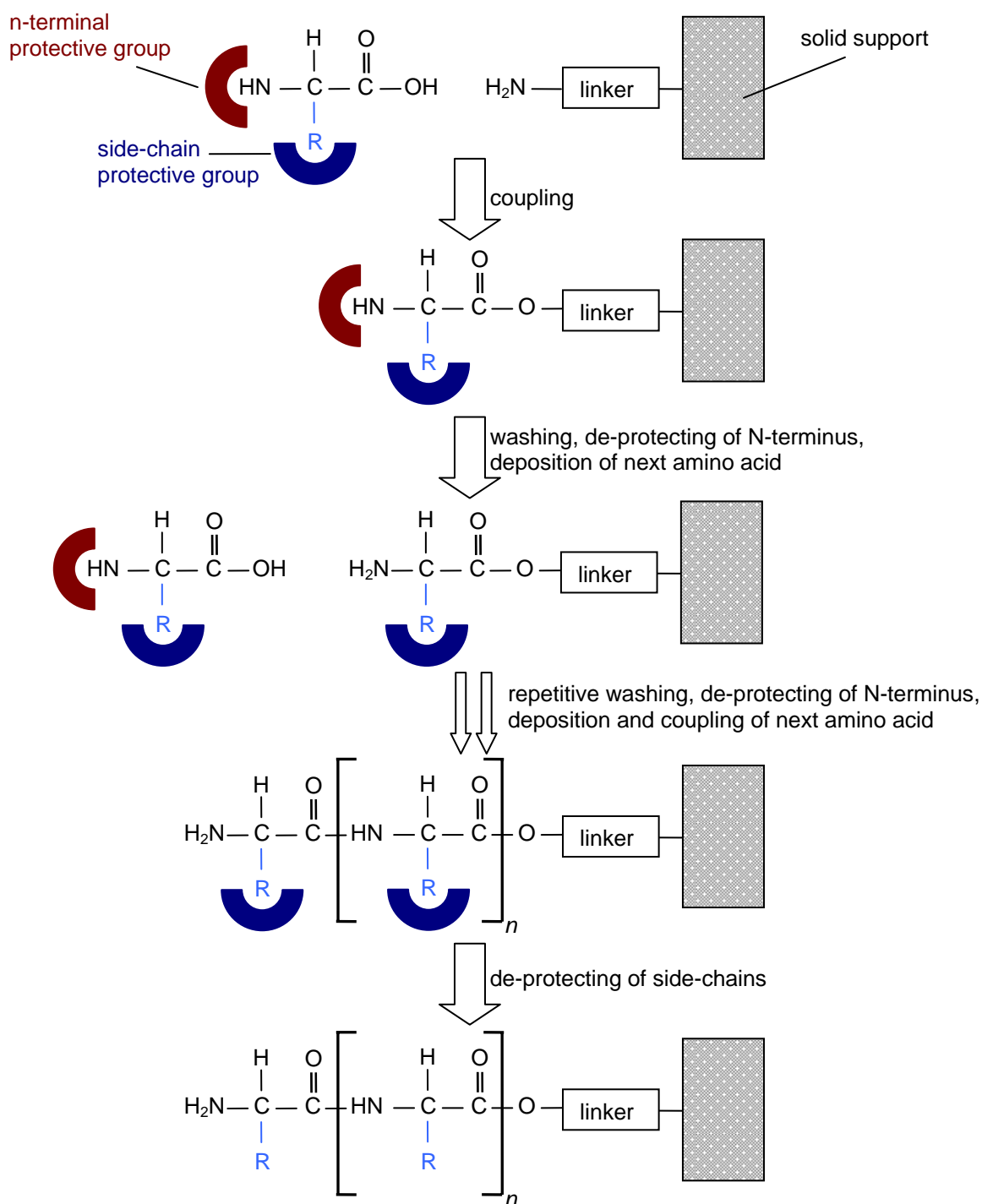


Fig. 1.1: Merrifield peptide synthesis (see text). Only amino acids having side groups that can participate in side reactions during peptide synthesis need to be protected by side-chain protecting groups. The protecting groups are bound to the protected group by covalent binding.

Two distinct methods of solid-phase peptide synthesis are in widespread use today. The first method follows the original Merrifield synthesis, and uses tert-butyloxycarbonyl (t-Boc) as N-terminal protecting group that can be removed by use of a weaker acid like trifluoroacetic acid (TFA), while the side-chain protecting groups are selected so that hydrogen fluoride (HF)

removes them. Due to the health hazards and handling difficulties associated with HF, this method is less preferred. An alternative method uses an N-terminal protecting group that is removed under basic conditions, and acid labile protecting groups for the side-chains. *Fmoc* (9H-fluoren-9-ylmethoxycarbonyl) is base-labile, and used as N-terminal amino acid protecting group which can be cleaved with mild bases such as piperidine in DMF. This leaves protecting groups labile to weaker acids (such as the protecting groups used for the backbone in the original Merrifield synthesis or other protecting groups labile to TFA) available for side-chain protection. As a side benefit, the Fmoc group is a chromophore, so absorbance measurements during de-protection can be used to measure synthesis efficiency of the previous coupling. As de-protection is very efficient, the number of Fmoc groups released is practically equal to the number of protected amino acids that were coupled during the previous coupling step.

In order to optimize synthesis yield, amino acids for synthesis may be *activated*, e.g. by adding chemical group to the amino group, which is replaced by the peptide bond during coupling. If properly chosen, such an *activation group* can increase reactivity of the amino acid. Care must be taken, however, for not all activation groups are compatible with long-term storage of the amino acids. One example of a commercially available, storage friendly activation group is *OPfp*, the ester of Pentafluorophenol. Fig. 1.2 shows the chemical structure of the protected and activated Fmoc-Ser(tBu)-OPfp amino acid, with backbone protecting group, side-chain protecting group and activation group marked.

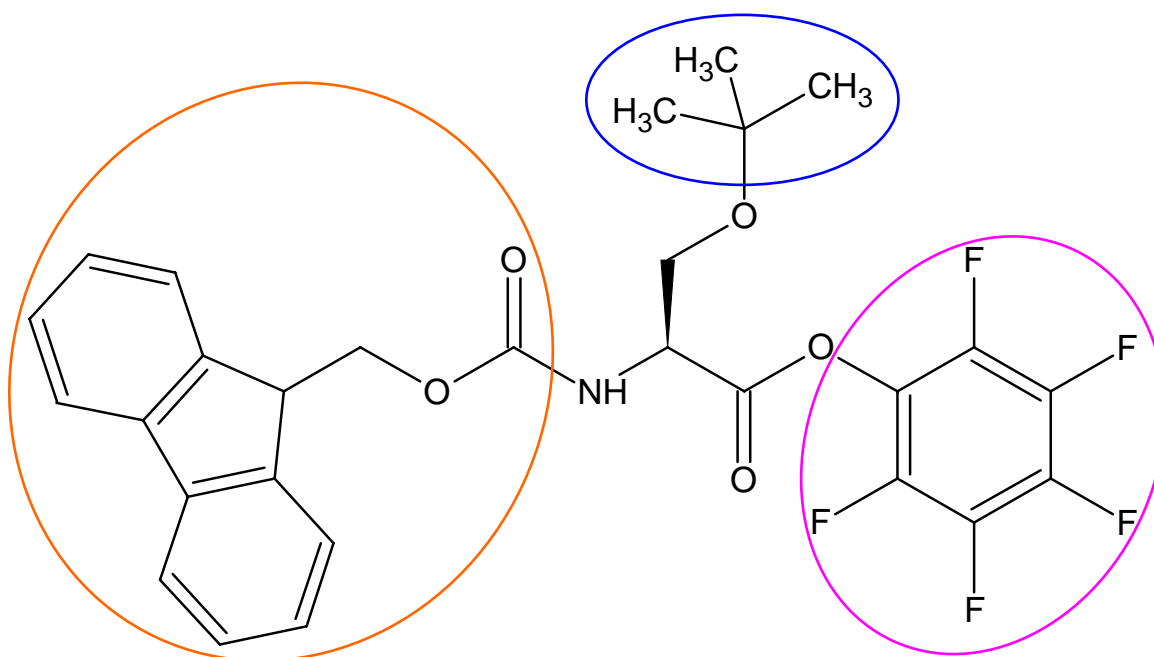


Fig. 1.2: Fmoc-Ser(tBu)-OPfp, an example of a protected and activated amino acid. The backbone amino group is protected with an Fmoc group (orange) and the alcohol group on the side-chain is protected by a tert-butyl group (blue). The carboxy group is activated by an OPfp group (magenta).

In between the first carboxyl group of the peptide and the support, spacers can be added before starting the synthesis to increase the distance between the peptide chain and the support, reducing steric hindrance. If peptides in solution are desired as the final synthesis product, a linker that releases the synthesized peptides upon exposure to a reagent or condition can be used. In case of Fmoc chemistry, that third reagent can be TFA, so that

peptides are released simultaneously to the removal of side-chain protecting groups, or yet a different reagent that is applied after the removal of side-chain protecting groups.

Further details on the chemistry of peptide synthesis, including protocols, can be found in other works [MÜL04, BEN06, BLO09, BEY05, BEY07].

1.1.3 Peptide libraries

Obviously, in the applications shown in 1.1.1, a large number of selected peptides (called a *peptide library*) may need to be tested for potential applications. Efficiency is maximized if numerous such tests are performed in parallel, both by reducing workload and by providing results with a higher comparability.

Peptide libraries may contain large numbers of peptides, even if they are only of short length. Using only the 20 standard amino acids for a peptide of n amino acids, there are, theoretically, 20^n possible combinations. For $n = 5$, this yields 3.2 million different molecules, for $n = 10$, there are about 10^{13} possibilities and for $n = 20$, we have over 10^{26} combinations¹. Fortunately, many applications only require a small subset of these possibilities; for example an experiment that would test all *permutations*² of a given peptide at only two amino acid positions still would require 400 different molecules to be tested. Yet, the possibility of synthesizing large arrays is very desirable – up to a range of millions of peptides per experiment [HOU91].

The most trivial parallelized setup is simply an X by Y array of labeled test tubes that are processed by lab workers in a manner similar to an assembly line. Alternatively, a pipetting robot can handle the tubes in a truly parallel manner. This setup is the basic *bioarray* setup, miniaturizations of which have since been developed for a variety of biomolecules, including RNA, DNA, antibodies or other proteins and peptides. Due to the fact that in solid phase peptide synthesis, the peptides are fixed to specific locations of the support by design, it can be parallelized with particular ease.

Three different strategies have been devised concerning the relationship of the peptides to their support: Coupling numerous pre-synthesized peptides onto a common support, synthesizing peptides in parallel on a common support, and synthesizing each peptide on an individual tiny support.

Spotting pre-synthesized peptides (from a first support) onto fixed locations on a new support to form the library used in the array experiment allows additional purification and concentration steps after synthesis. This method also allows using a distinct, optimized support for synthesis and another support for array exposure and detection of binding events. However, this comes at the price of extra processing steps that increase array production time and cost and may be sources of errors [GAO03].

Synthesizing the peptides directly on the support to be used in the experiment (*in situ*) is the most straightforward approach, without need for additional transfer steps. Some purification methods may be adaptable to this strategy, but this is more difficult than with pre-synthesized

¹ Some of these possibilities are not synthesizable with reasonable efficiency, however, due to steric hindrances.

² Differing from mathematics, in peptide biology “permutation” signifies the exchange of the amino acid at a given position of the peptide with a different amino acid (or all possible standard amino acids), leaving the rest of the peptide sequence untouched.

peptides. It should be noted that using this strategy, the support must be suitable for both synthesis and detection of binding events, making the design of the array system more challenging.

Split-pool (or *split-mix*) methods are an alternative to conventional array experiments. In this system, the single solid support with many distinctly located areas of one sort of peptides each is replaced by a large number of small resin beads, each bead containing one sort of peptides. The beads are split between the amino acids to be added for the next layer between synthesis steps and then mixed again, resulting in a very large number of different peptides. However, in order to determine, after the experiment, which peptide had actually been synthesized on a bead of interest, it must be sequenced (i.e. by Edman degradation). This adds extra process steps, and if the presence of all peptides from a list is to be guaranteed, due to the stochastic nature of the method, a much larger number of beads than of spots on a deterministic support is required. Furthermore, some (i.e. hydrophobic) peptides nonspecifically bind to any protein, and cannot be avoided due to the randomness of synthesis. They therefore add to the number of peptides that have to be sequenced. Additionally, such beads are not directly compatible with standard laboratory equipment based on microscope glass slides, rendering intervention or controls by the experimenter outside the synthesis machine difficult and thereby making process less flexible [HOU91, LAM91].

As this thesis is part of an effort to create a system useable for direct synthesis, only this case is considered in the following. A typical workflow of a peptide library experiment using this strategy can be summed up as shown in fig. 1.3.

The array system used must provide the required functions, in particular:

1. Synthesis chemistry allowing the sequential building of a polymer.
2. A support, and means to deposit the monomers onto distinct areas of it in a controlled fashion.
3. Means to expose the polymer (e.g. peptide) of each support area simultaneously to a target substance, and means to detect the strength of binding between the target substance and the polymer for each area.
4. For arrays of significant size, software support may be needed in order to design the array and to transform the data generated into meaningful results.

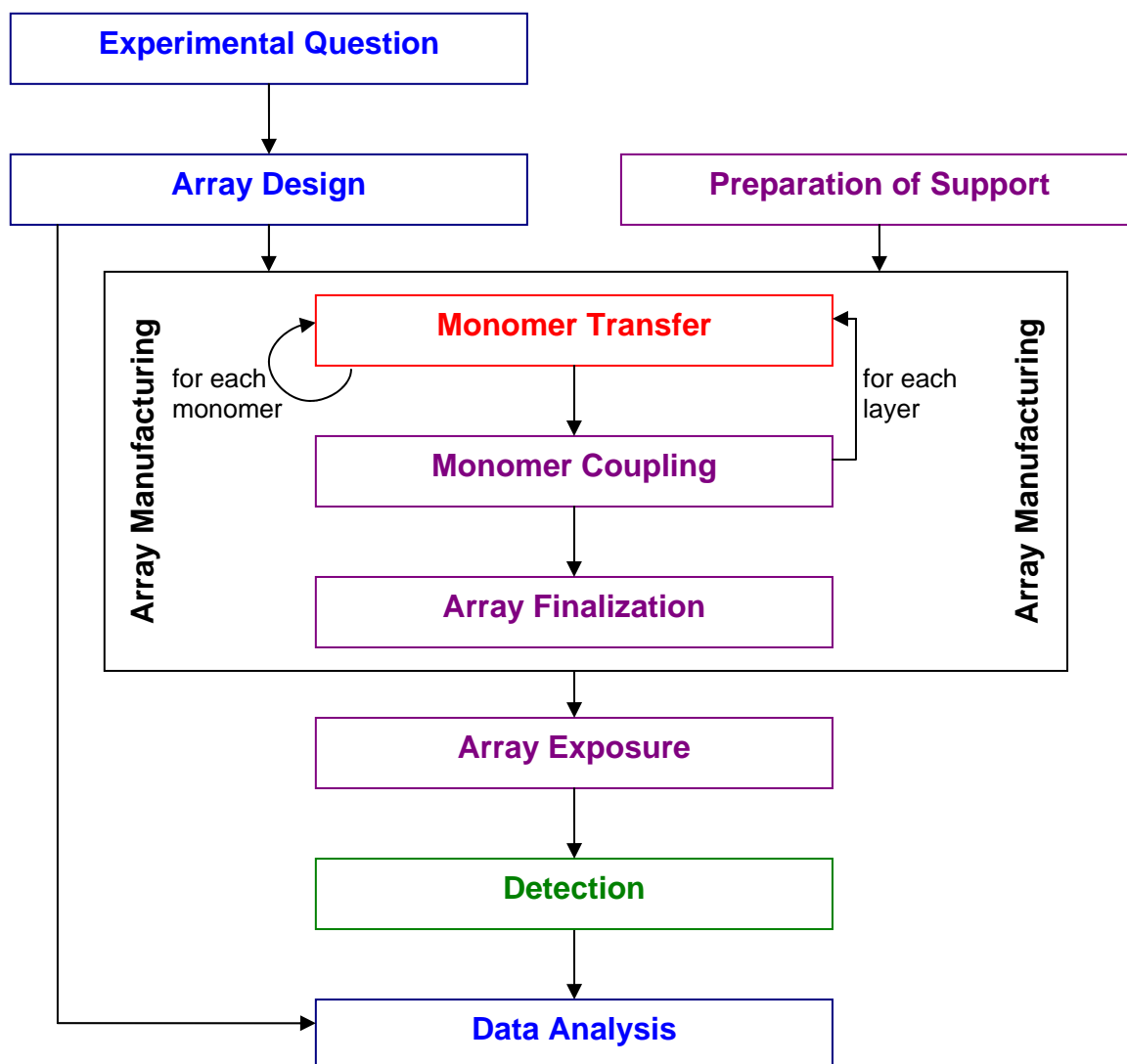


Fig. 1.3: Flowchart of a typical bioarray experiment. Data processing in blue, chemical steps in violet. Note that in many array systems, monomers must be coupled directly upon deposition for technical reasons, greatly increasing the required number of coupling steps. For each step, an appropriate verification step may be necessary depending on the reliability of that step and the requirements of the experiment.

1.2 Peptide Array State of the Art

1.2.1 Challenges in Peptide Arrays

1.2.1.1 Maximizing Spot Density and Minimizing Cost per Peptide Spot

As described in 1.1.3, the number of peptides theoretically possible is enormous, even for short molecules and even if using standard amino acids only. Cost per peptide spot may easily be the limiting factor in such experiments. As the cost of amino acid monomers and high-purity reagents required for synthesis, which depends on total array area, is high, increasing the number of spots per cm^2 is critical in order to provide more peptides per Euro. Additionally, in some applications, the amount of sample material that the array is exposed to

is limited or hard to provide (i.e. in experiments in which the array is exposed to serum). Here, high-density arrays are essential.

When creating peptide arrays using droplets of liquid, two factors limit the achievable spot density: First, liquids on surfaces tend to spread, and when two liquid droplets contact one another on a surface, they merge and mix. Thus, liquid spots on the surface need to be spaced sufficiently to prevent such contact. Second, when travelling in air, the evaporation of the liquid is proportional to the surface of the droplet. As the surface-to-volume ratio of droplets increases with decreasing volume, evaporation becomes more critical at lower volumes. As evaporation may also happen at the nozzle, clogging after evaporation of the solvent becomes more of an issue with smaller volumes and smaller nozzle diameters.

1.2.1.2 Maximizing Peptide Chain Length

While ribosome-based protein synthesis in living cells is capable of producing numerous peptides of several thousand amino acids, solid-phase peptide synthesis cannot produce arbitrary peptides of this length with good yield. Yield is defined as the number of desired peptides divided by the total number of peptides in the synthesis area. Yield Y can be calculated as the product of the synthesis efficiencies E_i of each step i , or

$$Y = \prod_i E_i . \quad (\text{Eq. 1.1})$$

For example, were a ten-mer peptide synthesized with a per-step efficiency of 0.9, only 35% of all peptides would be correctly synthesized, while for an efficiency of 0.95, about 60% correct peptides could be achieved. For a twenty-mer peptide, an efficiency of about 0.98 would be required in order to achieve more than 50% correct molecules. Synthesis efficiency is strongly dependent on the actual sequence, the properties of the support surface, and the linker. Additionally, ways to purify peptides both before spotting in case of deposition of pre-synthesized peptides and with in-situ synthesis have been devised [CHA00, STA08, BLO09].

Today, arrays of 10- to 15-meric peptides have been routinely synthesized in numerous experiments [ALB08, KNO99, ZHA10]. Having modified the classical SPOT technology, even peptide arrays with up to 53-mers have been synthesized [GAI05].

1.2.1.3 Optimizing Detection Specificity and Sensitivity

In order to be able to detect not only the strongest bindings between synthesized peptides and target molecules, but weaker ones as well, it is desirable to maximize the number of peptides per area in order to receive a detectable signal even for low binding ratios. Additionally, in order to be able to compare the strength of binding between different peptides, peptide density should be as homogeneous as possible over the whole support, independent of both the location of the synthesis site on the support and the sequence. Additionally, resistance of the support to non-specific protein binding is required in order to prevent a background signal. Details on detection can be found in 1.3.

1.2.1.4 Handling and Usability

Besides the hard figures of merit described above, whether a peptide synthesis system can be successfully employed in the laboratory also depends on its usability. The following factors, among others, may be decisive for some applications of microarrays:

- Time to manufacture an array.
- Time to achieve detection of binding events after exposure.
- Storability of manufactured arrays until exposure, i.e. how long and under which conditions can a manufactured array be stored.
- Robustness, i.e. how much care and manual skill is required in handling the support, and how tightly need the environmental conditions during the experiment be controlled.
- Ease of use, i.e. how complex are the procedures that must be observed.
- Compatibility to existing systems, i.e. whether the support can be manually examined in a microscope.
- Adaptability, i.e. how hard it is to modify the array system to allow for methods not foreseen during its design to be used on it.
- Upkeep and operational costs, including reagents, training and laboratory space requirements.

Users and providers of array systems alike must consider these factors both in choosing and designing their system.

1.2.1.5 Use of Non-standard Amino Acids

For certain applications, the user of a peptide array might want not only the standard proteinogenic acids, but various different or extended sets of amino acids to be synthesized on the support. A pharmaceutical user might require a set of D-amino acids corresponding to the biogenic L-amino acids to synthesize arrays of D-peptides to search for drug compounds, while a biologist interested in post-translational modifications of proteins might want the option to include selenoylated, methylated, hydroxylated or phosphorylated amino acids into the peptides.

Ideally, a peptide synthesis system allows for easy retooling, possibly even allowing to change the set of depositable amino acids during a running synthesis. Spare monomer transfer units, present in the system in addition to the ones for biogenic amino acids, could be re-configured for such syntheses according to the user's needs.

1.2.1.6 Synthesis in the Users' Labs vs. Synthesis at the Provider

In principle, array systems can be made available to the user by the provider of array systems following two strategies: First, the user can send the provider a description of the desired array, which is then manufactured by the provider and sent to the user. Second, the provider can sell the required machinery and materials to the user, which enables him to manufacture arrays for himself.

Which of these strategies are possible or preferable for the user depends both on the user's situation and some of the properties of the array system listed above. Especially, in order to enable manufacture at the provider, the synthesized array must be storable for sufficient time and under conditions that allow transport to the user (or alternatively the user must transport his test substance to the provider for array exposure and detection of binding events).

From the user's point of view, a certain throughput is required before the purchase of a synthesis machine is economic – for low throughput, ordering arrays from a provider is almost always more economical. Additionally, depending on the ease of use and robustness, staff with specialized training might be required in order to operate and maintain the machine. However, synthesis at the user's site would allow advanced users to introduce their own verification steps and modifications into the process as needed and be more economical at high volumes.

From the provider's point of view, shipping arrays increases vertical integration, potentially increasing profits. However, the required investments in the machinery and staff to handle customer requests bind capital and leave the provider to deal with the risk of fluctuations in demand for arrays.

1.2.2 Peptide Array Technology

The simplest array support nowadays are microwell plates, essentially a miniaturized array of test tubes in the form of depressions (wells) in a plate of plastic, glass or other materials. They have been standardized by the Society for Biological Standards [SBS04] and can be found in almost any biological lab for numerous applications. On an area of 127.76 mm × 85.48 mm at a height of 14.35 mm, plates with up to 1536 wells of down to 10 µl volume per well are available. Due to their standardized measurements, plate handler robots are available off the shelf.

If further miniaturization is desired, depressions are no longer practical due to capillary effects, and synthesis sites need to be created on a different support, normally level and without physical structures corresponding to the synthesis sites. While microwells are self-aligned, these level supports require precise alignment between different process steps to minimize offset. Various systems to dispense small volumes of liquid onto a defined spot are available, using direct contact or non-contact (e.g. piezo-based) methods similar to inkjet printers [MÜL04]. SPOT synthesis is a method in which solutions of activated and protected amino acids are spotted onto supports such as glass slides, paper or cellulose membranes [FRA92, VOL09]. This method has been developed into an array system that is now commercially available from JPT Peptide Technologies GmbH, Berlin [JPT] under the brand names of PepSpots and PepStar.

Synthesis using lithographic methods has also been demonstrated, both using photolabile protecting groups and using conventional acid-labile protecting groups in conjunction with acids photogenerated from precursor molecules. This method has allowed the synthesis of thousands of peptides per cm² on glass slides, but requires either numerous masks specifically manufactured for each array or sophisticated projection devices (i.e. micromirror arrays) [FOD91, GAO03, PEL02].

Several providers now offer peptide arrays or peptide array systems [MÜL04], but the purchase price for microarrays still is in the range of 5 € per peptide site [PET09], or 5,000 €

for an array of only 1,000 peptides, making peptide microarray experiments too costly for many potential users.

1.3 Detection of Bound Molecules

1.3.1 Labeled Molecules

Most molecules are too small to be seen and identified on a surface even with the best light microscopes available, as they are smaller than the resolution limit of visible light. Therefore, in experiments where the binding of a molecule to a surface is to be measured, other detection methods must be found. Sometimes, depending on the molecule and the setup, natural properties of the molecule can be used, such as its mass or natural fluorescence, but often this is not the case.

One common method to make arbitrary molecules detectable is to *label* them, that is to covalently bind the molecule to be detected to another molecule (or small solid object) which is designed to be easy to detect. Molecules containing radioactive atoms are a classic option, with the advantage of defined and selectable half-life and straightforward use, but the disadvantage of stringent safety regulations to be observed. Alternative methods in widespread use rely on visible, infrared or ultraviolet light, such as *chemoluminescence*, in which light is emitted as the result of a chemical reaction, or *fluorescence*, in which a molecule absorbs *excitation light* of a defined wavelength, and subsequently emits *fluorescence light* of a different, less energetic wavelength. This difference in wavelengths is called the *stokes shift* of the fluorescent molecule. These molecules may be more bulky than radioactive atom labels, and require more complex setups, but avoid the use of radioactives. In case of chemoluminescence, the light-generating chemical reaction must be compatible with the rest of the experiment. In case of fluorescence, the detector for the fluorescence light must be shielded from the excitation light by a very efficient filter, because excitation light tends to be several orders of magnitude stronger than the emitted light. Numerous fluorescence labels with different stokes shifts are commercially available.

In all cases, the label may interfere with the binding to be monitored, making positive and negative controls necessary. To reduce this risk, labels may also be linked to a second molecule that binds the molecule to be detected in what is called a *sandwich assay* – a method that is especially common when using antibodies [MÜL04, EIC05].

1.3.2 Detection of Bound Molecules in Bioarray Experiments

A variety of systems for detection of binding events on bioarrays after exposure is available, based on the labeling strategies described above, varying from manual examination by the experimenter under the microscope to specially designed array scanners that directly interface to analysis software, available commercially. Fluorescence scanners, for example, are table-top units that consist of a support holder (i.e. microscope slide holder) several sources of excitation light of defined wavelength (i.e. lasers) matched to frequently-used fluorescent dyes and a scanning detection unit with filters against the excitation light. Such units can scan arrays with a resolution in the range of few μm . Subsequent scans at different wavelengths creating a set of scans for different fluorescence molecules on one support are possible [MÜL05, EIC05].

2. Application Specific Integrated Circuits

2.1 Introduction

Electronic circuits, consisting of both passive components like resistors, capacitances and inductances and active elements such as diodes and transistors, are available as purely *discrete circuits* (where each component is a separate device soldered to a support such as a *PCB*¹) or with varying degrees of *integration*. In the context of microelectronics, integration stands for the process of combining several circuit components into a single package. Simple examples of integration are microchips containing several transistors, logic gates or other electronic devices on the same piece of silicon in one package, but without a fixed interconnect between them, that is each device is connected to the PCB independently. One example of this is the 74HC03 IC containing four separately contacted AND gates. More advanced examples are digital gates containing a few transistors in a fixed wiring or analog amplifiers consisting of several transistors and capacitances. Such devices are called *Integrated Circuits* or *ICs*.

The benefits of integration, namely a reduction in area (and thereby potentially significant improvements in speed due to lower parasitic capacitances, reduced power consumption, and improved mechanical ruggedness) and lower material costs far outweigh increased design and tooling overhead costs in many cases, especially in volume production. As foreseen by G. E. Moore [MOO65], integrated circuits with a geometrically growing number of transistors per unit are no longer limited to computing machines of ever increasing power, but now are present in most electronic devices, from assembly line machinery to cars, mobile phones and cameras, medical products and even simple toys. Microchips have even been implanted into the human eye as a means to restore sight to blind patients [GRA09].

Besides this *miniaturization*, the *development of new interfaces* was essential for this electronic revolution. Digital cameras as we know them would not be possible without photodiodes or other integrated CMOS photo detectors. Without HV-CMOS technology, conventional CMOS processes would still need external components to control high voltages required e.g. in machine tools or automobiles. CMOS-based *MEMS*² processes offer direct interfacing to the mechanical world, in applications as diverse as micro mirrors for optical transducers (DMDs³), driving aids (e.g. ESC⁴) and safety systems in vehicles (e.g. airbag controls) [FED05]. Chemical sensors allow for sensing of adsorbed molecules using gas-

¹ A PCB, or *Printed circuit board*, is a one- or multi-layered board of isolating material (such as woven glass and epoxy) with custom-routed metal tracks (usually copper, the tracks are obtained by a mask-based etching of a solid copper plane), *vias* (*Vertical Interconnect Access*, metal-filled holes connecting the metal tracks on different layers) and metal-lined holes or plates to connect devices to it in defined locations. PCBs can be obtained from various sources starting at a few 100€. Advanced processes offer a minimum metal track pitch of less than 150µm.

² Microelectromechanical systems.

³ Digital Micromirror Device – MEMS based mirror arrays used in video projectors

⁴ Electronic Stability Control

sensitive field effect transistors or capacitive sensors [HIE05]. Even a direct electronic interface between chips and neural cells is no longer fiction [FRO08].

Integrated Circuits can be divided into two varieties based on the purpose they were designed for: *General purpose ICs*, ranging from simple logic gates to operational amplifiers, digital-analog-converters, memory chips or field-programmable gate arrays (FPGAs) are designed for the *general market*: The intent is to produce a chip that suits many common applications, or at least fills a niche of end user needs. Some of these ICs may be extensively customizable, like FPGAs or microcontrollers, while in other cases, the user has the choice between thousands of similar components, with a wide range of specifications and packages, like in the case of operational amplifiers. Nowadays, for many applications, one can design the circuit required from chips and components readily available from various vendors and assemble it on a custom-made PCB [WIL05]. Many MEMS components, such as acceleration sensors for crash or rollover detection, are available in this way as well.

General purpose ICs can be very economic to use in many cases, but they are always a compromise. If an application has tight specifications, it is possible that no general purpose IC may serve. In case of the first level of detector readout electronics at CERN, for example, where very specific data needs to be analyzed at the highest speed and lowest power in a confined space, the IC must be tailored to the application. Such a specialized IC is called an *Application Specific Integrated Circuit*, or *ASIC*. In addition, designing your own ASIC is the only way to create fundamentally new interfaces between a CMOS chip and its environment.

In order to design an ASIC, one need not have a semiconductor process line of one's own. Many semiconductor companies offer *production services*: They make the specifications and rules for design in their semiconductor processes available to their customers and then produce the designs submitted to them. The designer is restricted by the *process parameters* (e.g. number and thickness of metal layers, doping strengths and depths, or physical properties of devices, such as MOSFET I-V-curves or parasitic capacitances) and *design rules* (requirements for guaranteed function of the components, for example minimum distances between isolated conductors), but otherwise has freedom down to the level of physical placement of doped areas and metal tracks.

2.2 High Voltage CMOS

2.2.1 HV CMOS Technology State of the Art

Along with reducing the feature size, miniaturization has continuously reduced the safe operating voltage of modern *deep submicron* CMOS processes, with gate lengths in the range of few hundred nanometers or less. One reason for this is the scaling of the electrical field along with the decreasing gate oxide thickness in order to prevent breakdown. Another reason is that with decreasing feature size and increasing clock speed, power density increases, potentially beyond levels that can be efficiently heat-sinked, which can at least partially be countered by reducing the operating voltage. Modern microprocessors therefore are operated at core voltages of less than one volt. In these processes, higher voltages (typically 5 V or 3.3 V) are required to efficiently drive the capacitive load of wires and PCB tracks to other chips or devices. In this case, these I/O devices may be designed using HV techniques.

However, even before the advent of such *dual-voltage processes*, some applications (motor controls, automotive, robotics and factory automation) required or could benefit from chips capable of handling voltages higher than their standard operating voltage (e.g. 5 V) [BLI81].

Means have been found to add limited HV capability without or with very few additional silicon processing steps to existing processes. Full HV capability up to several 10 V could also be achieved with a limited number of additional processing steps [BAL99]. These HV processes are also capable of handling comparably high power in the range of about 30 W, but at power ratings substantially beyond that, discrete power modules may be preferential [BLI81].

2.2.2 Voltage Limiting Effects in CMOS Processes

2.2.2.1 Gate Oxide Breakdown

An insulator will become conductive (break down) when exposed to a voltage V_{BD} that causes the electrical field to exceed the critical electrical field value E_{crit} of that material. If air is used as the insulator, molecules are ionized and air ions form a conducting path. In the case of solid insulators, currents or thermal effects may change their molecular properties or structure or shape so that they are destroyed (e.g. permanently conductive, causing a short circuit).

For structures resembling planar capacitors, the breakdown voltage is given by $V_{BD} = E_{crit} / d$, where d is the distance of the conducting plates. E_{crit} is a material constant, and strongly depends on impurities and surface quality (i.e. roughness). In practice, the critical field also depends on the thickness and area of the isolating sheet, as increased insulator thickness reduces the risk of an impurity or a defect causing the break-down of the whole sheet, and larger area increases the probability of a fatal defect being present anywhere on the sheet. For pure silicon dioxide under optimal conditions, for example, $E_{crit} = 12 \text{ MV / cm}$. Average oxides produced without special care, however, may have an E_{crit} of less than 1 MV / cm due to impurities. In semiconductor processes, however, silicon oxide sheets less than 10 nm thick have been used as gate isolation.¹ At a critical field of 8 to 12 MV / cm, on substantial percentages of dies all gates are functional, which equals only a few critical defects per cm^2 [BAL99].

In HV-CMOS, one important objective is to be able to use a low voltage signal to switch high voltage outputs. This cannot be efficiently achieved by simply increasing oxide thickness, as $I_{D,sat}$ would be extremely low for a safe oxide thickness. Compensating for this effect by increasing the channel width W would lead to an excessive consumption of silicon area. Therefore, a structure is needed that uses regular thin gate oxide, but somehow prevents the full high voltage from occurring over the oxide all the time during transistor operation.

2.2.2.2 Channel Hot Carrier Effects (HCE)

Without an external electric field, charge carriers in a semiconductor are in thermal equilibrium with the lattice. Under the influence of a small electric field E , they are no longer in thermal equilibrium with the lattice and move at a velocity $v = \mu \cdot E$, where μ is the charge carrier mobility. If the electrical field is strong, such as in the depletion region of a reverse-biased junction, they can reach kinetic energies well beyond thermal energy before colliding

¹ Maximizing gate capacitance, and thus minimizing gate oxide thickness is desirable in order to maximize the transconductance of a MOSFET of channel length L and width W since $I_{D,sat} = W / L \cdot \mu \cdot C_G \cdot (V_{GS} - V_{th})^2 / 2$ and $C_G = k \cdot \epsilon_0 \cdot A / d$.

with the lattice. If their kinetic energy is much greater than k_bT , such carriers are called *hot carriers*.

Hot carriers can occur in a MOSFET when carriers drifting in the channel reach the junction between the bulk and the strongly-doped drain, where electrical fields are high due to the strong doping. These charge carriers will sooner or later¹ collide with a lattice atom, where part of their kinetic energy W_{kin} is usually transferred to the lattice as phonons. However, if the energy of a hot carrier is high enough, harmful effects can occur:

- Charge carriers at energies higher than the potential barrier of the Si-SiO₂-Interface (electrons at $W_{kin} > 3.2$ eV and holes at $W_{kin} > 4.9$ eV) can be injected into the gate oxide. Some of them reach the gate and cause a gate current; while others are trapped in the oxide or at the Si / SiO₂ interface and cause device degradation by shifting V_{th} and reducing g_m .
- Charge carriers at energies higher than the ionization energy of the lattice ($W_{kin} > 1.3$ eV) can generate secondary electron-hole pairs by impact ionization. In an NMOS, generated electrons contribute to the drain current, while holes cause a substrate current. Both can also become trapped in the oxide if their energy is high enough.

In addition to degradation effects, hot carriers can also lead to destructive *avalanche breakdown* or *snapback breakdown*. For both effects, secondary electron-hole pairs generated by impact ionization cause the breakdown of the device, although by different mechanisms discussed for the NMOS as follows:

- In avalanche breakdown, the electric field is strong enough for secondary electrons to pick up sufficient kinetic energy in the electrical field that they can cause impact ionization themselves. Like in an avalanche diode, this effect of *avalanche amplification* results in a negative differential resistance in the device, and thus in high currents that usually destroy the transistor.
- It should be noted that the highest fields, and thus avalanche breakdown at the lowest voltage, are present in areas where the junction is curved, especially if the radius of curvature is small. External electric fields, such as from the gate or metal conductors near the surface can alleviate or aggravate this effect depending on their potential by extending or compacting the depletion region. Avalanche breakdown occurring due to the effect of conductors near the surface is called *surface breakdown*.
- Snapback breakdown is similar to latch-up in that it is caused by turning on a parasitic bipolar transistor with the substrate. As shown in fig. 2.1, an ordinary physical NMOS actually is a combination of an NMOS and a parasitic bipolar NPN transistor. In the parasitic bipolar, the drain and the source of the NMOS form the emitter and the collector, while the bulk underneath the channel is the base, which is held at V_{ss} via the substrate resistance R_{sub} . If R_{sub} is large, as in the case of a short channel, the injected hole current from impact ionization may cause a significant voltage drop over R_{sub} , thus increasing the voltage at the base of the parasitic NPN. This causes an additional current from source to drain underneath the actual channel, which generates additional

¹ This depends on their mobility, which is higher for electrons, leaving them more distance to travel in the field and pick up kinetic energy, which is why this effect is more significant for NMOS transistors.

secondary electron-hole pairs. As with avalanche amplification, the differential resistance turns negative, and breakdown occurs.

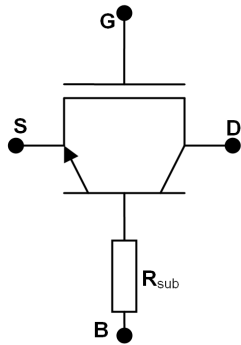


Fig. 2.1: Equivalent circuit of an NMOS with its parasitic NPN and the substrate resistance between the NPN and the substrate contact.

2.2.2.3 Drain-induced Barrier Lowering (DIBL) and Punchthrough

With decreasing channel length, the maximum voltage between drain and source must be considered even if the electrical field is not strong enough for avalanche breakdown. Obviously, the drain-source voltage of an open MOSFET cannot be increased indefinitely. As the reverse-bias voltage along the drain is increased, the depletion region at the drain-body p-n junction grows under the gate towards the source. This decreases the effective channel length, and increases the junction charge at the p-n junction. As a result, the potential barrier between the source and the channel, and with it V_{th} , decreases. Finally, the gate fails to adequately control the drain-source subthreshold current, and *punchthrough* occurs [TRO79].

This effect forces process engineers to increase doping levels in low-voltage deep submicron technologies, since the gate length must always be large compared to the depletion zone (which decreases with increased doping).

It depends on the parameters whether HCE or DIBL is the limiting effect for the operating voltage of a given process. While, for example, a thick gate oxide is desirable to minimize HCE, it increases the risk of DIBL; and if bulk doping is increased in order to reduce DIBL, HCE become the voltage limiting effect.

2.2.3 HV-CMOS Solutions

2.2.3.1 HV-CMOS Structures

In order to prevent gate-oxide breakdown while still allowing to control HV by LV, the voltage drop across the gate oxide must be limited, ideally to the same voltage as in LV transistors. This needs to be guaranteed for both the digital on- and off-states and transitions, and also for analog states if the device is to be used to generate an analog signal. The usual way to achieve this requires giving up the drain-source symmetry common in LV transistors. For example, such an HV transistor could be specified for V_{DS} and V_{GD} of up to 100 V, but a V_{GS} of only 7 V, and the bulk might be tied to the source voltage.

Looking only at the source and the part of the gate near the source, such a device might look just like an LV MOSFET. On the drain side, however, the effects of the high voltage need to be countered by introducing additional structures.

In the “on” state of the transistor, avalanche effects and snapback breakdown need to be prevented. An established way of achieving this is the introduction of a *lightly doped drain (LDD)*. This describes an extension of the strongly doped diffusion region on the drain side with a weakly doped area towards the channel. At given LDD doping levels, the higher the voltages that need to be handled, the greater the size of the LDD. The lower doping decreases the field gradients at the pn-interface, and thus increases the maximum allowed voltage above which impact ionization occurs. In some HV processes, the LDD may be larger than the minimum gate length (more than 10 μm wide). In contrast, many modern deep submicron processes use an LDD that is small compared to the minimum gate length, whereby both sides of the gate receive this doping in order to preserve device symmetry.

Additional measures taken for HV transistors may include field plates that shape the electrical field near the surface to prevent surface breakdown (for example, the gate may be extended on top of the field oxide on the drain side of the DMOS) and limiting of the device to a fixed channel length in order to prevent failure due to DIBL. Furthermore, closed diffusion guard rings surrounding the entire HV device may be required as bulk contacts to decrease R_{sub} and prevent snapback breakdown.

Several structures, called *DMOS (double-diffused metal-oxide semiconductor)* because their drain features two diffusion regions of different doping level, have been developed to counter the voltage limiting effects described above. Two structures can be distinguished as follows:

- In *vertical DMOS* structures, source and gate are on the active surface of the die, while the drain is below it. In practice, the drain may be equivalent to the bulk and connected from the back of the die. Alternatively, a strongly doped area buried within the silicon may be introduced for devices that need to have their drains contacted individually.
- A *lateral DMOS*, in contrast, is more similar in structure to a conventional MOSFET, even though drain and source usually are not symmetrical.

Both kinds of structures can be found in dedicated HV or extended LV processes; most discrete HV transistors use vertical structures, while many extended LV processes offer lateral DMOS structures, also because (except for SOI processes), combining vertical HV-NMOS and HV-PMOS transistors each with a buried drain in one process is not practical.

Vertical DMOS structures

In the simplest vertical DMOS transistors, as shown in fig. 2.2 for an HV-NMOS, source and drain contacts are on different sides of the die. The weakly n-doped bulk forms the LDD, strong n-doping and metallization from the backside are the drain contact, and a weakly p-doped well around the strongly n-doped source is used for the channel. In fact, half the structure in the figure would retain its function. Circular, square or finger structures, however, allow maximizing current density. Placing the gate in a V-shaped groove between the source diffusion regions turns the device into a VMOS structure – a technology widely used for discrete MOS power devices with maximized current density.

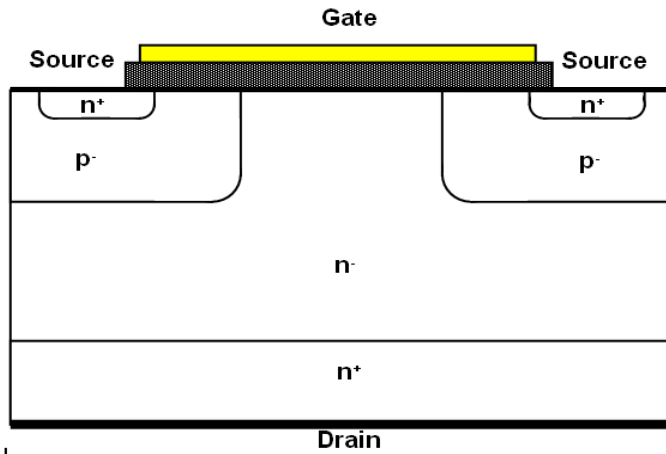


Fig. 2.2: Vertical NDMOS (for discrete devices). This structure can be created on an n^- -wafer by doping and metalizing on both sides.

If a vertical DMOS is to be used in an HV-ASIC process, the drain has to be connected to the surface of the die. This can be achieved by placing the strongly n -doped drain area not on the backside of the die, but rather in a *buried layer* underneath the n^- -channel silicon as shown in fig. 2.3.

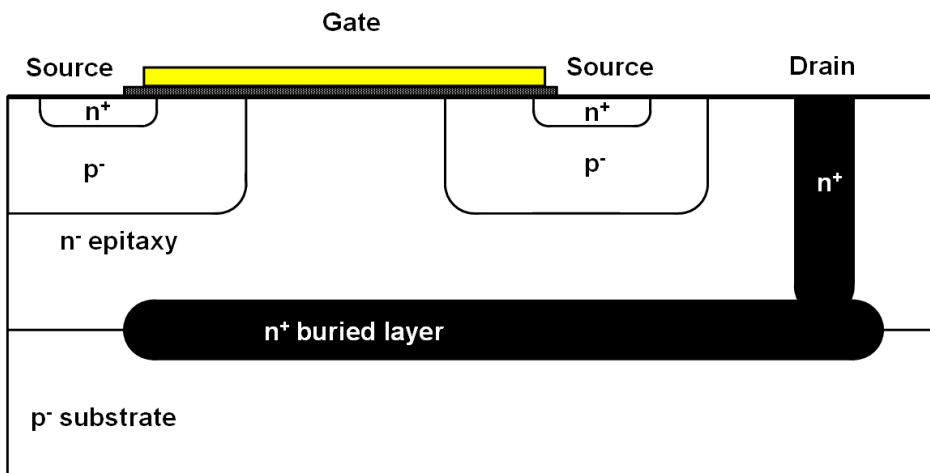


Fig. 2.3: Vertical NDMOS with buried layer and sinker (black) contacting the drain of the device from the surface of the die.

Creating a strongly doped layer underneath weaker doping regions is complicated, as it would require precise counter-doping of a layer, to a precision several orders of magnitude higher than in the first doping. Consecutive dopings of the same area must therefore each be stronger than the previous one. Instead, the highly doped layer is created on the surface of the wafer, and then this layer is buried by epitaxial growth of a weakly doped *epitaxy layer* over the whole surface of the wafer. Well and diffusion areas are then doped into this epitaxy layer in later process steps.

Lateral DMOS structures

The structure of a lateral DMOS is more similar to that of a conventional MOSFET insofar that drain and source are both on the same side of the die and that current flows in parallel to the surface (except for parasitic currents). These devices, as shown in fig. 2.4, also feature a

lightly doped drain region. Additionally, the gate is extended in order to form a field plate, increasing the depletion zone area and smoothing its curvature in order to prevent surface breakdown. As in the vertical DMOS, the p-doped channel area surrounds the source. It is usually tied to source potential.

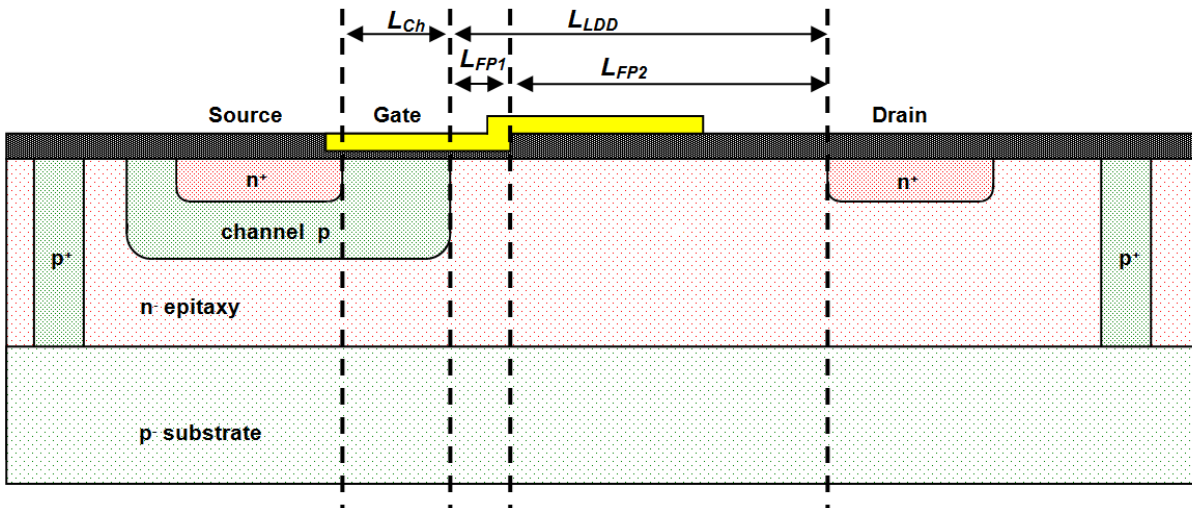


Fig. 2.4: Lateral n-channel DMOS structure. L_{Ch} denotes the channel length, L_{LDD} the length of the lightly doped drain. L_{FP1} and L_{FP2} denote the lengths of the two parts of the gate poly used as field plate on gate oxide and field oxide, respectively. In a variant of this structure, the p-doped region around the source is extended down to the substrate and merged to the left p^+ sinker (which is used to isolate the device) to reduce the area. In that case the source has to be connected to substrate potential, which limits the range of applications.

The DMOS can be divided into three devices connected in series, as shown in fig. 2.5: One dominant MOSFET, similar to a low voltage transistor, with L_{Ch} , one or two MOSFETs formed by the gate extension acting as field plates (the part of the gate with LDD underneath) also called *channel end MOSFET*, and a resistor formed by the LDD. In addition, depending on the actual implementation, parasitic diodes and resistors, e.g. to the substrate, may have to be taken into account. Detailed calculations of dimensions and real implementations of lateral DMOS structures can be found in [BAL99].

Inter-device-isolation

Breakdown is not only an issue within the individual HV transistors, but can also occur between HV transistors adjacent to each other or HV transistors and adjacent LV devices. While in low voltage processes it is often sufficient to require a certain small minimum spacing between diffusion areas on different voltages and to create thick field oxide from the silicon substrate there by *local controlled oxidation of silicon (LOCOS)*, much greater spacing is required in HV devices in order to keep the electrical field below the critical value. Introducing a *guard ring*, a ring of well-contacted strongly doped silicon absorbing all stray charge carriers and isolating the well of the HV device by a strongly doped reverse-biased diode junction may also be required.

Perfect isolation of individual devices can obviously be achieved by placing them on different patches of silicon on an isolating substrate as in silicon on insulator (SOI) technologies. This technique, however, is impractical for highly integrated HV-LV processes, but lateral dielectric isolation still is an option. In *shallow trench isolation (STI)* or *deep trench isolation (DTI)*, a trench is etched into the silicon substrate between two devices. In the case of DTI, it

is etched deeper than the deepest wells of the HV devices, while for STI it is only etched into the wells, but deeper than the diffusion zones. It is then filled up with an isolating material (such as SiO_2). If such trenches are small enough, spacing between devices can be greatly reduced [KAL94]. STI is also used in modern deep submicron processes to reduce inter-transistor leakage current.

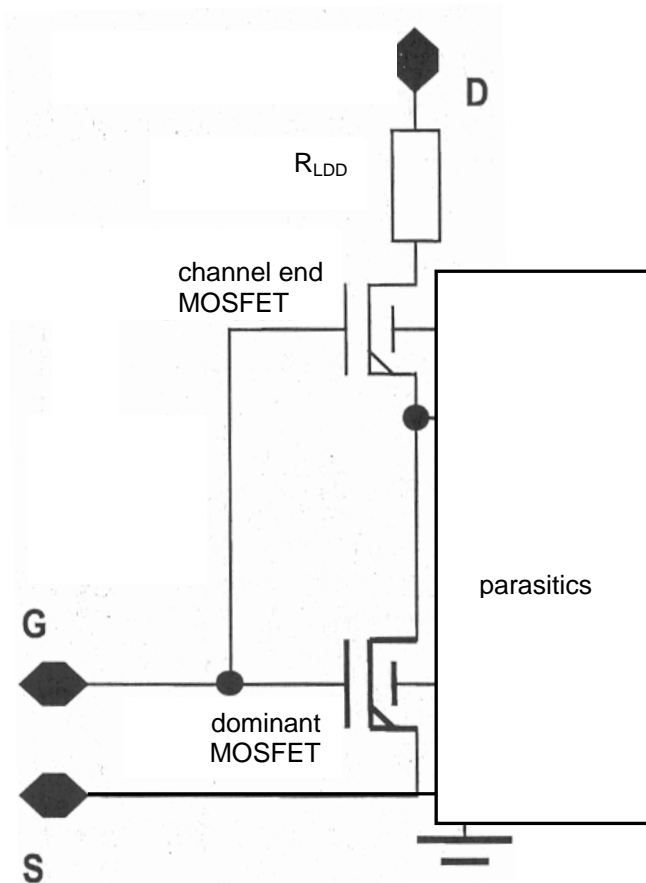


Fig. 2.5: Generalized schematic of the lateral NDMOS. This composition may also be used for circuit simulation (Modified from (KOE05, AMI)).

2.2.3.2. HV Interconnect

In general, interconnect on CMOS chips may be capable of handling much higher voltages than the operating voltage of the process before the oxide between different metal tracks breaks down. The oxide between metal tracks may be less perfect than the gate oxide, but usually it is about one hundred times thicker even at the weakest spots. Assuming a breakdown voltage of silicon oxide E_{BD} of roughly 1 MV/cm for low-quality oxide at a minimum distance of approximately $d = 0.5 \mu\text{m}$ minimum oxide thickness, we get $V_{max} = E_{BD} \cdot d = 5 \text{ kV}$, which is much higher than the HV operating voltages of the processes considered here.

However, metal tracks on high voltage still need special care because of possible interactions with the silicon. Fig. 2.6 shows the similarities between an HV track on the lowest metal layer and a low voltage MOSFET. In the worst case, a metal track at a high positive voltage runs over a weakly-doped p-area between two strongly-doped n-areas at different potentials. In this

case, the electric field can still be strong enough, even underneath the thick field oxide, to cause inversion and formation of a channel between the two n-doped areas, and a parasitic current may flow between them, possibly even creating a short circuit.

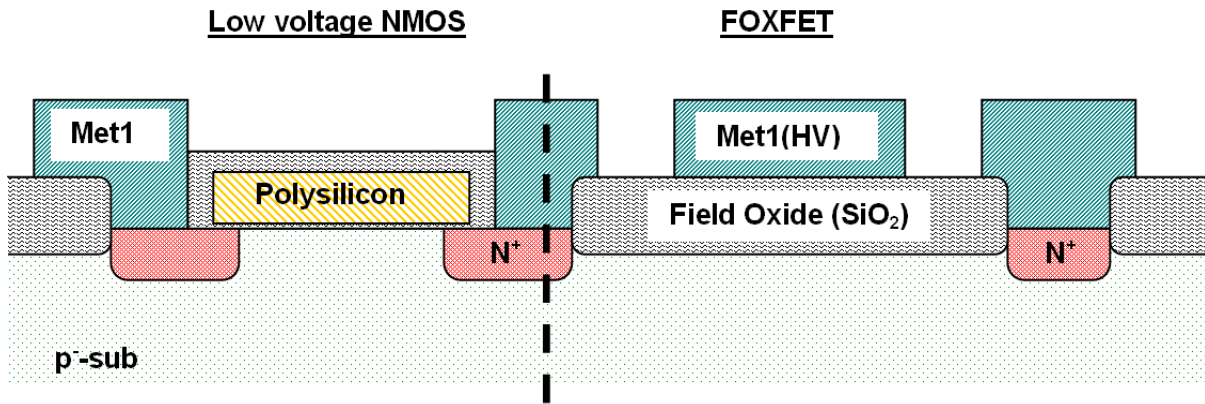


Fig. 2.6: Comparison between a FOXFET structure (right) and a standard low voltage MOSFET (left). The strongly negatively doped regions from other structures (i.e. low voltage MOSFETs) on both sides of the HV track form drain and source, the metal layer under high voltage is the gate of this parasitic transistor.

From the designer's point of view, there are several possibilities to avoid FOXFETs:

- The design kit and design software could provide checking for FOXFETs, but this is usually difficult to achieve and therefore not always implemented. However, a warning that marks all tracks leaving designated HV areas and entering LV areas for manual checking is very easy to generate and may be implemented in the design kit to aid the designer in manual verification.
- It is common practice to keep the HV and the LV areas of a circuit well-separated on the floorplan level. Routing of HV into or through LV areas is minimized or avoided altogether. However, cases where e.g. HV signals are run over a voltage divider and fed into LV circuitry must still be checked by hand. In addition, exotic designs e.g. with numerous HV outputs may prevent the separation of HV and LV parts due to prohibitive space requirements of interconnect.
- FOXFETs can be prevented on the physical level by breaking up the FOXFET structure. The voltage required at the FOXFET gate is increased if metal tracks farther away from the substrate are used for HV routing. If additional grounded (or LV) metal or polysilicon tracks are placed between the HV metal and the substrate, they shield the substrate completely from the electric field of the HV. Additionally, as strongly doped silicon requires higher "gate" voltages to deplete, introducing diffusion (like in a substrate contact) in the wells underneath the HV tracks increases the FOXFET's V_{th} to values that may be beyond the high voltage used in the process or design.

2.2.4 Commercially Available Dedicated HV Processes and Extended LV Processes

Semiconductor technology is mature, and despite high initial investments required for a production line, dozens of companies run general or niche processes, for internal use or making them available to external customers. Several companies also provide HV solutions, based on the techniques described in 2.2.3.

For academic or small and medium enterprise users of foundry services in the European Union, processes provided through the EU-supported Europractice consortium offer several advantages, e.g. easy access and low-cost low-volume prototyping [EUR]. Through Europractice, HV processes from two semiconductor foundries are available, and the key features of these and other HV processes will be highlighted below as examples of the state-of-the-art. A summary of process features is given in tab. 2.1.

- ON Semiconductor offers a family of processes originally developed by the company AMI Semiconductor (AMIS), which they now own [AMI]. These analog LV processes of various feature sizes have been extended with dedicated structures to gain full HV capability. These processes offer voltages up to 100 V controlled by a 5 V gate voltage and up to 5 metallization layers. The I3T50 process also enables reduced spacing between HV transistors by using DTI. A 100 V-capable 0.18 μm process is under development by ON Semi.
- austriamicrosystems also offers two HV process families, with the H35 family offering DTI-insulated 50 V transistors both for 5 V gate voltage and 20 V HV-capable gates to directly apply higher voltages to a transistor without need for a resistive voltage divider.
- X-fab, while not available via Europractice, is another provider of numerous mixed-signal HV processes from 1.0 μm to 0.18 μm feature size. Some of them are also optoelectronic processes with dedicated and characterized photo diode structures, while the 1 μm process is also available with MEMS extensions.

Process	Feature size [μm]	LV V_{DS} [V]	HV V_{DS} [V]	HV V_{GS} [V]	# of metal layers	Isolation
AMIS						
I2T100	0.7	5	30, 60, 100	5	2 - 3	LOCOS
I3T80	0.35	3.3 / 5	80	5	3 - 5	LOCOS
I3T50	0.35	3.3 / 5	50	5	3 - 5	DTI
I4T100 (upcoming)	0.18	up to 3.3	up to 100	3.3 ?	4 - 6 ?	DTI
austriamicrosystems						
CXZ	0.8	5	50	5 / 20	2	LOCOS
H35	0.35	3.3 / 5	50	5 / 20	3 - 4	DTI
X-FAB						
XC10 (opto, MEMS)	1.0	1.5 / 5	40, (80)	5	1 - 3	LOCOS
CX08 (opto)	0.8	3.3 / 5	50, 80	5	2 - 3	LOCOS
XC06 (opto)	0.6	3.3 / 5	16, 60, 100	5 / 18	2 - 3	LOCOS
XH035, XA035	0.35	3.3 / 5	14, 18, 45	3.3 / 18	2 - 4	LOCOS
XH018 (opto)	0.18	1.8 / 3.3	10, 40	3.3 / 10 / 18	5 - 6	STI

Tab. 2.1: Simplified overview of some HV processes [EUR, AMI, AMS, XFA]. Not all V_{DS} - V_{GS} combinations are available. Voltages in brackets are available for NMOS only.

Alternatively, *silicon on insulator* processes offer even higher voltages up to several hundred volts [XFA], at the drawback of higher cost per wafer and lower integration density due to the more complex process of fabricating semiconductor islands on a nonconductive wafer or creating a buried oxide layer inside a silicon wafer.

2.3 CMOS Photosensors

2.3.1 Physical Introduction

Semiconductor junctions can, besides their use in electronic devices, be used as photo detectors converting an optical signal into an electric current. Depending on the wavelength, visible light penetrates, on average, between 0.1 and 10 μm into silicon until it is absorbed (fig. 2.7). If the energy of the photon is larger than the bandgap (1.12 eV at 300 K for silicon¹), it may generate an electron-hole-pair. If this electron-hole-pair is generated within a reverse-biased diode junction, the electron and hole are separated in the electric field, and a *photocurrent* flows. Both in optical sensors such as CCD- or CMOS-cameras (highlighted in 2.3.2) and in energy converters such as solar cells, photocurrents in semiconductors have found widespread application. However, incident light can also cause parasitic effects in semiconductor circuits if no adequate precautions are taken (see 2.3.3) [SZE07].

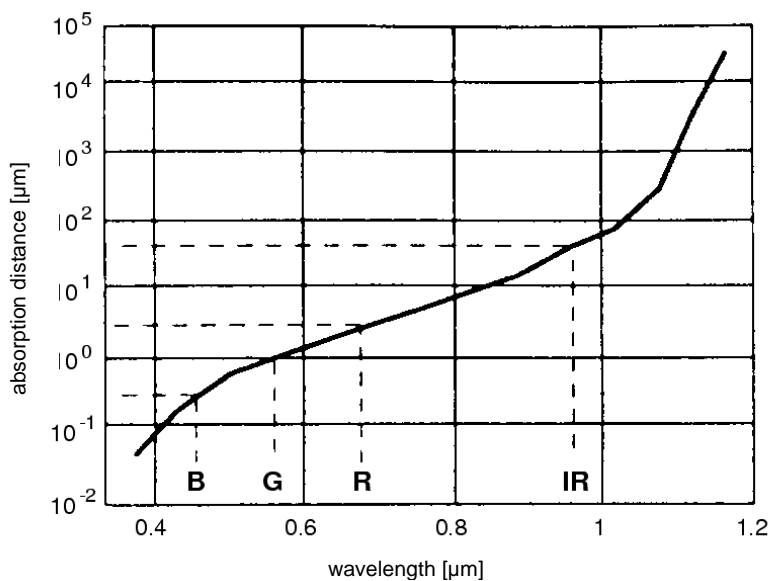


Fig. 2.7: Spectral *attenuation length* (distance in the medium at which the photon intensity has dropped to $1/e$ of the incident value) in silicon at temperature 300K. Wavelengths for blue, green, red and infrared are marked (Modified from [DAS55]).

2.3.2 CMOS Photosensor Devices

2.3.2.1 Characteristics of Photosensor Devices

Two types of silicon photosensor technology platforms exist: specialized *CCD* (*charge-coupled device*) processes and CMOS-based processes. Since CCD sensors require dedicated chips and usually are not co-integrated in a CMOS process, only CMOS photosensor devices will be considered here. The three standard photosensitive devices available in CMOS processes, the *photodiode*, the *phototransistor* and the *photogate*, are described below.

¹This is equivalent to about 1100 nm wavelength, or near infrared light. For infrared cameras, materials with a lower bandgap, such as germanium (0.67 eV at 300 K), must be used.

In the context of this thesis, response time of the photosensitive device is of minor significance. Spectral quantum efficiency is more important in this context, as fluorescent labeling provides rather low light intensities. The spectral quantum efficiency $Q(\lambda)$ is defined as

$$Q(\lambda) = \frac{n_q}{n_{phot}(\lambda)} \quad (\text{Eq. 2.1})$$

with

$n_{phot}(\lambda)$ = number of incident photons at wavelength λ

n_q = number of measureable charges created.

One prerequisite for high quantum efficiency is a large volume in which absorbed photons can be measured, while another requirement, depending on the wavelength, is an acceptable depth of the absorptive device within the semiconductor.

2.3.2.2 Photodiodes

Charge carriers that are created within the depletion layer in a reverse-biased semiconductor junction are separated in the electric field, creating a *photocurrent*. If fast reaction times are desired, the depletion region must be thin to reduce transit time, while highly sensitive devices require large depletion layers to absorb a greater percentage of the incident photons. The output of this device is just the photocurrent. If the light intensity is low, this current must be amplified before it can be read out. The photocurrent can also be accumulated on the junction capacitance for read-out using an integrating charge amplifier.

In principle, any semiconductor junction available in a given process could be used as a photodiode. Because of

$$d = \sqrt{\frac{2\epsilon_{Si}\epsilon_0}{e}(V_{ext} - V_{barrier})\left(\frac{1}{N_A} + \frac{1}{N_D}\right)}$$

with

d = thickness of the barrier

N_A = acceptor doping density

N_D = donator doping density

ϵ_{Si} = specific dielectric constant of the semiconductor material

ϵ_0 = dielectric constant

e = elementary charge

V_{ext} = external voltage

$V_{barrier}$ = barrier potential,

and the barrier potential given by

$$V_{barrier} = \frac{k_B T}{e} \ln\left(\frac{N_A N_D}{n_i^2}\right) \quad (\text{Eq. 2.3})$$

with

n_i = intrinsic charge carrier density of silicon¹

k_B = Boltzmann's constant

T = temperature of the semiconductor material,

in order to obtain a thick depletion layer for devices with high quantum efficiency, low doping and high reverse-bias voltage are desirable.

It should be noted that in addition to charge carriers created in the depletion zone itself, charge carriers created around the depletion layer diffusing into the depletion zone may also contribute to both signal and noise.

In single-well CMOS processes, three semiconductor junctions are available as photodiodes:

- the junction of n^+ -diffusion to p^- -substrate,
- the p^+ -diffusion to n^- -well junction,
- the junction of n^- -well to p^- -substrate,

or vice versa for a p-well process. Processes offering additional doping regions, such as *BiCMOS*² or HV processes, offer additional junctions that may be used as photodiodes.

The *avalanche photodiode* is a variant of the photodiode operated at high reverse-biased voltages. The avalanche effect is used in order to achieve high-gain amplification within the device. These devices may be used within specialized silicon detectors, but are not suitable for direct integration into a standard CMOS process on the same die. A detailed description of this device can be found in [SZE07].

2.3.2.3 Phototransistors

A phototransistor is, in principle, a bipolar NPN or PNP transistor with its base left unconnected. Instead of an external base current controlling the emitter-collector current, the photo current created in the base by the incident light is used. In comparison to a standard bipolar transistor, the base-collector junction, which is the light-sensitive part of the transistor, is enlarged (fig. 2.8). In an equivalent circuit, the light-sensitive effect can be modeled by a capacitance and a photodiode, in parallel, between collector and base. The output of the device is the collector current, which is the photocurrent times the β of the transistor.

Advantages of the phototransistor compared to photodiode are easier manufacturability especially for discrete devices, and the integrated amplification by the internal transistor action, allowing for gains of up to a few hundred, or even several thousand for heterojunctions (usually not available in CMOS processes). Its disadvantages include the nonlinearity of the gain with light intensity and the dark current being amplified by the transistor action as well. In addition, it tends to take up more space than a comparable photodiode in a CMOS process, and does not provide the freedom of choice for the junction used for photosensing as compared to the photodiode. Therefore, highly integrated CMOS light sensors such as digital cameras use a photodiode in combination with a MOSFET preamplifier instead of a phototransistor [SZE07].

¹ *Phonons* (lattice vibrations) at sufficient energy create free pairs of charge carriers in a semiconductor, contributing to the intrinsic charge carrier density n_i . As phonon energy is temperature dependent, so is n_i .

² BiCMOS processes offer additional doping layers that enable the use of optimized PNP and NPN transistors.

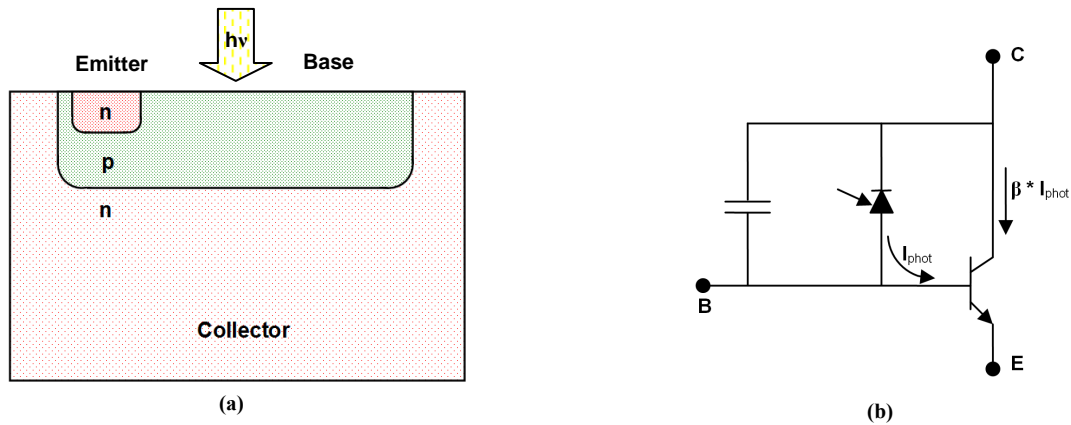


Fig. 2.8: (a): physical structure of an NPN-phototransistor. (b): equivalent circuit diagram.

2.3.2.4 Photogate

Of all CMOS photosensor structures, the photogate is the most similar to the CCD. Like the CCD, the photogate accumulates charges over a defined area for each pixel. Fig. 2.9 shows the structure of the photogate. A gate like that of a MOSFET is placed over weakly doped silicon (i.e. substrate), so that the gate voltage can deplete the silicon underneath. This area is contacted by a floating diffusion region of opposed doping, which forms a potential well for charges generated in the depletion region, which thus are collected there (in n-doped diffusion, electrons are collected while holes move to the substrate, and vice versa for p-doped diffusion). The output of a photogate is the accumulated charge over the integration time. Read-out may be achieved through a source follower connected to this diffusion region, converting the charge to a voltage signal. A reset transistor can be used to flush out accumulated charges for a new measurement.

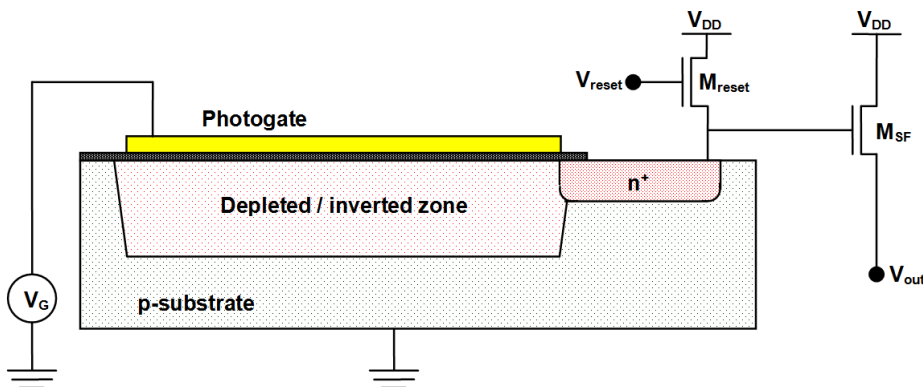


Fig. 2.9: The photogate structure. By biasing the gate, the silicon underneath it is depleted or inverted. The strongly doped region next to the photogate creates an electrical field in parallel to the gate. In this field, the electrons are attracted and accumulated there, while holes are drawn to ground. In this example, the accumulated charge converted to a voltage signal by the source follower M_{SF} and can be removed via M_{reset} . Note that the inverted zone does not differ in doping from the p-substrate; the inversion is only caused by the electric field of the photogate.

Even though the gate absorbs some of the incident light, especially in the blue part of the visible spectrum, quantum efficiencies of up to 40 % between 500 and 600 nm have been reported in standard CMOS processes. While it is slower than comparable photodiodes due to the lateral diffusion, its lower capacitance results in lower thermal noise. [LOE01, LUL00]

2.3.3 Parasitic Effects

2.3.3.1 Parasitic Effects of Light on MOSFETs

Most integrated circuits are *packaged* in some way suitable to their application. Often, the silicon die is encapsulated in a protective case that allows easy handling. It can be installed into a *socket* or soldered directly onto the PCB. Alternatively, the die can be glued and bonded directly onto the PCB. In that case, it is usually protected by *glob-top*¹. Glob-top is usually not transparent and standard chip packages are intended to completely cover the chip (special packages allowing optical interaction exist). Therefore, for chips without optical function, the designers usually need not consider the effects of charges generated by incident light on his chip.

However, dedicated optical chips such as camera chips need to receive light and therefore cannot be completely covered. In this case, parasitic interactions of charges generated by photons with the analog parts of the design, especially with the parasitic diodes between the transistors of the preamplifiers of the photosensors, need to be minimized by other means (e.g. metal shielding) or have to taken into account.

2.3.3.2 Passivation, Oxide and Metal Effects

In standard CMOS processes, several layers of metal interconnect with oxide insulation and the *passivation*² cover the semiconductor structures. Therefore, all light that is to reach the semiconductor devices of the chip must first traverse these layers. Both SiO₂ and Si₃N₄ are transparent to visible light in the form as they are used on microchips allowing this interaction in principle, while metallization in the path of incident light would prevent it. However, as their dielectric constants (3.9 for SiO₂, 7.5 for Si₃N₄) differ from each other and from that of crystalline silicon (11.9), reflection at the interfaces may reduce efficiency. [SZE07-1]

Metal interconnect tracks, being conductors, reflect practically all visible light on their surface. Therefore, interconnect must not be routed on top of the photosensitive structures if good detection efficiency is to be achieved. Conversely, the metal layers can be used to shield sensitive analog devices from incident light, thus reducing parasitic effects. A decrease of intensity of about two orders of magnitude can be achieved by using metal layers in this way [LOO96].

¹ Glob-top is the name for a kind of specialized epoxy glues. These are dripped onto a chip that is directly glued and bonded onto a PCB to cover the chip, the bond wires and the contacts on the PCB. After hardening, it provides protection from mechanical, chemical and electrical damage.

² A top layer of chemically inert and mechanically resistant insulator, usually silicon nitride, is used to cover the top metal layer in many CMOS processes. This is called the chip's passivation layer.

3. Microparticle Technology and Particle Transfer

3.1 Introduction

As the volume of a liquid droplet decreases, its surface-to-volume ratio increases, and so does its relative evaporation. Very small droplets of liquid may evaporate quickly, making transport of liquids in sub-nanoliter amounts difficult. Solutes that remain after evaporation may clog pipes or nozzles. In addition, liquids on surfaces may spread in undesirable ways unless guided. Therefore, in some applications, liquid droplets have been replaced by solid particles as the medium to transport material. *Particle science* and *particle technology* or *process technology of disperse substances* [STI09, STI97] cover the handling of particles in fluids. Gas filtration, as required in cleanrooms or particle filters for combustion engines, and gathering of disperse materials, such as cement or flour after production, are possible applications of particle technology. In the framework of the project as a part of which this thesis was written, particles have been loaded with amino acids for particle-based peptide synthesis. This concept is described in 3.2.

Laser printing may be one of the most widely-known applications of particles as a means of transport of functional molecules onto arbitrarily configurable locations on solid supports. In laser printing, *chromophores* (dye molecules) are immobilized within a solid *matrix* from which particles in a size range of about one to ten micrometers in diameter are formed. The particles are transported using electrostatic forces, with light being used to create an electric charge pattern on a revolving drum used for transfer from the particle reservoir to the target support. In 3.3, a system for peptide synthesis based on a laser printer is described.

3.4 and 3.5 highlight some of the properties of particles, especially of the laser printer toner and amino acid toner particles used in this work, with special attention on triboelectric charging. 3.4 describes particle manufacture and physical properties, while 3.5 remarks on their triboelectric chargeability.

3.6 elaborates on forces acting upon charged particles. Starting from general physical laws found in the literature, the special case of deposition of charged particles in settings like the ones used in this thesis is investigated. In 3.7 to 3.9, methods of spatially selective particle transfer that have been used previously are presented, namely direct (contact or near-contact) transfer, desorption of particles from a surface and adsorption of particles onto a surface are outlined.

3.2 Particle-Based Peptide Synthesis

Based on the requirements from 1.2.1, the possible benefits and challenges in replacing liquid droplets as “package” for the transport of amino acids to supports in array synthesis by particles are the following:

- In maximizing spot density, particles are extremely promising insofar that no evaporation in transit occurs and that no spreading can occur before melting if contamination-free

transfer is achieved. Even during melting, the risk for spreading can be reduced if a matrix (or “*solid solvent*”) is used that can be, upon heating for coupling, turned into a high-viscosity gel-like state instead of a low-viscosity liquid. This is the main motivation for the use of particles, and while particles may be more laborious to produce than amino acid solutions, the reduction in spot size should outweigh this effort, resulting in arrays that are less costly per sort of peptide synthesized.

- In order to match (or even improve upon) maximum possible peptide chain length achieved using liquids, the synthesis chemistry in the “solid solvent” must be investigated and optimized, as it was done for the conventional solid phase synthesis.
- If the particles are homogeneously loaded and homogeneously deposited on the synthesis loci, and the residues of the matrix thoroughly washed off, detection of binding events should be independent of whether the peptides were manufactured from particles or from solution.
- Handling and usability of the array during manufacture depends on the actual method that is used to deposit the particles, and will be considered separately below for different methods of particle transfer. As one special challenge, in all cases where *fine particles* that is particles of a diameter of less than 10 μm are used, it is essential to prevent them from becoming airborne outside the synthesis machine for health reasons [BRU05].
- Particles may *agglomerate* (be deformed and stick to each other upon contact), be adsorbed to surfaces or become electrically charged upon contact with other materials. These properties have to be considered in their handling, adapting the existing solutions from particle technology or devising new ones.

3.3 Peptide Laser Printing

3.3.1 Motivation

The straightforward approach to particle based peptide synthesis is to use technology that is already well-established in other applications as much as possible. Following this thought, a *peptide laser printer* based on a commercial printer has been built at DKFZ and peptide arrays printed using this machine are now commercially available through the start-up company PepPerPrint [STA08, PET09].

3.3.2 Laser and LED Printers

Laser printers make use of materials that become conductive upon exposure to light (for example *organic photoconductors*, or *OPCs*), charged particles containing dye molecules, and a system of transport mechanisms in order to obtain dye pattern on a solid support like paper (fig. 3.1). In a *cartridge*, the chargeable particles are stored, until picked up by the *transport drum*. A *charge drum* may be used to charge the particles *triboelectrically* (by friction). Selectivity of transport is ensured by the *image drum* or *OPC drum*. To achieve this, the image drum is built as a grounded conductor covered with a sheet of a material (e.g. the OPC) that is an electric insulator while in the dark, but locally becomes a conductor in the direction orthogonal to the drum surface upon exposure to light. The insulating drum surface / OPC is charged, e.g. by a coronary discharge. Thereafter, it is exposed to light in a defined pattern by a laser that scans the surface using a turnable mirror, whereby areas exposed to light are

grounded, while dark areas remain charged. Thereafter, the image drum passes under the transport drum, where the charged areas attract the oppositely charged particles, so that they “jump” to the image drum. The image drum surface next moves over the support (paper, foil, or other material to be printed on), where the toner is passed on again, e.g. by pressing the paper onto the OPC drum. Excess toner is scraped off the image drum and passes into a waste reservoir. The paper moves on and passes the *fuser* or *fixing unit*, where it is heated, releasing and permanently embedding the dye molecules into the support [MAC90].

For color printing, the support is passed through several (usually four) such printing units in sequence, commonly black, yellow, cyan and magenta. These units must be aligned with relation to the support to ensure a good print-out. Alignment may require a test print and configuration by the user or be performed automatically by the printer.

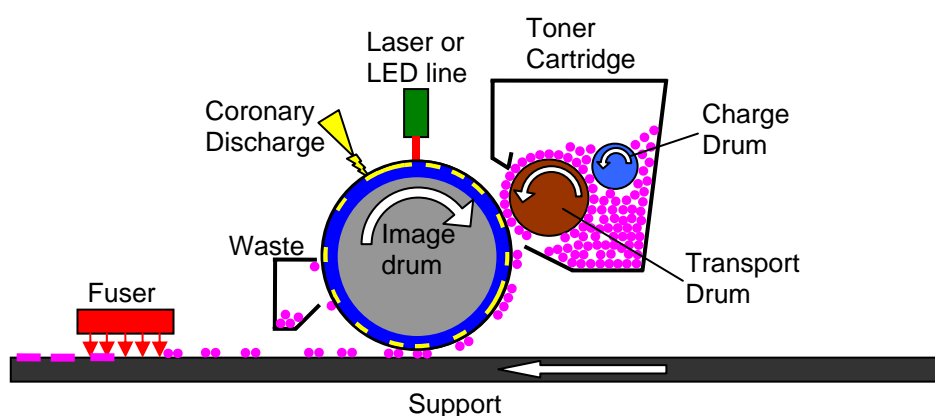


Fig 3.1: Principle of operation for a laser or LED printer. The image drum is completely charged by coronary discharge. A laser or LED selectively discharges the portions of the drum that are illuminated. The charged parts of the image drum pick up toner particles transported out of the cartridge on the transport drum. On the transport drum, the charge drum electrically charges the particles. Under a certain pressure, the toner passes on to the support (e.g. paper) being passed underneath the image drum. Excess toner goes to a waste reservoir before the drum surface is re-charged. A fuser heats the paper and melts the toner particles, releasing the dye into the paper and fixing the printout. Some or all of the drums and the waste bin are usually included in the cartridge, which is replaced or refilled upon depletion of the toner reserves contained therein.

LED printers are printers based on the laser printer concept, but the laser and mirror system is replaced by a line of LEDs that discharge the OPC drum. The high-precision mechanical parts required for moving the mirror are not required using this approach, allowing lower unit cost and greater robustness. However, LED printers are limited in resolution by the maximum density of LEDs that can be achieved. In commonly used language, all printers using toner and OPC drums are called “laser printers”, including LED printers.

1,200 *dpi* (dots per inch = dots per 2.54 cm) are a common value for laser printer “resolution” today, equivalent to about 50 dots per mm, or a theoretical dot size of 20 μm . However, in laser printing, the DPI number is not used to print precision lines, but to mix any color from the four primary colors available by varying the dot ratios. To this end, dots may and do overlap. The maximum density of non-overlapping reproducible color dots therefore is perhaps more than one order of magnitude worse than the DPI value. For the same reason, the alignment of the four color printing units in color printers is usually to a precision significantly worse than 20 μm (see 3.3.3).

3.3.3 The Peptide Laser Printer

In a collaboration between DKFZ and IPA (Fraunhofer Institut für Produktionstechnik und Automatisierung / Institute for Manufacturing Engineering and Automation, Stuttgart), a laser printer that prints particles loaded with amino acids has been designed and built. This printer is based on the OKI C7400 commercial color printer [OKI], but has been expanded from four to twenty toner cartridges, one for each standard amino acid. When calibrated, it achieves reproducible positioning of $\pm 5 \mu\text{m}$. Currently, 160,000 distinct spots on glass plates of $(20 \times 20) \text{ cm}^2$ can be printed, at a density of 400 spots per cm^2 [STA08]. The particles used are described in detail in 3.4.

3.3.4 Limitations of Peptide Laser Printing

Ultimately, the peptide laser printing method is limited in the density of peptide synthesis locations achievable insofar that it is not a *self-aligned* process. As the support is transported underneath each of the 20 or more printing units, each printing unit must be in the same alignment with respect to the support. Additionally, the exact position of the support must be restored for each layer, even with coupling and washing steps in between layers. With decreasing spot size and distance, mechanical precision becomes more and more difficult to achieve. At some point, calibration before printing runs by test prints or calibration for each print using alignment markers on the support becomes necessary. A self-aligned process, for example a method in which each synthesis site actively deposits particles onto itself in a configurable pattern, would not suffer from that limitation.

3.4 Particle Properties and Manufacture

3.4.1 Commercial Laser Printer Toner

The *commercial laser printer toner* used in this thesis is taken from cartridges for the OKI C 7000 series printers (magenta, cyan and black). The particles are of an irregular shape (see also 3.4.2.2). The diameter of these particles averages at about $10 \mu\text{m}$ (fig. 3.2), and their density is approximately $1 \text{ g} / \text{cm}^3$. When not charged triboelectrically, the average particle charge is smaller than $-0.1 \text{ mC} / \text{kg}$. When charged triboelectrically, values of -7 to $-3 \text{ mC} / \text{kg}$ as average charge have been measured using a Faraday cell [NES06]. The Faraday cell setup can only measure the average charge of a large number of particles “sucked in” through a pipe as an aerosol. Therefore, the exact particle charge distribution cannot be determined using this method. In principle, even positively charged particles might be present in such an aerosol. More details on these particles can be found in [NES06, NES08].

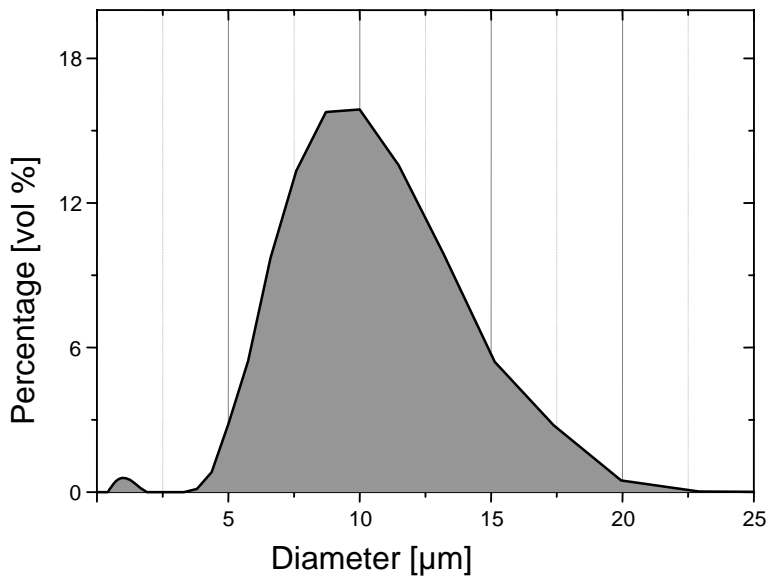


Fig. 3.2: Size distribution of Oki Magenta laser printer toner (taken from [NES06]).

3.4.2 Amino Acid Particles

3.4.2.1 Manufacture and Composition

The *amino acid particles* used in this thesis were manufactured at DKFZ for use both in the peptide laser printer (see 3.3) and for particle transfer onto CMOS chips [BEY05, BEY07, LOE09, BRE10]. Two objectives had to be met in developing these toners: First, the particles must mimic the OKI color printer particles insofar that they can be printed with the peptide laser printer. Second, all components of the particles must be compatible with peptide synthesis, that is they may not interfere with the coupling of the amino acids when the particles melt. The remains of the particles after coupling must be removable by washing with solvents compatible with peptide synthesis. The melting properties of the particles are such that they become a gel of sufficient viscosity for coupling to occur. Small (few μm) gaps between particles should be covered by the melt, but even if a heap several layers of particles high is molten, the melt should not spread farther than few μm to avoid spillover to neighboring spots. A coupling temperature of around $90\text{ }^\circ\text{C}$ has been chosen, as at this temperature the activated amino acids can efficiently couple, but still remain stable, especially regarding racemization (see also A1.2.1) [BRE10].

The particles consist of

- a *resin*,
- a “*solid solvent*”,
- the activated and protected amino acids and
- *charge control agents*.

The resin is used to provide thermal and mechanical stability and to form the bulk of the particles. In a typical mix, polystyrene or SLEC PLT 7547 from Sekisui is used and contributes 60 % of the total particle mass.

The “solid solvent” replaces the solvent used in liquid-based solid-phase synthesis. A molecule similar to the DMF (dimethyl formamide) commonly used as solvent in solid-phase synthesis, but with a melting point around 70 °C, is used here, for example the higher-order analogs DPF (diphenyl formamide) or DPSO (diphenyl sulfoxide) (fig. 3.3), typically at 25 mass percent.

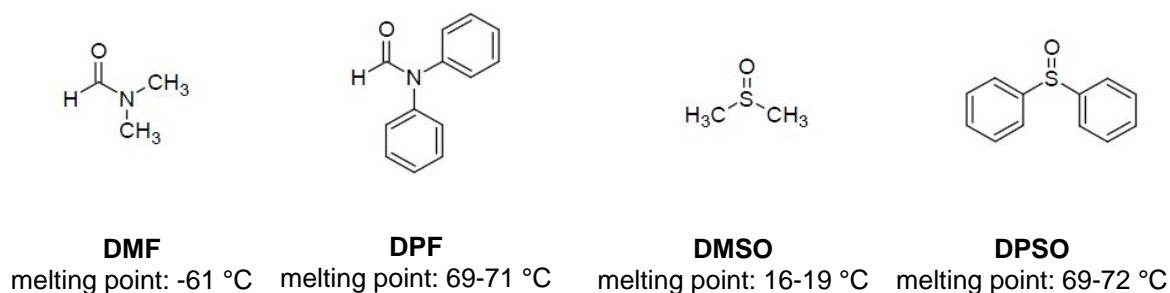


Fig. 3.3: Structures and melting points of solvents from conventional and particle-based peptide synthesis (taken from [BEY05]).

The amino acids are added in a protected and activated form, as Fmoc-Aminoacid-OPfp-esters (see 1.1.2). In standard toner, they take up 10 % of the total particle mass. This means that the molar amino acid load differs depending on the amino acid type. For the standard amino acids, the lowest molar amino acid content is about 59 % that of the amino acid with the highest molar content¹. This must be taken into account when determining the minimum particle density to be deposited on the synthesis site, e.g. by performing these experiments with the histidine particles that have the lowest molar content of amino acids.

Charge control agents are added to the toner in order to stabilize triboelectric charges on the toner, that is to slow down the discharge of the particles in air. In a standard amino acid toner mix, 4 % pyrazolone orange and 1% sodium-di(aqua)-di(2-hydroxy-3-napthoic acido) ferrate(III) are added to the toner mass.

Particles are produced from these constituents by mixing and dissolving in acetone, then removing the acetone by various drying steps. The resulting mass is milled in an air jet mill. During milling, silica nanoparticles (in the standard process 0.05 % of the particle mass) are added as anti-agglomerants. Using sieves and winnowers, the particles can be sorted into fractions of different particle diameter ranges (fig. 3.4).

3.4.2.2 Properties

Typically, a fraction similar to the Oki toner in size distribution (mean diameter 7 µm to 15 µm) is used for the printer, and may also be used with the chip. This fraction is referred to as the *coarse fraction* in the rest of this work. Particles of smaller average diameter, around 5 µm or less, that are too small for use in the printer, have also been used on the CMOS chip, and are referred to as the *fine fraction*. A fraction of even larger particles can also be

¹ While the molecular weight of the heaviest standard amino acid, Tryptophan, is more than twice that of Glycine, the lightest standard amino acid, the relative difference is less for the amino acid derivatives in the particles, including activation and protection groups. For the lightest standard amino acid, Fmoc-Glu-OPfp, the weight is 463.36 g/mol, while for the heaviest standard amino acid with side-chain protecting group, Fmoc-His(Trt)-OPfp, the weight is 785.77 g/mol, for a ratio of 59 / 100.

manufactured, but is not in regular use. As with the Oki toner particles, the amino acid particles are irregularly shaped (fig. 3.4), as it is common for particles created by milling.

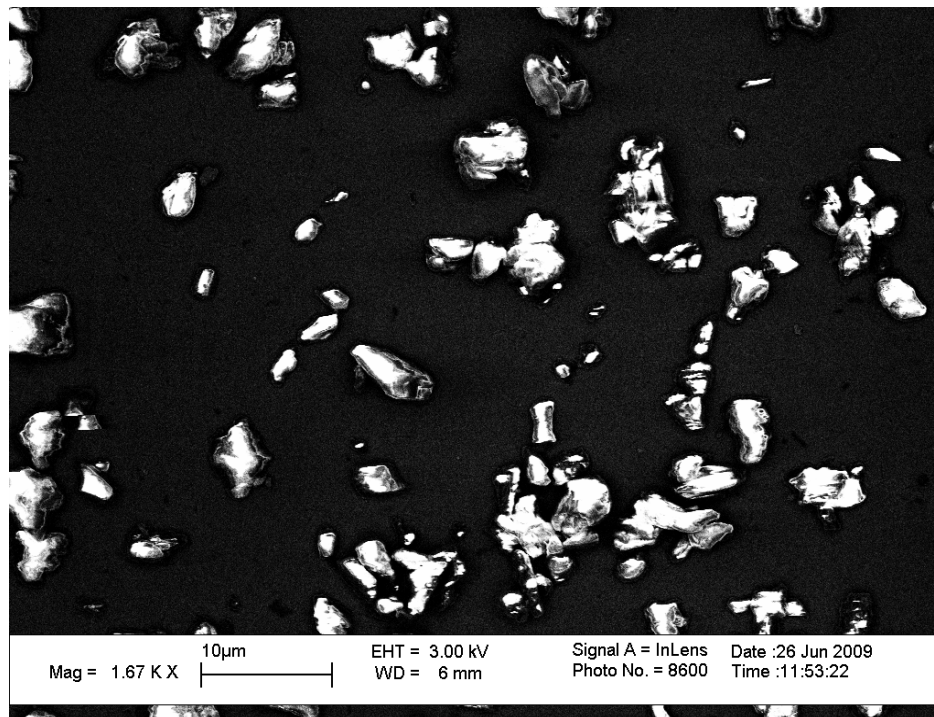


Fig. 3.4: Electron microscopy of amino acid particles (fine fraction, average diameter around 5 μm) on a microchip surface.

One surprising property of amino acid particles deserves to be noted: Embedded in the solid solvent, decay of Fmoc-amino acid-OPfp esters is greatly slowed down in comparison to such molecules stored in solution. At room temperature, for all standard amino acids except Arginine, the decay rates observed are less than 1 % decay per month, while for Fmoc-Arg-OPfp, which is known for rapid decay in solution, the decay rate is about 5 % per month [BEY07].

These low decay rates of the amino acids embedded therein allow long-term storage of the particles before use. Amino acid toner is stored in sealed falcon tubes under dry nitrogen atmosphere refrigerated at 4 °C to further slow down decay of amino acids and particle properties, especially to prevent them from drawing water from the ambient air. To avoid condensation, particles and tubes have to be allowed to heat to room temperature before the tube is opened for the retrieval of particles. Nevertheless, during particle-based chip synthesis, particles have been stored at ambient condition in air within the setup for months, and both transfer and synthesis remained possible (see chapter 7).

Due to the price of the constituents, especially of the activated and protected amino acids, and due to the work effort required for production, minimizing toner consumption is very desirable. Additionally, it should be mentioned that the health hazards associated with fine dust require that the number of particles escaping into the laboratory air is minimized in order to prevent exposure of laboratory personnel.

Some properties of particles depend on their size [STI09]. In general, for smaller particles, with increased surface-volume-ratio,

- tendency to agglomerate increases,
- pourability decreases,
- in an aerosol, drag forces become more relevant compared to mass-dependent forces (the small particles “follow the airstream” more closely, see 3.6.6.2),
- chargeability increases,
- adhesive forces increase, making smaller particles stick to surfaces more intensely, and
- forces due to electric fields become more relevant compared to mass-dependent forces, as particles can reach higher q / m ratios.

3.5 Triboelectric Charging of Particles

3.5.1 Motivation

It is a well-known effect that friction may cause charges to accumulate in objects. While at most times annoying, like the mild electric shock that is sometimes felt when touching a metal object after walking in shoes with insulating soles, this effect can be costly in electronics, where the voltages and charges that can be accumulated in this way may be sufficient to destroy unprotected CMOS gate oxides. However, this effect can be useful to intentionally charge materials, for example particles on the charge drum in the laser printer or in an airstream, by forcing them to move along a surface.

A brief summary on the theory is given in 3.5.2. As a more specialized diploma thesis on triboelectric charging in the context of the peptide chip project is available [LOE09], this chapter will only provide a short summary, both on triboelectric charging methods and on measurement of the charges generated. 3.5.3 describes some methods to measure q / m values of particles, and 3.5.4 investigates the properties of the amino acid particles.

3.5.2 Theory of Triboelectric Charging

Even though known to the ancient Greek, triboelectric charging remains poorly understood today, in spite of being used in numerous industrial applications. As it is a surface effect, disperse matter with large surface-volume ratios may be strongly affected by it. One or both of the materials used must be insulators or at least insulated from each other and a common ground, or any charge accumulated would immediately be grounded. Generally, for charging to occur, electrons or ions are transferred between the two materials between which there is friction. Therefore, it is ultimately the quantum mechanics of surfaces of solids that govern triboelectric charging. Thin films of moisture or other contaminations of either surface contribute to the difficulties in real applications, as do uncertainties on how the medium (i.e. air) contributes to the process.

For practical applications, use of empiric formulae may be more feasible than ab initio quantum mechanical considerations. One example is the *triboelectric series*, which is a tool for approximations of the behavior of two materials in contact.

The triboelectric series is somewhat similar to the series of *electron work functions* of metals (conductors and semiconductors), in which the metals are ordered by the work required to remove an electron from the *electron gas* in the metal. They can be used to calculate a *contact potential*, that is a voltage that occurs at a contact between two metals or a metal and a semiconductor, as in a Schottky diode. The metals are thus ordered by their work functions (in eV), and this order allows to predict which material will donate or accept electrons in a given junction. Similarly, the triboelectric series orders materials by their tendency to become positively charged upon contact with another material. A material will become positively charged when in contact with a material “more negative” in the series. However, as even objects of the same material can become charged when moved along one another, this model is clearly insufficient. Furthermore, it allows no good prediction on how strongly each material is charged. Moisture on the objects and in the air, contaminations and temperature, which may also influence the results, are not considered in this table, either.

An upper limit to triboelectric charging in air or other gases can be approximated based on the fact that charged materials rapidly lose their charge by ionizing the gas if the electric field exceeds a critical value ($E_{crit} \approx 3 \text{ MV/m}$ for air under standard conditions, depending on humidity). The maximum surface charge σ_{max} of an isolator is independent of the curvature of the surface in theory because of Gauss’ law, with $\sigma_{max} = E_{crit} \cdot \epsilon_0 \approx 27 \mu\text{C/m}^2$. This means that particles with a higher surface-to-volume ratio will have a higher q/m ratio, provided that their whole surface is uniformly charged. Unfortunately, for irregularly shaped insulating particles, this can not be guaranteed, as parts of the surface may not be able to contact the wall of material during triboelectric charging. Additionally, surface-to-volume ratio varies strongly between individual particles.

Whether the charge of particles triboelectrically charged will be positive or negative depends on the relative position in the triboelectric series of the resin to the contact material. In triboelectric contact with *PMMA* (poly-methyl-methacrylate) or metal at neutral charge, which are used for the walls of the aerosol chamber for particle transfer in this thesis, the amino acid particles used in this work are expected to acquire a negative charge.

3.5.3 Measurement of q/m -values

3.5.3.1 Faraday Cell

Measurement devices for q/m values based on a *Faraday cell* are commercially available. In these devices, a known mass of particles is put into a Faraday cage connected to an electroscope to measure the charge within. In this project, the Trek 210HS-2B q/m -Meter was used. This device is not sensitive enough to measure individual particles. Typically, batches of about 50 mg were measured, giving an average charge of these particles.

3.5.3.2 Induced Charges Measurement Method

An alternative measurement method has been developed, namely a system for charge measurement of particles in an airstream in a tube or hose based on induced charges in a metallic tubular probe [NES07, NES07-2]. This system is especially suited for selective deposition from an aerosol (see 3.9). In this method, a circular or tubular metallic probe is wrapped around the dielectric tube or hose in which the charged particles are transported in the aerosol. Particles passing through the tube inside the probe cause an induced charge on the

probe. If the probe is grounded, particles entering or leaving the tube cause a current flow between probe and ground, which can be measured (fig. 3.5).

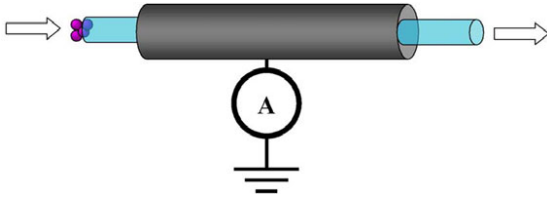


Fig. 3.5: Setup for the measurement of particle charges based on induced charges in a metallic tube, which surrounds a section of the hose or tube in which the particles are transported in an aerosol. Taken from [NES07-2].

According to Gauss's Law,

$$\frac{Q}{\epsilon_0} = \oint_S \vec{E} \cdot d\vec{A}$$

with

$$Q = \text{total charge} \quad (\text{Eq. 3.1})$$

ϵ_0 = dielectric constant

E = electric field, and

S = closed surface around the charge.

For a point charge Q , the electric field can be assumed to be homogeneous, even though only in approximation if other conductors are present. Under these circumstances, if neglecting the deformation of the field by introducing a conductor, the charge induced in this conductor is proportional to the spatial angle Ω it covers, as seen from the charge (fig. 3.6), or

$$Q_{ind} = -\frac{\Omega}{4\pi} Q.$$

with

$$(\text{Eq. 3.2})$$

Q_{ind} = charge induced on the conductor. (For a closed surface of a Faraday cup, obviously $\Omega = 4\pi$ and $Q_{ind} = -Q$.)

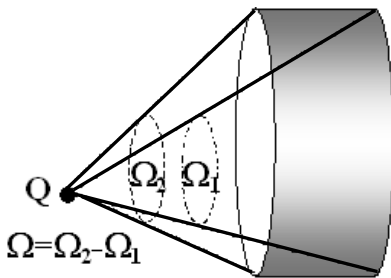


Fig. 3.6: The electric field of the point charge Q induces a charge in the tubular conductor roughly in proportion to the spatial angle covered by it. Taken from [NES07-2].

If the conductor is connected to ground, a change in the induced charge over time causes a current I_{ind} in the connection. Forming the time derivative of eq. 3.2, we get

$$I_{ind} = -\frac{d}{dt} \left(\frac{\Omega}{4\pi} Q \right) = -\frac{1}{4\pi} \left(\frac{d\Omega}{dt} Q + \frac{dQ}{dt} \Omega \right), \quad (\text{Eq. 3.3})$$

where the first term corresponds to the motion of the particles in the tubular conductor, and the second term corresponds to changes of the charge (e.g. through triboelectric charging within the tube). For a charge inside a tube with a length that is large compared to its diameter, $\Omega \approx 0$ while the charge is far away from the tube, and $\Omega \approx 4\pi$ while the charge is near the center of the tube, as the simulation result fig 3.7 shows.

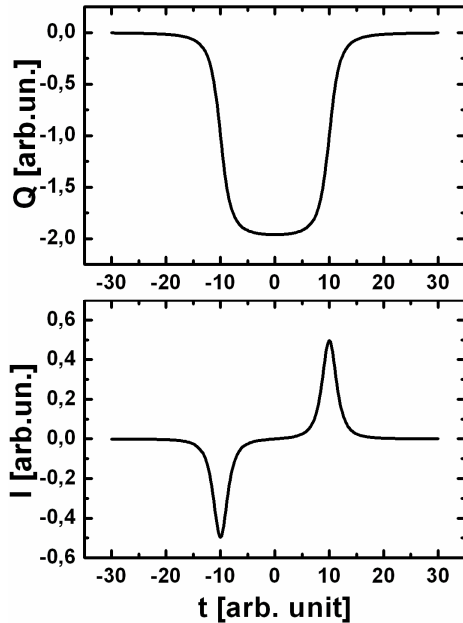


Fig. 3.7: Simulation of the induced charge $Q(t)$ (top) and induced current $I(t)$ (bottom) in a grounded cylindrical probe with a positively charged particle passing through with constant velocity (inlet at $t = -10$ a.u.; outlet at $t = 10$ a.u.). Taken from [NES07-2].

If the aerosol is piped through an appropriate filter which is weighted before and after passage of a cloud of particles, the mass and thus the q/m -ratio of the particles can be determined. Typically, I_{Ind} is measured, and Q_{Ind} is calculated from this. As it measures changes in the charge of particles in an airstream, this method is most suited to measurements on “packages” of particles and less suited to monitoring small changes in a constant flow of particles, which only result in tiny changes in I_{ind} .

This method has also been used to monitor the triboelectric charging process by friction on the walls of the tube or hose, or to compare different setups in their effectiveness in triboelectrically charging particles [NES07-2].

3.5.4 Triboelectric Properties of Amino Acid Particles

The triboelectric properties of amino acid particles have been studied in detail in [LOE09]. It is assumed that triboelectric charging is proportional to the force that brings the particles in contact with the wall. For charging in curved tube or hose or in a cyclone, this is the centripetal force F_Z , which can be calculated by

$$F_z = \frac{mv^2}{r}$$

with

m = mass of an individual particle

v = particle velocity relative to the wall

r = radius of curvature of the wall.

(Eq. 3.4)

In the case of non-laminar flow, turbulence also forces particles into contact with the wall at non-zero tangential velocities even in straight tubes. In experiments, triboelectric charging of different sorts of particles at a range of velocities against polyacryl (PA), poly(methyl)methacrylate (PMMA or acrylic glass) and aluminum walls at different curvatures was determined [LOE09]. In summary:

- average particle charges are typically in the range of -1.0 to -15 mC / kg for both OKI toner and biotoner particles,
- increased curvature results in higher q / m values,
- an increase particle velocity in a curved tube or cyclone results in a roughly proportional increase in q / m ,
- around 15 mC / kg, particle charge saturates, most likely due to gas ionisation discharges,
- charge control agents (CCA) are indispensable if stability of charges is required; without CCAs, particles may even charge positively,
- CCAs may be deposited on the walls of a PMMA cyclone during contact, contaminating it and changing its triboelectric properties, and
- aluminum may be a more suitable material for a charging cyclone, but more thorough investigation is needed at this point.

Additionally, particle sorts with a smaller mean diameter acquire a more than proportionally higher q / m if charged under the same conditions. Triboelectric chargeability seems to be mostly independent of the amino acid sort of a batch of particles.

3.6 Forces Acting upon Microparticles

3.6.1 Approach

Microparticles in a fluid are subject to forces of different categories: All such particles experience forces that are proportional to particle mass, such as gravitational and inertial forces, and forces that are proportional to the surface or the cross-sectional area of the particle, such as drag forces and aerodynamic lift [STI09]. In addition, charged or magnetic particles experience electromagnetic forces, most significantly electrostatic forces acting on electrically charged particles in an electric field. Small particles in dilute gasses may also experience diffusive forces due to Brownian motion of the fluid molecules, but these are not significant under the conditions in the experiments performed during this thesis.

A full-scale attempt to simulate the dynamics of particle transport and transfer is not undertaken in this thesis, for such simulations can be found in [NES06] and [NES08]. However, knowing how the numerous forces acting upon particles scale, particularly with regard to particle size, charge and velocity of the medium is invaluable even in a more experimental approach to spatially selective deposition.

3.6.2 Mass-dependent Forces

3.6.2.1 Gravitational Force

Due to their mass, all particles are subject to the *gravitational force* F_G :

$$\vec{F}_G = m \cdot \vec{g} = \rho \cdot V \cdot \vec{g} \approx \rho \cdot \vec{g} \cdot \frac{\pi}{3} \cdot r^3$$

with

m = mass of an individual particle

g = gravitational acceleration

ρ = particle density

V = particle volume

r = particle radius.

(Eq. 3.5)

As the gravitational force scales with r^3 , it tends to be small compared to other forces for micro- or nanoparticles.

3.6.2.2 Inertial Force

Particles that are accelerated experience an *inertial force* F_T proportional to their mass, with

$$\vec{F}_T = -m \cdot \vec{a} = -\rho \cdot V \cdot \vec{a} \approx -\rho \cdot \vec{a} \cdot \frac{\pi}{3} \cdot r^3$$

with

a = acceleration.

(Eq. 3.6)

Inertial forces occur if a particle is “forced” to change its velocity, e.g. by interaction with the fluid in which it is transported. Figuratively speaking, the particle mass “resists the change of velocity of the medium”. Particles can be sorted according to their density (or their concentration in a fluid of different density can be changed) using inertial force, e.g. in a cyclone, in which the *centrifugal force* F_z can be calculated as

$$\vec{F}_z = -m \cdot \vec{x} \cdot \omega^2 = -\rho \cdot V \cdot v^2 \cdot \vec{x} / x^2 \approx -\rho \cdot v^2 \cdot \frac{\pi}{3} \cdot r^3 \cdot \vec{x} / x^2$$

with

x = distance from the center of gravity of the particle to the rotational axis

ω = angular velocity around the rotational axis = v / x .

(Eq. 3.7)

Dense particles therefore will be found in increased concentration closer to the outer cyclone wall. In fact, this force is present in any curved air flow, including flow over any substrate onto which particles are blown in an airstream perpendicular to the surface.

Considering particles in an airstream accelerated along the same trajectory as the air, the air experiences the same forces as the particles. Thus, the particles experience a *resulting centrifugal force* F_{Zres} proportional not to their density but to the difference in density between particles and air,

$$\vec{F}_{Zres} = -m \cdot \vec{x} / x^2 \cdot v^2 = -(\rho - \rho_f) \cdot V \cdot \vec{x} / x^2 \cdot v^2 \approx -(\rho - \rho_f) \cdot \vec{x} / x^2 \cdot v^2 \cdot \frac{\pi}{3} \cdot r^3$$

with

(Eq. 3.8)

ρ_f = fluid (e.g. air) density.

While this effect is negligible for dense particles in air, if a liquid is used as the fluid, it may need to be taken into account.

3.6.3 Surface-dependent Forces

3.6.3.1 Dynamic Lift

If a fluid flows around an object in a non-symmetrical manner, a non-symmetric pressure distribution around the object ensues, which results in a force exerted upon the object by the medium. The projection of this force onto the plane perpendicular to the direction of flow at the particle, called *dynamic lift* F_L , can be described as

$$F_L = \frac{c_D}{2} \cdot A \cdot \rho_f \cdot w^2 \approx \frac{c_D}{2} \cdot \pi \cdot r^2 \cdot \rho_f \cdot w^2$$

with

(Eq. 3.9)

c_D = lift coefficient

A = particle cross-section, perpendicular to the flow

w = velocity of the medium relative to the particle.

The main causes for lift forces upon particles are

- irregularities in particle shapes resulting in torque upon the particle,
- rotation of particles (Magnus-effect) and
- proximity to (including contact with) a wall in laminar flow, where the velocity gradient results in a force directed away from the wall.

However, as the lift coefficient of the particles is hard to guess, and likely small, dynamic lift is not examined further in this work.

3.6.3.2 Drag Force

If particles and fluid are in motion relative to one another, surface-dependent forces occur, based both on pressure and on friction. While dynamic lift describes the force perpendicular to the flow of the medium, the *drag force* F_D is parallel to the direction of flow of the medium. One ansatz to describe F_D that is valid for both laminar flow and turbulent flow around the particle can be chosen according to [STI09] with

$$\vec{F}_D = \frac{c_w(Rn_l)}{2} \cdot A \cdot \rho_f \cdot |w| \cdot \vec{w} \approx \frac{c_w(Rn_l)}{2} \cdot \pi \cdot r^2 \cdot \rho_f \cdot |w| \cdot \vec{w}$$

(Eq. 3.10)

where

c_w = drag coefficient (depends on the particle Reynolds number Rn_l and w).

In simple terms, drag forces cause particles to follow an airstream; they describe the effect of the particles being “dragged along with the air”.

c_w is modeled depending on Rn_l , which in turn depends on w with

$$Rn_l = \frac{w \cdot l \cdot \rho_f}{\eta} \approx \frac{w \cdot 2r \cdot \rho_f}{\eta} \quad (\text{Eq. 3.11})$$

with

l = characteristic size of the particle (e.g. its diameter)

η = dynamic viscosity of the fluid.

Assuming a spherical particle, for laminar (Stokes) flow around the particle, at Rn_l smaller than approx. 0.25, friction of the particle in the fluid is dominant, and $c_w = 24 / Rn_l$, thus $F_D \sim w$ and $F_D \sim r$. For large $Rn_l > 10^3$, flow around the particle is turbulent, and dominated by inertial forces of the fluid in turbulence behind the object. c_w becomes constant at high Rn_l , and thus $F_D \sim w^2$ and $F_D \sim r^2$. For the transition region, approximative descriptions can be found in [STI09].

In air at room temperature and normal pressure ($T = 293$ K, $P = 101$ kPa), $\rho_f = 1.204$ kg / m³ and $\eta = 18.36 \cdot 10^{-6}$ Pa · s. Assuming velocities on the order of magnitude of 1 m / s and a particle diameter of approx. 10 μm, we get $Rn_l = 0.6$, and for larger 15 μm particles at 5 m / s, we get $Rn_l = 4.9$. In consequence, exact calculations would require the use of a transition region formula, but a laminar calculation still yields an acceptable approximation. Eq. 3.10 then simplifies to

$$\vec{F}_{D,lam} \approx 6\pi \cdot \eta \cdot r \cdot \vec{w}. \quad (\text{Eq. 3.12})$$

3.6.4 Electromagnetic Forces

3.6.4.1 Electrostatic Force

In an electric field E , particles with a charge q experience a *Coulomb force*

$$\vec{F}_c = q \cdot \vec{E} = \frac{q}{m} \cdot V \cdot \rho \cdot \vec{E} \approx \frac{4\pi}{3} \frac{q}{m} \cdot r^3 \cdot \rho \cdot \vec{E} \quad (\text{Eq. 3.13})$$

in parallel to the field. The higher the q / m ratio, the stronger the Coulomb force in relation to the mass-dependent and surface-dependent forces. When handling charged particles, each charged particle may experience electric fields caused by

- its own charge (such as the *image force* between itself and a nearby conductor due to induced charges from the particle),
- the charge of other particles nearby (causing a cloud of particles at the same polarity of charge to disperse),
- conductors in its vicinity, either isolated and charged or forced to a fixed electric potential (e.g. by a voltage source), and
- other electrically charged objects (e.g. insulators with surface charges).

As electrical fields of high strength and small dimensions are easily generated, they are the selective force of choice for spatially selective particle deposition, both in laser or LED printing and deposition on HV microchips.

In the case of the particles used in this thesis, which are surface-charged, the maximum q/m scales approximately with $1/r$, as maximum q scales with the area at r^2 and m scales with the volume at r^3 .

3.6.4.2 Dielectrophoretic Force

Dielectric particles in an inhomogeneous electric field, even if not electrically charged, are polarized, and thus experience the dielectrophoretic force F_{dep} that is directed towards a region of stronger electric field [NES06]. For a spherical particle with radius r , no dipole moment except that induced from the electric field, and an electric field E constant over time,

$$\vec{F}_{dep} = 2\pi \cdot r^3 \cdot \varepsilon_f \frac{\varepsilon_p - \varepsilon_f}{\varepsilon_p + 2\varepsilon_f} \nabla \vec{E}^2 \quad (\text{Eq. 3.14})$$

with

ε_f = fluid dielectric constant

ε_p = particle dielectric constant.

Due to the dependency on the gradient of the square of the electric field, the dielectrophoretic force is much more short-ranged than the Coulomb force in the chip setup, where strong field gradients only occur near the pixel metal edges. It tends to be significant especially in selective desorption, but less so in selective adsorption processes [NES06].

3.6.4.3 Other Electromagnetic Forces

Forces requiring the particle to be magnetized are not relevant in the context of this thesis, because such forces would be very weak for weakly para- or diamagnetic particles, and the bioparticles cannot easily be designed to be ferromagnetic because most metals adversely affect the synthesis process. The Lorentz force acting upon a charged particle moving in a magnetic field is hard to use for selective deposition because it requires strong fields. In general, creating strong magnetic fields on microchips by using inductive coils is much harder than creating electric fields because of the restrictions of CMOS technology. Therefore, using magnetic fields for particle deposition is not practical, and will not be considered further in this thesis.

3.6.5 Particle Adsorption and Desorption on Surfaces

Interactions of particles with surfaces such as walls of tubes or chambers that include removal from the aerosol (adsorption to the surface) or lift-off into the aerosol (desorption from the surface) are very difficult to model [STI09]. They depend on particle size and shape, the velocity and direction of the airstream relative to the surface, surface and particle humidity and roughness, and deformation of particles upon impact. They generally increase relative to other forces with decreasing particle size, with some components like the molecular force and the capillary force proportional to the particle radius, the electrostatic image force between surface charged particle and surface is proportional to r^2 , while the electrical force due to contact potential is proportional to $r^{2/3}$ [NES08]. Additionally, if a multilayer of particles is deposited, particle-particle-interactions must be considered. Extensive theoretical and experimental studies of particle adhesion have been undertaken in the framework of this

project, and can be found in [NES06, NES08]. For slow air speeds (1 m/s or less) and monolayers of particles, adsorption tends to be permanent. Larger agglomerates of particles on a surface may come off in groups, which may make the aerosol inhomogeneous in time. Furthermore, the adhesive forces for individual particles may vary widely, making adhesive force strength an unreliable factor in selective transfer. Particles may also be reflected or scattered upon contact with a surface, and if agglomerates contact a surface, they may spread upon impact.

3.6.6 Comparison of Forces Acting Upon Particles in an Aerosol

3.6.6.1 Scaling with Airstream Velocity and Particle Size

Summarizing the forces described in the previous sections yields tab. 3.1.

Force	F_G	F_T & F_{Zres}	F_D	F_C	F_{dep}	F_{adh}
Scaling with v	const	v^2	v	const	const	const
Scaling with r	r^3	r^3	r	r^2	r^3	$r^{2/3}$ to r^2

Tab. 3.1: Scaling of forces in particle transfer with particle velocity and particle size. For F_{Zres} , constant curvature is assumed, for F_C , constant surface charge is assumed. Adhesive forces tend to increase relative to the other forces with decreasing particle size, but the exact dependence is not known.

Note that inertial and gravitational forces scale with r^3 , while the drag force scales with r . This means that the drag forces become more significant for smaller particles, which thus have a weaker tendency to separate from the airstream in curved flows.

Only the electric forces F_C and F_{dep} can be used for selective deposition. They are independent of particle velocity, while nonselective forces increase with particle or airstream velocity. Therefore, it is desirable to reduce airstream velocity to the minimum necessary to transport the particles into (or out of) the area in which the selective electrical forces dominate. As, for smaller particles, the electrostatic force increases in significance over the dielectrophoretic force, and adhesive forces grow proportionally stronger, it may be preferable to use adsorption methods over desorption methods for these particles.

3.6.6.2 Comparison of Forces for Typical Particles

For typical OKI or amino acid particles of about 10 μm in diameter, the forces acting upon a particle have been calculated in [NES06]. Expanding upon these data, fig. 3.8 shows an order-of-magnitude comparison of the forces involved in deposition of particles of 15 μm , 10 μm and 5 μm in diameter d . Particle density is around $\rho = 1,000 \text{ kg/m}^3$ [NES08] and $g = 9.81 \text{ m/s}$. As a best guess approximation, a radius of curvature of $x = 2 \text{ mm}$ for the airstream over the chip is assumed. The drag force is calculated for $w = v$ (particles being lifted off a surface), and also for $w = v/10$ (particles deviating from the airstream). Taking experimental results from [LOE09] as guideline, particle q/m is assumed to be 1.5 mC/kg for $d = 15 \mu\text{m}$, 3 mC/kg for $d = 10 \mu\text{m}$, and 4.5 mC/kg for $d = 5 \mu\text{m}$. The electrical field is approximated as $E = U/L$, where L is the pixel pitch and U is the pixel voltage [NES08]. This approximation assumes a “thin” aerosol, so the electric interaction between particles can be neglected in comparison to the field induced by the support. In a “dense” aerosol, the “cloud” of particles would create a significant electric field, causing particles to separate from one another, leading to strong nonselective deposition on all surfaces limiting the aerosol. Due to its short range, the dielectrophoretic force is disregarded.

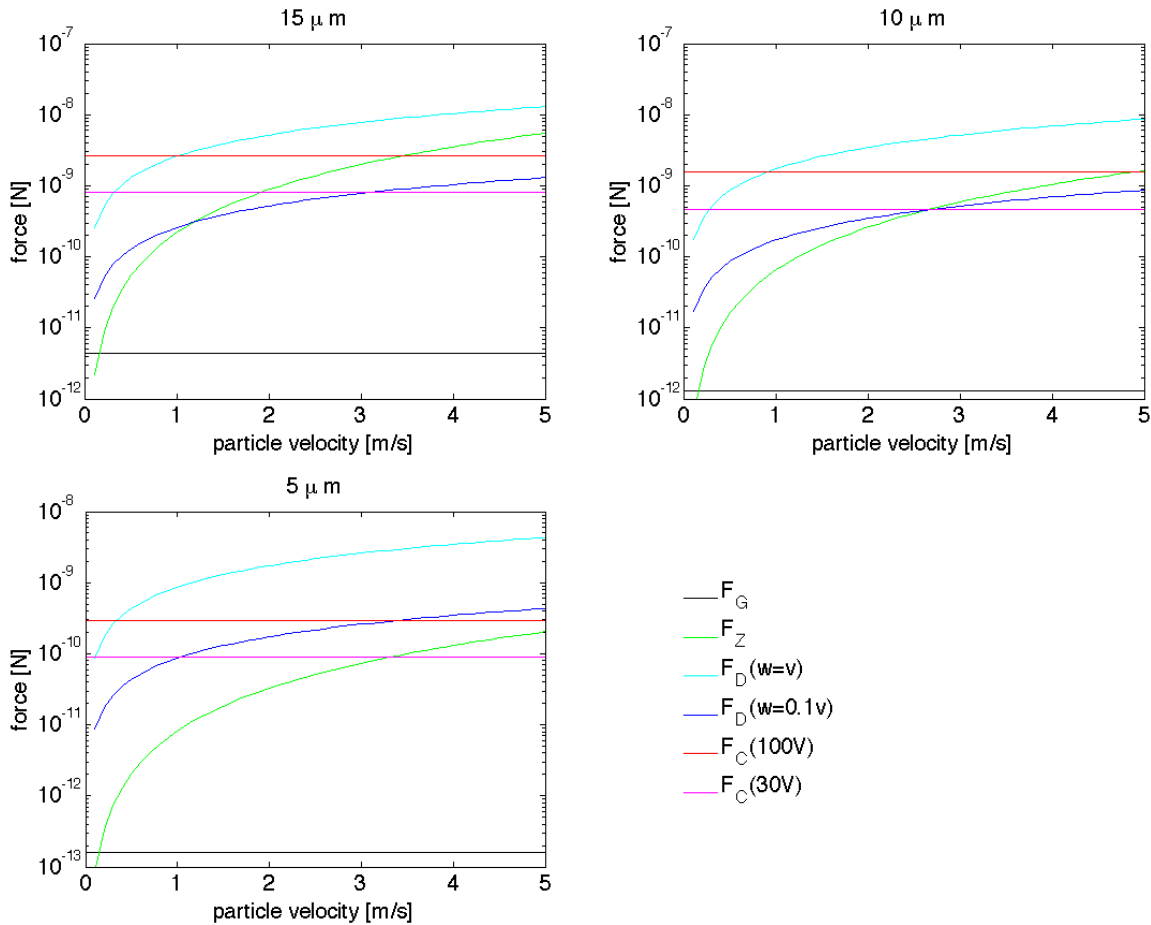


Fig. 3.8: Forces acting upon particles in an aerosol and an electric field, for particle size $15\ \mu\text{m}$, $10\ \mu\text{m}$ and $5\ \mu\text{m}$. F_G : gravitational force, F_Z : centrifugal force, F_D : drag force, given for different particle velocities w relative to the velocity of the medium v , F_C : Coulomb force, given for different voltages.

Fig. 3.8 shows that the gravitational force is very small compared to the other forces down to very low particle velocities. For large particles, inertial forces are significant in relation to drag forces for velocities greater than $1\ \text{m/s}$, allowing these particles to diverge from the airstream in a laminar curved laminar flow, which increases the probability of particles contacting surfaces. For $5\ \mu\text{m}$ particles, however, F_Z is much smaller than F_D for the velocities considered. Therefore, these particles follow the airstream along its curved trajectory, and are less likely to contact surfaces in a laminar curved flow. This effect could be used to reduce contaminations during spatially selective particle transfer. For small particles, the relative drag forces increase in comparison to the electric forces, as well. Therefore, to achieve selective deposition from the airstream, a slow laminar flow over the chip is critical for small particles. Adhesive forces are not shown in this figure, but experiments have shown them to be significantly larger than the electric forces even for $100\ \text{V}$ (particles cannot be detached from the chip by electrical forces alone), but comparable to the drag forces at high velocities at least for particles around $10\ \mu\text{m}$ (as particles can be desorbed from the chip by using pressurized air at $8\ \text{bar}$) [NES06, NES08, KÖN05].

3.7 Direct Particle Transfer

In direct particle transfer, a uniformly particle covered support (e.g. glass slide) is brought in close proximity to a support capable of exerting spatially selective forces upon particles, e.g. an HV microchip, so that the surfaces are parallel (fig. 3.9). The medium (typically air) between the surfaces is stationary. As the electric field $E = V/d$ is proportional to the inverse distance, and the voltage on microchips is limited, a small distance between source and target surface is required [NES08, KÖN05]. If the source is not a conductor, a conductor at a high voltage may have to be placed behind it (seen from the target) to achieve sufficient field strength, resulting in a selective and a non-selective component of the electric force. Using glass slides as the particle source and chips as the target, positioning with an accuracy of around 10 μm is required using this technique for 100 μm spot pitch, making it mechanically challenging. The absence of free particles in an aerosol and the hard-to-control forces and conditions associated with it, however, make this choice attractive. As yet another downside, the adhesive forces between the particles and the source substrate are also hard to predict or control, which is why this method was not the method of choice for this work [KÖN05]. However, it is developed further in other works [CHE].

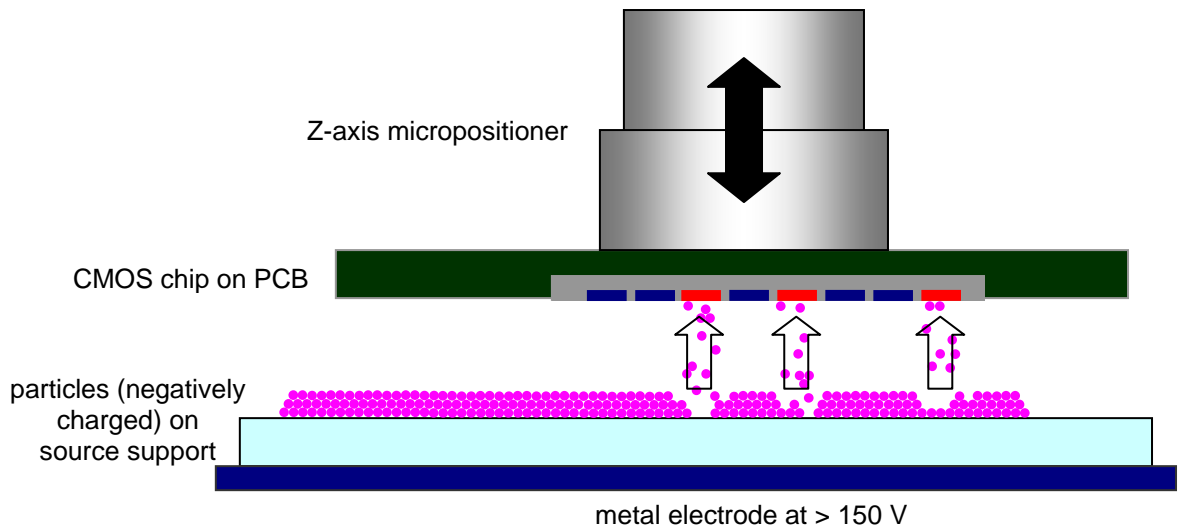


Fig. 3.9: Direct particle transfer. The target support (chip) is placed close to the particle-covered source support. An electric field of sufficient strength is used to overcome the adsorption forces on the source substrate and transport the particles to the target substrate.

Using direct particle transfer, it is possible to employ the chip not as the synthesis substrate but as a transfer substrate, similar to a printing head. Particle transfer would be a two-step process in this case: First, particles are selectively deposited onto the chip (by the direct transfer method or any other method), then they are transferred from the chip to a target substrate (such as a glass slide or another chip).

Some drawbacks of using the chip as a printing head are:

- Use of the direct transfer methods with its associated drawbacks (see above) is required.
- Precise lateral alignment of the target support is necessary, limiting synthesis locus size.
- Particle transfer becomes a two-step process, making the machinery more complex.

However, such a system could offer the following benefits:

- Larger supports can be used by stepping the printing head chip over them.
- Any support can be used for synthesis, e.g. glass slides which are much cheaper and more robust than microchips. This alleviates the need to make surface modifications and synthesis process compatible to the CMOS support. Alternatively, a second chip, optimized for integrated detection, could be used as target support.

The particles on the covered support may even be put in direct contact with the target surface by pressing the surfaces together, as long as the pressure does not exceed the tolerances of the chip. This has the advantage of the adsorbing force of the target helping to overcome the adsorbing forces on the source, but due to the unreliability of adhesive forces (3.6.5), this entails an increased risk of contaminations when used for transfer from a fully covered source. However, in using the chip as a printing head, it may be possible to avoid this difficulty: If the chip entered the process free of contaminations, it cannot contaminate the target. If particles already on the target are fused to the target by brief heating in between different amino acid printing steps, they can be prevented from contaminating the chip by “reverse” particle transfer. Thus, the combination of deposition from the aerosol to the chip, and then printing from the chip onto a glass slide is conceptually possible. Verification of the pattern on the chip by image processing between the two transfer steps may reduce the risk of contamination on the synthesis substrate further [WAG10].

3.8 Selective Desorption into an Airstream

In selective desorption, particles are removed from a support by the nonselective forces F_{nonsel} of an airstream passing over them. First, the support is prepared by homogeneously dispersing particles on it. Then, forces from switchable electric potentials on the support F_{sel} add to or subtract from the adhesive forces F_{adh} , making desorption selective at a certain airstream velocity, where $F_{adh} < F_{nonsel} < F_{adh} + F_{sel}$. If these conditions are fulfilled, all particles at locations where the electric field is turned off are “blown off” in the airstream, while particles on locations where the electric field is active are retained. Other works indicate that electrophoretic forces are the dominant selective electric forces in case of selective desorption [NES06]. While functional on unmodified chips, the usability of the desorption method in combination with PEGMA-modified surfaces (see 4.1) still needs to be verified, as the adhesive forces tend to be stronger on these films.

3.9 Selective Adsorption from an Aerosol

Adsorption of particles from an aerosol is known both in *dust removal* (the cleansing of gasses from particulate contamination, i.e. in a cleanroom), and in *particulate collection*, where useful disperse matter is gathered from an aerosol (i.e. after transport or production) [STI07]. In neither case, spatial selectivity is required, making spatially selective microparticle deposition unusual.

Electrostatic precipitators are in general use, and usually consist of a *spray electrode* to charge particles in the gas by coronary discharge and an *adsorption plate* of opposite polarity that attracts and gathers the charged particles. Most of them are operated at several ten kilovolts [STI07], well beyond the voltage range of microelectronic chips, and require no

spatial selectivity. Nevertheless, spatially selective particle deposition onto a surface from an aerosol using smaller electric fields has been demonstrated previously [JAC02].

As shown in (3.6.6), below a certain particle velocity, electrostatic forces dominate even for voltages of 100 V and below, which are available on HV-CMOS chips. Thus these forces can, given an appropriate setup, ensure selective deposition. An airstream loaded with particles can be used to transport a steady supply of particles into the range of the electric fields generated by the CMOS support. Using this concept, toner particles have been deposited on CMOS chips in a variety of patterns at voltages down to 30 V [KÖN05]. Fig. 3.10 shows the steps of such a deposition. Selective adsorption from an aerosol is the primary method for particle transfer used in this thesis.

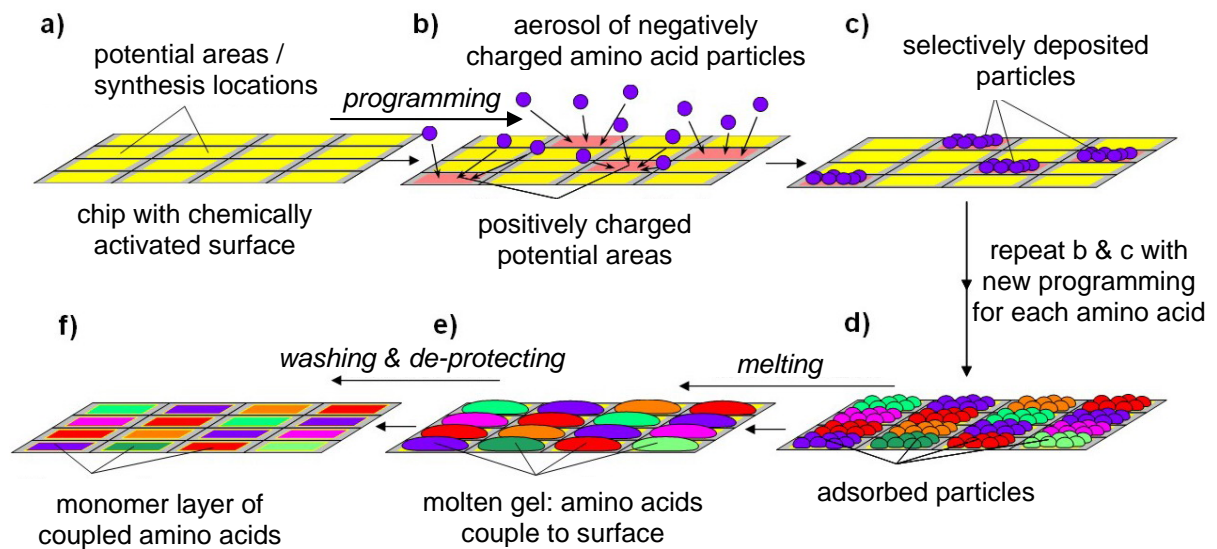


Fig. 3.10: Deposition and coupling of a single amino acid layer. a) The chip with a chemically modified and activated surface (see 4.1) enters the process. b) After being programmed with the pattern for the first amino acid sort, potential areas (corresponding to synthesis spots) to be patterned are positively charged, while the rest of the potential areas is grounded. The chip is exposed to an aerosol of negatively charged particles, which are deposited on the positively charged potential areas. c) The chip is removed from the first aerosol. Adhesive forces prevent deposited particles from being removed in the following steps. d) Steps b) and c) are repeated for each amino acid particle sort: The chip is programmed with a different pattern and exposed to the corresponding particle sort for each amino acid. e) The chip is heated until the adsorbed particles melt, releasing the amino acids and initiating their coupling to the activated support (see 3.4.2). f) Excess amino acids, solvent and other particle components are washed away. Subsequently, the coupled amino acids are de-protected. The chip is now ready for the next amino acid layer.

PART II

NEW MATERIALS AND METHODS

4. Particle-Based Peptide Synthesis - Related Works

4.1 Preparation of Support with PEGMA Films

Peptide synthesis requires a support surface that allows for covalent coupling of activated and protected amino acids. For this purpose, the surface is functionalized with a polymer coating terminally presenting amino groups. Those amino groups function as an anchor group, allowing the specific binding of amino acids with an activated carboxyl group.

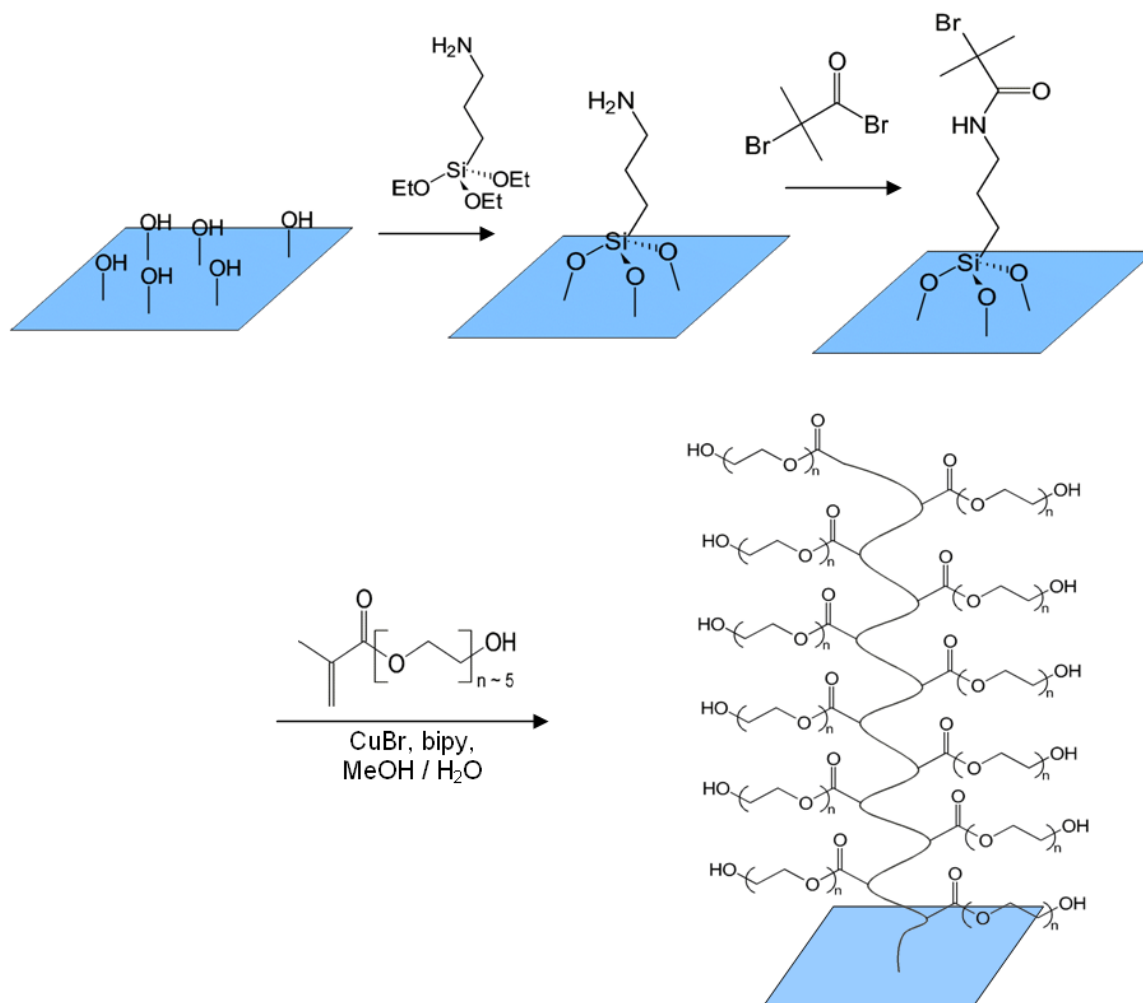


Fig. 4.1: Structure and synthesis of the PEGMA graft polymer layer. First, hydroxy groups are generated through oxidation of the surface. Chip surfaces may consist of silicon nitride, silicon oxide, silicon or aluminum. Afterwards, a silane is coupled to the hydroxy groups and converted to a bromide-substituted silane, which serves as starting point for copper(I)-induced graft polymerization. The OH-terminated poly(ethylene glycol) side-chains of the graft polymer are subsequently converted into amino groups by esterification with Fmoc- β -alanine (Fmoc: 9-fluorenylmethoxycarbonyl protection group) (not shown). Residual hydroxyl groups are blocked by acetylation prior to Fmoc de-protection [SCH08]. Linker molecules can also be added at this point, e.g. to increase accessibility of the synthesized peptide. Modified from [BLO09].

Using a branched polymer offers the advantage of an increased number of starting amino acid groups (up to 40 nmol / cm² of amino groups at film thicknesses around 100 nm) through its three-dimensional structure. The *poly(ethylene glycol)-methacrylate (PEGMA) graft polymer* films (fig 4.1), which are used in peptide laser printing, provide these benefits. In addition, they prevent non-specific protein adsorption, reducing background i.e. in antibody-based sandwich assays for peptide detection [STA07, BEY05].

In chip-based synthesis, the surface to be modified is the bond pad aluminum or the passivation silicon nitride. PEGMA polymers had been created on such surfaces previously, and successfully used in the peptide laser printer. However, no particle deposition had been performed on CMOS chips surface-modified with PEGMA films (see 6.5, [STA07]).

It should be noted that these films slowly degrade (on a timescale of weeks or months) by exposure to oxygen at room temperature. Therefore, surface-modified supports are kept at 4° C under nitrogen atmosphere for long-term storage.

4.2 Aerosol Generation

An aerosol chamber (fig. 4.2) made of Plexiglass parts glued with Fixogum sealing glue has been used to create the aerosol from which the particles are deposited as described in (3.9). It consists of the following parts:

- The *air inlet* consists of a flow adjusting valve and a tap valve that enables influx of pressurized air into the system while pushed. It can be connected to a pressurized air supply or gas bottle with pressure regulator. In the standard setup, a flow regulator is connected between the pressure regulator and the inlet. Standard operating range of the chamber was between 5 and 30 l / min at 1 to 8 bar.
- The *injector* is the part of the chamber where particles are added to the airstream. The air passes underneath a hole to the particle reservoir through an injector jet, in an arrangement designed to “suck in” particles from the reservoir.
- From the injector, the air moves through a tube into the *cyclone*, a cylinder of 28 mm diameter, for triboelectric charging. On the top, in the centre of the cyclone, the air outlet is mounted. As particles move along the walls due to the centrifugal force (3.6.2.2), only few particles escape through the air outlet unless the air is excessively saturated with particles. At the bottom of the cyclone, the particles pass through a conical connector into the main transfer chamber.
- As the *transfer chamber* is a large volume, the air stream coming out of the cyclone expands and air velocity decreases. This layout generates a disperse aerosol with slow-moving air and particles. The chip was placed in a holder behind an aperture at the top of the chamber. Originally, the aperture was planned to be completely closed by the chip, but a certain air flow past the chip out of the chamber was found to be required for good deposition results.
- The *particle reservoir* is located at the bottom of the transfer chamber. Enough particles for several ten to hundreds of depositions can be stored there.

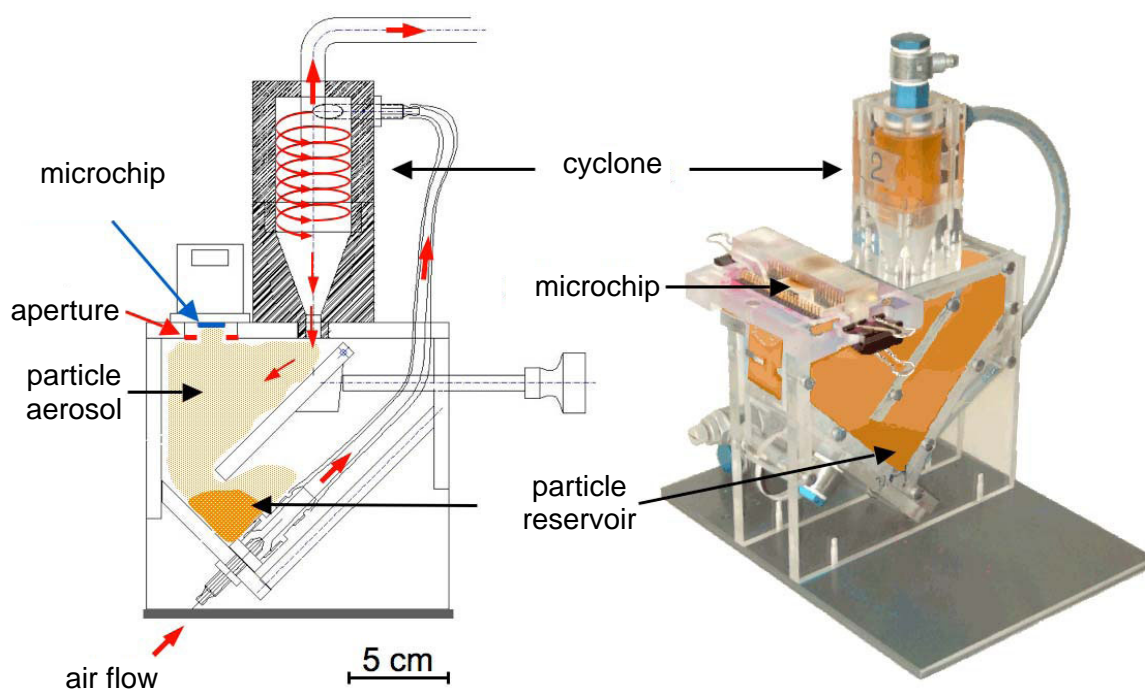


Fig 4.2: Schematic drawing and image of the aerosol chamber used for particle deposition from the aerosol. The flow path of air is shown by arrows. See text for details. Taken from [BEY07].

This chamber design was found to be workable, and a protocol for the use of this chamber in chip-based peptide synthesis could be written. This protocol, along with a detailed analysis of the chamber and its components had not been performed previous to this work, and can be found in (6.2).

4.3 Fixed-Pattern Chips

4.3.1 Structure and Function of Fixed-Pattern Chips

Fixed-pattern chips are, in the context of this work, microchips that can create electrostatic patterns on their surfaces like the CMOS chips described above. Like CMOS chips, fixed pattern chips contain metal interconnect on a silicon die, but in contrast to CMOS chips, no semiconductor structures are available. Therefore, unlike CMOS chips, they are limited to one (or few very specific) patterns that they can create. This drawback makes direct combinatorial synthesis impossible on such chips, but although limited to few patterns, all steps of particle transfer and synthesis can be tested on them. Chips manufactured in such processes cost only a fraction of CMOS chips of the same silicon area, making them attractive for use as prototypes.

In this project, fixed-pattern chips have been used to test and develop surface modification, deposition and synthesis procedures before investing in more costly CMOS chips. Especially for surface and synthesis tests, where die sizes larger than those affordable in CMOS were required, fixed-pattern chips were used. Indeed, the first on-chip peptide synthesis in this project was performed on a fixed-pattern chip [BEY07].

Reproducibility of results obtained on fixed-pattern chips on later CMOS chips could not be taken for granted; therefore these results had to be verified using prototype CMOS chips. These early CMOS chips had to be of small size for economic reasons. Indeed, some notable differences in behavior were encountered during this work, as the silicon nitride surfaces of chips from different manufacturers proved to differ notably in their physical properties. The relation between fixed-pattern chips and prototype CMOS chips in developing the fully combinatorial CMOS chip and the deposition and synthesis system is detailed in 4.4 and 5.2.

4.3.2 Particle Deposition on Fixed-Pattern Chips Using Color Toner Particles

Using OKI color toner particles and fixed-pattern chips manufactured at the Technical University of Dresden, Institute of Semiconductor and Microsystem Technology [TUD], particle deposition from an aerosol was achieved [NES06], establishing a test system (fig 4.3).

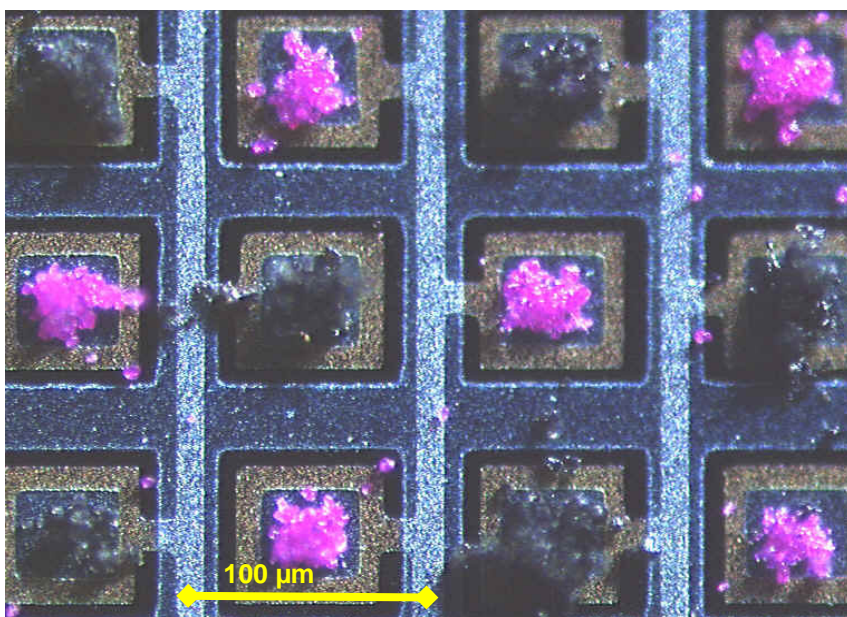


Fig. 4.3: Result of complementary transfer of OKI black and OKI magenta toner particles onto a fixed pattern chip, pixel pitch 100μm (taken from [NES06]).

Fixed-pattern chips with a pixel pitch of 100 μm and 50 μm were shown to yield successful deposition from the aerosol, both with commercial toner and amino acid particles. The desorption method (3.9) and the direct transfer method (3.7) were also tested using these chips [NES06, NES09].

4.4 Peptidchip 3

4.4.1 Objectives

The objective of previous works in microelectronics [KÖN05] was to achieve proof-of-principle combinatorial transfer on CMOS chips, and to determine how pixel size, shape and spacing influence particle transfer. For the CMOS chips, deposition from the aerosol (3.9) was the primary method chosen for selective particle transfer, using the aerosol chamber described in 4.2. On Peptidchip 2, first successful transfer was achieved, while Peptidchip 3 was used for a comparative analysis of numerous different pixel layouts. Additionally,

Peptidchip 3 was the first chip to be used to investigate the possibility of integrating CMOS photodiodes into the pixels for detection of fluorescence-labeled ligands (see 5.2.4).

Furthermore, all results obtained with fixed-pattern chips had to be verified using CMOS chips, preferably chips manufactured in the exact same semiconductor process as the “application chips”. This was necessary because of possible differences in structure and design or differences in the surfaces (due to the different processes used) influencing synthesis.

4.4.2 Microchip Design

In order to meet the objectives, Peptidchip 3 was designed to feature a number of different matrices of 8×8 pixels with a range of pixel sizes and layouts, at maximum voltages between 30 V and 100 V [KÖN05]. The pixels in these matrices can be controlled either by a direct control using switches on the main board, which configures all 4×4 sub-matrix on the chip in equal patterns, or by an I²C interface using a lab PC, whereby arbitrary patterns can be programmed. The I²C interface of Peptidchip 3 was designed to be scalable for control of up to 2^{19} or 524,288 pixels, allowing re-use of the interface in application chips.

Each pixel consists of a *low voltage control* (5 V), which is basically a memory cell that can be set or reset via the interface. Connected to the memory cell is a *high voltage inverter* designed as an NDMOS inverter with PDMOS pull-up. The PDMOS gate is held at a bias voltage near its threshold voltage, so that it is conductive with a high R_{on} , in order to limit HV currents. The output of the HV inverter is connected to the *potential area*, which is a plate of metal on the topmost (third) metal layer that projects the electric field in the volume above the chip. Each potential area directly corresponds to a synthesis site.

Certain differences in layout between the fixed-pattern chips and the CMOS chips should be noted. First, fixed-pattern chips are free in whether to put passivation over the potential areas or to leave the aluminum conductor exposed. On the fixed-pattern chips, the aluminum was usually left exposed in order to obtain stronger electric fields, even though the differences were expected to be almost negligible. On CMOS chips manufactured in the AMIS I2T100 process, however, the design rules require the chip to be covered by passivation except for passivation openings at the bond pads¹. While some deviations from this rule are accepted (at the risk of the customer), a closed area filled with the topmost metal layer underneath each passivation opening is indispensable according to the design rules. Logic under passivation openings is prohibited, and designing it anyway is possible, but very difficult because generated layers required for logic would have to be drawn by hand. Therefore, Peptidchip 3 features only few pixels with passivation openings, namely one matrix of 78 μm , one of 65 μm and one of 44 μm pixel size, which do not have their own logic but are connected to the output of an adjacent matrix. Additionally, integrated photodiodes require the potential areas to have *holes* in the metal layer (which are filled with silicon oxide) in order to allow the passage of light to the silicon underneath. These holes were designed to be larger than the wavelength of visible light, and a number of different sizes up to about the average diameter of the particles, with hole-to-metal ratios of 1:1 to 1:8 were present on Peptidchip 3. These holes, due to the strict requirement of a closed metal area underneath all passivation, can only be manufactured in passivated areas.

¹ Bond pads are special structures intended to electrically contact the chip. Usually, the layout of these structures is tightly regulated.

The second difference between fixed-pattern and CMOS chips is that in the fixed-pattern chips, all pixels and their respective interconnect are located on the first (bottom) metal layer, without the need for pixel interconnect wires crossing over each other. On CMOS chips in our process, such a layout is not possible, as part of the bottom metal layer in each pixel is required to connect the logic and HV devices, while bottom and intermediate metal layers are required for interconnect, control and supply wires. Metal at a high voltage may never directly cover active silicon devices, so that metal on the first layer tied to a low voltage must be used as a field plate to prevent triggering of FOXFETs (2.3.3). Where spatial constraints require HV to be routed in bottom layer metal, no silicon devices can be integrated underneath. Thus, only the topmost metal layer is available for potential areas in our CMOS process.

A certain distance (roughly 5 to 25 μm) between the potential areas of each pixel is desirable to avoid merging of particle melts from different pixels during coupling. However, just leaving a gap of this size between the potential areas does not guarantee that space to be free of fields, indeed conducting tracks underneath that area will project an electric field through the insulation and passivation into the area above the chip. Therefore, the space between the potential areas is covered with a (passivated) metal *grid electrode* on the top metal layer that can be set to an arbitrary fixed voltage. This voltage may even exceed 100 V or be below substrate potential (0 V). The grid electrode is also present on fixed pattern chips, but differs from the CMOS chips in layout insofar that the grid electrode is not always passivated and, on most chips, it is located on the metal layer above the potential areas instead of being placed on the same layer. On some fixed-pattern chips, grid and potential area even overlapped as a consequence of this, while on the CMOS chips they had to be spaced by 1.5 μm .

4.4.3 Particle Transfer Results

Selective particle transfer with good quality was shown in [KÖN05] using OKI toner in a checkerboard pattern, on pixels with a pitch from 100 μm down to 43 μm , at voltages between 100 V and 30 V, with the grid electrode between 0 V and 15 V (fig. 4.4). Pixels with exposed aluminum tended to attract more particles than those covered with passivation, but both kinds of pixels could be covered with ample amounts of particles. At 25 V, only the 100 μm pixels could be selectively deposited, and below 25 V pixel voltage, selective deposition failed regardless of pixel size. Voltages above 30 V had little effect in improving the transfer quality further. Complementary transfer of OKI particles with different colors was also achieved and it was shown that one previously deposited particle layer does not hinder a subsequent deposition (fig. 4.5).

Non-checkerboard patterns were also examined (fig. 4.6 and fig. 4.7) and deposition was generally successful for patterns with less active pixels down to only one pixel in 16 being active. Setting the grid electrode to half the pixel voltage improved the deposition quality for patterns with few active pixels. Patterns with most pixels active yielded less coverage of pixels to be deposited on due to a “halo effect” (fig. 4.8), where attracting pixels directly adjacent to the repellent one received only very few particles. The holes in potential areas were found to have no measurable influence on particle transfer. The integrated photodiodes of Peptidchip 3 had not been tested in [KÖN05], as particle transfer was of a higher priority.

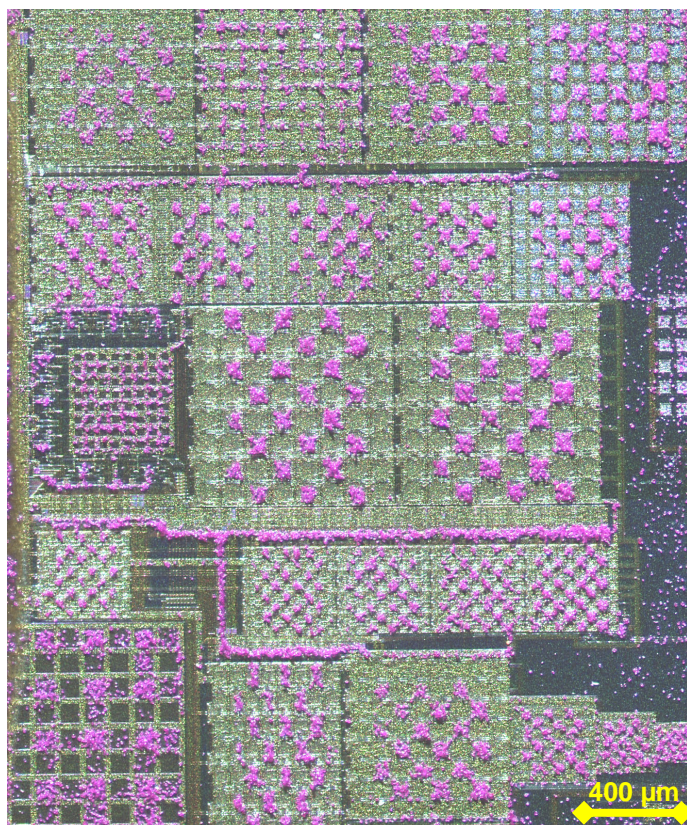


Fig 4.4: Deposition result on Peptidchip 3 at 30 V pixel voltage, 15 V grid voltage. Taken from [KÖN05].

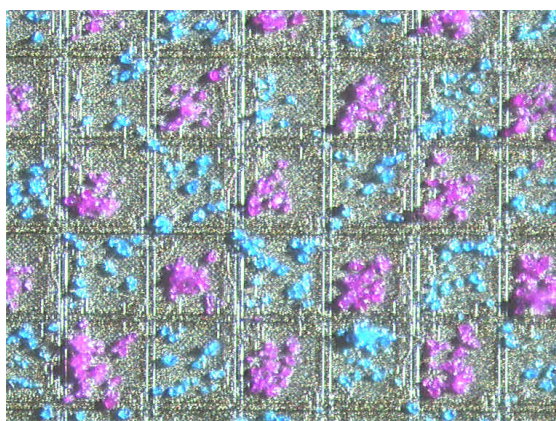


Fig 4.5: Complementary deposition of OKI Cyan and OKI Magenta commercial toner (30 V, 100 μm). Taken from [KÖN05].

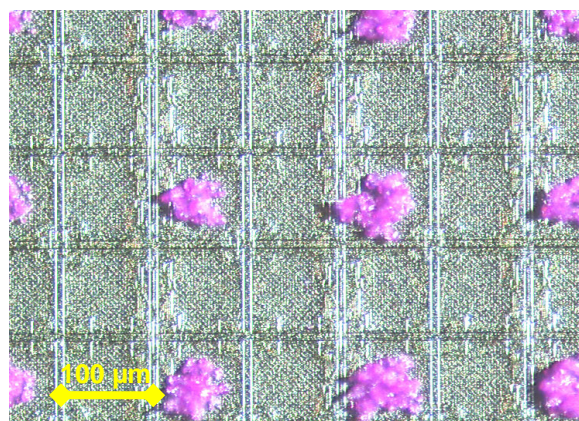


Fig 4.6: Deposition on one in four pixels (30 V, 100 μm). Taken from [KÖN05].

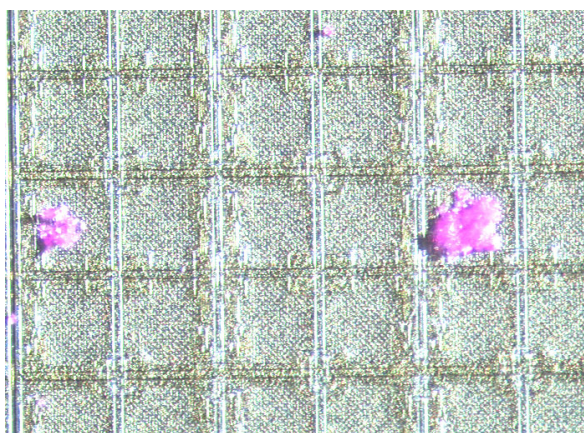


Fig 4.7: Deposition on one in sixteen pixels (30 V, 100 μm). Taken from [KÖN05].

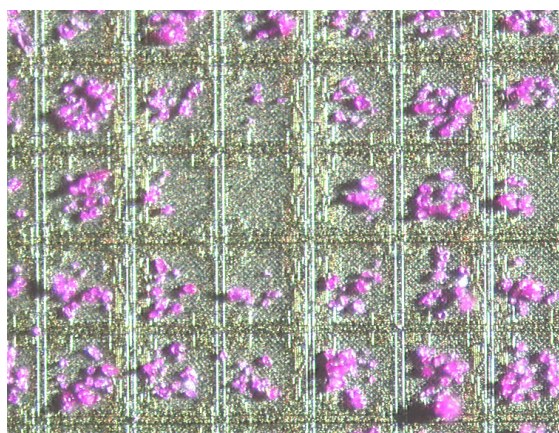


Fig 4.8: Deposition on all but one in sixteen pixels (30 V, 100 μm). Taken from [KÖN05].

In chapter 6, experiments expanding upon these results are shown, including deposition using amino acid particles, complementary deposition of four different particle sorts, and investigations into compatibility of particle transfer with surface modifications required for peptide synthesis. The chips designed and used in this thesis and their development path from Peptidchip 3 are shown in 5.2.

5. Microchip Development

5.1 Introduction

In chip-based peptide synthesis and array experiments, the microchips used are the material connection between all required components. Unlike any other known concept for peptide synthesis, the Peptidchip concept merges the amino acid transfer pattern generation system and the deposition support into one single microchip. Therefore, the requirements of both of these functions must be fulfilled by this single device. For pattern generation, the chips must provide the configurable electric fields that guide the particles to their desired locations. As synthesis support, they must accept surface modifications required to fix peptides to their surface and be capable of enduring chemical synthesis. Compatibility of all the required functions and modifications cannot be guaranteed without being tested. Due to the cost of masks and low-volume production, prototypes of small silicon areas that can be manufactured in low-cost *MPW runs*¹ or fixed-pattern chips (see 4.3) were used for testing until a reasonable degree of certainty that a large-scale chip will be functional had been reached.

Continuing on the development on the chips described in 4.4, an overview of the chips in the Peptidchip project and their purpose is given in 5.2. In 5.3 and 5.4, the chips that were built in the course of this thesis are described in detail. PCBs, packages and coverings, synthesis chambers and chip control software are described along with each chip.

5.2 Microchip Versions

5.2.1 Overview

In order to achieve the diverse goals in the Peptidchip project, three kinds of chips, designed for distinct purposes, have been used (fig. 5.1):

- Fixed-pattern chips have been utilized to investigate particle transfer in general and the behavior of typical chip surfaces during all stages of use. Furthermore, they have been serving to test the chemical processing and cleaning steps of synthesis.
- Fully combinatorial synthesis chips are required to investigate particle transfer in arbitrary patterns, to verify the results obtained with fixed-pattern chips and ensure suitability of the selected CMOS process for the Peptidchip application in all stages, in addition to their main purpose of actually performing combinatorial syntheses.
- Fully combinatorial synthesis chips with detection features pave the way to integrated fluorescence signal detection. In the future, syntheses on chips with integrated detection structures might be performed.

¹ In an MPW run, or *multi-project wafer run*, several microelectronic designs are co-located on the same mask set, and processed at once. This results in a lower number of dies for each design per run, but as the expensive mask costs can be shared between numerous designs (potentially belonging to different customers), this is much cheaper than buying an individual mask set for design prototyping. For large dies, however, MPW runs become uneconomical, as not enough designs can be co-located on the mask set to yield sufficient advantages in price.

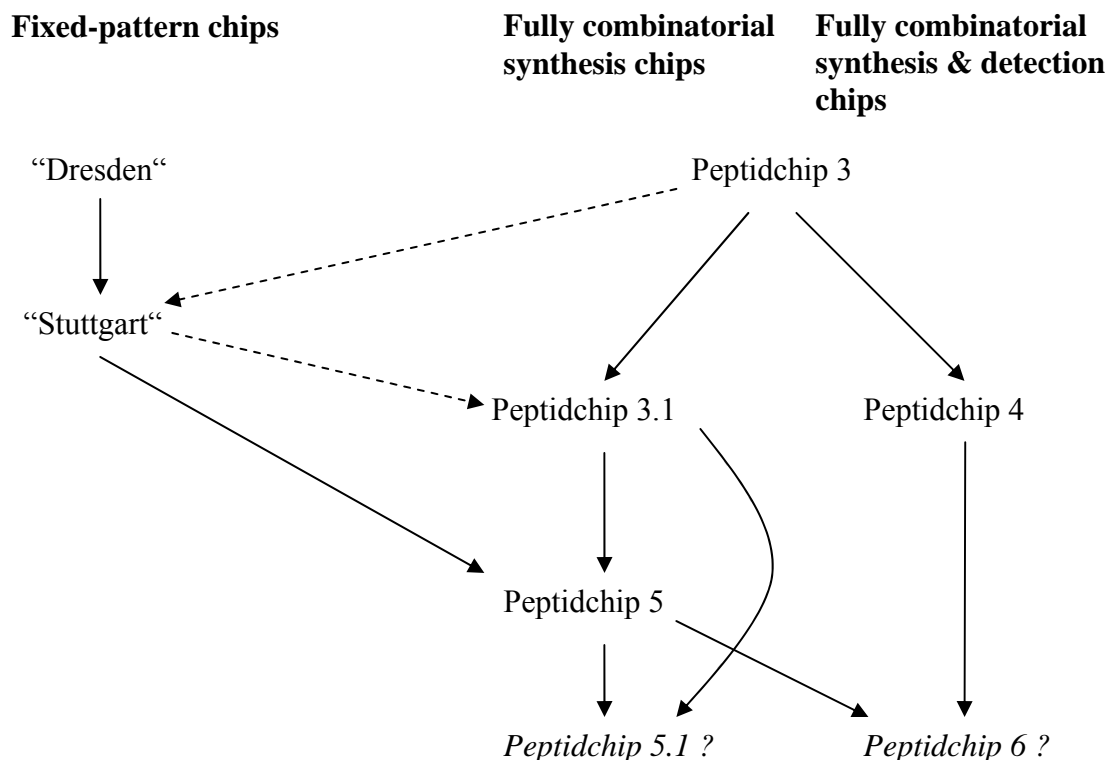


Fig. 5.1: Versions of the Peptidchip generations (see text).

5.2.2 Fixed-pattern Chips

Fixed-pattern chips were used to answer special questions regarding the aerosol, the surface modifications and the chemistry (e.g. 6.5.4.2). Some of them are described in greater detail elsewhere (4.3), [NES06, NES08]. Two sources of custom fixed-pattern chips were utilized, which are called "Dresden" [TUD] and "Stuttgart" [IMS] in this project. Several different chips are actually summarized under these labels. In all cases, they consist of a silicon wafer as support, aluminum wiring with silicon oxide insulation and silicon nitride passivation, but no active silicon elements (transistors or diodes). Therefore, pixels in these chips must be hard-wired to bond pads through which a voltage is supplied. Since several pixels must, for space reasons, share a bond pad, they cannot be used truly in a truly combinatorial way, but only in few specific patterns (usually checkerboard pattern or variants thereof). "Stuttgart" chips were used for the first on-chip synthesis [BEY07], after which their main purpose was achieved.

5.2.3 Fully Combinatorial Synthesis Chips

5.2.3.1 Peptidchip 3

Peptidchip 3, as described in 4.4, is the precursor of the fully combinatorial chips developed in the course of this thesis. As the semiconductor process used for this chip [AMI] was shown to be suitable, it was retained for all fully combinatorial chips.

5.2.3.2 Peptidchip 3.1

Peptidchip 3.1 was designed as a replacement for Peptidchip 3 when it became clear that the number of chips available was insufficient. Since Peptidchip 3 had been submitted in an MPW run, reuse of old masks was impossible. Therefore, it was possible to implement changes to the chip in order to improve usability without extra cost. Still, in order to save design time and allow re-use of the PCB, the coverings and the main board, most parts of the design of Peptidchip 3 were retained. As one significant change, it was decided to use a dedicated chip to further investigate optical detection, freeing room and bond pads on Peptidchip 3.1 by allowing the removal of all detection features. Peptidchip 3.1 is described in detail in 5.3.

5.2.3.3 Peptidchip 5

Peptidchip 5 is the first fully combinatorial CMOS chip for peptide synthesis. As such, it is built upon the experiences gained using the prototype chips Peptidchip 3 and Peptidchip 3.1, which were designed using the same semiconductor process. Additionally, it is the successor of the “Stuttgart” chip in being the support for large-scale synthesis [BEY07]. Peptidchip 5 is detailed in 5.4.

5.2.3.4 Peptidchip 5.1

One natural path of further development for the Peptidchip would be to minimize the spot size. The maximum spot size critically depends on what voltage is required by particle deposition, as the high voltage transistors that handle this voltage are dominant in determining pixel size. On Peptidchip 3 and Peptidchip 3.1, smaller pixels than those in Peptidchip 5 were already prototyped. Retaining the architecture of Peptidchip 5, a chip with a pixel pitch of 80 μm at 100 V maximum voltage, or 65 μm at 60 V, or 45 μm at 30 V could be built using the AMIS I2T100 semiconductor process (see 8.3).

5.2.4 Fully Combinatorial Synthesis and Detection Chips

5.2.4.1 Peptidchip 4

As the first CMOS chip specially designed for the development of integrated optical detection, Peptidchip 4 is based on the Peptidchip 3 design. Particle deposition and digital control components from Peptidchip 3 are reused in this chip. Only a summary of Peptidchip 4 is given here, as it is described in detail in [ZHA06].

At the time Peptidchip 4 was designed, no dedicated process with both HV and qualified optoelectrical components was available for use in this project. Therefore, the optical properties of the AMIS I2T100 process used [AMI] had to be investigated on this chip. Another key design objective was to retain the possibility of combinatorial particle-based synthesis on this chip, so besides some test photodiodes, this chip features 8×8 pixel matrices for deposition. A proof-of-principle synthesis and detection of fluorescent light, e.g. from an antibody binding experiment as those described in chapter 7, should be possible on this chip. However, due to its tiny size (total pixel area of ca. $2.5 \times 2 \text{ mm}^2$), performing a peptide synthesis on this chip is difficult for handling reasons.

A serious drawback of integrated detection compared to the use of fluorescence scanners is that no arbitrarily chosen spectral filter can be placed between the synthesized peptides and the photodiodes, thus limiting the fluorophores that can be utilized to those that lie in the range of the natural filtering properties of silicon. By burying the semiconductor junction deep in the chip, using UV light (which has a low penetration depth in silicon) as incident light and fluorophores with a large Stokes shift, sufficient filtering might be achievable [MER99]. Therefore, Peptidchip 4 features sandwich photodiodes, containing a combination of a surface photodiode and a buried photodiode in a P-N-P semiconductor structure. Signal read-out can be selected to use either only the buried photodiode or both photodiodes in parallel, depending on the application. An alternative method for filtering is the use of evanescent light generated by total reflection in a glass prism placed on top of the chip surface after peptide synthesis and array exposure.

The main components of the chip are the digital and direct controls taken from Peptidchip 3, four 8×8 pixel areas, and a read-out block for each pixel area. All pixel areas feature 30 V pixels, two of 100 μm and two of 150 μm pixel pitch. Each pixel contains a pre-amplifier in the form of a current mirror. A test current source can be used to characterize the amplifiers independent of the photodiodes. Using the digital control, individual pixels can be selected for read-out. The read-out blocks consist of an operational amplifier in integrator configuration with an external reset. It is connected to a comparator, which compares the integrator output to an external voltage, thus the signal strength can be determined by measuring the time between integrator reset and comparator triggering for each pixel. A second operational amplifier can be used with arbitrary external components and connected to an external analog-digital-converter.

The PCB of Peptidchip 4 was designed to have the same physical dimensions as that of Peptidchip 3 and 3.1, and a chip covering similar to the one for these chips was built, allowing to process this chip in the existing synthesis chamber (see 5.3.3.2). A main PCB for control and read-out of this chip was also built. This chip is currently being tested and characterized [TOR].

5.2.4.2 Peptidchip 6

A second development path for the Peptidchip system might be to integrate yet another function into the large-scale CMOS chip. Using results obtained with Peptidchip 4, photodiodes for detection could be integrated into a successor of Peptidchip 5 (see 8.3).

5.3 Peptidchip 3.1

5.3.1 Objectives

When performing experiments in particle transfer, in compatibility of the Peptidchip with surface modifications, and peptide synthesis chemistry, chips must be considered consumables, as they can only be surface-modified once. The number of Peptidchip 3 (see 4.4) samples obtained by the MPW run performed during [KÖN05] was not sufficient for all experiments needed. Therefore, new chips of similar specifications were required. The design was modified slightly based on previous experiments as described in 5.3.2. Notably, all integrated photo detection devices had been removed; as a separate chip for optical detection experiments was designed and submitted simultaneously to Peptidchip 3.1 (see 5.2.4.1).

Changes in the PCB and a newly built protective template and a chamber for peptide synthesis are described in 5.3.3.

5.3.2 Microelectronics

5.3.2.1 Changes from Peptidchip 3 to Peptidchip 3.1

Peptidchip 3.1, having been built to continue the experiments begun with Peptidchip 3, was to be designed to be compatible with the main and support PCBs designed for Peptidchip 3. Therefore, most of the design was retained. A top-level layout overview is shown in fig. 5.2. However, a number of changes have been implemented, as listed below.

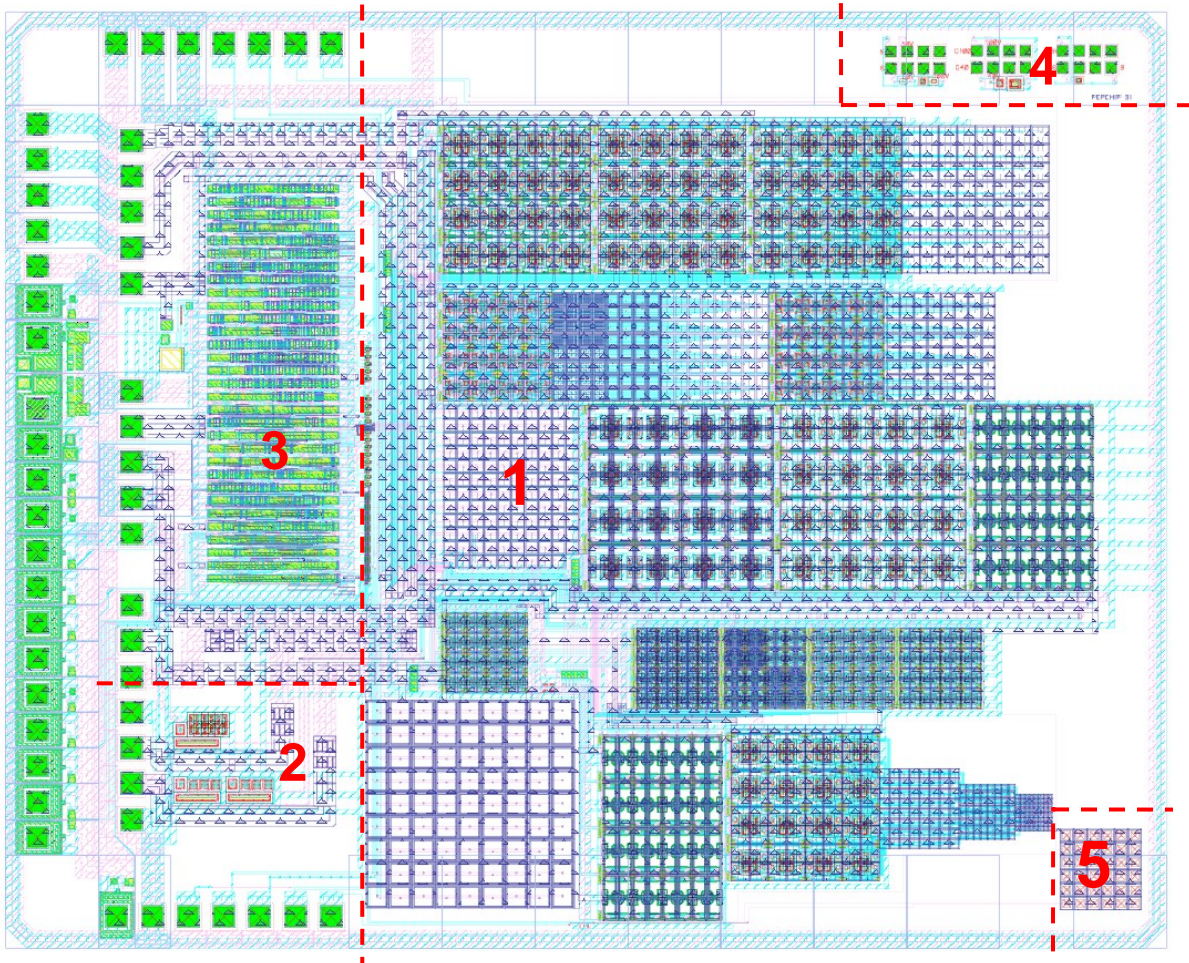


Fig. 5.2: Peptidchip 3.1 Layout. 1: pixel arrays (passivated). 2: bias voltage supply. 3: digital control. 4: test structures. 5: pixel array with passivation openings.

All structures for testing different semiconductor junctions for optical detection were removed, as the tests had been completed using Peptidchip 3. Thereby, all bond pads on the right side of the chip could also be removed. One additional pixel field of $100\ \mu\text{m} \times 34\ \mu\text{m}$ pixels at 30 V was added in the area thus made available.

All detection features were removed as well, as further detection experiments were to be performed with the dedicated Peptidchip 4. This simplified pixel and supply layouts, freeing both silicon and interconnect area. This also reduced the number of bond pads required by 10.

In order to free further bond pads and chip area, the test outputs connected directly to the HV pixels were also removed.

The multipol pixel arrays [KÖN05, NES06] were removed, with further testing of the multipol concept to be conducted on fixed-pattern chips. They were replaced with arrays of $50\ \mu\text{m} \times 50\ \mu\text{m}$ and $100\ \mu\text{m} \times 100\ \mu\text{m}$ fixed-pattern pixels which can be used to test functionality of particle deposition independently of the electronics (see 5.3.2.2 and 6.5). In addition, all pixels in the main area of the chip are completely passivated in Peptidchip 3.1, with the intention of reducing the risk of chemicals intruding into the chip. In a corner of the chip, an independent fixed-pattern 4×4 array of $50\ \mu\text{m} \times 50\ \mu\text{m}$ pixels with passivation openings has been added for cross-checking such influences.

Using the space made available by removal of detection-related devices and interconnect, the high voltage interconnect was re-routed. In the area of the pixel arrays, all HV interconnect at 60 V or 100 V was routed to lower metal layers and covered with ground or 30 V tracks to avoid the higher voltage tracks from influencing particle deposition as it was observed with Peptidchip 3 [KÖN05]. Since Peptidchip 3 produced shorts with some frequency, seemingly at random (see also A3), the HV routing was also modified to increase spacing between HV tracks in critical areas where melting of metal tracks and the chip surface was observable after shorts.

As a side effect of these changes, the number of bond wires required could be reduced to 46, and the number of contacts to the main board to 38, which allowed (with one minor modification in the main board assembly and a new support PCB) to contact the chip using only one instead of the previous two connector cables. The number of second-row bonds, which proved difficult to handle as their length and height made them mechanically sensitive e.g. in strong air streams, was reduced from 28 to between 5 and 12, though such bonds could not be completely avoided without giving up compatibility to Peptidchip 3 electronics.

5.3.2.2 Description of Pixel Arrays

A detailed list of all 25 pixel areas on Peptidchip 3.1, including their logical addresses for using the I²C interface, is provided in tab. 5.1, with their locations on the chips shown in fig. 5.3. Most pixels were designed for minimum size possible using the high-voltage inverters for the given voltage. The size given is total pixel pitch p (distance from the center of a pixel to the center of an adjacent pixel). This includes the grid electrode between pixels (width $g = 6\ \mu\text{m}$ unless noted otherwise) and spacing between grid electrode and potential area (always $2\ \mu\text{m}$ each), as shown in fig. 5.4. The size of the potential area x thus is given by

$$x = p - g - 2 * 2\mu\text{m} . \quad (\text{Eq. 5.1})$$

All of these pixel areas, except for pixel area y) are completely passivated.

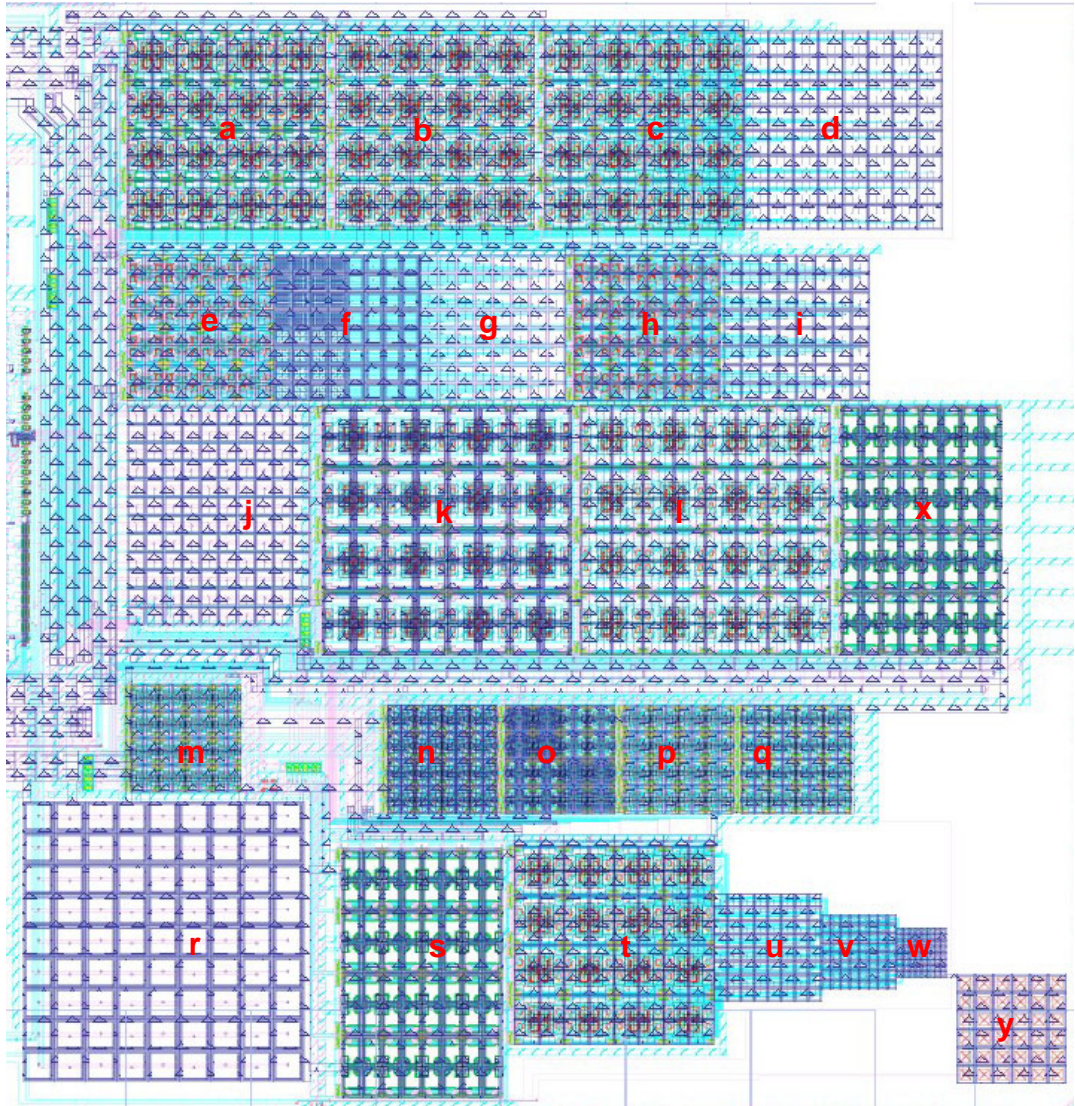


Fig. 5.3: Positions of the pixel arrays on Peptidchip 3.1. See tab. 5.1 and text.

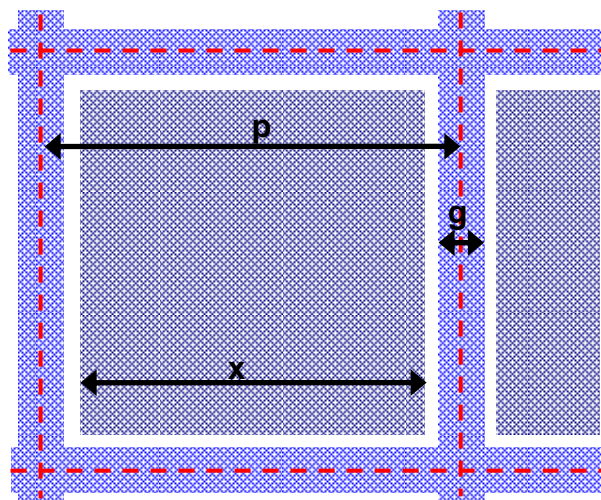


Fig. 5.4: Relation between pixel pitch p , grid electrode width g and potential area size x . The borders between pixels are drawn in red dashed lines.

Position	Address				pixel pitch [$\mu\text{m} \times \mu\text{m}$]	max. voltage [V]	notes
	Xblock	Yblock	X	Y			
a)	0	0	0	0..7	79.7×79.7	100	
b)	0	0	1	0..7	79.7×79.7	100	$g = 21 \mu\text{m}$
c)	0	0	2	0..7	79.7×79.7	100	
d)	0	0	2	0..7	79.7×79.7	100	
e)	0	1	0	0..7	58.6×58.6	60	
f)	0	1	0	0..7	58.6×58.6	60	
g)	0	1	0	0..7	58.6×58.6	60	
h)	0	1	3	0..7	58.6×58.6	60	$g = 12 \mu\text{m}$
i)	0	1	3	0..7	58.6×58.6	60	
j)	hard-wired, 10×12				50.0×50.0	100+	
k)	0	2	1	0..7	100.0×100.0	100	
l)	0	2	2	0..7	100.0×100.0	100	
m)	0	3	0	0..7	43.8×43.4	30	
n)	0	3	1	0..7	43.8×43.4	30	
o)	0	3	2	0..7	43.8×43.4	30	
p)	0	3	3	0..7	43.8×43.4	30	
q)	0	3	4	0..7	43.8×43.4	30	
r)	hard-wired, 9×9				100.0×100.0	100+	
s)	0	4	1	0..7	43.8×100.0	30	
t)	0	4	2	0..7	79.7×79.7	100	
u)	0	4	2	0..7	43.4×43.4	100	
v)	0	4	2	0..7	30.0×30.0	100	
w)	0	4	2	0..7	20.0×20.0	100	
x)	0	2	3	0..7	43.8×100.0	30	
y)	hard-wired, 4×4				50.0×50.0	100+	passivation openings

Tab. 5.1: List of the (normally 8×8) pixel arrays on Peptidchip 3.1, see fig. 5.3 for positions.

The hard-wired pixels are directly contacted to a bond pad by metal tracks, like in fixed-pattern chips. The passivated fixed-pattern areas j) and r) can be configured into repeating 2×2 patterns using four supplies, while the independent area with passivation openings y) only has two supplies, each wired to every other pixel. All of these hard-wired pixels are limited in voltage only by the break-down voltages of the oxide between metal tracks, the PCB and the air between the bond wires. Preliminary tests found them to be able to withstand at least 280 V.

The I²C software for controlling the chip using a LabView VI and the parallel port of any PC was updated to support these changes by its author [TOR].

5.3.3 Packaging, Electronic and Mechanical Supports

5.3.3.1 Support PCB

While the main PCB remains mostly unchanged from [KÖN05], the support PCB was simplified. Fig. 5.5 shows the layout of the two-layered Peptidchip 3.1 support PCB.

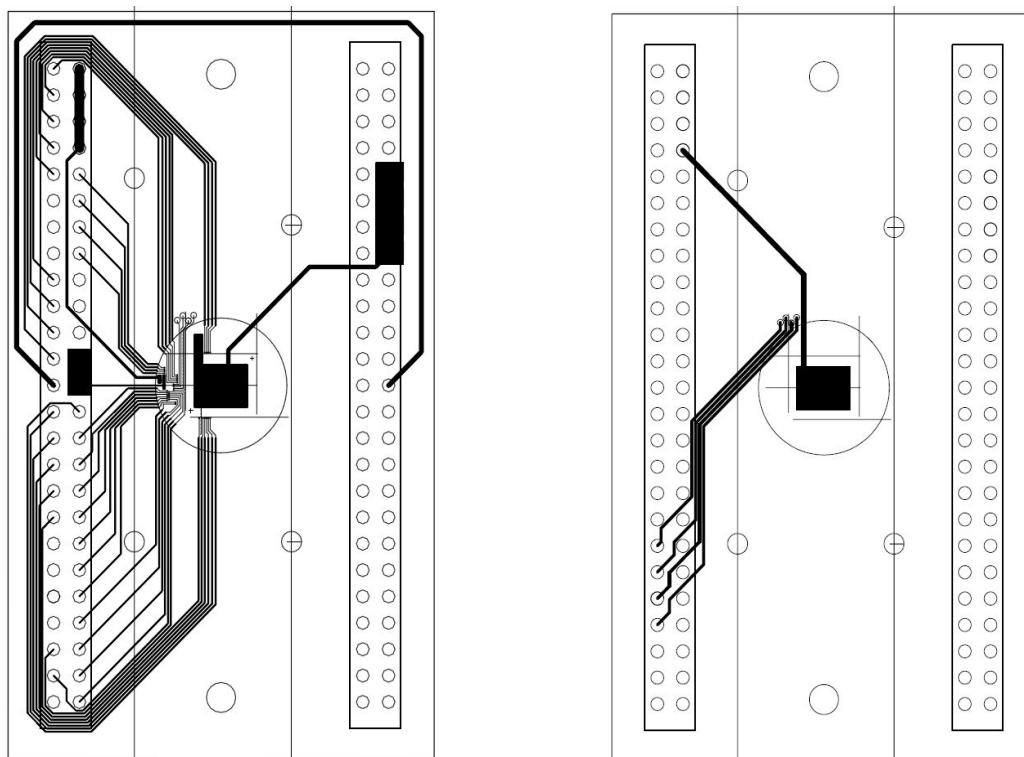


Fig. 5.5: The support PCB for Peptidchip 3.1. Left: top layer, right: bottom layer. See A2.1 for a detailed view of the bond area. Only the left connector is used. Six holes are provided for mounting the chip covering.

In contrast to the previous board, where holes for mounting the chip covering (see 5.3.3.2) had to be drilled by hand, the new board includes holes for fixing the chip covering. The pin layout of the connector cable can be found in A2.1. The connector on the right is retained for compatibility with Peptidchip 3, but remains unused in the standard setup.

5.3.3.2 Chip Covering

While the chip itself is resistant to all chemicals used in peptide synthesis, standard PCBs are less resistant to these substances. Additionally, the bond wires are sensitive to the mechanical stress of liquids moving by them during chemical steps, and to a lesser extent to the moving air during deposition or cleaning of a chip in a strong air stream. GlobTop also proved unable to withstand the chemicals used [KÖN05], and is difficult to apply without covering the pixel areas as well. Therefore, mechanical coverings made of Teflon were designed to protect both the bond wires and the PCB. They are fitted to the PCB using an aluminum back-covering. First, the PCB is pushed onto the back-covering using alignment pins. Then, the Teflon covering is cautiously slid onto the pins, and fixed with four screws. As there is insufficient room on the chip for the use of an o-ring seal and Teflon exhibits some plastic flow under pressure, the Teflon template is simply pressed onto the chip to form a tight seal. It should be noted that, for lack of space, some of the outer pixels are hidden under the covering when it is installed. These pixels can only be tested in the aerosol when the covering is not in place.

While the pressure applied by the covering alone is sufficient to seal the bond wires and board against the airstream and particles, that pressure is not sufficient to guarantee a seal that is impermeable to liquids. The seal becomes liquid-tight when mounted into the matching synthesis chamber (fig. 5.6). The connection between chamber and covering is sealed using a

resistant o-ring. The chamber and covering allow the chip to be exposed to any liquid, while the chamber also offers room for a magnetic stirring bar.

In A3, further instructions for mounting the chip covering and installation into the synthesis chamber are given.

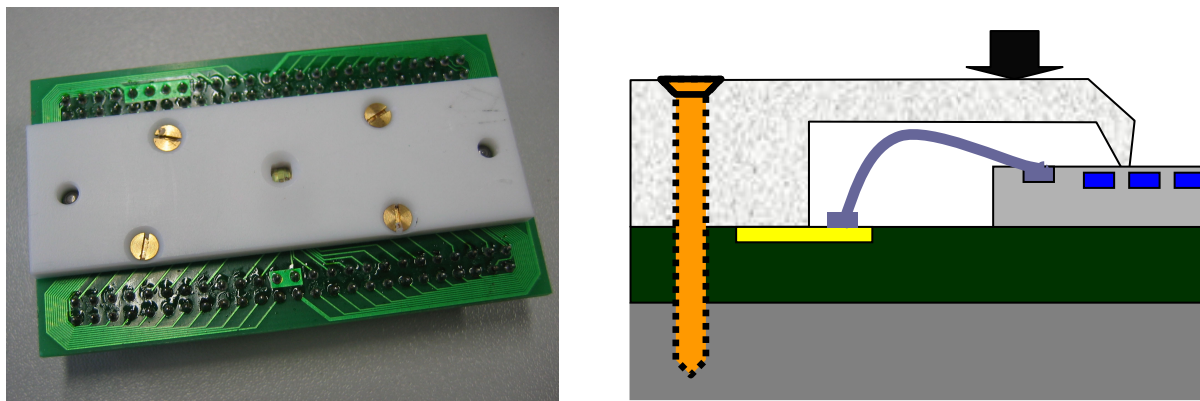


Fig. 5.6: Left: Peptidchip 3 mounted in chip covering. The chip is exposed through the central opening in the Teflon covering. Right: Sectional drawing (not to scale) of the chip and its covering, showing the area around the seal and bond wires. The arrow shows the area where the synthesis chamber o-ring contacts the covering.

5.4 Peptidchip 5

5.4.1 Design Requirements

Peptidchip 5 is the first Peptidchip to be useable in peptide array experiments of a large scale. To this end, not only a large number of synthesis sites are required, but it must also be reliable and easy to use. It should be adaptable to an automated deposition and synthesis environment, which is currently being developed [PAI10, LOE].

Design components from Peptidchip 3.1 were reused in Peptidchip 5 in order to reduce design time where possible, taking the larger size of the chip into account. In particular, the same semiconductor process as used for Peptidchip 3 and Peptidchip 3.1, AMIS I2T100 [AMI], was used, both because the surfaces in this process had already been tested (see 6.5) and to allow straightforward reuse of design components. Future availability of this process, which is widely used in other applications such as automotive components, was ensured by the manufacturer.

Key design objectives of Peptidchip 5 were:

1. *Reliability*: Good chances for a chip to survive particle transfer and the synthesis process are more important than extra features or synthesis site density.
2. *Suitability for development*: The chip must be suitable and conveniently usable in experiments to develop the other components of the particle transfer and peptide synthesis systems until they are ready for application.
3. *Suitability for application*: The chip must be easy-to-use in peptide array experiments once the complete synthesis system is ready.

4. *Large number of synthesis loci:* Only if a significant number and density of synthesis sites are provided, the use of a chip is worth the cost and effort. For this chip, a minimum of 10,000 sites was set as a design requirement.
5. *Design for reuse:* As the deposition and synthesis system was still in development, the possibility for a need for changes in the chip design to improve suitability to deposition and synthesis could not be ruled out. In case of a need for changes, or in case of future miniaturization, design parts should be reuseable in order to minimize redesign time.

This chip was submitted in two mask variants of the pad window mask and the top metal mask. In the first variant, the passivation over the pixels was closed, which should make the chip more resistant, but requires special care with the surface modification to avoid shielding of electric fields (see 6.5). The second mask variant features pad openings similar to bond pads in each pixel, increasing flexibility and reliability with regard to the surface modifications. The performance of each of these variants is described in 6.3.

5.4.2 Microelectronics

5.4.2.1 Overview and Top Level Design

The design of Peptidchip 5 was performed with several aspects considered:

- Layout of the pixels (synthesis sites) for electrostatic particle transfer
- High-voltage design of the pixels, using full-custom layout techniques.
- Design of the digital interface using VLSI techniques.
- Combining the digital and analog parts into a mixed-signal design.
- Considerations of mechanical stress imposed by a liquid-tight package and handling.

The design is described by component in the following chapters: In 5.4.2.2 the synthesis sites are detailed, in 5.4.2.3 supply and control are shown, while the mechanical considerations are elaborated on in 5.4.2.4. Top-level design and floorplan aspects are detailed below.

Maximum chip size limits the number of pixels, and in turn is limited by the reticle size of the semiconductor process. The chip size was chosen to be 19.8 mm × 19.0 mm, which is close to the absolute maximum. The 0.9 mm × 19.0 mm area on the “left” edge of the chip was designated for the digital part, supply components and bondpads (see 5.4.2.3), while the remaining 18.9 mm × 19.0 mm were used for the main part of the chip. The latter consists of the pixels in the center surrounded by a seal area without semiconductor structures and the sole purpose of supporting a sealing o-ring from the chip covering (see 5.4.3.3) (fig. 5.7).

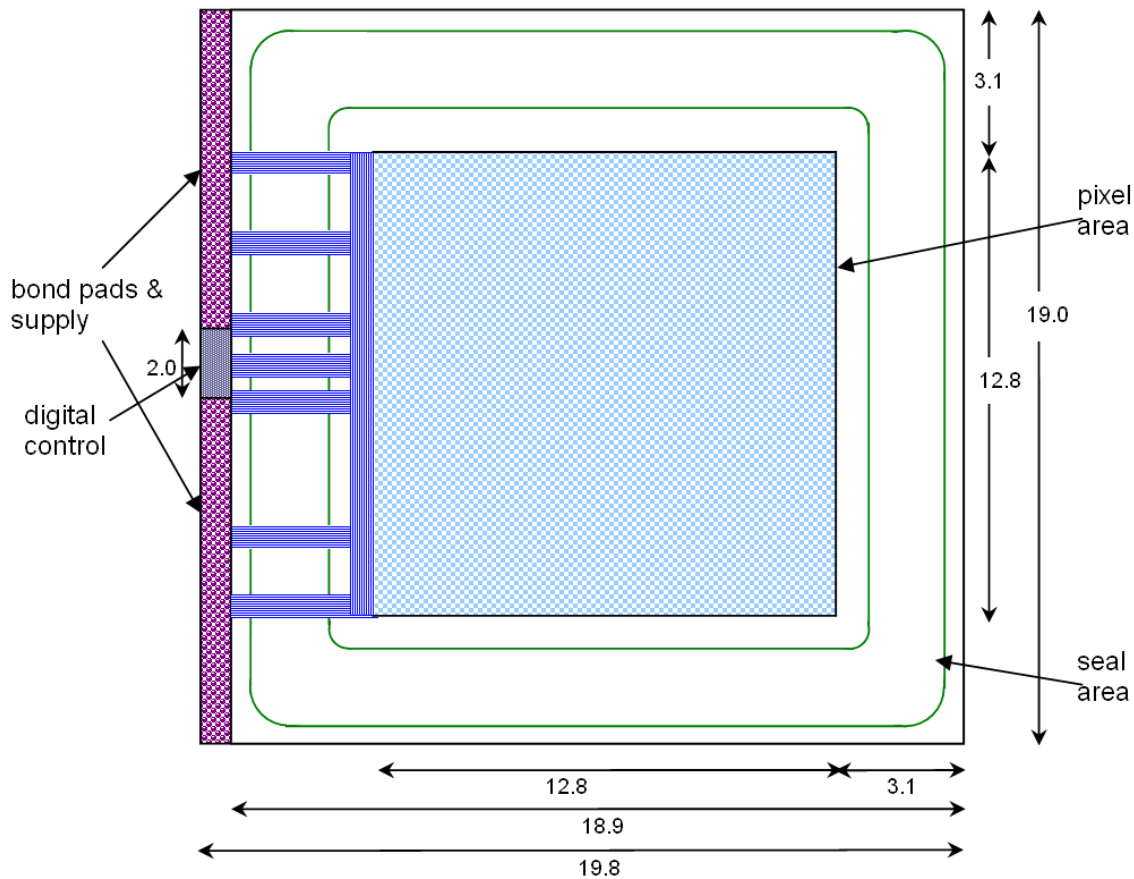


Fig. 5.7: Floorplan of Peptidchip 5. The pixel area is surrounded by the seal area where the o-ring seal contacts the chip, protecting the bond wires and PCB. The pixel area is connected to the digital control, supply area and bond pads outside the sealed area, which connect the chip to the main PCB. All measurements in mm.

5.4.2.2 Pixel Area

Overview

Only one type of pixels and no test structures except for a set of test transistors contactable by probe needles have been implemented on this chip. A conservative pixel size of $100\ \mu\text{m} \times 100\ \mu\text{m}$ was chosen for this chip in order to improve both particle transfer quality on an area that is large compared to the particles and electric reliability by making more room for high voltage supply metal tracks. This size still allowed 128×128 pixels to be implemented on the chip, which exceeds the requirement of 10,000 pixels total by a factor of more than 1.6. The schematic of these pixels could be copied from Peptidchip 3.1, but the layout (fig. 5.8) had to be remade in order to enable higher power densities. Pixels are controlled in rows of eight that are written simultaneously by the digital control.

All local routing is kept on polysilicon and the bottom metal layer, part of which is also used for routing parallel to the Y-axis of the chip. The second metal layer is used for routing in parallel to the X-axis exclusively, while the third metal layer is used for the pixel and grid electrodes.

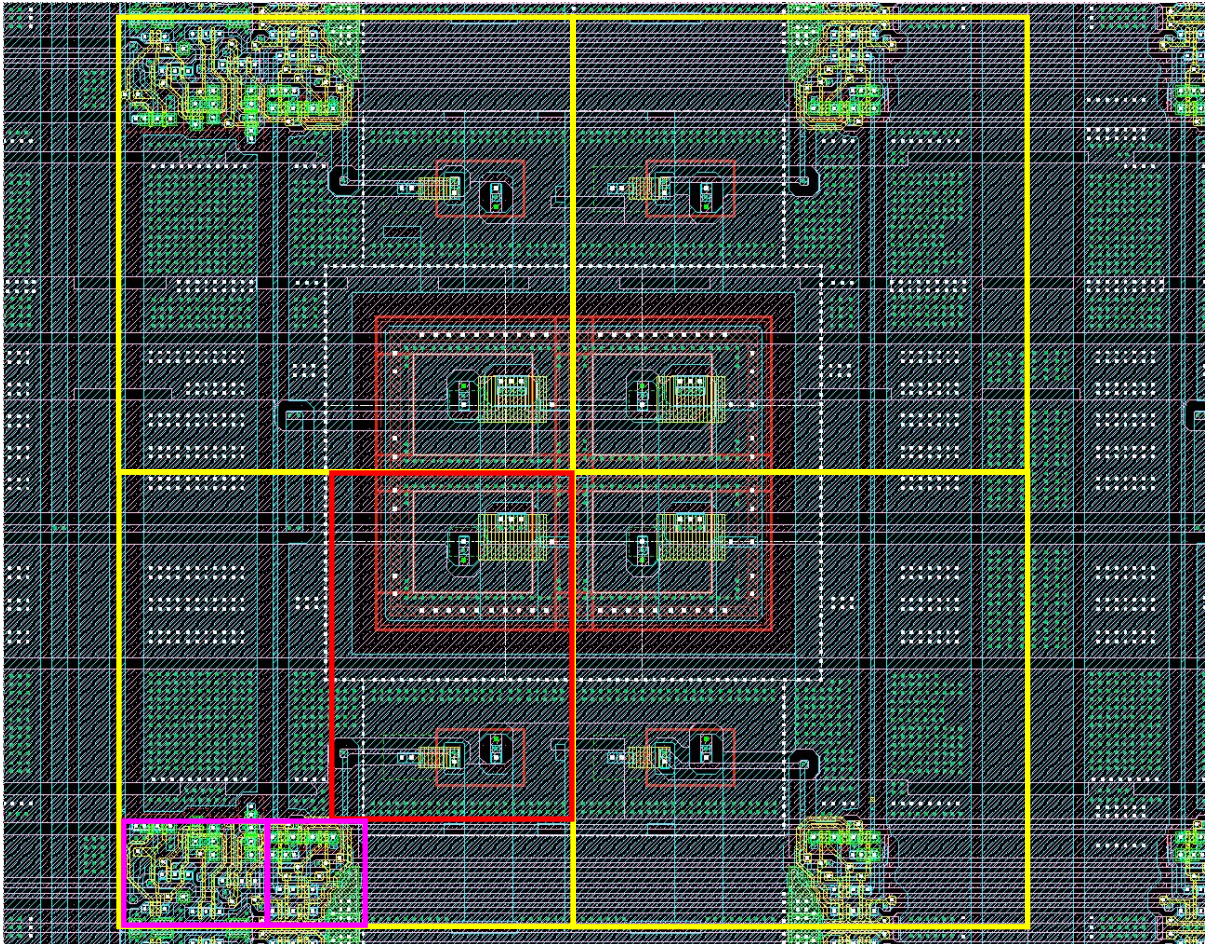


Fig. 5.8: Group of four pixels (yellow rectangles). In the lower left pixel, the high voltage inverter (red) and the digital control (magenta, left part: common control for a row of 8 pixels, right part: control of each pixel). Top metal layer and pad window layer are not shown for better visibility of other layers.

Pixel Low-Voltage Control

As in the previous Peptidchip models, rows of eight pixels are simultaneously written by the interface [KÖN05]. A common control (fig. 5.9) for every row of eight pixels is implemented under the first pixel of each row, generating complementary write signals (DATAENABLE and NOTDATAENABLE) for writing data to the pixels and read signals (READBACKENABLE and NOTREADBACKENABLE) for reading the pixel memory cells back out via the I²C interface. The read signals are not used, however, because the buffers for the serial data signals DATA[0..7] are for write only, as previous Peptidchips showed little need for the read back functionality. The area used by each common control cell fits into a $42\ \mu\text{m} \times 26\ \mu\text{m}$ rectangle.

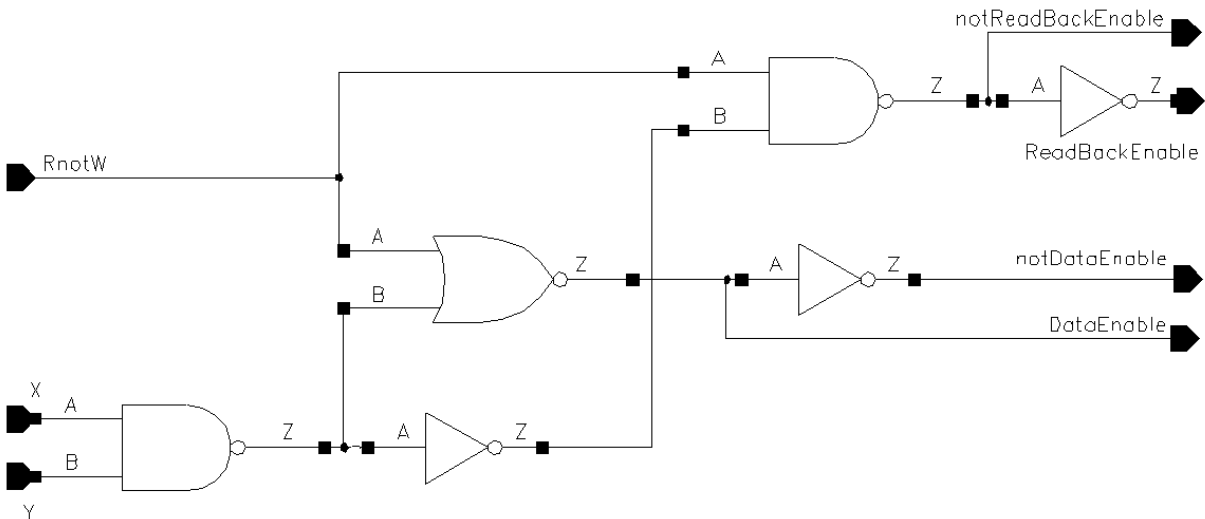


Fig. 5.9: Common control for a row of 8 pixels (modified from [KÖN05]).

Each pixel contains a memory cell (fig. 5.10) of two tri-state inverters and one inverter plus one tri-state inverter for reading back (not used), the area consumed by each memory cell is less than $25 \mu\text{m} \times 26 \mu\text{m}$. The total for one block containing common control and memory cell is only $54 \mu\text{m} \times 26 \mu\text{m}$ because of synergy effects (shared guard rings, substrate and well contacts). The inverting output of each pixel memory cell is connected to the input of the high-voltage inverter of the corresponding pixel.

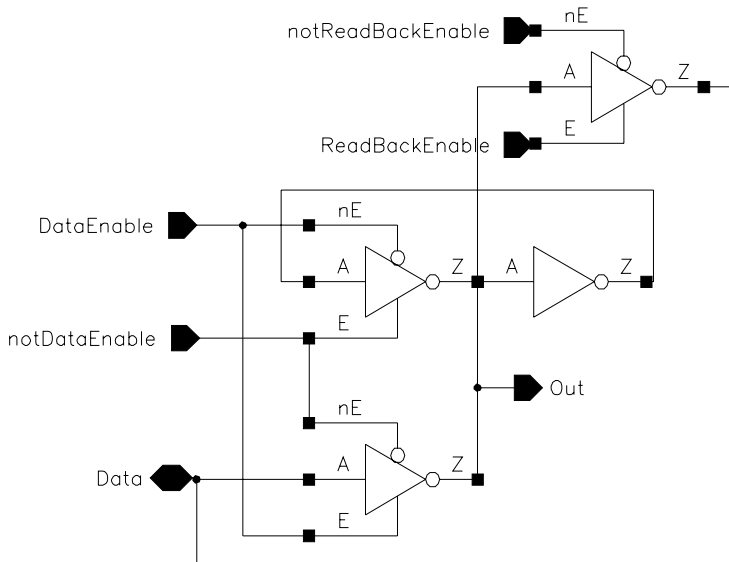


Fig. 5.10: Schematic of a Peptidchip pixel memory cell using tristate inverters (taken from [KÖN05]).

Pixel High-Voltage Components

The high-voltage “output” of each pixel is the potential area, which projects the electric field for selective particle deposition into the volume above the chip surface. Each potential area is sized $84 \mu\text{m} \times 84 \mu\text{m}$. On the chips with passivation openings, the central $76 \mu\text{m} \times 76 \mu\text{m}$ of

each potential area aluminum are exposed. The capacitance of each potential area has been approximated as less than 1 pF [KÖN05].

The potential area is connected to an HV-NMOS and an HV-PMOS which form an HV-pull-up-inverter. The resistance of the HV-PMOS can be tuned by setting the bias voltage, generated on chip, which allows to trade-off power consumption and pixel charge time (see 5.4.2.3).

5.4.2.3 Supply and Control

Digital Control

The digital control used in Peptidchip 5 is a re-laid-out version of the Verilog design (including I/O delay and bondpads) described in [KÖN05], consisting of a modified I²C interface [PHI00] and a memory control capable of addressing up to 65,536 rows of eight pixels, for a total of up to 524,288 pixels. As the memory cells in the pixels are level sensitive, not edge sensitive, in order to save space, the address signals must be glitchless. This is ensured by the design of the XYEnable and XYEnableGenerator components, that only enable the address signals after their settling times and disables them before the start of the next I²C cycle by using a delay generated from the I²C clock signal SCL, which is also the only clock used on the chip.

Like in previous Peptidchip series, the pixels are organized in bytes of eight that are simultaneously written, and the whole chip can be written by a single I²C access. The address of each byte consists of four coordinates, with logical addresses between 0 and 15 for each coordinate: Y, the row coordinate, X the column coordinate, YBLOCK, the coordinate of the Yblock of 16 rows in relation to the other Yblocks, and XBLOCK, the coordinate of the Xblock of 16 columns. Of these addresses, only XBLOCK = 0 and YBLOCK = [0..7] are needed to address the 2,048 bytes of pixels on the chip. The chip is divided into matrices of 8 × 8 pixels both by layout and by organization, which are written by a consecutive write in ascending order of YBLOCK, X and Y as shown in fig. 5.11. Alternatively, each byte can be written individually.

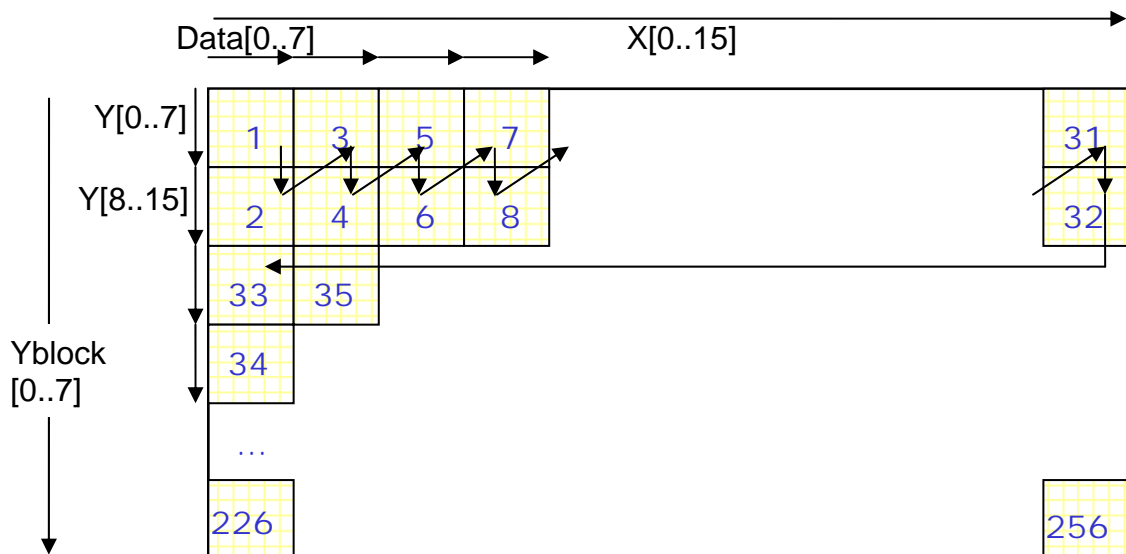


Fig. 5.11: Write order of the matrices of pixels on a Peptidchip in a consecutive write starting at YBLOCK = 0, X = 0, Y = 0. The numbers give the order in which the matrices are written by an I²C consecutive write. Within each matrix, its 8 lines (Y[0..7]) are sequentially written, top to bottom.

The bytes transmitted in each I²C access are interpreted by the memory control as follows: The first byte contains the address of the I²C device (14 for all Peptidchips) and the mode bit (read or write mode). In write mode, the following byte contains eight command bits that are written into the CommandReg register, which are used for the timing of the XYEnableGenerator. Normally, this byte should be “00000000”, which sets the values to their defaults. In the future, this data could be used for other purposes, as the chip is functional using the default timing. The following two bytes contain the address of the first pixel to be written to during this I²C access, in order XBLOCK, YBLOCK, X and Y, with four bit each, which are concatenated into the XYReg register. Each subsequent byte sent to the chip via the I²C is written to the DataReg register, and transferred to the pixels during the subsequent I²C cycle. After each byte is written to the pixels, the address stored in XYReg is counted up by one, so that the next byte is written to the subsequent address. Note that due to this mode of operation, after the last byte of data to be written to the chip is sent, another dummy byte of data must be sent over the I²C, in order to ensure transfer of the last byte from DataReg to the pixels. In I²C read mode, the contents of CommandReg and XYReg (the current address) are written onto the I²C bus by the chip, but read back of the pixels as in previous Peptidchip versions has not been implemented.

Direct Control and Buffers

The direct control, which has been retained in the design from Peptidchip 3.1, allows programming Peptidchip 5 with simple repetitive 4×4 patterns without using the I²C. As the direct control is completely asynchronous, no signals over the I²C, including the clock signal, are needed, and programming is possible using simple switches, which is favorable for quick tests of function in the aerosol. The direct signals are multiplexed into the wires routed from the digital control to the pixel areas using multiplexers. The DATA[0..7] signals are generated within the digital part for both modes, but in the direct mode, they do not require the I²C clock SCL.

All data signals are routed through the seal area in a straight line on the intermediate metal layer with no bends or different signals or supply crossing over one another, and all spacings have been at least doubled from the design rules in order to increase the maximum pressures the chip can withstand (see A3). Parallel to all data or supply lines, ground lines on the bottom metal layer used as substrate contacts are routed.

Due to the increase in size compared to Peptidchip 3, an additional set of buffers for all signals has been implemented on the edge of the pixel area. There, a set of Y signals is generated for each Yblock using AND gates (fig. 5.12).

An order of magnitude approximation for the capacitive load of wires has been performed. For a wire of 30 mm on the lowest metal layer, a resistance of less than 1 k Ω and a total capacitance of less than 10 pF have been calculated, resulting in an time constant $\tau = RC$ of less than 10 ns. This calculation assumes a perfect driver, but has been verified by a Cadence simulation using the model of a comparable driver, which resulted in a delay of 6 ns. These values are several orders of magnitude smaller than the 125 μ s of one I²C clock cycle, and thus satisfactory.

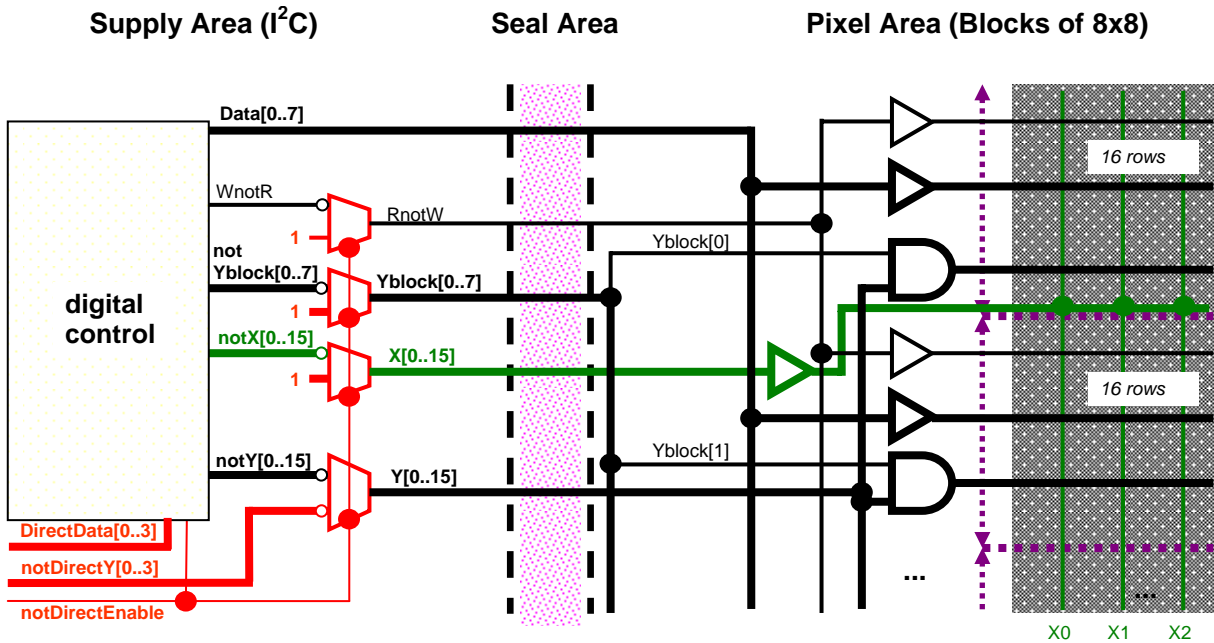


Fig. 5.12: Concept drawing of the relationship between supply area and pixel area. The direct control is triggered by NOTDIRECTENABLE, which is directly connected to a number of select gates, inside the digital part written in Verilog for DIRECTDATA and in the full custom part for the other signals. All address signals are routed from the supply area through the seal area into the pixel area where the signals are distributed over all blocks, with extra buffers to compensate for the long wires.

Bias Voltage and Power Supply

Power consumption of Peptidchip 5 is dominated by the HV inverters. With the HV-NMOS in the off-state (pixel at 100 V), transient power consumption is minimal, but with the HV-NMOS in the on-state (pixel at 0 V), power consumption is high, and depends strongly on the resistivity of the biased HV-PMOS. The concept of the bias voltage generator has been retained from Peptidchip 3 [KÖN05], however, an 100:1 current mirror has been used for Peptidchip 5 instead of the 10:1 current mirror of Peptidchip 3 in order to be able to increase the external current to around 100 μA for a transient power consumption of around 1 μA per pixel. At 100 V, this corresponds to a power density $P = U \cdot I$ of 100 μW per pixel or 10 mW / mm^2 . This value resulted in no significant heating of the chip on Peptidchip 3.

Supply metal width was maximized, and is capable of providing more than 3 mA per row, or more than 23 μA per pixel within the process specifications, thus leaving a more than 20-fold margin of security under worst case conditions (maximum power consumption, all pixels turned off). Supply tracks from the bond area to the pixel area are designed at similar maximum power. Together with the pixel area buffers, these supply tracks take up another 0.3 mm on the left side of the pixel area.

5.4.2.4 Mechanical Considerations

In order to allow secure placement of the o-ring seal with an o-ring of 1 mm width by hand, a seal area of at least 2 mm was considered desirable. With the pixel area including associated buffers and supply tracks occupying the central 1.31 mm \times 1.28 mm, the seal area is 2.7 mm on the smallest side (towards the I²C) and 3.1 mm on all other sides.

In order to allow contact or near-contact particle transfer techniques, which were still in the conceptual stage during the design of Peptidchip 5, three contact sensor pads have been added to the design. These pads, called *contact detection pads*, are simply $580 \times 280 \mu\text{m}^2$ (size of passivation opening) bond pad structures on the edges of the chip, near the corners of the pixel area, that are connected to bond pads in the bond area. If a suitable conductive spacer, such as the ball of a ball bond², is placed onto the contact detection pads, they can be used to detect contact to a conductor using external circuitry connected to the output bond pads. In addition, a ring of additional bond pad structures without electric functionality, called *spacer pads*, has been placed onto the three edges of the chip that are not used for electrical contact bonds (fig. 5.13). These structures could be used to add ball bonds or other metallic structures functioning as spacers in the sub-millimeter distance range, or alternatively to mount the chip as a flip-chip on a PCB with a hole in the center to expose the potential area. Due to their location on the edge of the chip, outside the seal area, the contact detection pads and spacer pads are not useable with the chip covering installed.

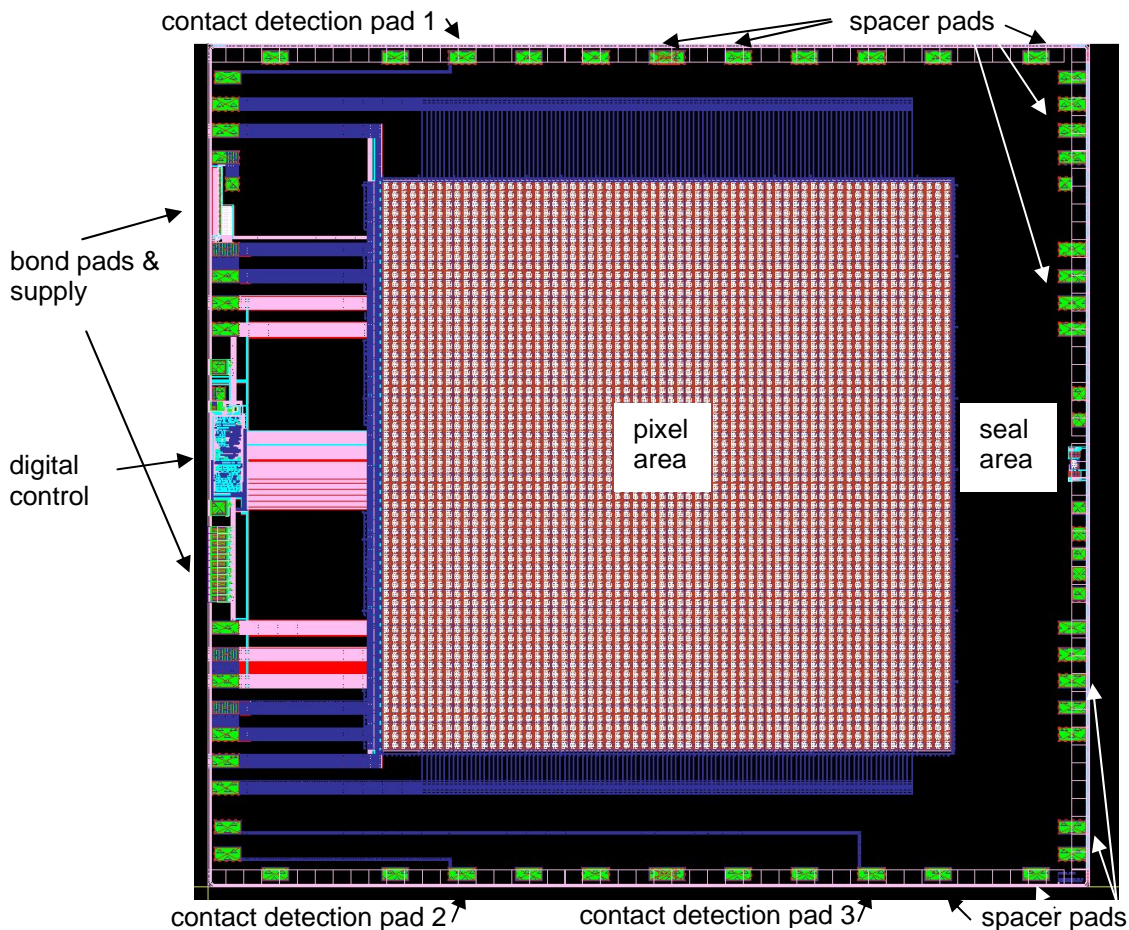


Fig. 5.13: Top-level layout of Peptidchip 5. The locations of all main components (see fig 5.3) and of the contact detection pads and spacer pads are shown.

² Ball bonds are an alternative to wire bonds in which a ball of metal (e.g. gold) is placed onto the chip in each bond location. Wires are then drawn from these balls to the corresponding site on the PCB, or vice versa. Alternatively, in flip-chip bonding, only the balls are placed without wires being drawn, and the chip is then “flipped over” onto a matching PCB, with contacts in locations directly corresponding to the bond pads on the chips, and then pressed onto the balls. The diameter of such balls can range from approx. $20 \mu\text{m}$ to $80 \mu\text{m}$.

5.4.3 Packaging, Electronic and Mechanical Supports

5.4.3.1 Support PCB and Bonding

The PCB used for Peptidchip 3 was built for use in particle transfer experiments, and not optimized for handling in a peptide synthesis. Connecting the PCB using pin connectors is hard to automatize and requires an amount of mechanical force that makes careful handling difficult. Furthermore, pins are prone to bending. Long bond wires were prone to detachment and failure due to mechanical stress in the airstream or in case of accidental contact with objects. Finally, in synthesis experiments, the Peptidchip 3 PCB cannot fit into standard array scanners for glass slides that are normally used, so the chip had to be removed from the PCB and fitted into a custom-made holder for detection.

In order to avoid these issues, the PCB for Peptidchip 5 was designed to match the format of a standard microscope glass slide. The 0.5 mm thick chip is placed inside a cavity, so that the chip surface is on level with the PCB front (see 5.4.3.3). This also ensures minimal bond wire length, as the wires run straight from the PCB contact to the chip (fig. 5.14). The PCB size is within the tolerance limits of microscope glass slides and measures 76 mm × 26 mm × 1.1 mm (except for indents at the side of the PCB that is used as connector), so the PCB fits into array scanners for glass slides. Other equipment, such as transport boxes and microscopes for handling or examining glass slides, which is standard equipment in most biology laboratories, can also be used with no or little adaptations. For contacting the chip, contacts are placed on the PCB similar to PCI cards in PCs. The PCB thus can be plugged into part of a standard PCI connector socket. The contacts are large enough to allow for the use of contact pins as an alternative.

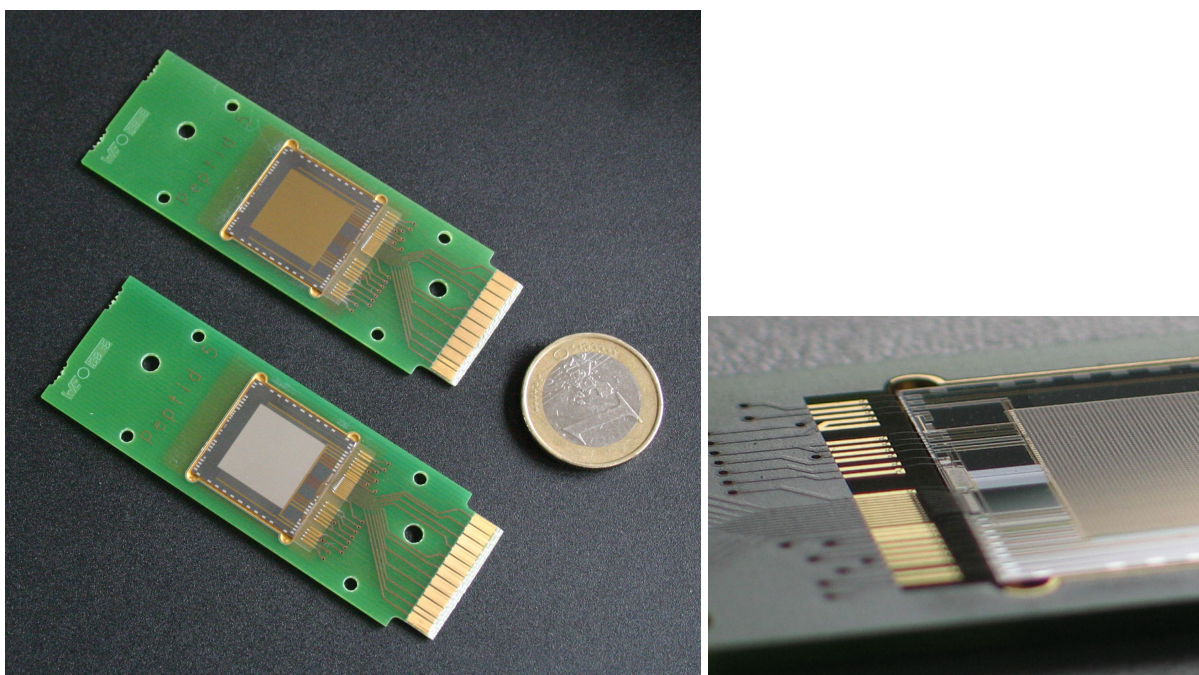


Fig. 5.14: Left: Both mask variants of Peptidchip 5 on the support PCB (with 1 Euro coin as size reference). The potential areas of the pixels can be seen as the large golden or silver area in the center of each chip, surrounded by the dark seal area. Top chip is completely passivated; bottom chip has a passivation opening on each pixel. The bond wires and bond contacts are on the right side of each chip. They are wired to the PCB connector on the right edge of the PCB. Right: Close-up of the chip in the cavity, showing the flat and short bond wires.

5.4.3.2 Main PCB

The *main PCB* (fig. 5.16) is used to connect the chip to the required power supplies, the laboratory PC for I²C programming, and for direct programming. It also provides the bias current from which the bias voltage for the HV-PMOS in the pixel HV inverters is generated on-chip. In addition, it contains probe contacts for all important signals.

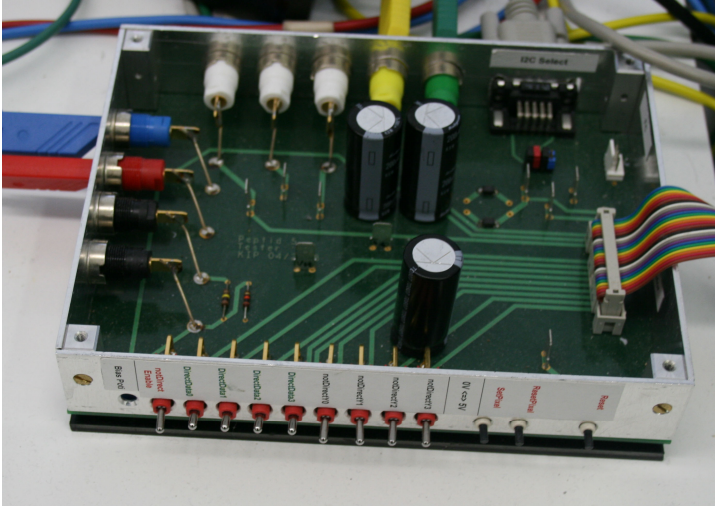


Fig. 5.16: Main PCB for Peptidchip 5 power supply, bias current generation, I²C interface, and direct control, in its casing.

In detail, it consists of the following parts (the corresponding schematics are found in A4):

1. The *chip connector jack* is where the ribbon cable connecting to the chip is plugged in. This ribbon cable ends in a modified PCI jack, into which the support PCB fits.
2. The *I²C connector* includes a D-SUB and a pin connector to receive the signals from the I²C master controlling the chip. It also contains the overvoltage protection diodes required.
3. The *power supply* provides the banana jacks to plug in the required laboratory power supplies for LV and HV. Filtering capacitances are also included. The contact detection pads are connected to banana jacks, as well.
4. A set of *direct control switches* is used to program the chip via the direct control.
5. The *bias current generator* allows measuring and fine-tuning the current provided to the chip using a voltage divider. The complete schematic of the biasing circuit is shown in fig. 5.17.
6. The *reset buttons* activate the low-active reset signals: NOTRESET resets the I²C interface, NOTRESETPIXEL sets all pixels to 0 V, NOTSETPIXEL sets all pixels to HV.

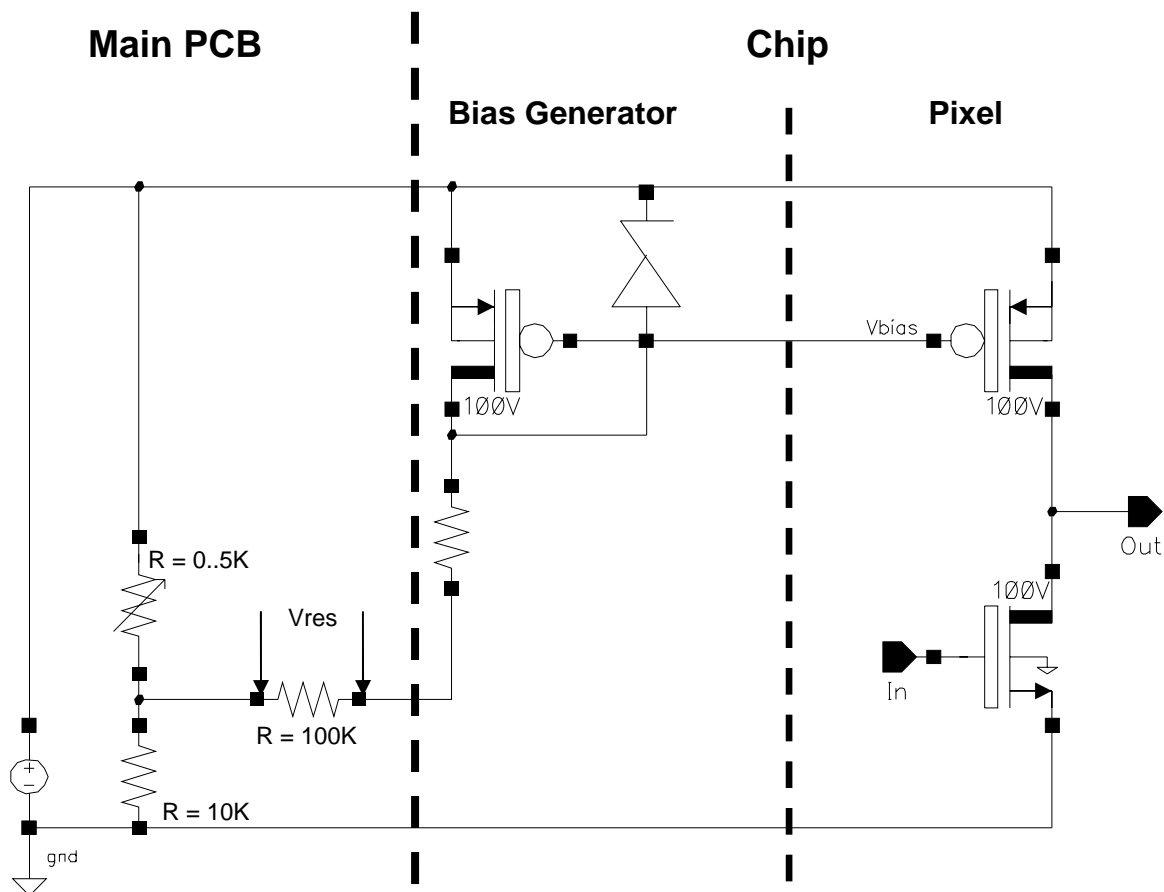


Fig. 5.17: Complete schematic for the biasing of the HV inverter, including components on the main PCB and on chip. Taken from [KÖN05].

The current PCB contains all circuitry necessary for both routine use and testing of Peptid-chip 5. For use in a synthesis machine, a more compact variant of the board could be built, in which all testing circuitry not required during normal operation is omitted. Details of the changes that could be implemented in such a minimal PCB are noted in A4.

5.4.3.3 Chip Covering

Given the increased seal area implemented on the chip, a covering using a resistant o-ring (Parafluor Parker V8545-75, material: FFPM 75Shore A) is used as a seal. The covering is wider than the board so that another o-ring seal can form the contact between the covering and the synthesis chamber. As in the covering of Peptidchip 3.1, an aluminum back-covering is used. With the covering mounted, the chip fits into a variant synthesis chamber adapted for the larger chip (fig. 5.18, 5.19, 5.20).

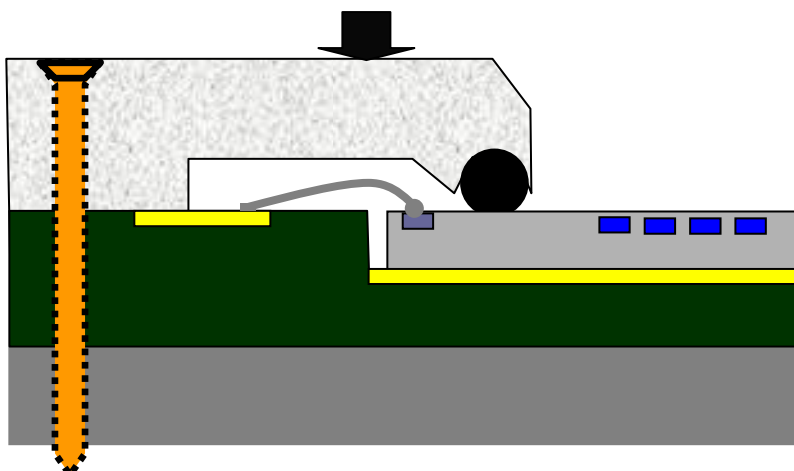


Fig. 5.18: Sectional drawing (not to scale) of Peptidchip 5 and its covering, showing the area around the seal and bond wires. The arrow shows the area where the synthesis chamber o-ring contacts the covering.

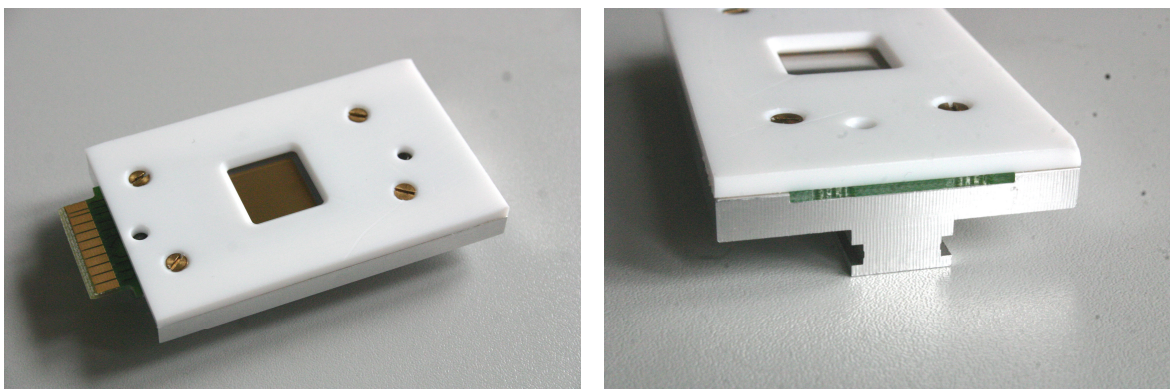


Fig. 5.19: The PCB is mounted in a cavity in the back-covering, after which the covering is placed on top, guided by alignment pins, and screwed into place. The contacts remain exposed in order to allow operating the chip while in the covering.



Fig. 5.20: Peptidchip 5 on PCB with covering, installed into the synthesis chamber. The silvery area in the center is the pixel area of the chip.

5.4.4 Control Software

A control software analogous to the LabView VIs for Peptidchip 3 and Peptidchip 3.1 was written [TOR], which allows to contact the chip and write a pattern of data corresponding to activated (HV) and inactive (0 V) pixels from a file to the chip using the I²C interface (fig. 5.21).

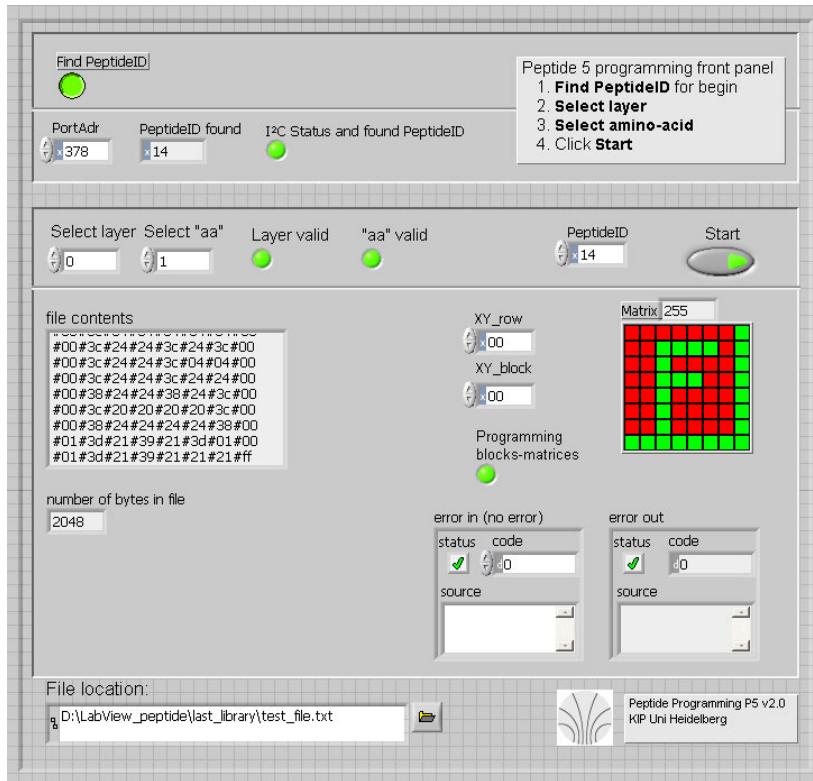


Fig. 5.21: LabView virtual instrument for chip programming. The deposition pattern is read from a file, and the chip is programmed according to the pattern via the I²C interface.

This VI allows writing a pattern encoded in a text file into the Peptidchip 5. For text file generation, an Excel-based pattern file generator can be used to obtain pattern files from a graphical input, while a second program is available to generate pattern files from an input of desired peptide sequences [TOR].

For later applications, this file could also be generated by software for generating peptide arrays from biological databases or user-defined specifications, such as the software available for the laser printer described in 3.3.

PART III

RESULTS AND DISCUSSION

6. Transfer of Amino Acid Particles

6.1 Introduction

Prior to this work, not all prerequisites for on-chip synthesis were met. While additional tools for particle analysis were made available in other works [NES06, NES07, NES07-2, NES08, LOE09, NES10] and used to gain further insight into particle properties, this thesis focuses on using aerosol chambers for particle transfer in a CMOS chip based system suitable for peptide synthesis. The following issues have been addressed:

- A general analysis of the aerosol chamber concept, including reproducibility considerations, is provided in 6.2.
- The first tests of amino acid particle deposition on CMOS chips are detailed in 6.3.
- In 6.4 and 6.5, the effects of surface modifications required for hydrogen detection and peptide synthesis based on selective deposition are described and solutions for achieving compatibility are given.
- 6.6 describes proof-of-principle experiments on particle deposition using a liquid as the transport medium instead of generating an aerosol.
- Finally, in 6.7, these results are summarized and discussed with regard to peptide synthesis.

6.2 Aerosol Chambers

6.2.1 Aerosol Chamber Concept

The original concept of the aerosol chambers (fig. 6.1) used in this work is similar to that of a toner cartridge (fig. 6.2) with a large reservoir of particles. Making these chambers useable for deposition of amino acid particles onto CMOS chips was one objective of this thesis. Enough toner for a large number of depositions is available in a reservoir, and an airstream replaces the drums used in laser printer cartridges for particle transport. Particles are present in the whole system. Other methods of particle deposition are investigated in other works [NES06, NES08, CHE].

The original concept of the aerosol chamber (fig. 6.2) is described as follows (see also 3.9): Air pressure is used to power the deposition system. Supply air coming from the *air inlet* (1) flows through the *injector* (2) where it picks up particles and mixes with air already present in the *reservoir* and *deposition chamber*. The particle-loaded air then passes through a hose (3) to the *cyclone* (inner diameter: 28 mm, length: 35 mm) (4), where the centrifugal force causes the particles to move along the cyclone wall, charging them triboelectrically. In the center of the cyclone, an *air outlet* (7) is used to remove excess air and thus prevent pressure built-up. As the centrifugal force causes a gradient in the particle concentration in the cyclone, the air leaving through the central outlet has a reduced particle concentration. From the cyclone, air and particles pass into the deposition chamber (width: 3,2 cm, maximum height: ca. 12 cm, length: ca. 20 cm) (6), where the air speed is reduced due to the expanding cross-section of

the flow, as the deposition chamber is large compared to the other parts. Mounted top-down on the deposition chamber is the chip (5), on which particles are to be deposited. According to this first concept, the chip is to be tightly fixed to the deposition chamber, such that *leakage* past the chip is minimized. From the deposition chamber, the air can pass on into the particle reservoir and the injector where it mixes with fresh supply air. The chamber is built of MMA (Plexiglas), which allows observing the aerosol inside. Polyamide hoses are used for air supply and to connect the injector to the cyclone.

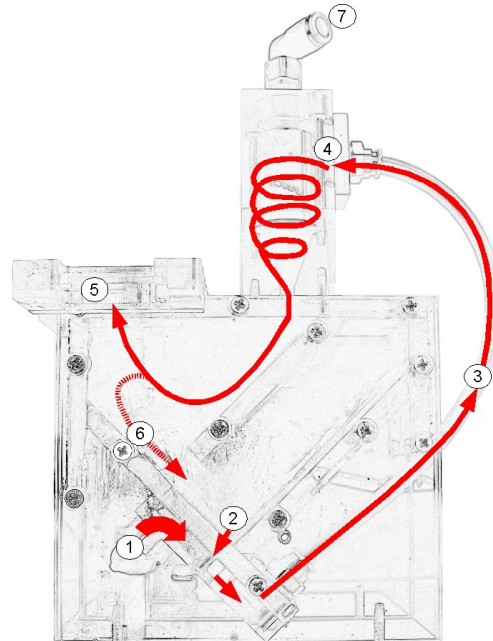


Fig. 6.1: Aerosol chamber, first generation. 1: Air inlet. 2: Particle injector for uptake of particles from the reservoir into the airstream. 3: Air-particle-hose. 4: Cyclone for triboelectric charging. 5: Chip holder aperture. 6: Particles and air returning to the particle reservoir. 7: Cyclone air outlet. Taken from [BEY05].

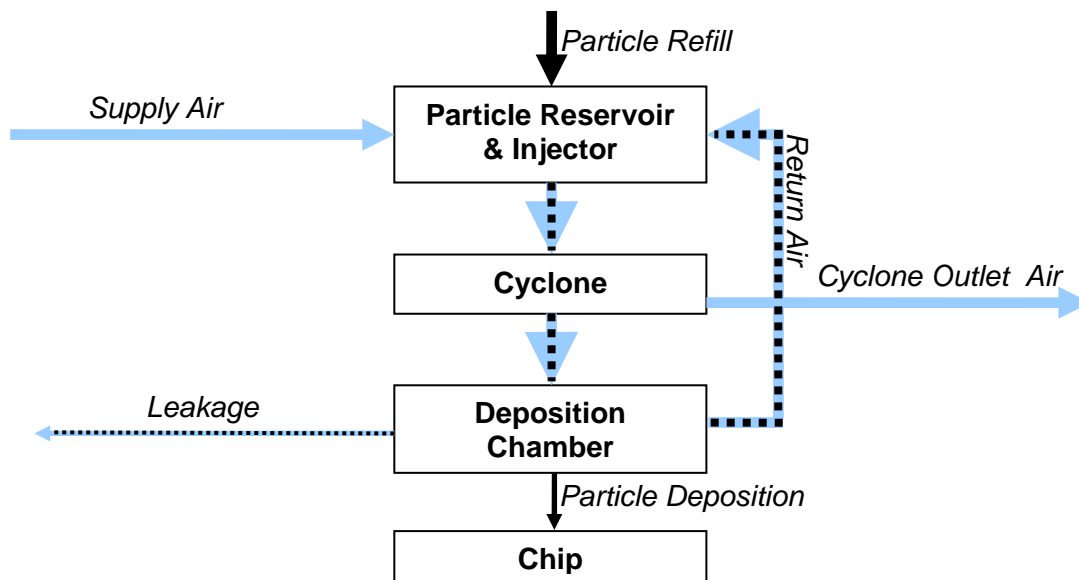


Fig. 6.2: First idealized concept of the aerosol chamber particle deposition system. Blue arrows: airflow without particles. Dashed arrows: Airflow transporting particles. Black arrows: Particles leaving or entering the airstream or reservoir.

6.2.2 First Generation Aerosol Chambers in Experiments

Experiments showed that the original description of the aerosol chamber had to be modified to account for the effects observed during use in the following ways (fig. 6.3):

First, the particles in the reservoir are exposed to the airstream not only via the injector, but also directly, since the reservoir is not physically separated from the deposition chamber. The particles are simply poured in through the chip holder aperture, and thus heaped up on the bottom of the chamber, around the injector which is initially covered completely with particles. The first bursts of supply air into the chamber after refilling the chamber therefore are oversaturated with particles until the injector is cleared. In subsequent depositions, particles from the remaining heap around the injector opening are used. Even then, however, the amount of particles in the aerosol at a given supply air pressure and flow is strongly dependent on the amount of particles remaining in the chamber, as there is no mechanism for the dosage of particles. After a number of depositions, the area around the injector is nearly free of particles, and too few particles are injected. By shaking the chamber, particles from further away from the injector can be redistributed, making these particles available for uptake into the aerosol. This process is not perfectly reliable in creating reproducible aerosol conditions. Use of the deposition chamber as a reservoir for a very large number of depositions, with the injector and chamber bottom completely covered with a large heap of particles, proved completely impossible, as it resulted in a massively oversaturated aerosol.

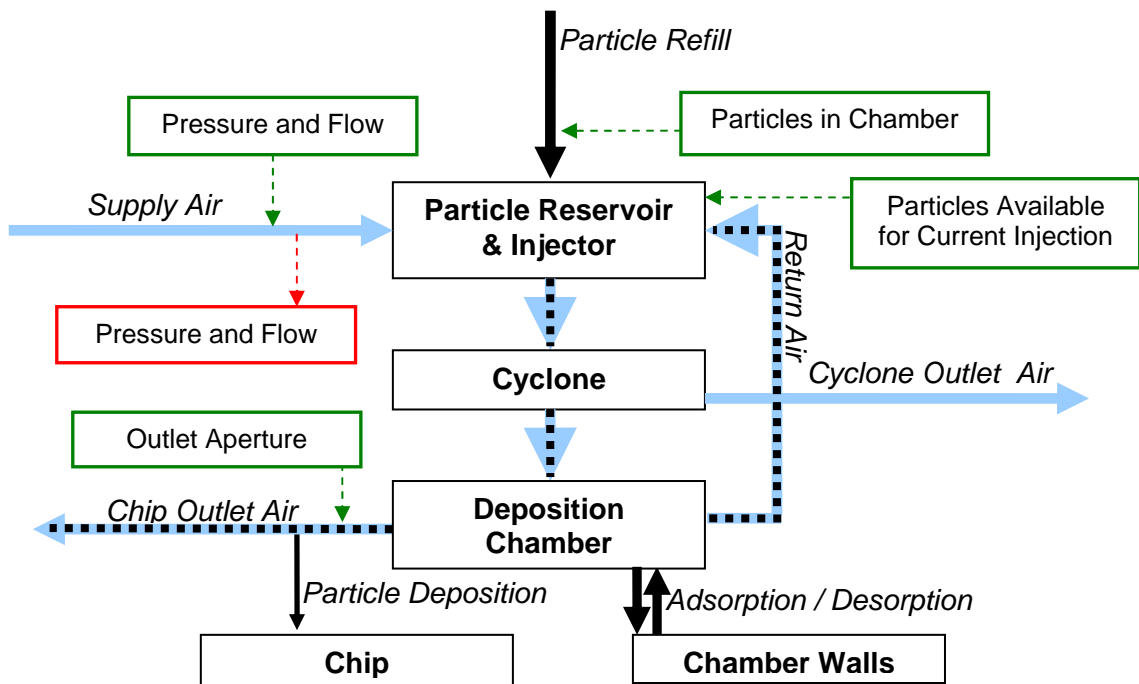


Fig. 6.3: Realistic description of air and particle flows in the aerosol chamber, including points for measurement and regulation. Measured parameters in red, adjustable parameters in green. Blue arrows: airflow without particles. Dashed arrows: Airflow transporting particles. Black arrows: Particles leaving or entering the airstream or poured as powder.

Second, it turned out that if leakage is minimized by tightening the seal between chip and chamber, deposition fails as insufficient particles reach the chip. Only if some air leaves the chamber as close to the chip as possible, deposition succeeds in these aerosol chambers. (In practice, this can be achieved either by using the chip without covering, when air can pass between the contact pins that cause between 1 and 2 mm of spacing, or by using a *spacer*,

which creates a 2 mm gap between the chip covering and the chamber. The disadvantage of this change is that non-negligible amounts of particles leave the chamber in an uncontrolled way, making them difficult to recover and contaminating the surrounding air, requiring the setup to be placed in a closed flow hood.

Additionally, interactions of particles with the deposition chamber walls must be considered, as large numbers of particles can be deposited onto the walls and taken up into the aerosol from the walls depending on airflow, pressure and aerosol density. Deposition of particles on walls is generally more significant at places in the chamber where air speed is slow due to a large cross-section. In particular, there is little deposition on the walls of the cyclone during deposition due to the high speed of the airflow along the cyclone wall, but much stronger coverage of the walls near the reservoir. Wall interactions were found to be hard to predict, with large groups of accumulated particles detaching from the walls in random intervals.

6.2.3 Regulating Aerosol Parameters

6.2.3.1 *State of the Art and Objectives*

Using the setup described in 6.2.2, particle deposition on chips has been performed with good results [KÖN05] by adjusting only supply air pressure, airflow, and the amount of particles available for uptake by the injector (by refilling appropriate amounts and shaking the chamber). The downside of this approach is that adjusting chamber parameters for good aerosol is a matter of time, experience and intuition. Due to the fact that ideal conditions vary with the amount of particles within the chamber, particle batch and the way the particles are heaped in the chamber (which is changed by shaking), it has not been possible to “set” a chamber to an ideal configuration of parameters and operate it under these conditions indefinitely. Usually, a chamber’s parameters must be readjusted after storage of the chamber, but if the chamber is not moved, they are retained for about 5 to 15 depositions or several hours.

In case of “critical” depositions, such as during peptide synthesis, a test chip must be used to establish good aerosol conditions, with the “critical” chips being exposed to the aerosol only after good aerosol conditions have been achieved. The test chip is “blown clean” with a strong (8 bar) airstream using a pressurized air outlet with a pistol valve after each deposition and thus can be reused.

The following protocol can be used as a guideline to find good aerosol conditions. A flow meter / regulator of 52 l/min maximum flow is used.

1. If the chamber is empty: Fill in 500 mg (about 5 spatulas) of particles through the chip aperture.
2. Connect the chamber to the supply air. Set air pressure to 2 bar and airflow to 20 % of maximum flow.
3. Perform deposition by pushing the tap valve for about 5 s and examine the chip under the microscope.
 - a. If too many agglomerates were deposited: Retry, if the condition persists, change particles.

- b. If too many particles were deposited: reduce flow to 17.5 % and retry. If still too many particles are deposited, retry at the given parameters until the particle concentration has been reduced sufficiently.
- c. If too few particles were deposited, perform one of the following steps, starting on top, and retry:
 - o Rise the chamber on one side and gently tap it onto the floor of the flow hood.
 - o Rise the chamber on one side and vigorously knock the chamber into the floor. Repeat for all four sides.
 - o Increase the flow by 5 %. This can be repeated up to about 35 % flow. Pressure can also be increased up to 3 bar.
 - o Fill in 2 to 4 spatulas of particles through the chip aperture. Reset air pressure to 2 bar and airflow to 20 %.
- d. If the amount of particles deposited is good, but there are too many contaminations, vary the flow between 15 % and 40 %. If deposition still fails, change particles.

As a rough guideline, when the aerosol is activated, particles in the aerosol should be just barely visible by eye for good aerosol. Suitable places for observation are the inlet of the cyclone or the chip aperture. If a clearly visible cloud of particles escapes the chamber at the chip aperture, the aerosol is much too dense for good deposition.

Changing particles requires the chamber to be at least cleaned with a vacuum cleaner to remove the old particles. It is preferable to completely disassemble the chamber and wash all parts with ethanol before reuse with new particles; this is mandatory if a particle sort containing a different amino acid is refilled.

Using either dry laboratory air or nitrogen for supply air, no influence of ambient air temperature from 20° C to 28° C or of relative humidity up to 50 % could be observed. It is recommended to store and use aerosol chambers containing particles within this range of temperature and humidity until further experiments regarding acceptable conditions are conducted.

Using the given protocol, the aerosol chambers could be used for successful experiments studying particle transfer (6.4-6.7), and even for combinatorial synthesis (chapter 7).

6.2.3.2 An Aerosol Chamber with Monitored Aerosol

Concept

The following questions need to be addressed in order to increase reliability and usability:

- o How can an aerosol chamber be designed which produces aerosol conditions suitable for high-quality particle transfer without requiring extensive configuration steps?
- o In order to reduce waste of particles, can the use of a test chip be made unnecessary? Can the aerosol be monitored and stabilized while the chamber is closed?
- o Is it possible to design a chamber that can be, using feedback loops, brought into stable conditions by control software?

Using the previous chamber, the chip is exposed to an aerosol immediately after the supply air is activated. This prevents verification of the aerosol quality before deposition. Therefore, an

approach aimed at depositing only after good aerosol quality has been achieved requires a *shutter* that, while closed, separates the deposition chamber from the chip. The shutter remains closed until the aerosol is brought into an acceptable state, and then opened for deposition.

Loss of particles past the chip is still accepted for the first proof-of-principle version of the chamber. However, it would have to be addressed in chambers to be used in routine deposition for peptide synthesis.

Three parameters are deemed important in establishing conditions in the aerosol chamber that lead to good deposition:

- particle properties, such as q/m , size and shape,
- airflow relative to the chip, and
- aerosol density.

Particle charge must be uniform, that is all particles in the aerosol have to be charged to the same polarity. Variations in the amount of charge are tolerable within a certain range as long as the pixel voltage on the chip is high enough [KÖN05]. In this work, particles from various batches of OKI Magenta and OKI Cyan laser printer toner and amino acid particles with average diameters between 7 μm and 15 μm were used. The influence of particle properties on deposition has been investigated in [LOE09], and is not subject of this work.

Airflow close to the chip can be adjusted by changing supply airflow and pressure. However, this changes the airflow throughout the chamber, which in turn influences aerosol density as the injection rate and wall interactions depend on the velocity of the air stream. Still, in the previous chamber, successful depositions have been achieved at a range of flows from 8 to 20 l/min, which could be used to compensate for varying aerosol density.

Aerosol density is the hardest parameter to control in the first chamber, as it can neither be measured nor directly controlled in that setup. It also proved to be the parameter most likely to leave the region in which good deposition is achievable. It is thus the most critical parameter, and in a chamber that is to provide controlled aerosol conditions, aerosol density must be measured and controlled.

In addition, using suitable sensors [NES07], the correct charge of particles could also be monitored. This would allow early detection of particle batches that have lost the ability to become charged uniformly and in the desired way (e.g. due to aging or deficiencies in production).

Aerosol density can be measured optically using the Lambert-Beer law which relates concentration c of an optically absorbing (or scattering) substance (particles) within an optically non-absorbing (or scattering) substance (air) to the absorbance A , and thus the ratio between incident light I_0 and transmitted light $I(c)$ according to

$$A = -\lg \frac{I(c)}{I_0} = \varepsilon \cdot l \cdot c$$

with

ε = extinction coefficient (a material constant of the absorbing substance)

l = distance in medium

c = concentration of the absorbing substance.

(Eq. 6.1)

Thus, by sending a beam of light through the chamber and measuring the decrease in intensity, we could measure the particle concentration in the chamber.

For a good measurement, stray light from the laboratory must be prevented from reaching the detector. This can be achieved by using a *spatial filter*, that is a long tube with blackened inner walls coaxially aligned with the light source and the detector. Furthermore, the chamber walls in the beam path need to be free of particle depositions that occur on most chamber walls. This is achieved by putting the chamber walls in the beam area in a recess behind extra air inlets into the chamber. These *seal air inlets* cause an inflow of fresh air into the chamber at the critical sections of wall, displacing the particle-loaded air there.

Fig. 6.4 depicts the concept for such a chamber. The particle reservoir is removed from the circular airflow in the chamber, even though it is still connected to the deposition chamber. Particles pass through a mill that is used to break up agglomerates, and are transported into the injector with a rate dependent on the rotational frequency of the mill, which can be set. Particle injection rate thus becomes independent of the amount of particles in the reservoir. In the deposition chamber, aerosol density is measured optically (see below). Feedback loops are closed, either manually by the experimenter or later automatically: In *aerosol density control*, aerosol density in the deposition chamber is measured and compared to the desired value, while particle injection rate is changed accordingly. Similarly, in *air supply control*, supply air pressure and flow are kept at the desired values. If both parameters are within the specification and the chip is installed for deposition, the shutter is opened for the set deposition time.

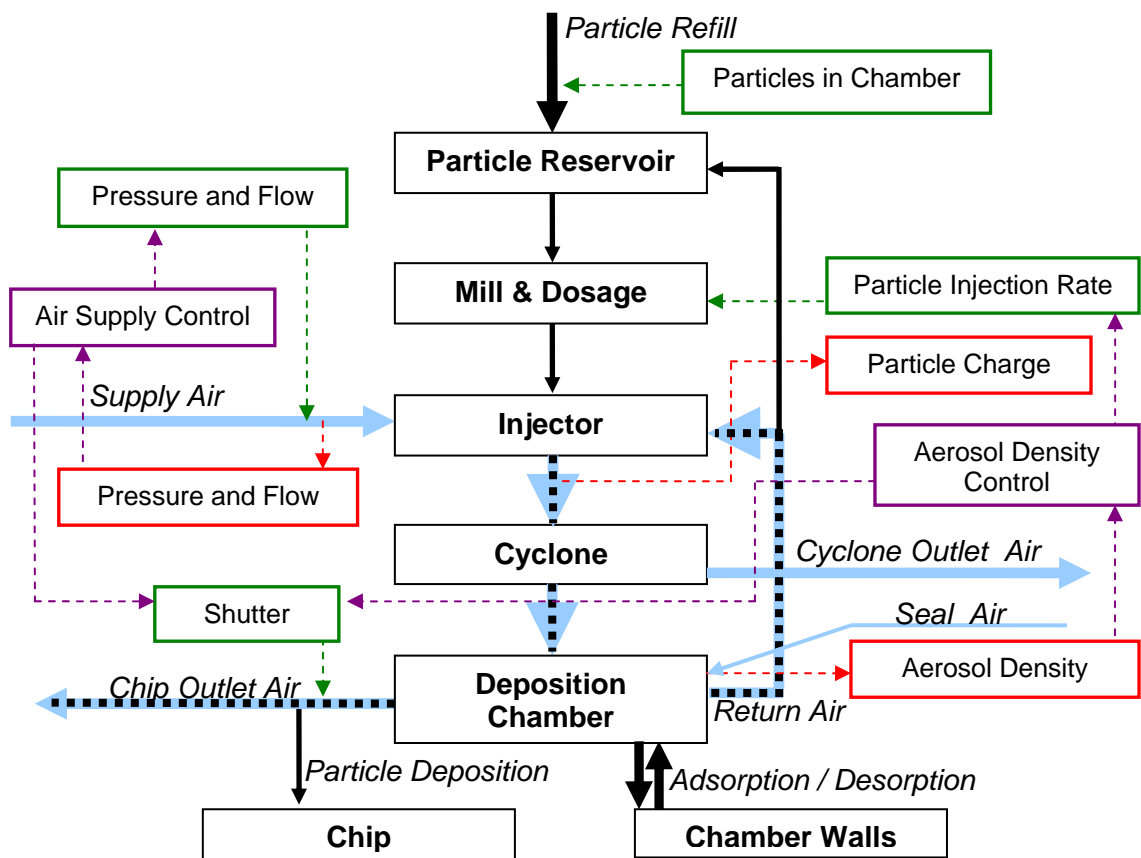


Fig. 6.4: Concept of an aerosol chamber for generating a controlled aerosol. Measured parameters in red, adjustable parameters in green, control modules closing feedback loops in violet. Blue arrows: airflow without particles. Dashed arrows: Airflow transporting particles. Black arrows: Particles leaving or entering the airstream or poured as powder. See text.

Realization

An aerosol chamber was built according to these specifications. The cyclone is reused from the previous chamber. It is now mounted on the side of the deposition chamber, and connected by a diagonal tube. The deposition chamber is smaller and of a more simple geometry than in the previous chamber, reducing the wall area. It is separated by a metal plate with holes from the particle reservoir, allowing excess particles fall back into the reservoir. Situated underneath the reservoir is the *dosage mill*, a rotating conical cylinder in a conical chamber. The rotating cylinder pulls particles out of the reservoir into the gap between it and the wall, which is adjustable via the mounting height of the cylinder. Agglomerates are broken up, and particles fall down through the gap onto a circular shelf. At one point in the shelf, a hole connects to the injector, and a pair of metal *wipers*, mounted coaxially to the mill cylinder, pushes the particles along the shelf until they fall into the hole and are injected. The injection rate is thus proportional to the rotational frequency of the mill and wipers. An air bypass channel within the Plexiglas wall leads from the deposition chamber to the injector, where it is mixed with supply air before passing at the particle injector. As in the previous chamber, the air passes from the injector to the cyclone via a hose. The chip is mounted top-down on the deposition chamber, with the option of tight fitting (no air outlet) or a spacer being installed for allowing a chip outlet airflow. A manual shutter with o-ring seals allows opening the chip aperture by rotating a window in the aperture shutter plate into the opening.

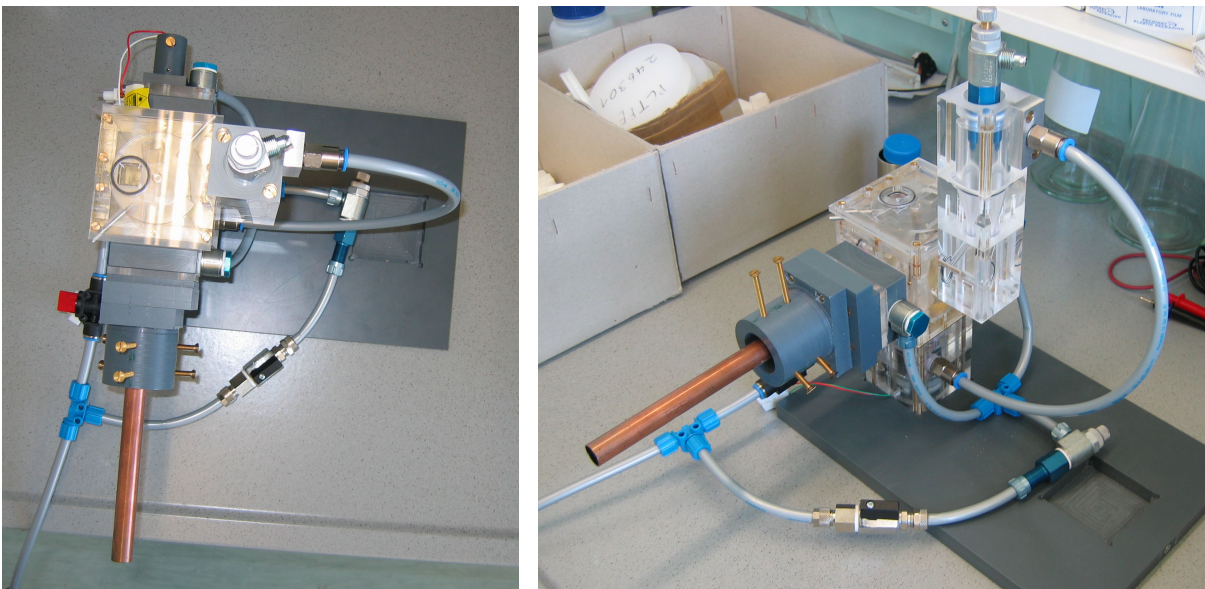


Fig. 6.5: Top-down (left) and overview (right) images of the new aerosol chamber with a makeshift optical setup for measuring aerosol density installed (grey parts on the sides of the chamber). See text.

Fig. 6.5 shows the new chamber with a makeshift setup for optical measurement of aerosol density in the chamber partially installed. In the left image, the components for optical measurement of aerosol density can be seen. In the top part of the picture, the lamp/laser mounting for the light source is visible, while in the bottom part, the spatial filter, a copper tube with blackened inner walls, is mounted with alignment screws. The photo detector can be mounted directly on the spatial filter. On the bottom of the right image, the air supply hoses to the seals including a flow adjustment valve are shown.

Usability of the new chamber

Particle deposition in the new chamber was tested using OKI Magenta particles and Peptidchip 3.1 (fig. 6.6). Good aerosol conditions were established, with optimum pressure and flow tending to be lower than in the previous chamber (around 9 l/min at 2 bar). While the results of deposition were comparable to the previous chamber as far as single particles were concerned, a comparatively large number of randomly deposited agglomerates of around 50 μm in diameter was observed on the chip, reducing overall deposition quality drastically. The same strong tendency to form agglomerates was observed using OKI Cyan particles.

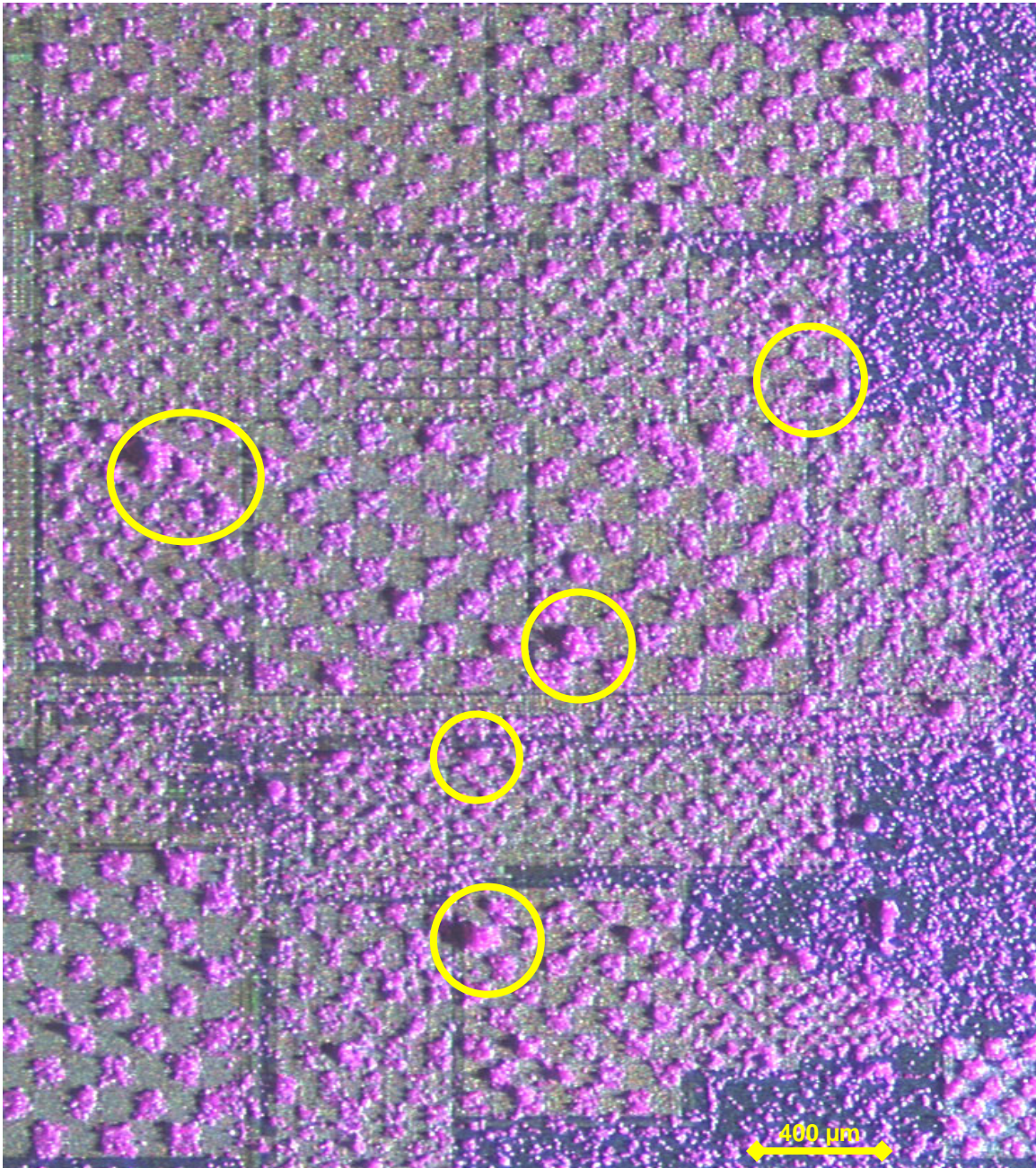


Fig. 6.6: Example of particle deposition on a Peptidchip 3.1 in the new aerosol chamber. Deposition succeeded with few single-particle contaminations, but a large number of agglomerates reduce quality (yellow circles). Stitched microscope images.

Disassembly and optical inspection of the chamber revealed the presence of numerous agglomerates near the injector and at the wipers and at the gaskets of the shutter. These moving parts may exert forces onto piles of particles that are deposited there, thus causing the formation of the agglomerates. As these structures are passed in the airstream only behind the mill which is used to break up agglomerates, no structure prevents the agglomerates from reaching the chip. This flaw renders the new chamber unusable for selective deposition at high qualities. In an improved chamber, no moving parts may be inserted into the airstream. The wipers at the injector could be made obsolete by an improved mechanical design, and the chip opening could be sealed by an airstream into the chamber in a similar way as the seals in the path of the optical measurement setup.

The optical measurement setup was also tested. The air-based seal prevented the deposition of particles onto the chamber walls in the light path, while not significantly affecting deposition, already at flow rates a fraction (approx. 20%) of that of the supply air.

A Coherent FieldMAX II photometer was used for optical measurements. Using the spatial filter, the signal with the incident light deactivated was reduced to the detector's dark current. Both light sources tested, an LED flashlight and a red laser, resulted in stable signals from the detector. This signal was expected to be reduced according to Lambert-Beer's law upon activation of the aerosol. However, upon activating the mill and pressurized air (with the chip shutter closed) in order to obtain an aerosol, the detector showed an erratic signal which changed over several orders of magnitude within seconds. During chamber operation, the signal did not settle. Even with the mill and wipers for toner injection deactivated, an unsteady output signal was observed while the pressurized air is activated, persisting over several minutes during which the aerosol was expected to become homogeneous. Inhomogeneity of the aerosol could be observed even with the eye. Contrary to the expectations, the aerosol did not become homogeneous even with longer periods of continuous chamber operation. It is thus concluded that adsorption and deposition of particles to and from the chamber wall cause an inhomogeneous aerosol. The experiments with the new chamber were thus abandoned.

Therefore, while successful depositions, with a quality sufficient for peptide synthesis, were achieved using the first generation aerosol chambers, the aerosol concept might not be suitable for an automated system. For this purpose, an alternative concept with reduced wall areas and an improved particle reservoir might be preferable.

6.2.3.3 Alternatives to the Aerosol Chamber Concept

In order to achieve a controlled aerosol, alternatives to the concept of an aerosol chamber with a circular flow of particles, which by its nature requires complex geometries, must be considered. A simpler alternative would be a linear system, which consists of, in sequence of airflow:

1. An air inlet
2. A system to inject particles into the air
3. A cyclone (or other method to charge the particles)
4. The chip, placed directly into the airstream at a position with sufficient cross-section
5. An air outlet

The schematic of such a system is depicted in fig. 6.7.

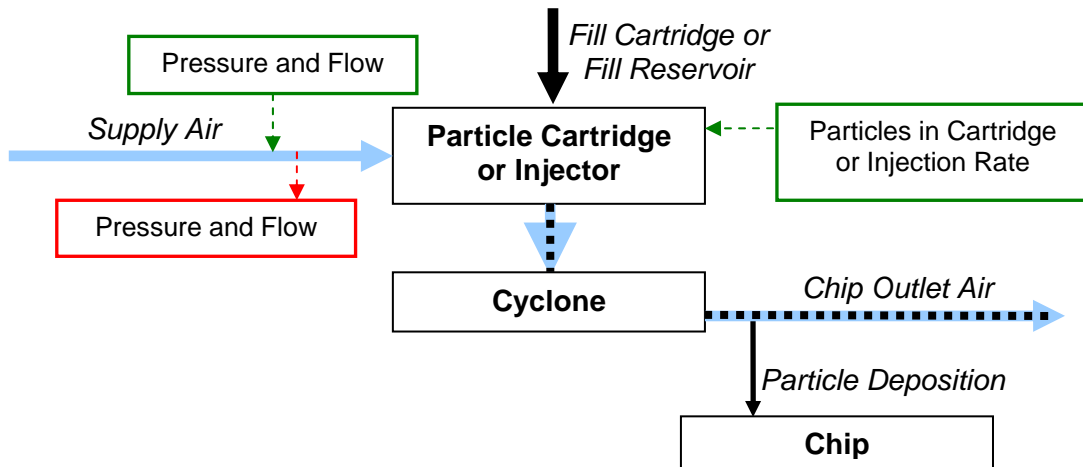


Fig. 6.7: Description of air and particle flows in a linear deposition system. Measured parameters in red, adjustable parameters in green. Blue arrows: airflow without particles. Dashed arrows: Airflow transporting particles. Black arrows: Particles leaving or entering the airstream or poured as powder.

In this system, air pressure and flow are regulated at the inlet as in the aerosol chambers. In a radical implementation, the injector might be replaced by a *cartridge* pre-filled with only the amount of particles needed for one deposition step, which is replaced after each deposition. Alternatively, if a method for reliable dosage is found, the injector could be retained, using a reservoir that is not connected to the aerosol except through the injector. The cyclone for triboelectric particle charging is retained from previous designs, and as the air is fast-moving in all parts except the last section before it reaches the chip, adsorption of particles onto the chamber walls should be minimal.

The drawback of this method is that the outlet air passing the chip still contains particles that are not deposited on the chip, which are lost. The method therefore has to include a filter or some other device for particle recapture.

6.2.3.4 Conclusions and Outlook

A realistic description of the aerosol chambers used for particle deposition has been found. Increased understanding of these chambers led to a protocol for manual deposition using these chambers, which therewith have been used successfully for all other selective deposition experiments described in this thesis, including deposition for synthesis (chapter 7).

Using the experience gained with the first aerosol chambers, a new aerosol chamber was designed in order to achieve tightly controlled aerosol and deposition. Testing this chamber showed the conceptual weaknesses of aerosol chambers, namely the need for moving mechanical parts that are prone to cause particles to agglomerate, and a large area of walls with which the particles interact. A linear deposition system, which transports as small amounts of particles as possible directly from a cartridge or an injector capable of good dosage to the chip might circumvent these difficulties. Such a linear deposition system with dosage injectors based on modified commercially available components is currently being tested [LOE]. An automated system for deposition of 20 or more different sorts of particles is being built from this system.

6.3 Transfer of Amino Acid Particles onto CMOS Chips

6.3.1 Prerequisites

Previous works [KÖN05] showed only the deposition of OKI laser printer particles used for reference onto CMOS chips, but synthesis of peptides requires the use of particles loaded with amino acids. Therefore, testing the transfer properties of amino acid particles in order to compare their behavior to that of the OKI toner particles (6.3.2) was necessary before particle based peptide synthesis could begin. Additionally, only two different sorts of particles had been successfully deposited in sequence in [KÖN05], while up to twenty such depositions are required for synthesis. Sequential deposition had to be tested, verifying that particle layers already deposited do not interfere with deposition on adjacent pixels (6.3.3). Experiments comparing different batches of amino acid particles were performed in order to examine whether the requirements of chip-based particle deposition are more stringent than those for amino acid laser printing (6.3.4).

Unless noted otherwise, all work in this chapter used Peptidchip 3.1 CMOS chips and first generation aerosol chambers. The batch of particles used varied for different experiments, as availability of particles from each batch was limited. For most experiments not focused on comparing particle batches, particles from a batch known for good performance were chosen.

6.3.2 Amino Acid Particle Deposition on Peptidchip 3.1 and 5

6.3.2.1 Peptidchip 3.1

Using the same setup as described in [KÖN05], that is the original aerosol chamber described in 6.2.2, particle deposition experiments using amino acid particles were performed, with the objective of reproducing the results obtained with OKI Magenta particles.

Particle deposition is also used to test the new chips designed during this thesis. If the pattern of deposition matches the programmed pattern, the chip displayed the correct electrical field pattern, and thus be electrically functional.

On Peptidchip 3.1, patterns of alanine amino acid particles were deposited, using a checkerboard pattern (fig. 6.8). Deposition quality was slightly worse than with OKI Magenta particles due to stronger contaminations, but considered acceptable for eventual synthesis.

These results show that at least this batch of amino acid particles performs comparably to OKI Magenta toner particles used as reference particles until then, with only slightly poorer performance, at least in checkerboard patterns. Electrical functionality of Peptidchip 3.1 was also demonstrated by depositing particles in different patterns for each pixel area. For synthesis of peptides on Peptidchip 3.1, additional batches of amino acid particles were tested. It was noted that patterns with few (one in sixteen or less) pixels active for deposition resulted in strong contaminations, unlike the good results achieved with OKI Magenta particles in [KÖN05]. On the small pixel areas of only 8 x 8 pixels per area of Peptidchip 3.1, this was difficult to investigate further. Also, further experiments with Peptidchip 3.1 focused on achieving compatibility with the PEGMA layer surface modification (6.5) and in synthesizing a pattern of six different peptides on the chip (chapter 7), before moving to more complex synthesis patterns. Therefore, these effects were investigated in detail later, using Peptidchip 5 (see 6.3.4).

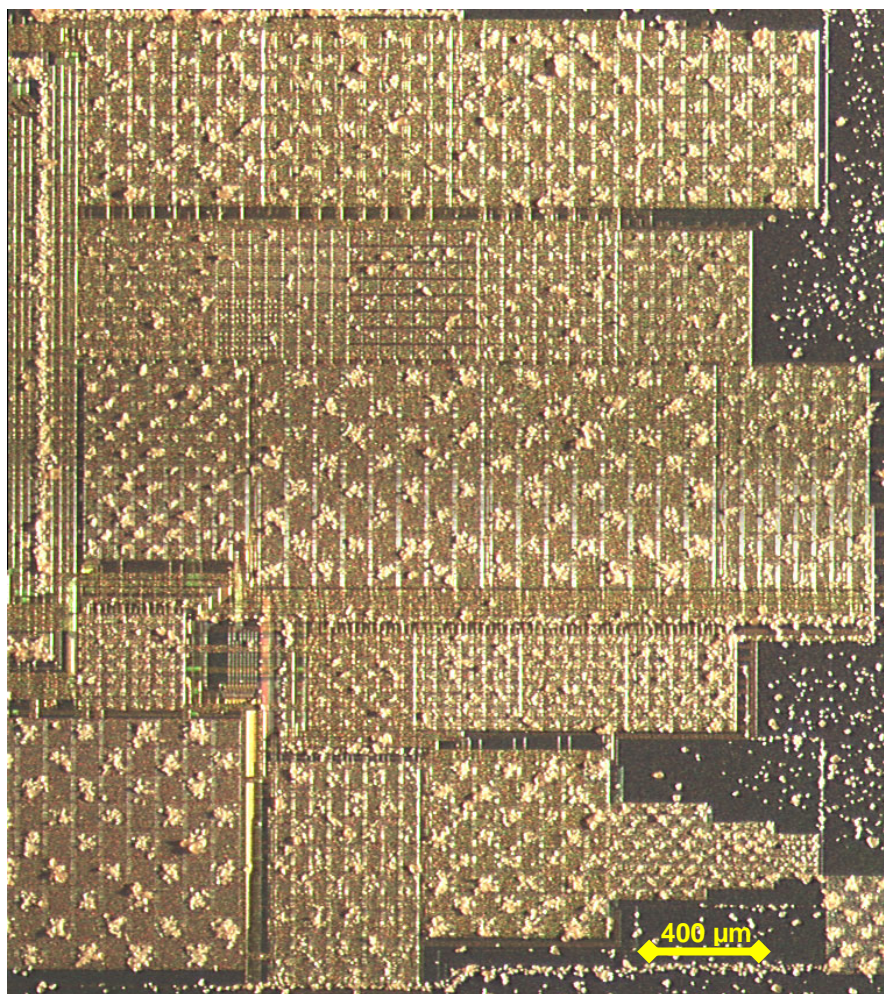


Fig. 6.8: Particle deposition in checkerboard pattern of alanine amino acid toner particles on a Peptidchip 3.1. Stitched microscope images.

6.3.2.2 Peptidchip 5

After production, Peptidchip 5 was tested in the aerosol. A running pattern of numbers and letters was programmed into the chip for deposition of glutamic acid particles with an average diameter of $10.2\ \mu\text{m}$. The chip was operated at 100 V pixel voltage and 0 V grid electrode voltage. The results (fig. 6.9, 6.10) showed a deposition pattern matching the programmed pattern, proving the chip to be electronically functional. The pixels were strongly saturated with particles. Evenly spread contaminations were noticed in areas where the distance between two active pixels was three or more pixels.

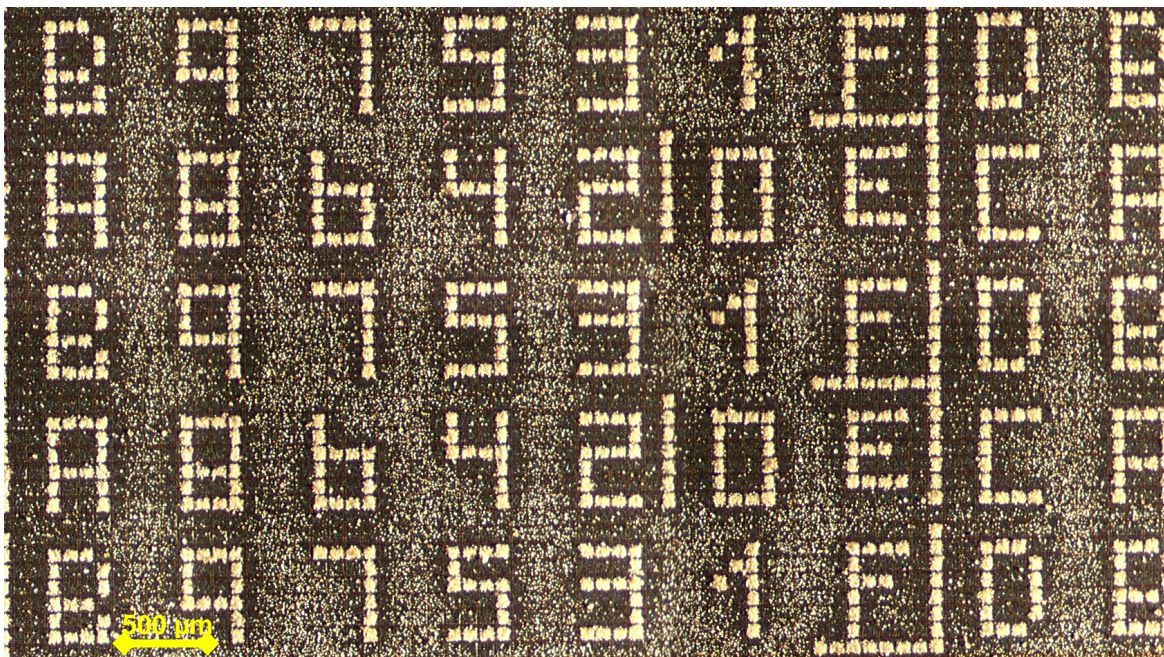


Fig. 6.9: Part of the particle deposition in ordered numbers pattern of glutamic acid alanine amino acid toner particles on a Peptidchip 5. Stitched microscope images.

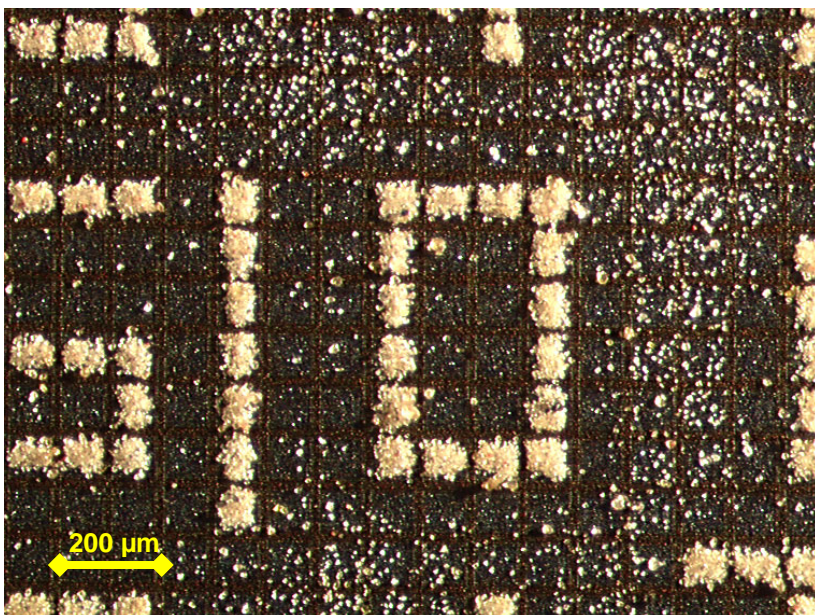


Fig. 6.10: Detail of the particle deposition in ordered numbers pattern of glutamic acid particles (average particle diameter 10.2 μm) on a Peptidchip 5.

These results are in contrast to those obtained in [KÖN05] with OKI Magenta particles, but confirm the difficulties encountered with amino acid particles on Peptidchip 3.1 (6.3.2.1). The contaminations observed here would be too strong for a combinatorial synthesis.

As OKI Magenta particles could selectively be deposited with much lower densities of active pixels, it should be possible to create amino acid particles with similar performance. However, due to the effort needed to create new particle variants, making the existing particles usable would be preferred. A simple compensation strategy would be to use some pixels as dedicated “particle dump” pixels that are active in every deposition. Between one in

four and one in nine pixels might be required to achieve this effect. Alternatively, the grid electrode, if set to a higher voltage, might be used as particle dump. In 6.3.4, further investigations on pattern dependencies of particle transfer are shown, and solutions are presented.

6.3.2.3 Minimum Voltage for Particle Transfer on Peptidchip 5 with and without Covering

While Peptidchip 5, with a pixel pitch of 100 μm , is capable of providing 100 V of high voltage, lower voltages would be required if smaller pixels are to be used in future chips, or photodiodes for optical detection are to be integrated. Therefore, the minimum voltage for particle deposition on Peptidchip 5 was determined.

For this experiment, the same glutamic acid particles as in 6.3.2.2 were used. As these particles were found to be unsuitable for patterns with few pixels to be deposited, the experiment was performed using a checkerboard deposition pattern only.

During previous experiments, a subjective tendency for chips with covering installed to achieve poorer deposition results than these without covering was noted, which is why most particle transfer experiments were performed without using a chip covering. In order to compare deposition with and without covering more objectively, minimum voltage for successful particle transfer was determined for both a chip without covering and a chip with covering installed, as the voltages at which deposition quality breaks down are easier to compare than the qualities of two good depositions. Grid voltage was held at 0 V for these experiments.

Both with and without covering, deposition yielded good results at 100 V pixel voltage. Deposition at 30 V pixel voltage succeeded for chips with and without covering. Without the covering installed, the quality differed little from that at 100 V, but with the covering, the deposition quality was reduced. At 20 V and below, selective deposition with the covering installed failed. Deposition without covering still yielded good results for 20 V. At 15 V and 10 V, the deposition pattern was still discernible, but the number of contaminations increased to levels not acceptable for synthesis. At 7.5 V, random deposition without a discernible pattern was observed.

These findings indicate that voltages below 30 V can not be guaranteed to be suitable for particle transfer with these particles, on pixels of 100 μm pitch though voltages of 20 V might also be acceptable. These experiments should be repeated with the better-suited fine particles (diameter < 5 μm , see 6.3.4), and with different patterns, before chips with smaller pixels are actually designed. Deposition at 30 V would be sufficient to allow miniaturization down to 45 μm pixel pitch, which would be about a threefold increase in density of synthesis sites.

Furthermore, these experiments confirm that the covering indeed impedes deposition. Therefore, it might be advantageous to use the chip without covering in deposition. For automation, a synthesis machine with a synthesis chamber that directly seals against the seal area of the chip could be constructed. As the bond wires of Peptidchip 5 are very robust in comparison to those of Peptidchip 3.1, this could be achieved with little risk of bond wire damage during deposition.

6.3.3 Sequential Deposition of Different Sorts of Particles

With four colors of OKI toner particles and amino acid particles available, deposition of several sorts of particles in sequence can be attempted. The different colors of the particles allow tracking of contaminations, and thus to judge the influence that previously deposited particles have on subsequent depositions.

On a Peptidchip 3.1, OKI Magenta, alanine amino acid (white), OKI Cyan and OKI Black particles were deposited in sequence, with the 100 V maximum voltage pixels at 100 V, the rest of the pixels at 30 V and the grid electrode at 15 V. Fig. 6.11 shows the results, with fig. 6.12 and fig. 6.13 showing detail views of 80 μm pixels and the small pixel areas down to 20 μm at 100 V, respectively. Even though there are some contaminations, and the amino acid toner is deposited in excess of the required amount, the pattern is good for the 80 μm pixels, and can be considered adequate for attempting peptide synthesis. For the 40 μm pixels, contaminations are strong due to spill-over on adjacent pixels, but the pattern can still be recognized. As expected, the smaller pixel areas show the limitations of these particle sorts with an average diameter between 8 μm and 15 μm , and at 20 μm , no selective deposition is discernible.

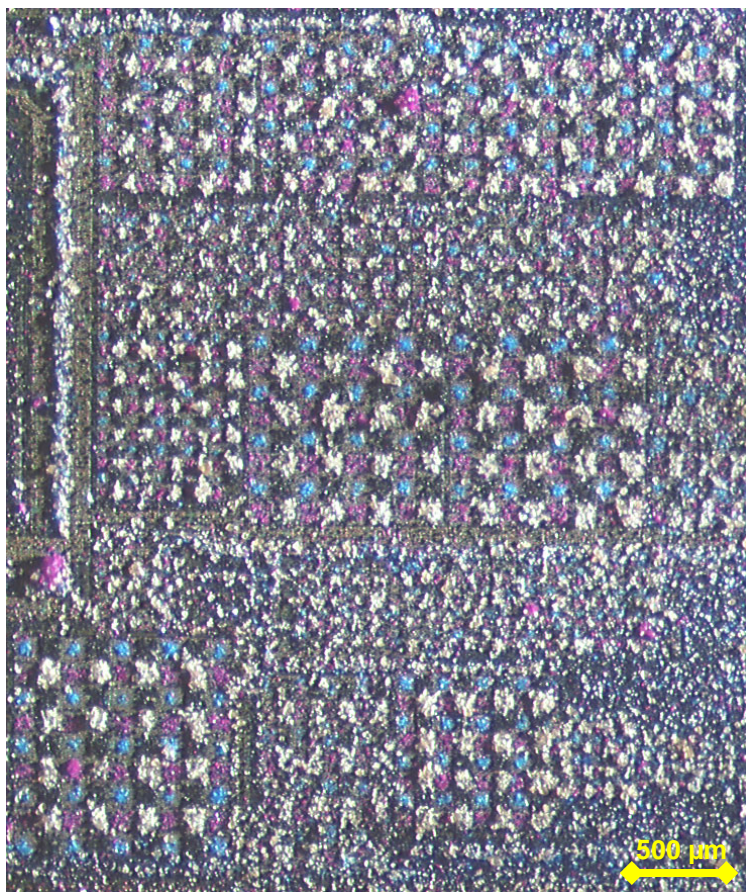


Fig. 6.11: Particle deposition result on a Peptidchip 3.1. OKI Magenta, alanine amino acid (white), OKI Cyan and OKI Black particles were deposited in sequence in a complementary pattern. Stitched microscope images.

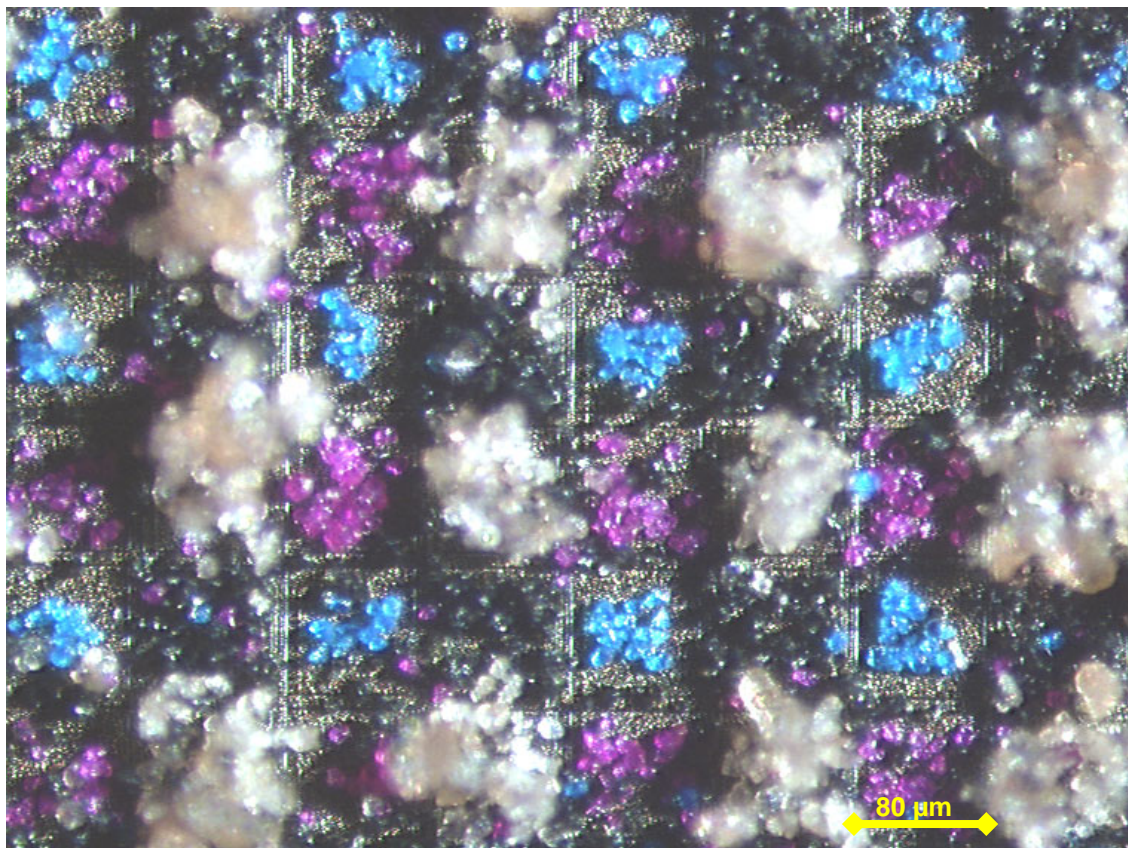


Fig. 6.12: Detail of particle transfer in four colors, 80 μm pixel pitch.

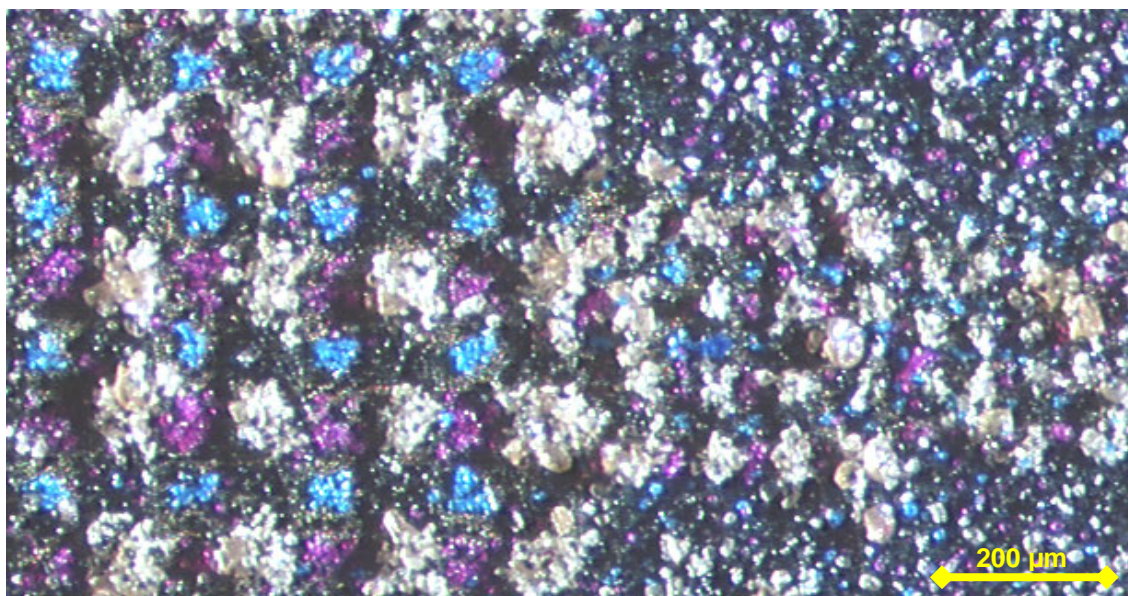


Fig. 6.13: Detail of particle transfer in four colors, pixel areas of 80 μm , 40 μm , 30 μm and 20 μm pixel pitch.

With these results, feasibility of sequential deposition of particles in complementary patterns has been shown. In future complementary depositions, e.g. for synthesis, the process could be made easier if particles of each deposition step could be blown off independently in case of a bad deposition, without having to repeat deposition of the entire layer. This can be achieved by *fusing* the particles after each deposition, that is by melting for a short time in order to

increase adhesion of the particles to the support. This method is used in the depositions for synthesis described in chapter 7, and should be used in depositions for synthesis until aerosol reliability can be improved further upon the state described in 6.2.

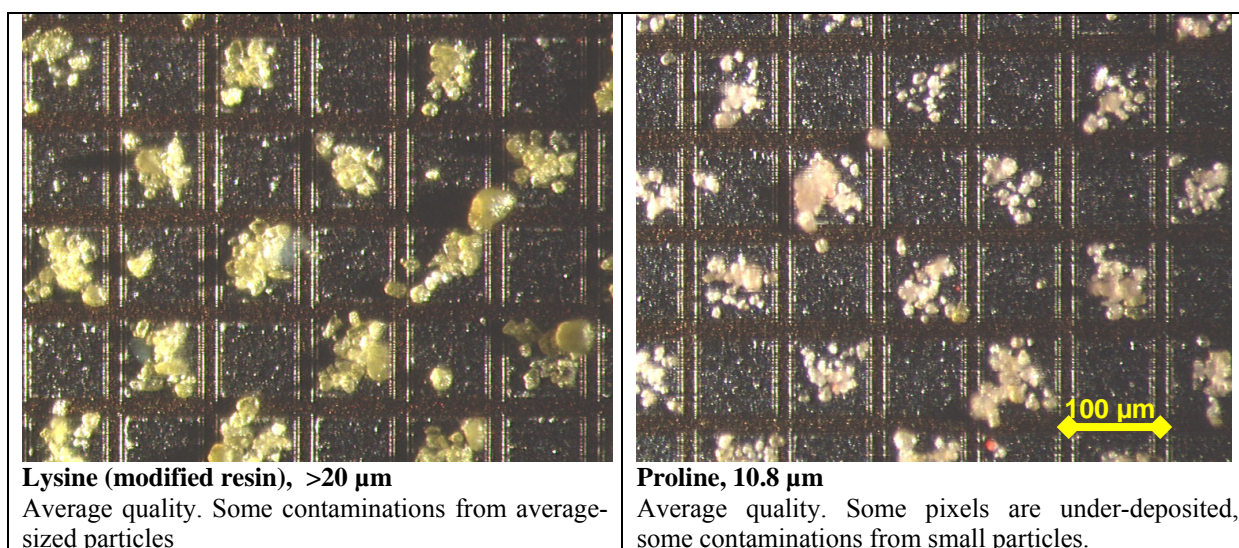
6.3.4 Influence of Deposition Patterns and Particle Properties on Transfer Quality

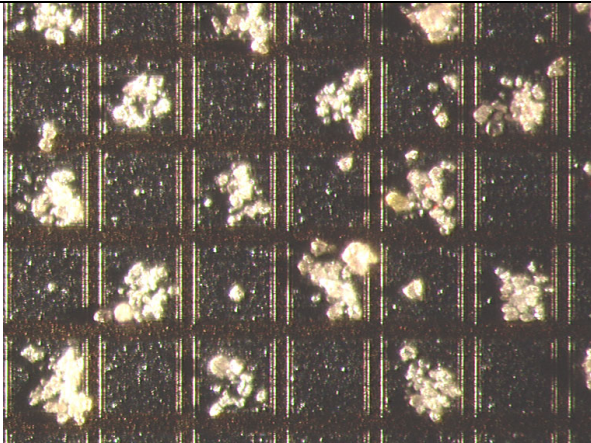
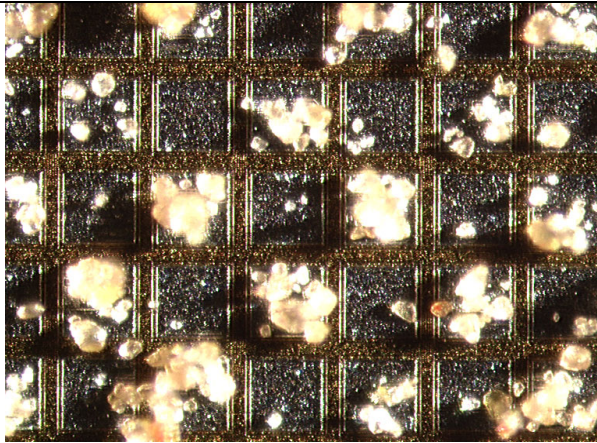
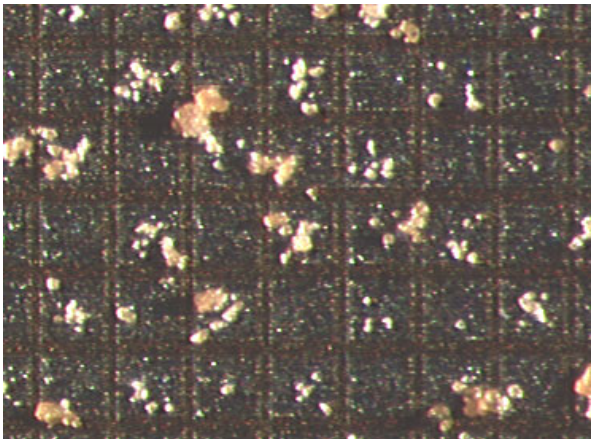
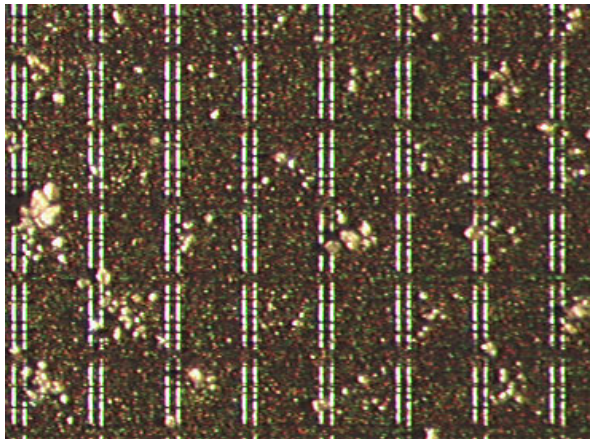
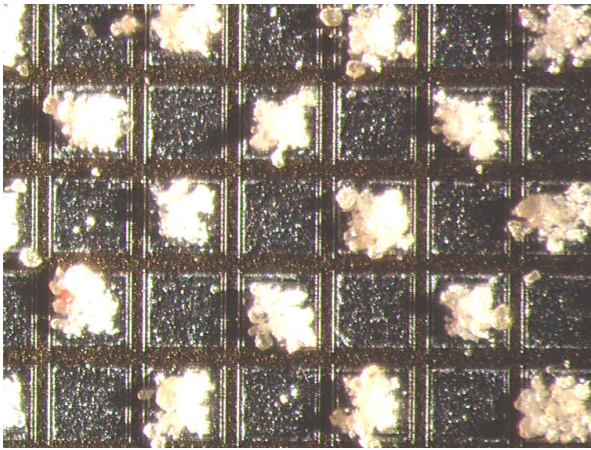
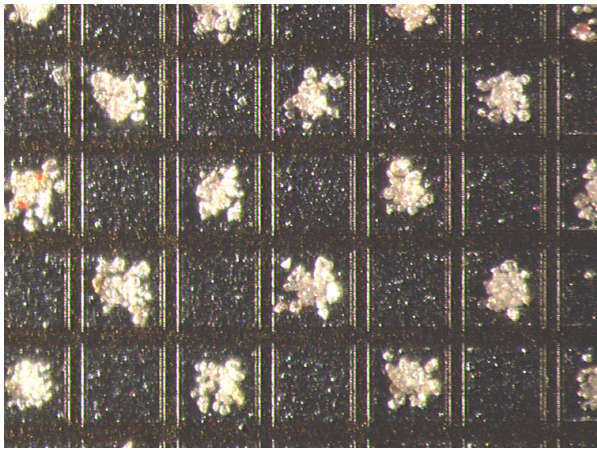
6.3.4.1 Coarse Fraction Particles

Different batches of amino acid particles were tested by deposition experiments in preparation for combinatorial synthesis, in order to ascertain the availability of the particles required for synthesis. The different batches were compared with regard to their performance in the aerosol, in order to elucidate the range of transfer quality of different batches. While the experiments in this work focused on particle tests in deposition experiments with the objective of finding useable particle batches for synthesis experiments, other works [LOE09] also investigated particle properties under laboratory conditions.

More than 20 different batches of particles from the coarse fraction (average particle diameter between 8 and 20 μm), which is standard for use in the peptide laser printer, were tested in the aerosol, with different average particle size, resin and charge control agents used, and amino acid, with the objective of finding acceptable batches of particles for all 20 standard amino acids. A batch of reference particles, containing all components of standard particles but no amino acids, was also tested. For the synthesis on Peptidchip 3.1, only patterns with more than one in nine pixels active were tested, in order to avoid the difficulties described in 6.3.2.2.

For the sake of brevity, not all depositions are described here. Examples of good and bad deposition quality for a number of causes are shown in tab. 6.1. Particles from the same batch showed similar behavior in different particle transfer chambers, and even though aerosol parameters had to be varied with changes in the amount of particles in the chamber, previous deposition quality levels could be retained for weeks of storage of a chamber filled with particles in air.



	
<p>Histidine (modified CCA), 8.8 μm Average quality. Some contaminations from average-sized particles</p>	<p>Aspartic Acid, 15.8 μm Poor quality. Some pixels are over-, others under-deposited, contaminations with small to large particles.</p>
	
<p>Alanine, 13.7 μm Poor quality. Many pixels are under-deposited, contaminations from small particles and agglomerates.</p>	<p>Alanine, 11.4 μm Very poor quality. Strong under-deposition.</p>
	
<p>Alanine (modified CCA), 9.7 μm Good quality. Few contaminations from small particles.</p>	<p>Glutamic Acid, 10.2 μm Very good quality. Very few contaminations.</p>

Tab. 6.1: Examples of particle deposition results. The amino acid used is noted below each image (deviations from the standard in resin and charge control agent are noted) along with average particle diameter. Quality of deposition is described for each deposition.

Unfortunately, no correlations between physical or chemical particle properties and deposition quality could be found. Neither particle size, nor presence and sort of amino acid was shown to be the crucial parameter in deposition quality, and with all resins or charge control agents tested, deposition quality varied with particle batch. Aging of particles might be an issue, as some batches of particles yielding bad results had been stored for over four years. However, some of the older batches of particles yielded good results even after four years of storage, and while most newly-made particles showed at least average performance, not all of them were superior to the older batches.

In some batches with poor performance, particle performance improved noticeably upon adding a spatula tip (ca. 5 mg) of silica nanoparticles into the aerosol chamber or the falcon tube containing the particles, while for other batches this had no effect.

Particle batches with at least average deposition quality could be found for all 20 standard amino acids. While particle production may need to be improved if coarse fraction particles are to be used for routine syntheses in order to guarantee the highest particle qualities possible, these experiments provided the required particles for the syntheses described in chapter 7.

6.3.4.2 Sparse Deposition Patterns

In order to investigate the effects of the pattern on deposition results further, new test patterns were used. In these patterns, Peptidchip 5 is divided into four square parts of equal size. The first part is deposited in a 1:1 checkerboard pattern, the second at one active pixel in four, the third at one active pixel in sixteen, and in the fourth part, fifteen pixels out of sixteen are active. Typical results are shown in fig. 6.14. Deposition in 1:1 and 1:4 patterns is good, while the 1:16 pattern shows contaminations. For the 15:16 pattern, saturation of target pixels with particles is low compared to the sparse patterns, especially on the pixels adjacent to the inactive ones (this behavior was also observed for OKI Magenta in [KÖN05]). Similar results were achieved with all other batches of coarse fraction amino acid particles tested. These results confirm the difficulties with the deposition of coarse fraction particles in sparse patterns. Increasing the grid electrode voltage was attempted in order to use the grid as a “dump electrode”, attracting particles that would otherwise be deposited as contaminations on other pixels. For the coarse fraction particles, this showed no effect.

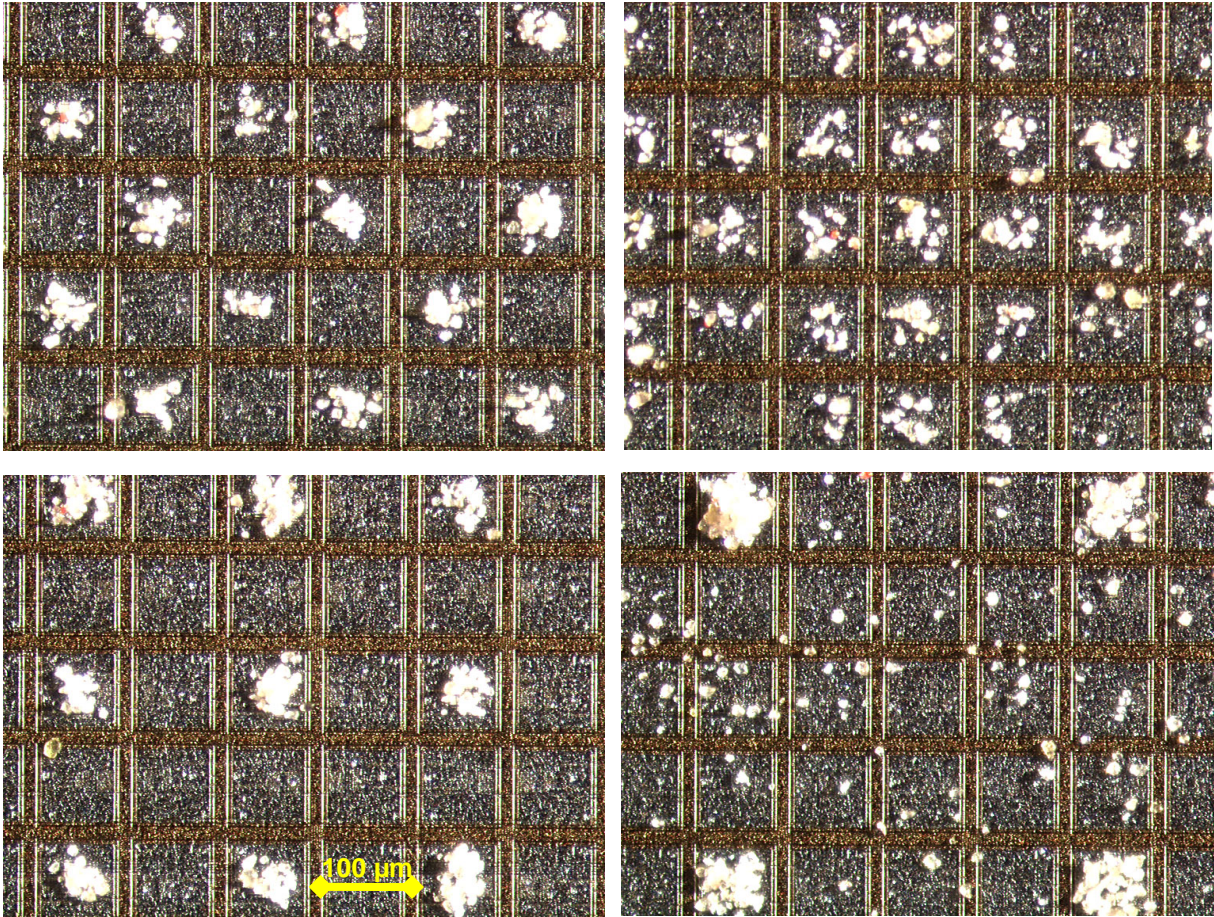


Fig. 6.14: Particle deposition results for glutamic acid particles, 10.2 μm average diameter. Pixel voltage 100 V, grid voltage 15 V. Top left: 1:1. Top right: 15:1. Bottom left: 1:3. Bottom right: 1:15.

If sparse deposition could be achieved at improved quality, the low saturation of particle deposition for dense patterns could be easily circumvented by splitting deposition for each layer. This is achieved by picking a checkerboard pattern subset of the chip and activating all pixels to be deposited on within this subset. Thereafter, the procedure is repeated on the complementary checkerboard pattern. Therefore, if arbitrarily sparse deposition could be achieved at low levels of contaminations, difficulties with dense deposition patterns could be easily compensated for. A method to achieve this is shown in 6.3.4.3.

6.3.4.3 Fine Fraction Particles

As shown theoretically in 3.6.6, drag forces are stronger compared to inertial forces at low velocities (around 1 m/s) for smaller particles. Thus, particles smaller than the coarse fraction of around 10 μm average particle diameter, i.e. the fine fraction particles with an average diameter of 5 μm , should have a lower tendency to cause contaminations. Electrostatic forces are stronger compared to drag forces for small particles at these velocities, as well, which also indicates that small particles may show a favourable behaviour with regard to contaminations.

Using batches of particles that still contained a large number of particles with a small diameter, it was observed that these small particles are sometimes deposited differently from

those with larger diameters [LOE09]. During amino acid particle production for laser printing, usually only the coarse fraction of particles, with a diameter between 7 and 15 μm is used. Smaller particles, the fine fraction, are not used in laser printing. Some fine fraction batches of particles produced for laser printing, which had remained after sieving and winnowing, had been stored for eventual future use.

Using these stored fine fraction particles, it was shown that the grid electrode can be used to reduce contaminations on the pixels by drawing off some particles there. First results of deposition, even with only one in 64 pixels active, showed excellent results for different amino acid particle batches (fig. 6.15 and fig. 6.16).

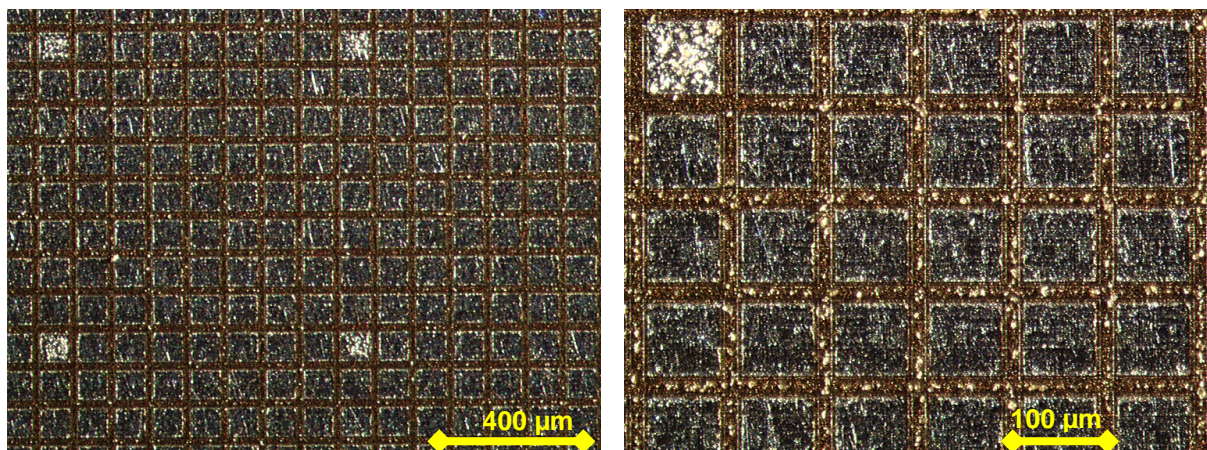


Fig. 6.15: Deposition result of tryptophan particles in a 1:63 pattern. Pixel voltage 100 V, grid voltage 30 V. While some particles were deposited on the grid electrode, the pixels are remarkably free from contaminations.

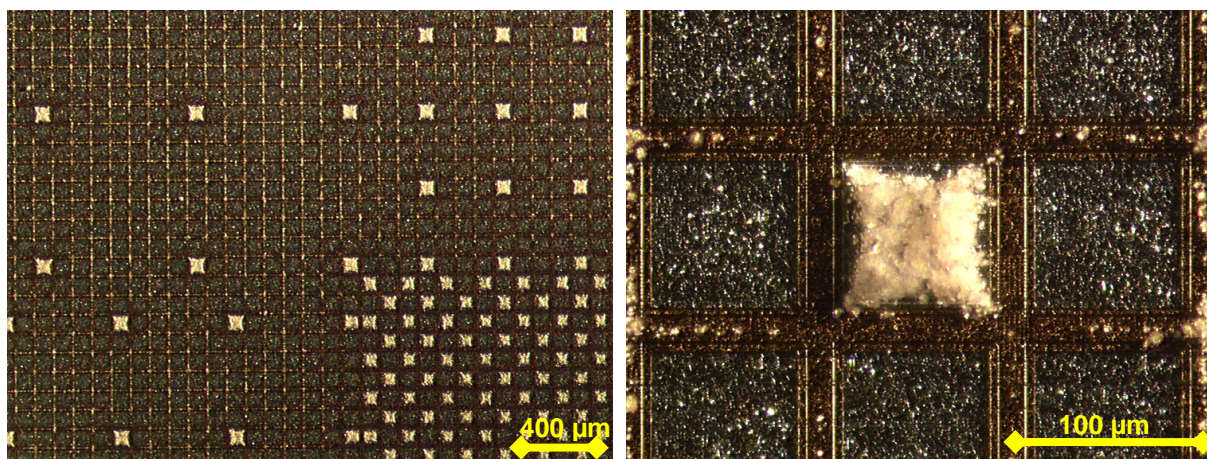


Fig. 6.16: Deposition result of alanine particles in a 1:63 pattern. Pixel voltage 100 V, grid voltage 30 V. While some particles were deposited on the grid electrode, the pixels are remarkably free from contaminations.

These preliminary results indicate that fine fraction particles are superior to coarse fraction particles for use on CMOS chips, and that further deposition research should focus on these particles. Detailed theoretical and experimental considerations of particle transfer using fine fraction of particles, including a modified setup for improved particle transfer, will be found in future works [LOE].

6.4 Metal-Oxide Layers on the Chip Surface

6.4.1 Motivation

One possible application of the Peptidchip system is the search for catalytic peptides or catalysts containing peptides (e.g. complexes of peptides and metal atoms). Finding substances that catalyze reactions resulting in the generation of hydrogen molecules are one example of particular interest e.g. for energy storage or conversion of solar energy if such a reaction was light-driven. The Peptidchip support could be used to test numerous peptides for this ability in parallel if a means to detect molecular hydrogen being generated on specific pixels could be devised. Tungsten oxide (WO_3) is known to be able to take up hydrogen into its bulk structure, whereupon its electrical conductivity and optical transmission properties change noticeably. For example, electrical conductivity of a thin film of tungsten oxide changes by six orders of magnitude when exposed to 1% hydrogen in nitrogen atmosphere, while transparency for light between 600 nm and 1000 nm decreases [NAK03, SEK00]. Absorption rates of hydrogen into tungsten oxides are low for practical use, but they can be enhanced to sufficient levels by adding a layer of platinum or palladium on top of the tungsten oxide. Resistive hydrogen detection is hard to combine with high voltage potential areas, and therefore would result in much larger pixels if implemented. However, using changes in optical transmissivity of tungsten oxide films on semiconductor photo detectors for hydrogen detection [LEE00] in a spatially selective way on a Peptidchip with integrated photodiodes could be envisioned without increasing area requirements. In this work, compatibility of both tungsten oxide – palladium film generation and influence of these films on Peptidchip operation and particle deposition have been examined.

6.4.2 Results

6.4.2.1 Effects of Film Generation on Electronic Functionality

A tungsten oxide film of 400 nm and subsequently a palladium film of 5 nm were evaporated onto naked Peptidchip 3.1 dies, which exposes chips to thermal and chemical stress. The whole chip, including the bond pads, is covered unless precautions are taken.

It is difficult to pierce a tungsten oxide layer using a wire bonder, as the bond tool clogs regularly and an increased percentage of wires fails to bond to the chip under these conditions. Protecting the bond pad area of the chip with a small Teflon covering prevents formation of the films in that area, and thus allows bonding using standard procedure.

The surface of three chips was modified in the described process, with the Teflon covering protecting the bond pads. Subsequent electronic testing via the I²C (writing and reading back data to and from the pixel memory cells) showed the digital components of the chips to be fully functional.

6.4.2.2 Particle Deposition

Two of the three modified chips were tested in an aerosol of OKI Magenta particles, with a checkerboard pattern programmed. Even at optimal aerosol conditions, however, this repeatedly resulted in failed depositions, with most of the pixel matrices covered by particles as though there was no electric field present on its surface. The only exceptions to this were the pixel areas with passivation openings, where the desired deposition pattern was produced

as expected (fig. 6.17). This experiment was repeated using leucine bioparticles (12 μm average diameter), with the same results.

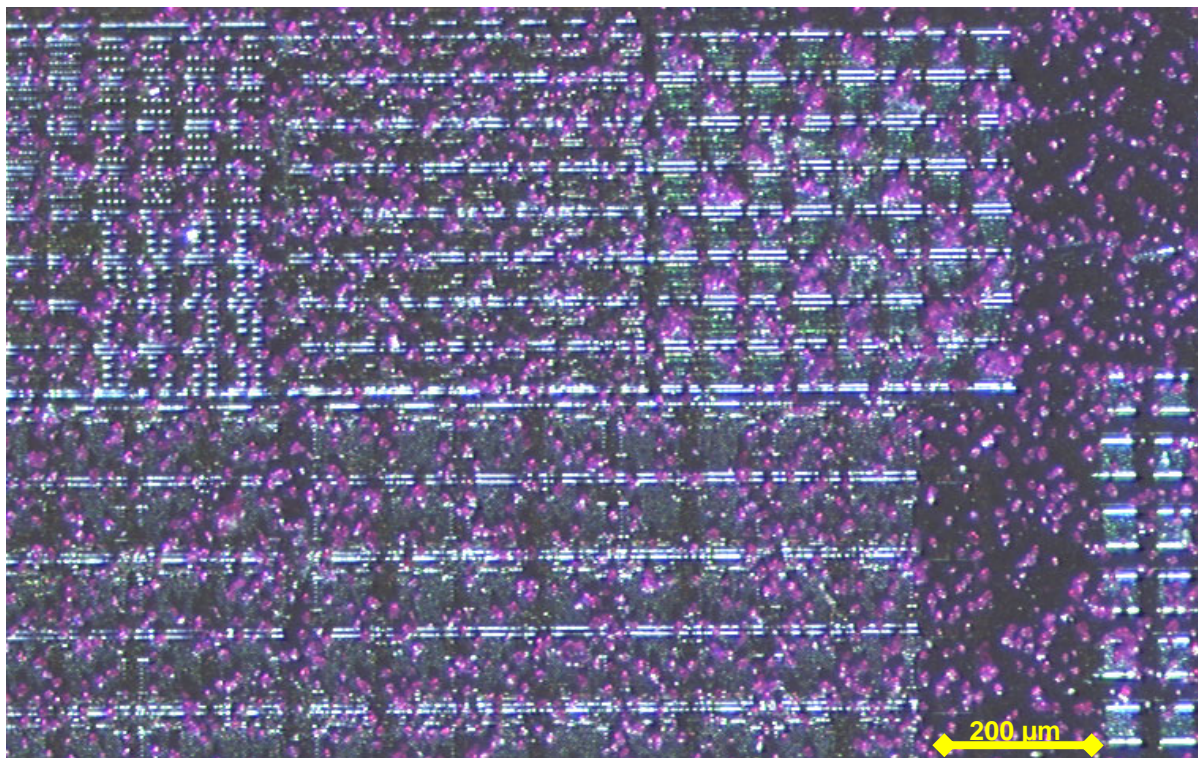


Fig. 6.17: Transfer of particles on a Peptidchip 3 with surface modifications for hydrogen detection. The pixel area in the top right corner has passivation openings, all other pixels are passivated.

6.4.3 Discussion

Random deposition on most pixel areas of the chip could have two main reasons: First, the pixels in question might have been destroyed in their electronic functionality, or second, the films might *block* the electric fields that effect the spatially selective deposition.

Due to the stress of film generation, electric failure was a possibility. While failure of the low-voltage parts could be ruled out by the tests described in 6.4.2.1, the high-voltage pixels cannot be tested with this method. However, the pixel areas with passivation openings were functional, and they do not have their own electronics, but each is directly connected to the potential area of the corresponding pixel in the adjacent pixel area to the left (see 5.3.2). Both potential areas, being connected by a metallic conductor, must be at the same voltage, which must be the correct one as correct deposition is observed on the non-passivated pixels. Therefore, the pixels have to be electronically functional, including the high voltage part.

Interference of the films with the electric fields is conceivable. Even at a thickness of only 5 nm, the palladium layer on top of a modified chip is a closed conductor in the electric field generated by the pixels. This confines the electric field to the dielectric between the potential areas and the palladium layer, leaving a homogeneous potential in the volume above the chip (fig. 6.18, left side).

However, if all pixel areas are covered by the film, the pixel matrices with passivation openings should be non-functional, as well. Aside from the possibility that the film generation

failed completely in these areas, which is unlikely in the vapour deposition method used, WO_3 might not be a perfect insulator. If that were the case, the potential area of each non-passivated pixel would be electrically connected to its neighbors by a high-resistance connection. Assuming the oxide and the palladium film to be continuous, each pixel would be connected to its neighbors via a series resistance of $R_{Pd} + (R_{Pd} \parallel R_{WOx}) + R_{Pd}$ (fig. 6.18). Disregarding the resistance of the potential areas, HV inverter and power supply, $R_{Pd} \parallel R_{WOx} > 2 \cdot R_{Pd}$ would be a required condition for a sufficient voltage drop over the palladium film between two pixels. However, at the given geometry, for pixels of $80 \mu\text{m}$ pitch and $76 \mu\text{m} \times 76 \mu\text{m}$ passivation openings and a checkerboard pattern, this would require a ratio of specific resistivities of $\rho_{WOx} < 3 \cdot 10^8 \cdot \rho_{Pd}$ ¹. Literature values are $\rho_{WOx} \approx 10^5 \Omega \text{m}$ [TRI99] and $\rho_{Pd} \approx 10^{-7} \Omega \text{m}$ [IPA], thus even though Pd resistivity may be increased due to surface effects in this thin film, and WO_3 resistivity may be reduced due to interactions with other materials than hydrogen, this explanation is unlikely.

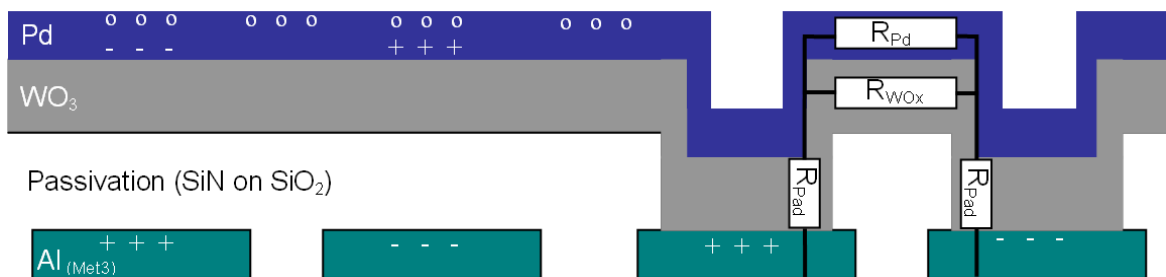


Fig. 6.18: Possible explanation for shielding of electric fields: The conductive palladium layer shields the volume over the chip from electric fields where it is continuous over a number of pixels (left). If WO_3 was not a perfect insulator, a current would be present between each pixel and its neighbors at a different voltage. If the conductivity of the thin Pd film was low, the voltage drop over the Pd film between two pixels might be sufficient for deposition (right).

Another explanation for the absence of shielding on the pixels with passivation openings could be that the palladium film is interrupted in these areas, e.g. at the pixel edges (fig. 6.19). In that case, charges in the palladium could not be transferred between pixels, and the field would not be shielded. Reduced thickness of the Pd layer at the edges resulting in an increased resistivity of the layer might also contribute, allowing the previous explanation.

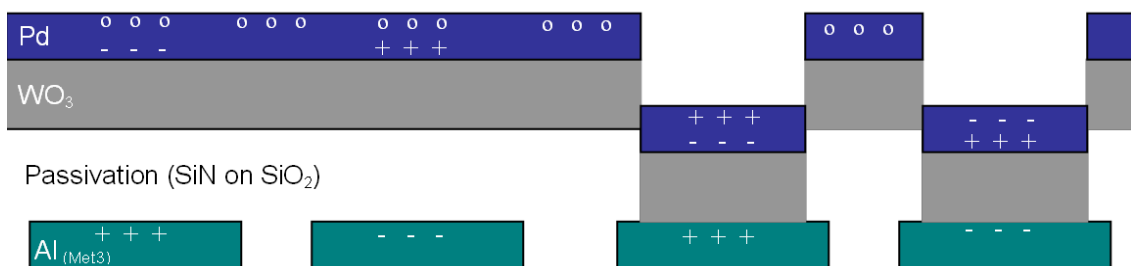


Fig. 6.19: Possible explanation for shielding of electric fields: The conductive palladium layer shields the volume over the chip from electric fields where it is continuous over a number of pixels (left). If it were interrupted between each pixel, it would not have this shielding effect (right).

¹ Using $R = \rho \cdot d / A$, we get: $R_{Pd} \approx \rho_{WOx} \cdot 70 / \text{m}$; and assuming $\rho_{WOx} \gg 80 \rho_{Pd}$, we get $R_{Pd} \parallel R_{WOx} \approx R_{Pd} \approx 4 \rho_{Pd} \cdot 5 \mu\text{m} / (80 \mu\text{m} \cdot 5 \text{nm}) \approx \rho_{Pd} \cdot 4 \cdot 10^9 / \text{m}$. Thus, $R_{Pd} > 2 R_{Pd}$ requires $\rho_{Pd} \cdot 4 \cdot 10^9 > \rho_{WOx} \cdot 140$ or $3 \cdot 10^8 \cdot \rho_{Pd} > \rho_{WOx}$.

6.4.4 Conclusions

The CMOS chips used can survive the deposition of WO_3 and Pd films as required for hydrogen detection, but a closed metal layer blocks electric fields, making selective particle deposition impossible on chips with closed passivation. Pixels over which passivation openings are implemented remain capable of selective particle deposition, presumably because the palladium layer is not continuous there, or because the layer is connected to the pixels via a high resistance. Passivation openings, however, are incompatible with the “holes” required in the potential area metal for optical detection (see 5.2.4).

One option to circumvent this incompatibility might be to use islands of palladium smaller than the individual pixels on fully passivated chips instead of a closed film. Alternatively the palladium could be structured, e.g. cut parallel to the grid lines between the pixels, but such a process would require additional research and engineering effort.

6.5 Compatibility of PEGMA Films with Particle Deposition

6.5.1 Approach

Previous to this work, particle deposition had not been tested on CMOS chips surface-modified with the PEGMA layers (approx. 100 nm thick) used to increase the number of amino groups available on the chip surface and for protein resistance (4.1). Such depositions had been performed successfully on fixed-pattern chips surface-modified in this way, however [BEY07]. Particle transfer on surface-modified Peptidchip 3 CMOS chips was therefore not expected to differ from particle transfer on pristine CMOS chips. Nevertheless, the first attempts to deposit particles on surface-modified CMOS chips failed, with the chips showing random particle deposition on the entire chip or large parts of it, as though the chip potential areas were not displaying any electric fields (fig. 6.20). This chapter shows reasons behind this effect, and describes methods to perform selective deposition on chips covered with such films.

Hypotheses for failed deposition on surface-modified chips were:

- The surface modification process disables the electric contact between the bond wires and the chip.
- The surface modification process damages or destroys the electronics of the chip.
- Electric fields are blocked by the polymer due to dielectric effects.
- Electric fields are blocked by the polymer, which acts as a conductor.

Each of these hypotheses was tested, with the results described below. In all experiments, good aerosol conditions were verified by testing spatially selective deposition in the same pattern on a *reference chip* with pristine surface before and after deposition. It should be noted that, at the time of these experiments, average aerosol quality was still rather poor, which is reflected in the images.

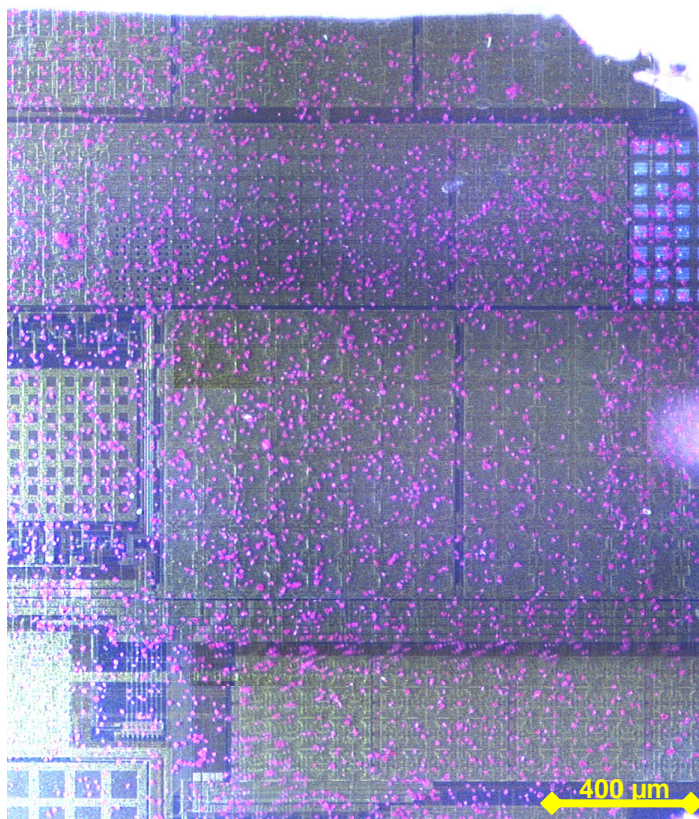


Fig. 6.20: Typical deposition result of Peptidchip 3 with PEGMA polymer. Deposition and photography were performed with the protective covering installed. (Stitched microscope images)

6.5.2 Step-by-step Testing of Surface Modification Procedure

In order to verify whether it is the PEGMA layer or any other step of the surface modification procedure that causes spatially selective deposition on the chips to fail, the procedure was performed step-by-step on three Peptidchip 3 chips. The standard surface modification procedure of that time was broken apart into (see also 4.1):

1. Cleaning of the chip surface with ultraviolet radiation.
2. Silanization of the surface.
3. Exposure to PEGMA monomers and graft polymerization.
4. Aminoderivatization of the “tips” of the PEGMA groups.

After each step, the chip was tested in the aerosol, whereupon the particles were removed and the procedure was resumed.

Selective deposition, comparable to the results on pristine chips, was observed after cleaning and after silanization. After graft polymerization of the PEGMA layer, random deposition was observed, which persisted after aminoderivatization. These results show that either the presence of the PEGMA layer or a mechanical, electrical or chemical influence on the chip during this step causes the failure of selective deposition observed.

6.5.3 Integrity of Bond Contacts and Electronics after Surface Modification

The presence of a PEGMA layer makes bonding more difficult, as greater forces are needed to penetrate it in order to weld the aluminum wire to the bond pad, which increases the risk of the bond tool clogging. Still, having found suitable bond parameters, reliable wire-bonding through the PEGMA layer was routinely achieved.

As fixed-pattern chips did not fail to achieve spatially selective deposition even with a PEGMA layer present, failure of the electronics of CMOS chips was suspected. After PEGMA layer generation, chips were tested electronically using the I²C (writing and reading back of data into the pixel memory cells), which showed the digital components of the chips to be fully functional.

Further experiments showed that pixel matrices with passivation openings reproducibly yielded good deposition results (fig. 6.21), even though their adjacent matrices with closed passivation with which they shared the controlling electronics did not. This effect is similar to observations on compatibility of films for hydrogen detection (6.4). The presence of a PEGMA layer on the aluminum was verified by ellipsometry, ruling out the possibility of a failed PEGMA layer generation on the aluminum pads.

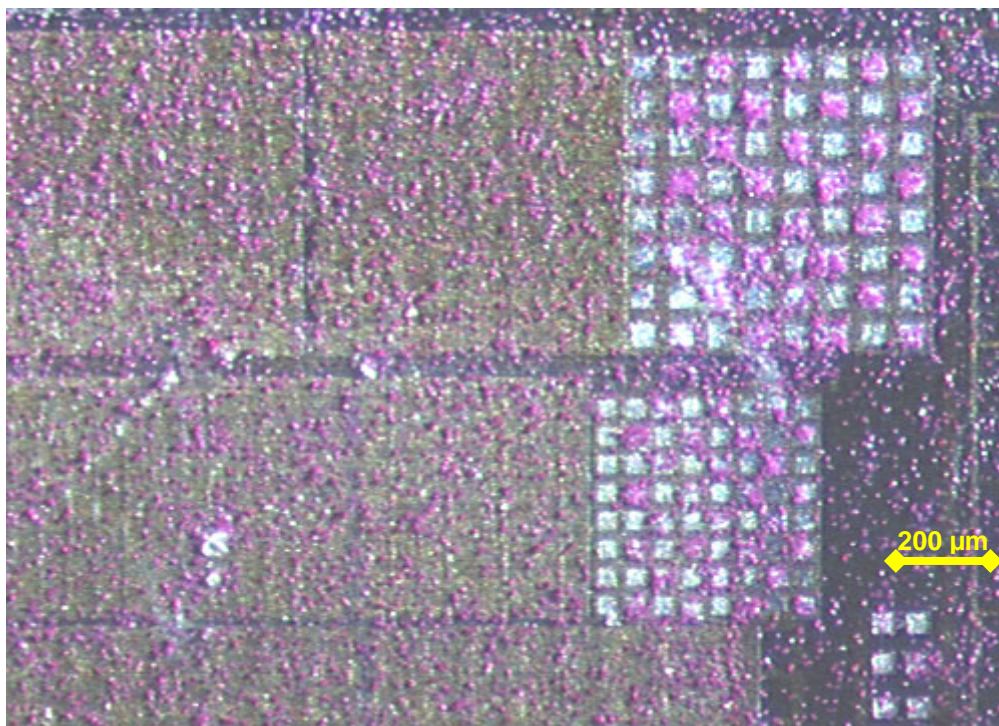


Fig. 6.21: Deposition result of Peptidchip 3 with PEGMA polymer, in checkerboard pattern. The left matrices, with passivation openings (“shiny” pixels), show regular deposition, while the other matrices are deposited randomly.

In further experiments, Peptidchip 3.1 chips were exposed step by step to only the cleaning procedure using UV light, the cleaning procedure and silanization of the surface, as described above. Finally, the synthesis of a film was *simulated*, that is all these steps plus exposure to chemicals as they are used in film synthesis were performed, however, the poly(ethylene glycol) monomers were omitted. This simulated the stress imposed on the chip by contact with the chemicals used in PEGMA layer generation, while making formation of a polymer layer impossible due to the lack of the required monomers. In all these experiments, the chips

were not affected in neither their electronic integrity nor in their ability to effect selective particle deposition after exposure.

Finally, a chip was surface-modified with the PEGMA polymer, and also found to be non-functional in selective deposition except for the pixels with passivation openings. By exposure of the chip to 90° C in air for three hours the polymer was thereafter “burnt off” and thus destroyed. Selective transfer in the aerosol was successful on the whole chip, as on pristine chips, afterwards.

Taken together, these results prove beyond doubt that the procedure of PEGMA layer generation does not significantly damage the electronics of a Peptidchip.

6.5.4 Blocking of Electric Fields

6.5.4.1 Introduction and Theory

If selective deposition fails completely despite of good aerosol conditions and good particles as verified by reference chips, the absence of the selective force, and thus of the electric field, may be suspected. If the chip is electrically intact, we could expect the electric fields to be *blocked* by some mechanism, similar to the observations in 6.4.

Two physical mechanisms could be responsible for the blocking of electric fields: First, as with the metal layer in 6.4, a conductor could “short-circuit” the electric field, and second, a strong dielectric could decrease the range of the field. As noted in 3.6.4, the range of the electric field in air on the chip is approximately equal to the pixel size. In a dielectric, that range is reduced approximately proportional to the relative dielectric constant ϵ_r . Indeed, the passivation of about 500 nm silicon nitride at $\epsilon_r \approx 7.5$ is roughly equivalent to 4 μm of air, which is still small compared to pixel sizes between 34 μm and 100 μm . For the PEGMA layer of about 100 nm to shield the field of a 100 μm pixel, the layer would need to have an $\epsilon_r > 1,000$, which is not realistic for such materials. Furthermore, there would be no explanation why the presence of passivation makes a difference between adequate function and total failure of selective deposition. This rules out dielectric blocking of the electric field.

Assuming a polymer like PEGMA to be conductive runs against our intuitive understanding of materials. An electron gas like in metals can not be imagined in such a substance. However, ions in a liquid, such as tap water, are known to be quite an effective conductor. PEGMA layers are known to be hydroscopic [STA07], and water or metal ions, taken up from the chip surface or any traces of dust or contamination during layer generation could diffuse freely between the polymer chains in such a film. Indeed, ionic conduction in polymer films is not unheard of in the literature [ALI98]. One possible explanation why the pixels with passivation openings are not affected could be that the conductive layer is interrupted at the edges of the passivation openings (see 6.4), another possibility is neutralization of charge carriers on the exposed potential areas (fig. 6.22), and the third is simply a highly resistive connection between adjacent pixels similar to the one shown in fig. 6.18.

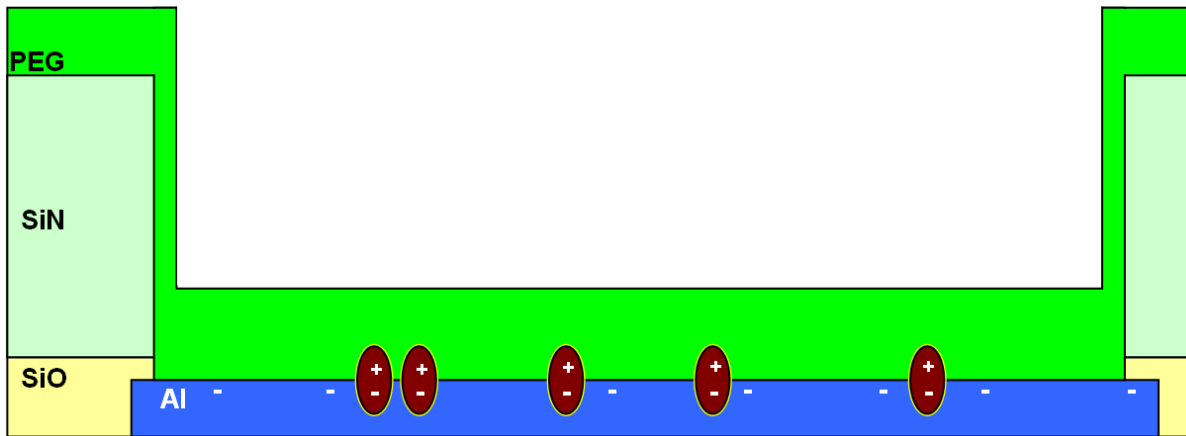


Fig. 6.22: Possible explanation of results in selective deposition on chips with PEGMA surface modification. Charge carriers (e.g. positively charged ions) migrate to a potential area of opposite (here: negative) charge in the electric field, come into direct contact with it, and pair with an opposite charge on the surface. As the potential area is held at a constant voltage, charges thus neutralized are replaced on the potential area from the power supply, while the PEGMA layer is depleted of charge carriers. Invert charges in the drawing for pixels at HV.

6.5.4.2 Experimental Verification using Fixed-Pattern Chips

A fixed-pattern chip has been designed for manufacture at TU Dresden [TUD], that enables the verification of the hypotheses on the blocking of electric fields. On this chip, three kinds of pixels have been realized, differing only in the passivation over the potential areas. In addition to standard passivated pixels and pixels with passivation openings etched down to the aluminum, a third variant of pixels has been implemented which is etched using the same etching process as the standard pixels with passivation openings, but the etching process is stopped before the aluminum is reached (fig. 6.23). This should ensure comparable “edges” on the etched spots, but no exposed aluminum in case of these special pixels. If such edges indeed interrupt a conductive PEGMA layer, both sorts of etched pixels should be capable of spatially selective deposition. However, if no selective deposition is observed on the partially etched pixels, presence of exposed aluminum is required for selective deposition, which would support the explanation of charge neutralization on the PEGMA-aluminum interface.

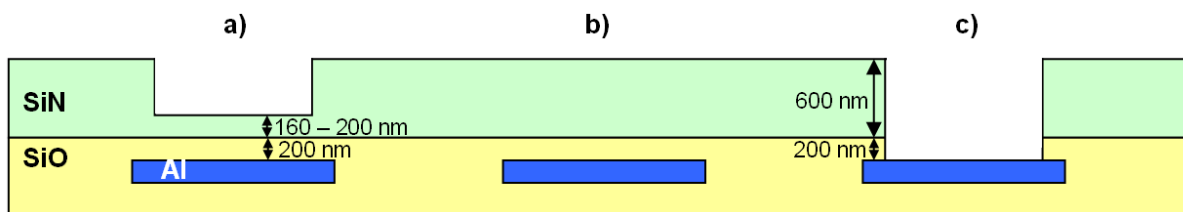


Fig. 6.23: Cross section of a fixed-pattern chip for direct comparison of passivated and non-passivated pixels. Section a) shows the layout of the pixels on the left part of the chip, where the passivation is partially etched. Section b) and c) are used as references, with closed passivation and completely etched passivation, respectively.

Two chips were tested in an aerosol of amino acid toner particles. Without a PEGMA layer present on the chip, all pixels showed selective deposition, thus verifying the chips to be functional. Four chips were covered with a PEGMA layer, and showed selective deposition only on pixels with completely etched passivation openings (fig. 6.24). This confirms the necessity of exposed aluminum for spatially selective deposition, and provides evidence against the hypothesis of an interrupted PEGMA layer on pad window edges.

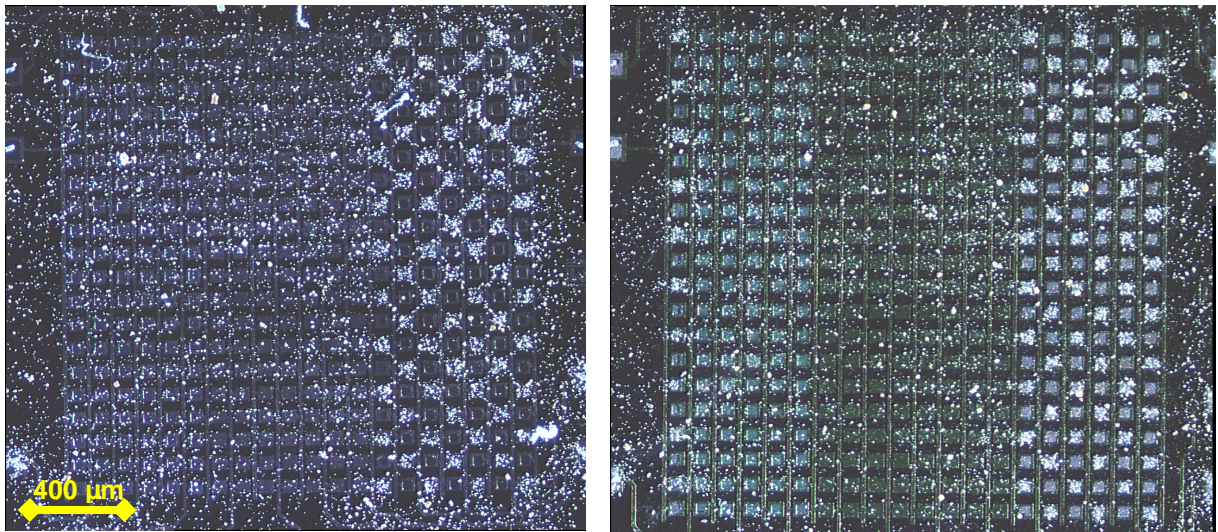


Fig. 6.24: Typical results of particle transfer onto two surface-modified fixed-pattern chips with different passivation variants. Pixel pitch is $100\ \mu\text{m}$. Pixels with completely etched passivation openings (right) show regular selective deposition, while both standard passivated (center) and partially etched (left) pixels exhibit random deposition. (In the right picture, the leftmost row of pads was completely etched due to a manufacturing error.)

6.5.5 Thin Polymer Layers

A small percentage of CMOS chips modified with PEGMA layers showed partial function even on some passivated pixels (fig. 6.25), especially on pixels at 100 V. PEGMA layers created by the polymerization protocol employed at that time were known to be inhomogeneous in thickness. Their thickness was maximized (at around 100 nm) in order to provide as large a number of synthesis sites as possible. It was speculated that the PEGMA layer was thinner, due to inhomogeneity of the polymerization, on the pixels that showed spatial deposition.

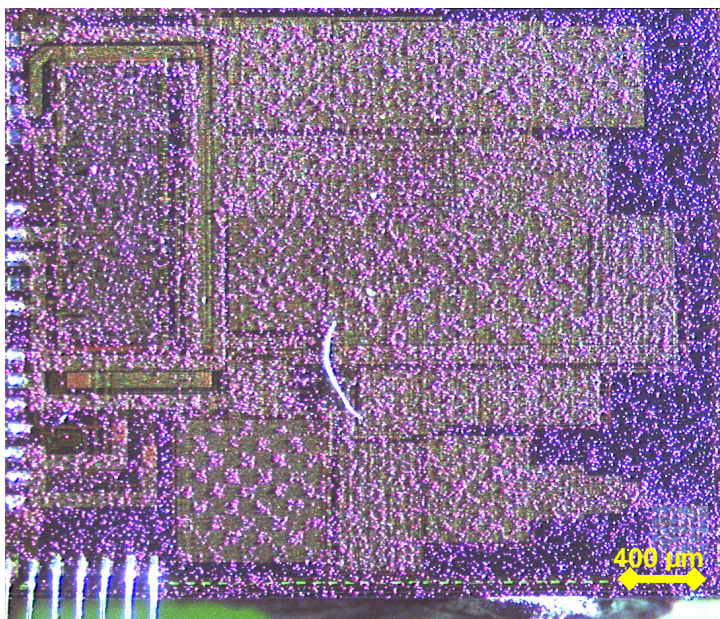


Fig. 6.25: Example of a Peptidchip 3.1 with partially successful deposition. Some of the 100 V matrices show successful deposition in a checkerboard pattern, while others, including all 60 V and 30 V matrices show random deposition.

In order to verify this hypothesis, three Peptidchip 3.1 chips were surface-modified with thin (approx. 35 nm) PEGMA layers. All three chips showed only partial selective deposition, though on some chips even pixels at 60 V and 30 V showed successful transfer, while 100 V pixels on the same chip showed random deposition (fig. 6.26, 6.27). It is thus concluded that thin PEGMA layers are not a reliable solution to achieve selective particle deposition on CMOS chips surface-modified for peptide synthesis.

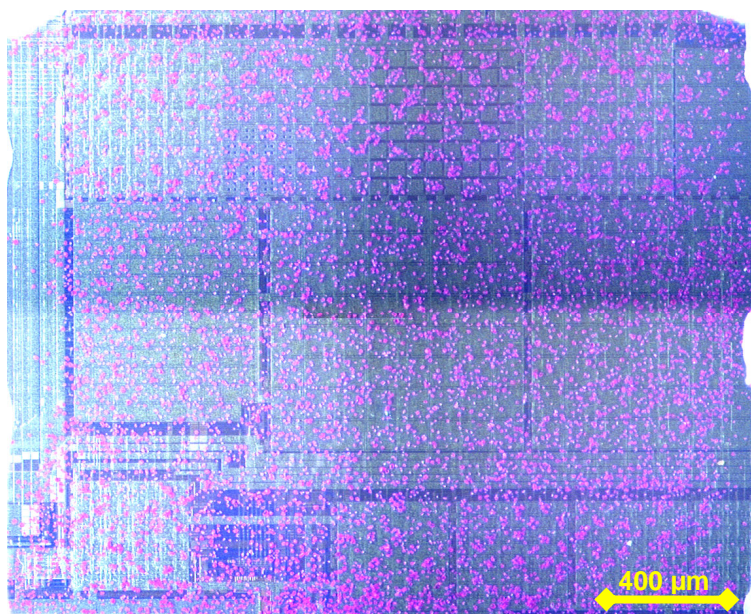


Fig. 6.26: Example of particle deposition on a Peptidchip 3.1 with thin PEGMA layer ($\approx 35 \mu\text{m}$). Selective particle deposition is successful only on some pixel matrices. Deposition was performed with chip covering installed. Stitched microscope images.



Fig. 6.27: Example of particle deposition on a Peptidchip 3.1 with thin PEGMA layer ($\approx 35 \mu\text{m}$). Selective particle deposition is successful only on some pixel matrices. Deposition was performed without chip covering installed. Stitched microscope images.

6.5.6 Heteropolymers

PEGMA polymer layers are quite hydroscopic, and thus may take up moisture from the ambient air. The effort to handle chips under controlled atmospheres exclusively during deposition experiments, microscopy and storage would be enormous, and thus was not attempted. However, heteropolymers made up of PEGMA and methyl methacrylate (MMA) monomers are known to be less hydroscopic [STA08-2], especially at high MMA contents. These heteropolymers retain the favorable protein resistance of pure PEGMA layers. Unlike the PEGMA monomers, each of which can be aminoderivatized to allow formation of a peptide, the MMA monomers are not aminoderivatized, thus a high MMA content decreases the number of synthesis sites available.

Peptidchip 3.1 chips surface-modified with heteropolymers of different PEGMA to MMA ratios, of varying thicknesses between 30 and 80 nm, were tested in the aerosol. As compromises between number of synthesis sites and hydrophobicity, molar ratios of 50:50, 25:75 and 20:80 were tested, focusing on the peak in hydrophobicity found around a ratio of 20:80 [SAT08-2].

At the ratio of 50:50 PEGMA to MMA, two chips were tested. They showed random deposition on all pixels, except pixels with passivation openings (fig. 6.28).



Fig. 6.28: Example of particle deposition on a Peptidchip 3.1 with 50% PEGMA, 50% MMA layer (thickness ca. 50-100 nm). Selective particle deposition failed, except for the pixels with passivation openings (lower right).

Using layers of 25% PEGMA and 75% MMA, a total of six chips from of three surface modification runs were tested. The two chips from the first run were tested after polymer generation, but before aminoderivatization of the PEGMA molecules, and showed spatially

selective deposition results in the aerosol. After aminoderivatization, they showed very bad results with only hints at selective deposition. The two chips from the second polymerization run showed very bad results already before aminoderivatization, and were not treated further. The two chips from the third run were tested after aminoderivatization and storage in dry nitrogen atmosphere for three days and showed no selective deposition on one chip and selective deposition only in some areas of the chip on the second chip (fig. 6.29). As in some chips, and in previous experiments (6.5.4), failure already occurred before aminoderivatization, it could be speculated that it is not the amino groups added to the polymer but exposure to air during this process (and thus humidity) caused the failure (this is investigated further in 6.5.7). On any account, this polymer layer proved too unreliable for synthesis.

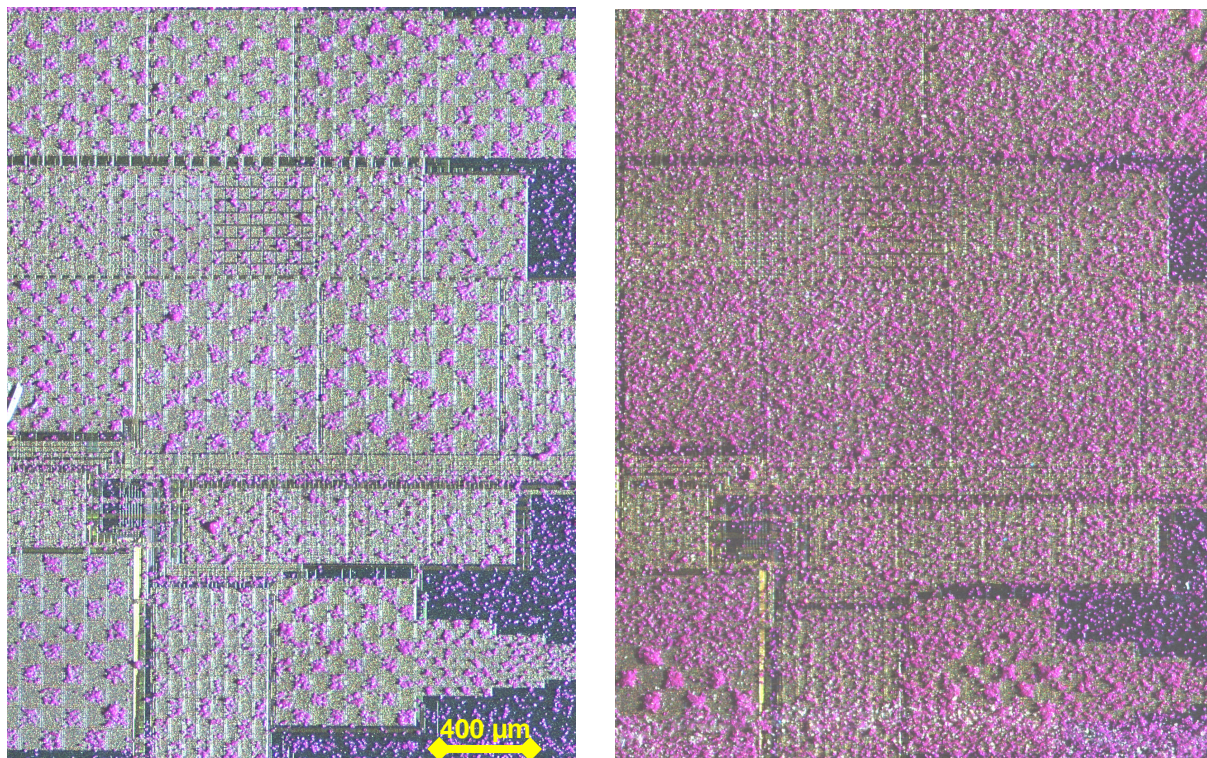


Fig. 6.29: Example of particle deposition on a Peptidchip 3.1 with 25% PEGMA, 75% MMA layer (≈ 50 - $100 \mu\text{m}$), before (left) and after (right) aminoderivatization. Selective particle deposition succeeded on all pixel areas before aminoderivatization, but largely failed afterwards. Stitched microscope images.

Layers of only 20% PEGMA and 80% MMA were first tested on three chips from two polymerization runs including aminoderivatization. All three chips showed good deposition results (fig. 6.30). This kind of polymer layer was used for all synthesis experiments (chapter 7), and did not exhibit any blocking of electric fields.

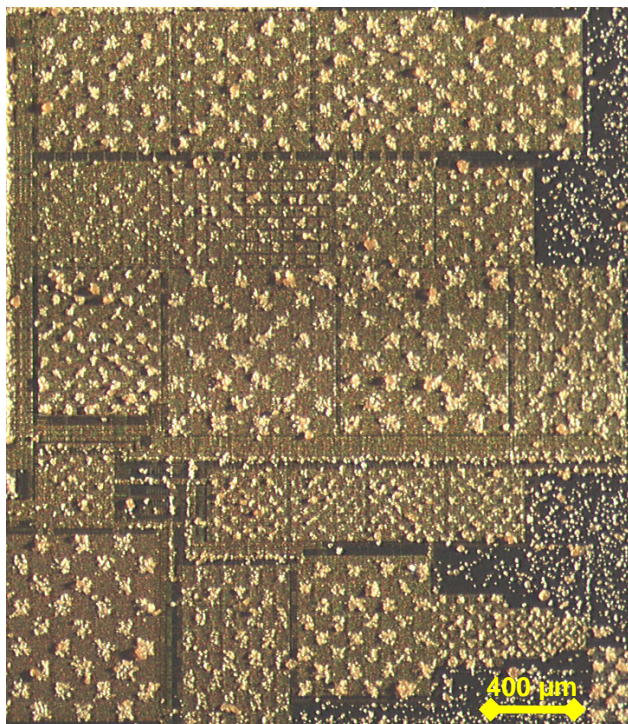


Fig. 6.30: Example of particle deposition (alanine amino acid particles) on a Peptidchip 3.1 with 20% PEGMA, 80% MMA layer ($\approx 50\text{-}100\ \mu\text{m}$), including aminoderivatization. Selective particle deposition succeeded on all pixel areas. Stitched microscope images.

6.5.7 Effects of Water and Ions on Heteropolymer Layers

Even though heteropolymers of 20% PEGMA and 80% MMA prevent electric field blocking for the purposes of on-chip peptide synthesis, it remains interesting to know whether it is indeed the presence of water, and ionic conduction therein, that blocks the electric fields on the chip. Therefore, it was attempted to *force* functional chips with 20% PEGMA, 80% MMA into blocking the electric fields by exposing them to water and ions, and to *recover* them afterwards. Two Peptidchip 3.1 chips with the aforementioned surface modification were exposed to pure (Milipore) water dripped onto their surfaces, then left to dry in air for about 45 minutes. Testing in the aerosol resulted in failed deposition in a circular area in the center of the chip, and successful deposition on the rest of the chip (fig. 6.31). After about 36 hours of storage in nitrogen atmosphere at room temperature, deposition was repeated, and was successful on the entire chip.

Polymers of the sort used in these experiments tend to collapse onto themselves, making parts of the volume inaccessible, which could slow uptake or release of water or ions. However, upon exposure to solvents such as dimethyl formamide (DMF), they swell, and accessibility is increased [STA08-2]. The two Peptidchips from the previous experiment were exposed to DMF for 20 minutes, then blown dry and immediately exposed to 0.5-molar potassium chloride dripped on the surface in excess and left to dry for 80 minutes. Directly thereafter, particle deposition was attempted, which was only successful on part of the chip. After one day of storage under dry nitrogen atmosphere, deposition was repeated, again with selective and random deposition on parts of the chip. After an additional day of storage under dry nitrogen, selective deposition was again achieved on the whole chip (fig. 6.32).

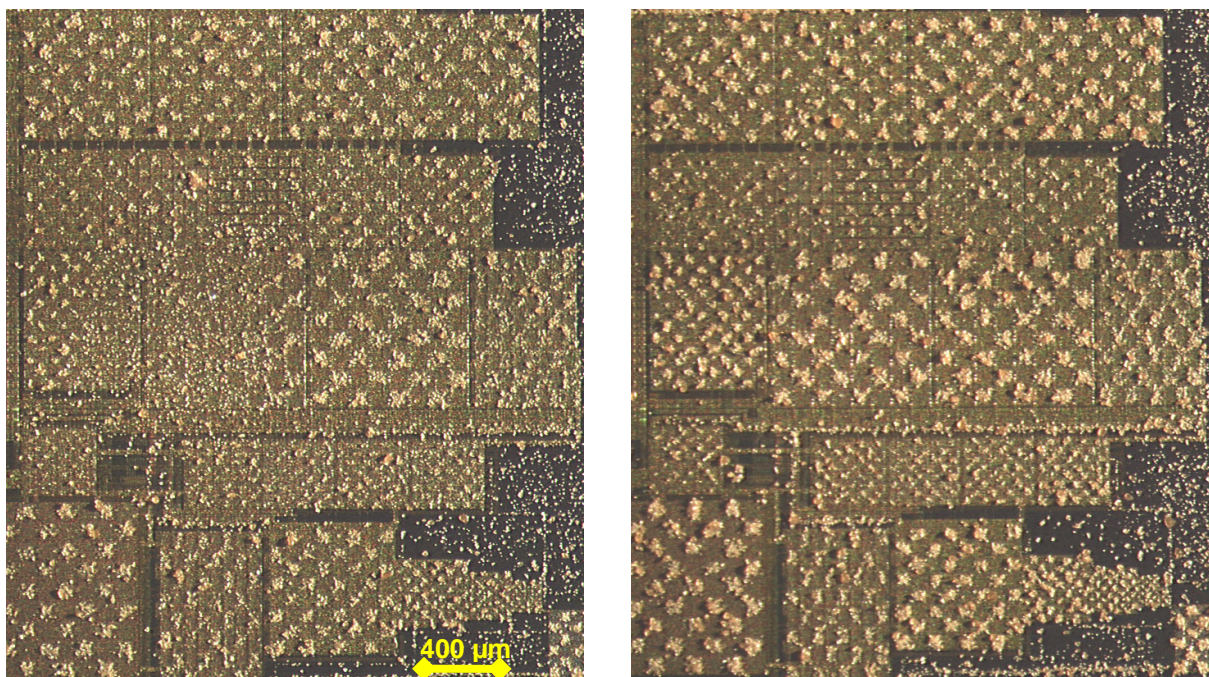


Fig. 6.31: Example of particle deposition (alanine amino acid particles) on a Peptidchip 3.1 with 20% PEGMA, 80% MMA layer (thickness between 50 and 100 μm) after the surface had been exposed to water (left) and after subsequent storage in dry nitrogen atmosphere for 36 hours (right). Selective particle deposition failed in one circular area directly after exposure to water, but the chip recovered the ability to selectively deposit particles during the day under dry nitrogen atmosphere. Stitched microscope images.

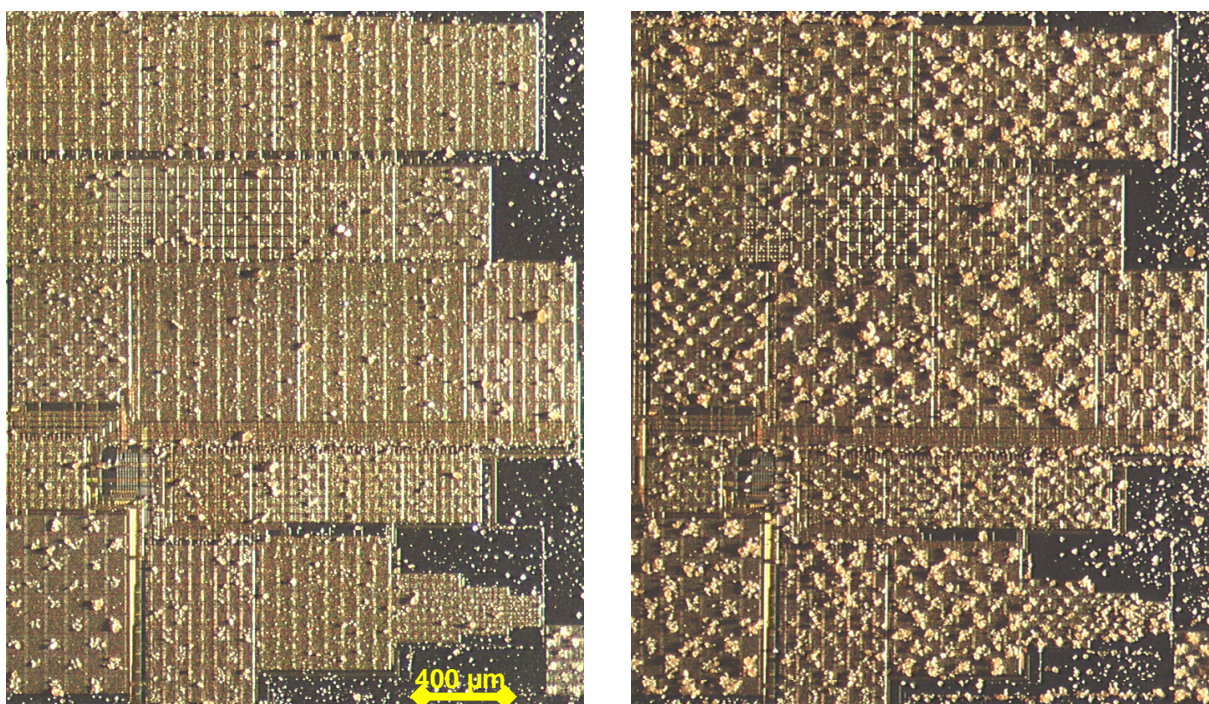


Fig. 6.32: Example of particle deposition (alanine amino acid particles) on a Peptidchip 3.1 with 20% PEGMA, 80% MMA layer (thickness between 50 and 100 μm) after the surface had been exposed to a solution of potassium chloride in water (left) and after subsequent storage in dry nitrogen atmosphere for two days (right). Selective particle deposition failed after exposure in most parts of the chip, but the chip recovered the ability to selectively deposit particles during the time under dry nitrogen atmosphere. Stitched microscope images.

These results show that the PEGMA-MMA polymer layers can indeed be forced into blocking the electric fields by exposure to water. However, while films at 25% or more PEGMA content block electric fields in their “ordinary” state after polymerization, and may revert to this state, layers with 20% PEGMA and 80% MMA do not commonly block electric fields. If water is forced into these polymers, they can be regenerated by storage in dry nitrogen atmosphere.

It might be possible to “dry” chips with other polymers, as well. To avoid re-hydration from ambient air, however, these chips would have to be handled under nitrogen atmosphere exclusively, which is why this was not investigated further.

Chips with this 20-80 heteropolymer were successfully used in all synthesis experiments described in this thesis, and random deposition due to electric field blocking did not occur with this kind of polymer. Additional investigations into the performance of different polymers in synthesis are shown in 7.3.

6.5.8 Conclusions

It has been demonstrated that PEGMA layers on CMOS chips can block electric fields, thus preventing selective deposition. Ionic conduction involving water and ions mobile within these films have been identified as the most likely cause for this phenomenon. Workable solutions to prevent this effect have been found, and include:

- The use of pixels with passivation openings. This method yields improved deposition results, and allows for the use of any polymer.
- Substitution of 100% PEGMA homopolymers with 20% PEGMA, 80% MMA heteropolymers. This may reduce the number of amino groups available for peptide synthesis on the chips, but is compatible with all current chips.
- Combination of both methods.

Having established compatibility between particle deposition on CMOS chips and surface modifications for peptide synthesis, these results enable peptide synthesis on Peptidchip 3.1.

6.6 Selective Deposition from Liquids

6.6.1 Objectives

Air is not the only medium that can be used to transport particles onto CMOS chips. In [JAC02], for example, nanoparticle deposition from both the aerosol and particles in liquid is shown. Even if the focus in this project is on particle transfer from the aerosol, the option of particle transfer from a liquid remains valid.

Using passivated chips and matching Teflon coverings in order to prevent electric discharges between pixels and bond wires and mechanical stress to the bond wires, Peptidchips should be capable of operation in most solvents. The properties of amino acid particles and PEGMA layers are more limiting in their chemical compatibility, however. Water or ethanol are likely not useable as they chemically interact with the amino acids in the particles. Acetone or dichloromethane might be useable, but their effects on the particles are uncertain. Hexane is quite likely to have no effect on either particles or PEGMA layers, and is therefore used in these experiments.

OKI Magenta toner particles form a suspension with particles evenly distributed in the liquid in hexane. Standard amino acid particles, however, agglomerate in hexane, and remain on the surface of the liquid, making transfer of these particles in hexane impossible. Therefore, the transfer of OKI Magenta particles is investigated only in preliminary experiments in order to indicate whether it might be worthwhile to find a combination of (existing or newly-designed) amino acid particles and a liquid medium for deposition.

6.6.2 Particle Transfer in Hexane

Using a magnetic stirrer with a stirring bar in a glass jar, 300 ml of hexane were stirred at 500 rpm and ca. 60 mg (two spatula tips) of OKI Magenta toner were added. A Peptidchip 3.1 with covering installed and placed inside an open synthesis chamber for protection was programmed to a pattern of one active pixel in four, with active pixels at 30 V for the 45 μm pixels and 50 V for the rest. The grid electrode was kept at 0 V. The chip was submerged in the stirred hexane for about 10 seconds, with the chip surface perpendicular to the flow of the liquid. Fig. 6.33 shows the results of this deposition.

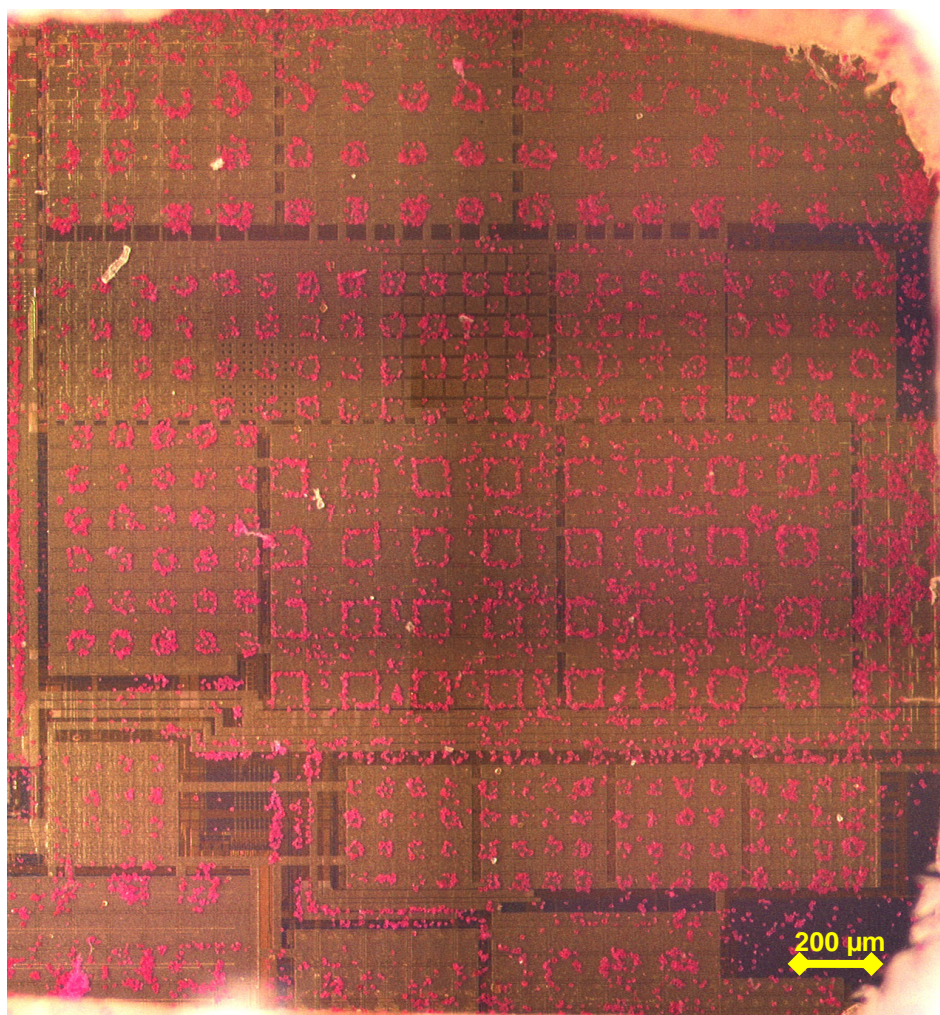


Fig. 6.33: Particle deposition of OKI Magenta toner particles on a Peptidchip 3.1 from Hexane in a “one active pixel out of four” pattern. Stitched microscope images.

This deposition matches the set pattern for all pixel areas. Interestingly, the largest (100 μm) pixels show the worst deposition results, with numerous contaminations on the pixels that were turned off, while the pixels to be deposited only show deposition on their edges. As the electric field gradient is strongest on the edges, this may indicate that deposition in liquids depends more strongly on the field gradient than on field strength, which indicates that dielectrophoretic forces may be dominant (see 3.6.4). On smaller pixels, deposition patterns look similar to those from deposition from the aerosol, with only few contaminations. Fig. 6.34 shows a detail of a 45 μm pixel area from this deposition with good results.

While other deposition patterns have to be tested as well, these results provide proof-of-principle that deposition of microparticles from suspension in hexane onto Peptidchips is possible. This may offer an alternative to particle deposition from the aerosol, especially for future chips with small pixels.

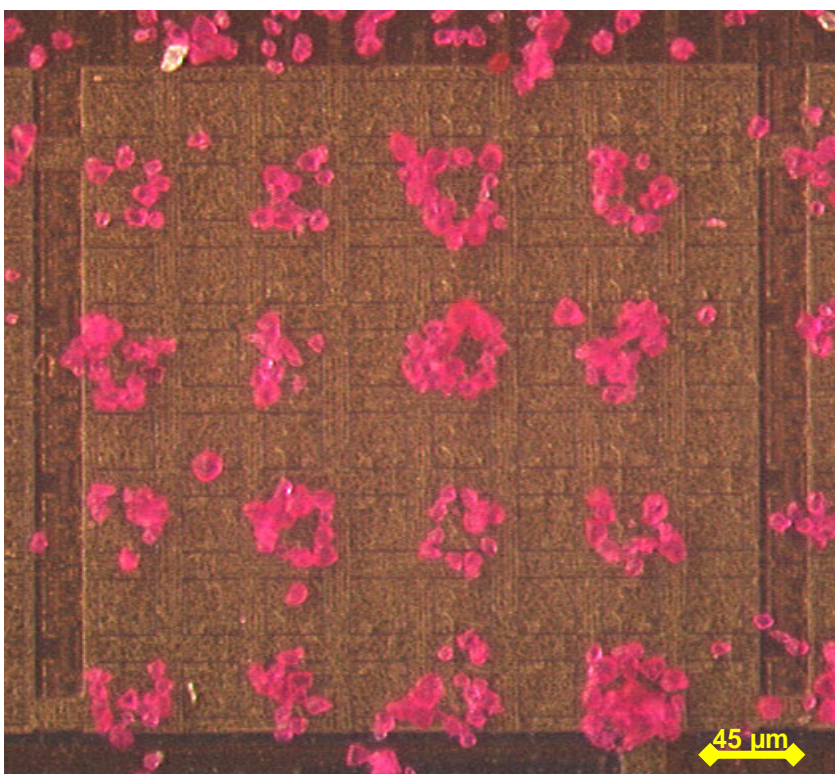


Fig. 6.34: Detail of Particle deposition of OKI Magenta toner particles from suspension in hexane on 45 μm pixels of a Peptidchip 3.1.

6.6.3 Conclusions

Selective deposition using hexane as a medium has been achieved, simply by placing a chip into a jar of OKI Magenta reference particles in hexane while stirring. Deposition results differ from deposition in aerosol in pixel coverage especially for 100 μm pixels, indicating that dielectrophoretic forces may more significantly influence deposition. The good results for the 45 μm pixels make this method promising for further miniaturization.

For any solvent, its effect on amino acid particles has to be tested, i.e. if the amino acid remains unchanged if exposed to the solvent. This could be verified by exposing the particles to the solvent, drying them and performing an HPLC. In addition, a functional test could be

performed by using exposed particles to synthesize an amino acid to a surface-modified glass slide and blue staining with bromphenol blue. Likewise, the effects on PEGMA layers would have to be tested. Finding a suitable combination of amino acid particles and solvent is a prerequisite before using this method for chip-based peptide synthesis. Additionally, if it were suitable for other applications, this method might be worth further consideration and investigation.

6.7 Summary and Outlook

While the standard aerosol chambers are not ideal, they are useable with extra work and care on part of the experimenter. The use of particles with an average diameter of 5 μm or less improves reliability. For routine experiments or even automation, a linear particle deposition system should be given preference over aerosol chambers with a circular flow of particle-loaded air. Such a system is currently in development [LOE]. Transfer of particles from suspension in a liquid might be a long-term alternative, especially if the pixels are to be miniaturized further, but this would require significant additional research efforts.

Aerosol chambers, amino acid particles and surface modifications for peptide synthesis have been tested in selective deposition for peptide synthesis. The functionality of the Peptidchip 3.1 and Peptidchip 5 chips has also been tested in the aerosol. Amino acid particles adequate for on-chip synthesis have been found. Using a system of conventional aerosol chambers and amino acid particles on chips with heteropolymers of 20% PEGMA, 80% MMA as surface modification, synthesis experiments can now be performed.

7. On-Chip Peptide Synthesis

7.1 Introduction

A proof-of-principle synthesis is required in order to demonstrate the compatibility of all components of the Peptidchip system (chip and electronics, surface modification, particle deposition, chemical synthesis, ect.). Due to the fact that deposition and synthesis are still performed manually and due to the difficulties in finding particles suitable for high-quality deposition, this first synthesis was to use few amino acids and few deposition and synthesis steps in order to minimize the required effort and risk of errors.

A model application for proof-of-principle synthesis should allow easy and reliable detection of synthesized peptides using standard methods and tools. A variety of antibodies is commercially available, binding certain short peptides with high specificity and affinity. Those antibodies can be labeled, e.g. by adding chemical groups that act as fluorescent dyes. For the detection of a distinct peptide, labeled antibodies can be employed, which bind to the target epitope with high specificity. In a method called sandwich assay, a primary non-labeled antibody binds the target peptide, which interacts further with a secondary antibody, which is labeled. Signals are detected using standard fluorescence scanners (1.3). Antibody binding studies are also a significant real application for peptide arrays e.g. in epitope mapping approaches (1.1.1).

For the first proof-of-principle experiments, three well-characterized peptide epitopes of average length (8 to 11 amino acids) have been chosen, namely FLAG, HA and c-myc [BLO09]. Anti-FLAG, anti-HA and anti-c-myc antibodies are commercially available purified from the mouse or rabbit. They can be bound by commercially available anti-mouse-antibody or anti-rabbit-antibody secondary antibodies in a sandwich assay. Both of these secondary antibodies are available with red or green fluorescence labels (AlexaFluor 647 and AlexaFluor 546, respectively). A scanner compatible to these fluorescence dyes and capable of a resolution in the range of less than 10 μm (Axon Instruments GenePix 4000B) [AXO] was used for spatially resolved detection of fluorescence signals.

Particle-based synthesis of FLAG and HA peptide epitopes using the peptide laser printer had been performed on glass slides, and the detection using labeled antibodies and the fluorescence scanner had been verified [BLO09]. A particle-based synthesis on fixed-pattern chips had been performed previously, using chips with fixed checkerboard patterns. These chips consist of two parts, one with spot / pixel electrode densities of 10.000 spots / cm^2 and one with 40.000 spots / cm^2 [BEY07, BLO09].

This chapter shows the first particle-based peptide syntheses on CMOS chips. In 7.2, a combinatorial synthesis attempt on Peptidchip 3.1 is described [KÖN10], while 7.3 depicts a large-area synthesis on chips with and without passivation using different polymers as surface modification [KÖN10]. This synthesis was again performed in a checkerboard pattern in order to investigate homogeneity of synthesis over the chip area.

7.2 Synthesis on Peptidchip 3.1

7.2.1 Objectives and Preparation

Objective of the synthesis on Peptidchip 3.1 was to perform a proof-of-principle for peptide synthesis on CMOS chips and to establish a working system or standard protocol. A slightly more complex pattern than the one used on the fixed-pattern chip was chosen for this synthesis. Six different epitopes were synthesized, three of which are detectable by known antibodies. Two of these epitopes had already been tested in the project (see 7.1). The other three epitopes are variants of each of the detectable epitopes, differing only in one amino acid, which serve as negative controls. From the literature and previous experiments with the peptide laser printer, it is known that these specific permutations of a single amino acid completely remove the ability of the respective antibodies to bind the modified epitope [BLO09]. Therefore, these modified epitopes can be used as negative controls in order to test for contaminations during the deposition. Since cross contamination would lead to partial synthesis of the original epitope, a positive signal after assaying with the corresponding antibodies should be observed in this case. The epitopes used are listed in tab. 7.1.

Epitope name	Amino Acid Sequence												
HA			NH ₂	Tyr	Pro	Tyr	Asp	Val	Pro	Asp	Tyr	Ala	support
not-HA			NH ₂	Tyr	Pro	Tyr	Asp	Val	Pro	Pro	Tyr	Ala	support
FLAG				NH ₂	Asp	Tyr	Lys	Asp	Asp	Asp	Asp	Lys	support
not-FLAG				NH ₂	Asp	Asp	Lys	Asp	Asp	Asp	Asp	Lys	support
c-myc	NH ₂	Glu	Gln	Lys	Leu	Ile	Ser	Glu	Glu	Asp	Leu	Asn	support
not-c-myc	NH ₂	Glu	Gln	Lys	Leu	Ile	Ser	Ser	Glu	Asp	Leu	Asn	support

Tab. 7.1: List of synthesized peptide epitopes and their amino acid sequences. Three of these epitopes can be bound by specific antibodies. For each of these epitopes, a second epitope was also tested, with one amino acid exchanged (red). The changed amino acid was chosen such that the antibody does not bind to the changed peptide. The peptides are written following standard IUPAC rules, however synthesis is performed from right to left, according to the Fmoc synthesis approach used.

The surface of four Peptidchip 3.1 chips was modified with a heteropolymer of 20% PEGMA, 80% MMA, a β -alanine linker and a C11-linker to increase distance between the polymer structures and loci of peptide synthesis and increase accessibility. The C11-linker terminates with a free amino group, allowing for the coupling of amino acid as starting point of peptide synthesis. The functionalized chips are glued to the PCB and electronically connected by bonding. Between processing steps, chips were stored at 4 °C in nitrogen atmosphere. They were heated back to room temperature before exposure to air in order to avoid condensation.

The synthesis of the peptide epitopes from tab. 7.1 required 11 layers of amino acids to be deposited, with up to four different sorts of amino acids deposited per layer, for a total of 28 depositions per chip. Amino acids were deposited using the aerosol chambers described in 6.2.2. After each deposition step, deposition quality was verified manually using a microscope. In case of a satisfactory result, the particles were fused by placing the chips into an oven at 90°C for one minute (in air), otherwise the particles were blown away by pressurized air and the deposition was repeated. Even though the appearance of particles on the chip is hardly changed by fusing, fused particles cannot be removed by pressurized air at the pressures used (up to 8 bar), thus only the failed deposition, instead of all depositions within one layer, has to be repeated.

A repeating 4 × 4 pattern was chosen for deposition on the regular pixel areas, as shown in fig. 7.2. For the fixed-pattern pixel areas, a 2 × 2 pattern of FLAG, HA, not-FLAG, and not-HA was chosen.

1a	2a	1	2
3	1a	2a	3a
2a	3a	1	2
1	2	3	1a

Fig. 7.2: Synthesis pattern. Peptides were synthesized in the repeating 4×4 pattern shown above. 1: HA, 1a: not-HA, 2: FLAG, 2a: not-FLAG, 3: c-myc, 3a: not-c-myc. Particles were deposited in numerical order.

As twelve different amino acids are used in this synthesis, twelve different batches of amino acid particles were used. As described in 6.3.4, particle quality varied. With some batches, good deposition was achieved on the first try in most cases, while others were less reliable, occasionally requiring deposited particles to be removed and deposition to be repeated. The batches of valine, glutamine, serine and glutamic acid particles used in this synthesis were noted to be more difficult to deposit correctly than the other batches (see also fig. 7.3).

7.2.2 Amino Acid Particle Deposition and Peptide Synthesis

The synthesis was completed only on two out of the four chips used. On one chip, one out of four rows of its pixels did not function after the polymer coating was completed. Some bond wires of this chip were damaged later during the synthesis and could not be re-bonded, making it unusable. Another chip failed due to a short circuit during deposition of the second amino acid layer. In one of the chips, one out of four rows failed during deposition of the 10th layer (at that point, synthesis of the FLAG and HA epitopes was already complete, so only the c-myc epitope was affected).

As noted in chapter 6, Peptidchip 3.1 was difficult to handle for both deposition and synthesis. Occasionally, bond wires were disconnected from the chip and had to be replaced. Furthermore, the Teflon lid of the covering failed in two instances, exposing the PCB to liquid solvents during cleaning and removal of protecting groups.

The quality control of the particle deposition was performed manually, by using a microscope and optical judgment. Fig. 7.3 shows three typical examples of particle deposition with good to average batches of particles, with tab. 7.2 summarizing the deposition quality of these samples. However, only selected pixel areas of few deposition steps were investigated and marked due to the prohibitive effort of performing such analyses manually. A quantitative control of deposition quality via image processing software might be preferable, and is currently in the development process (8.2) [WAG10].

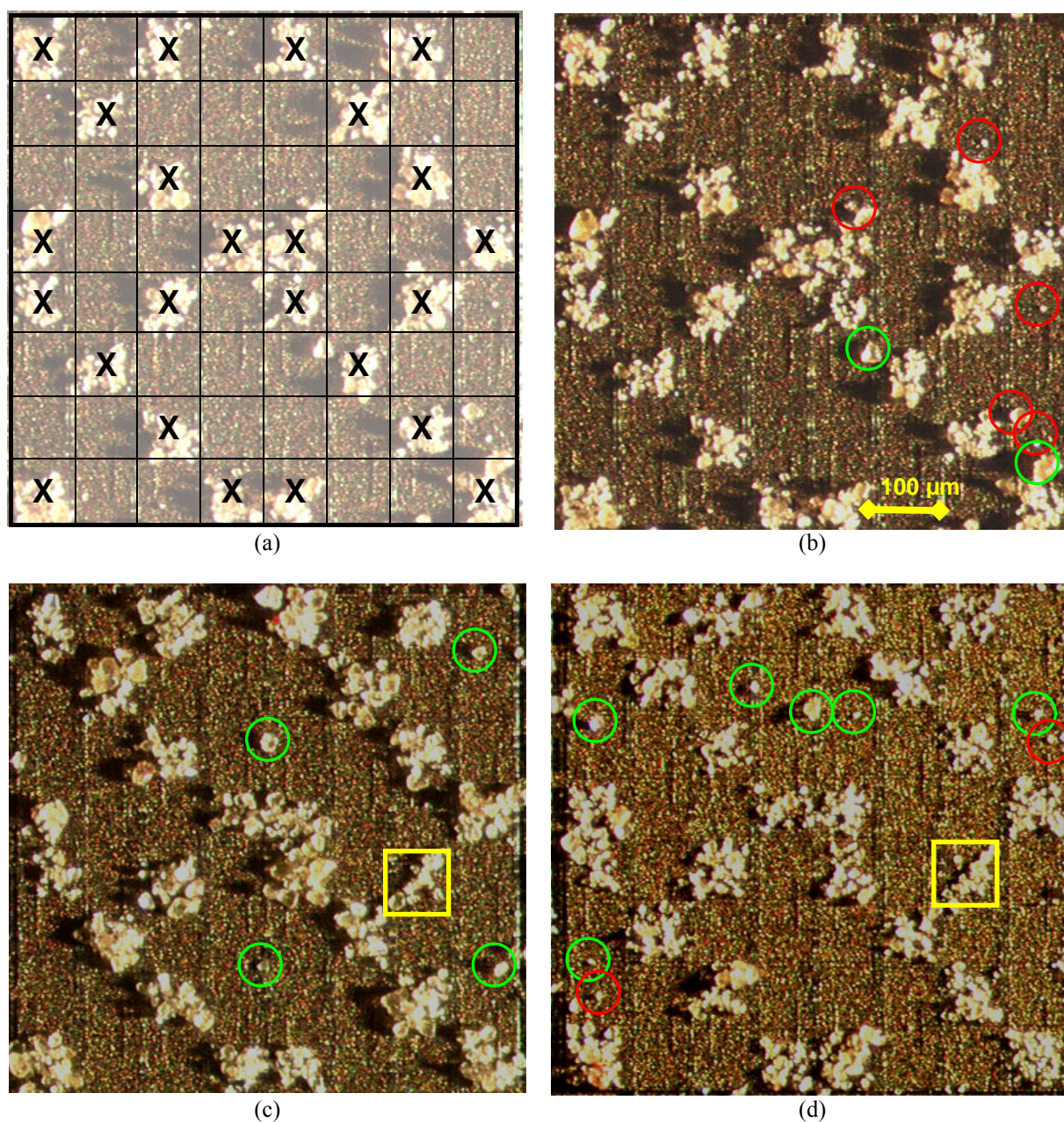


Fig. 7.3: Quality analysis of selected deposition steps, for 100 μm pixels. (a): Desired pattern, overlaid on Ala deposition. (b): Ala particles. (c) Tyr particles. (d) Asp particles. Poorly covered pixels are marked with a yellow square, contamination particles on pixels are encircled in red, while contamination particles on the grid are encircled in green.

amino acid	pixels patterned		contamination particles	
	well-covered	poor cover	on pixels	on grid
Ala	24 of 24	0	5	2
Tyr	23 of 24	1	0	4
Asp	23 of 24	1	2	6

Tab. 7.2: Summary of deposition results from fig. 7.3.

As the amino acid particles used in these experiments are very similar in appearance, only the first deposition per layer was investigated in detail for contaminations. However, for the

example of the amino acid particle deposition in the first layer from tab. 7.2, the chip is shown after the subsequent deposition steps and the appearance of the molten amino acid particles after heating and coupling are shown in fig. 7.4.

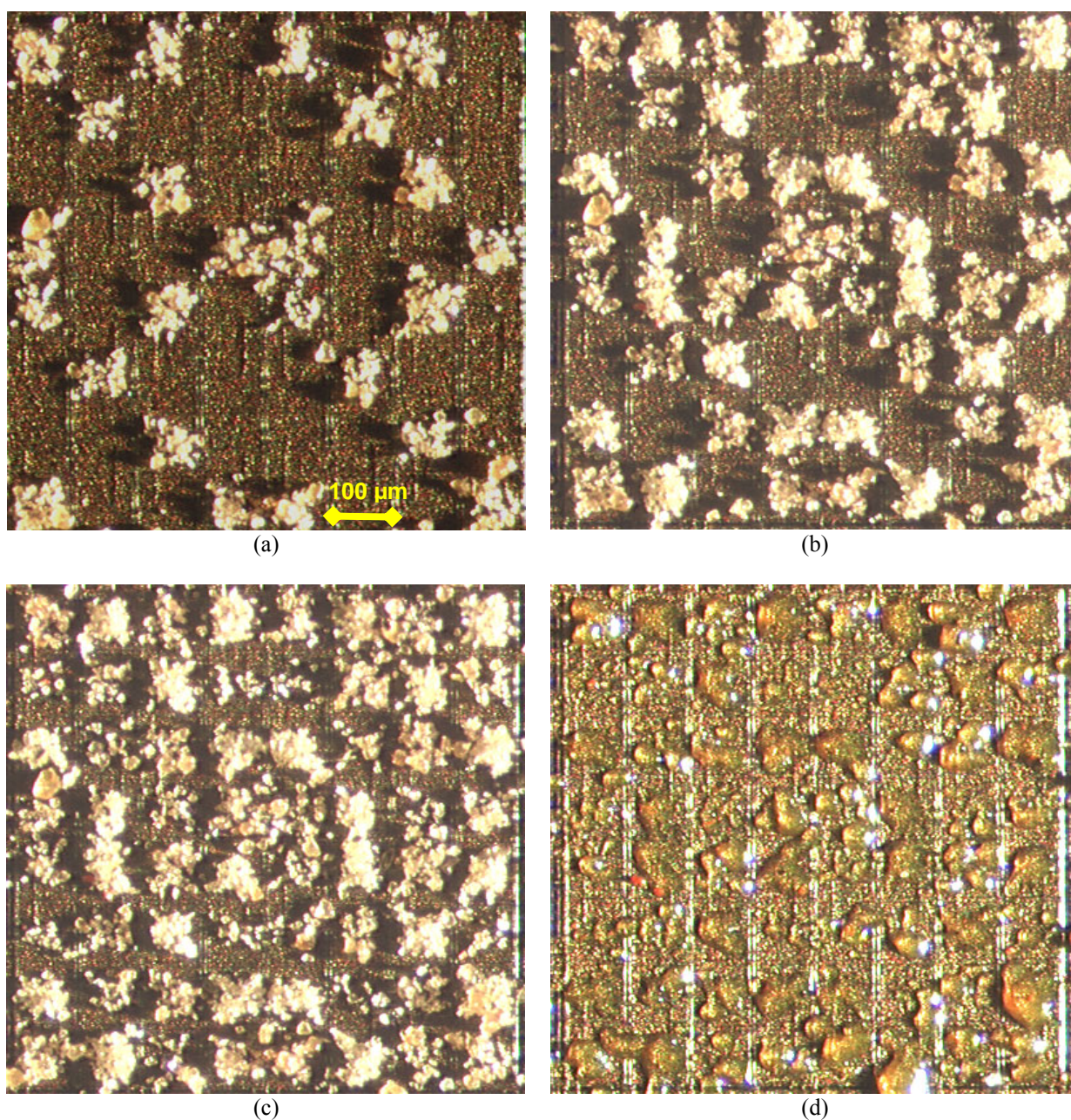


Fig. 7.4: Pictures of subsequent depositions of one layer, and of the particles after coupling (90 min at 90° C in nitrogen atmosphere). (a): Ala particles, from tab. 7.2, for reference. (b): Ala and Lys particles. (c): Ala, Lys and Asn particles. (d): Particles after heating and coupling. In (d), spreading of the melt to adjacent pixels can be observed.

Some particle batches yielded poorer results with increased cross-contamination of non-targeted pixels during deposition. Fig. 7.5 is a worst-case example of contaminations for this synthesis. As repeated depositions did not result in decreased contaminations, they had to be accepted for some batches of particles.

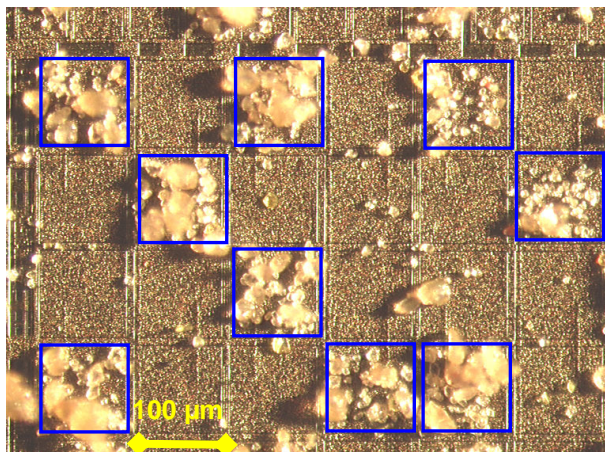


Fig. 7.5: Deposition of valine particles with numerous contaminations on the 100 μm pixels, desired electrodes marked with blue squares for reference.

In some deposition steps, excessive or low amounts particles were deposited. While a high particle load on electrodes may lead to merging and mixing of particle melt from different pixels during the heating process, low coverage of pixels decreases coupling efficiency, or may cause parts of pixels to receive no amino acids for coupling, so that peptide synthesis is terminated there. Examples of such events are shown in fig. 7.6 and fig. 7.7.

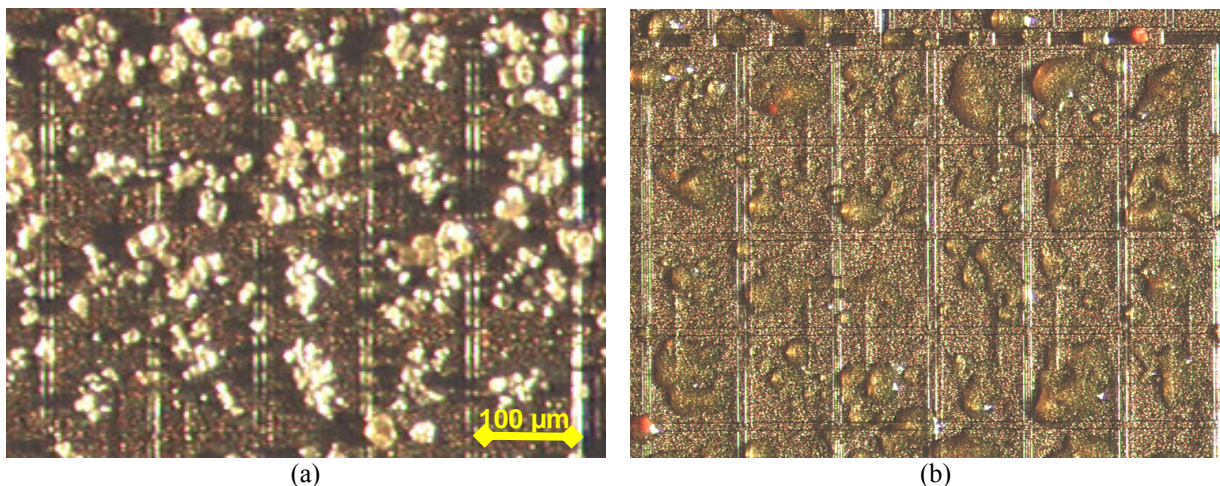


Fig. 7.6: Pixels with low particle coverage and typical melting result of such particles. (a): Ala, Lys and Asn particles, low deposition density. (b): Matrices of particles deposited at low density, after coupling, before washing. Parts of pixels not covered with particle melt may result in incomplete peptide synthesis or poor yield.

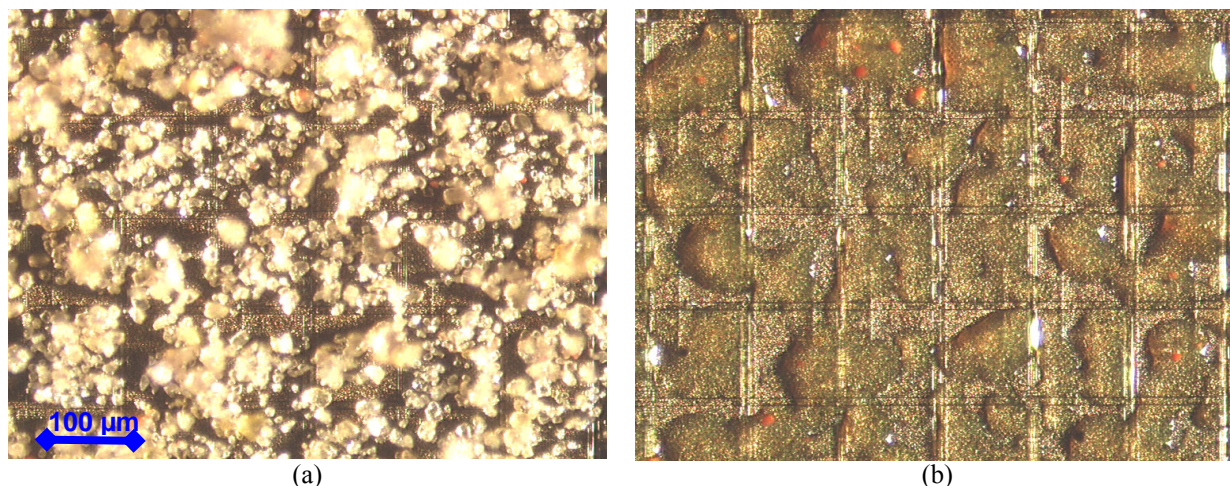


Fig. 7.7: Pixels deposited with excessive amounts of particles and typical melting result of overdeposited particles. (a): Tyr, Asp and Val particles, excessive deposition. (b): Matrices of particles deposited at excessive density, after coupling, before washing. Merged particle melts may result in cross-contaminations and incorrect peptides being synthesized.

7.2.3 Removing of Side-Chain Protection Groups, Staining and Detection of Epitopes

After completion of deposition and coupling cycles, the remaining chips were removed from the PCB. Protective side-chain groups were cleaved with trifluoroacetic acid and the chip was intensively washed to remove remains of the acid. For detection, a sandwich assay was applied. While one chip was incubated with specific primary anti-FLAG rabbit antibodies and anti-HA mouse antibodies, the other chip was incubated with a primary anti-c-myc mouse antibody in solution. Afterwards, both chips were incubated with corresponding (anti mouse and anti rabbit) fluorescence-labeled secondary antibodies. The chips were air dried, mounted to a custom-made holder in the size of a standard microscope slide, and detection was performed employing a fluorescence scanner. Results of the fluorescence scan are shown in fig. 7.8.

Synthesis of the FLAG epitope could be proven due to the achieved staining pattern in some pixel areas. Although the spots are irregular in size and intensity, the desired pattern can be clearly discerned on the right 100 μm pixel area (fig 7.9). On HA and c-myc spots as well as on the not-FLAG pixels, no or very little green signal is discernible, as desired. Even some of the 45 μm spots (fig. 7.8 lower right corner) show the desired pattern.

Except for traces on the fixed-pattern 50 μm pixels (fig 7.10), however, the HA epitope (red fluorescence signal) could not be detected. c-myc could not be detected, either.

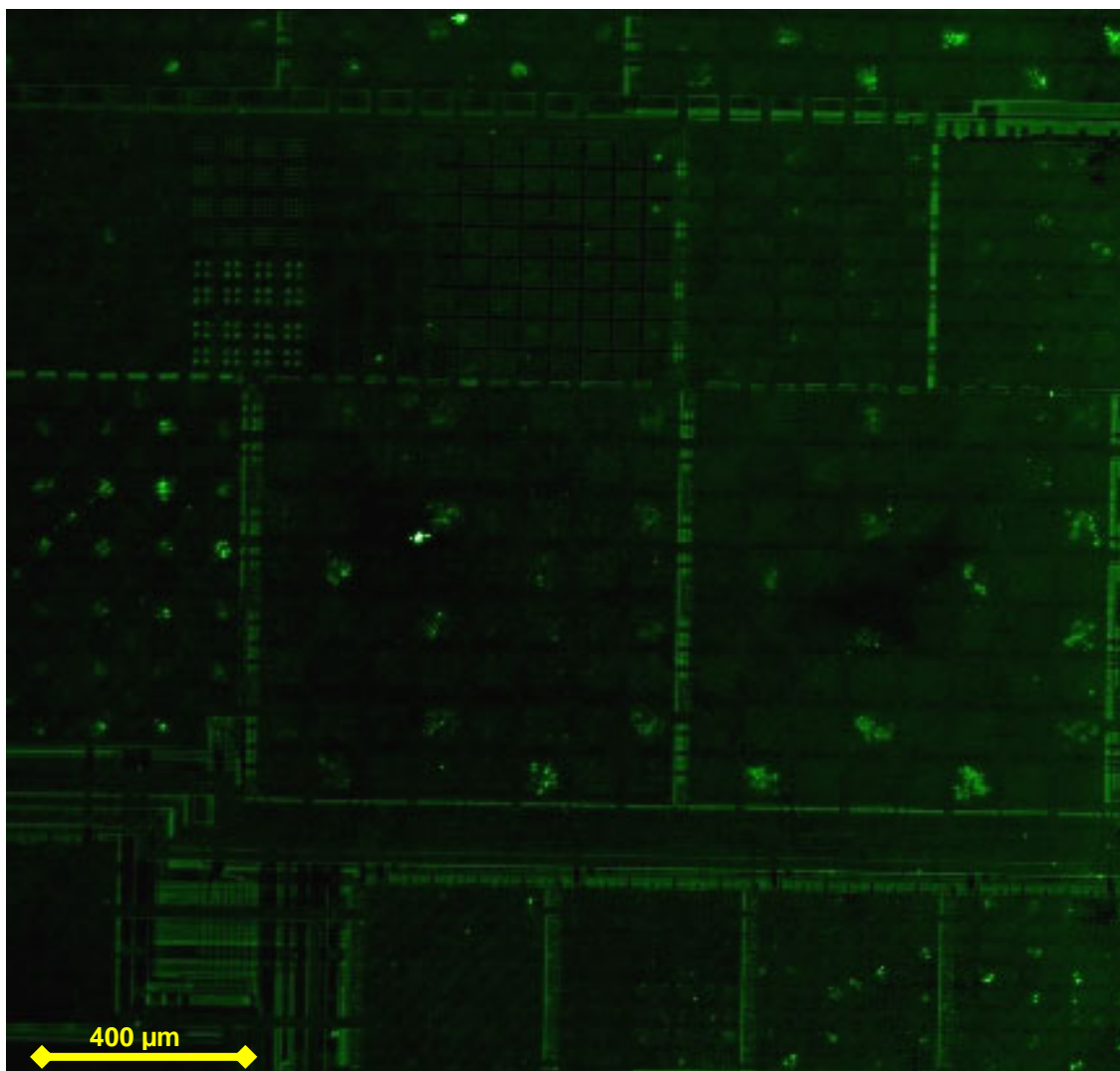


Fig. 7.8: Synthesis results for FLAG epitope after immunostaining (green).

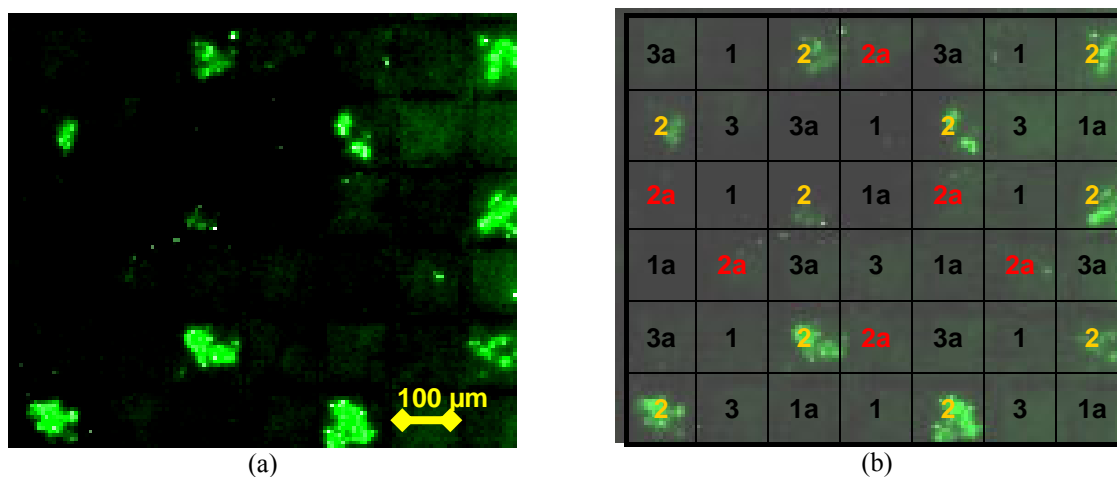


Fig. 7.9: Synthesis results for FLAG epitope after immunostaining, 100 μm pixels. (a): Synthesis result. (b): Desired pattern, with synthesis result in background. 1: HA, 1a: not-HA, 2: FLAG (desired pattern), 2a: not-FLAG (negative control), 3: c-myc, 3a: not-c-myc. (left: original image, right: synthesis image with synthesis pattern). Contrast and brightness adjusted for better visibility.

On fig. 7.10, autofluorescence of the chip in the range of the red fluorophore (around 647 nm) is apparent in the form of red lines co-located with parallel metal tracks in routing areas between pixel areas. To a lesser degree, green autofluorescence can be observed in fig. 7.8. This autofluorescence is limited to areas where metal tracks on the intermediate or bottom layer run in parallel, and are not covered by top metal layer tracks. Covering top metal tracks, located where black areas intersect the red lines in the image, suppress this effect. The phenomenon of chip autofluorescence is described in detail in [NES08].

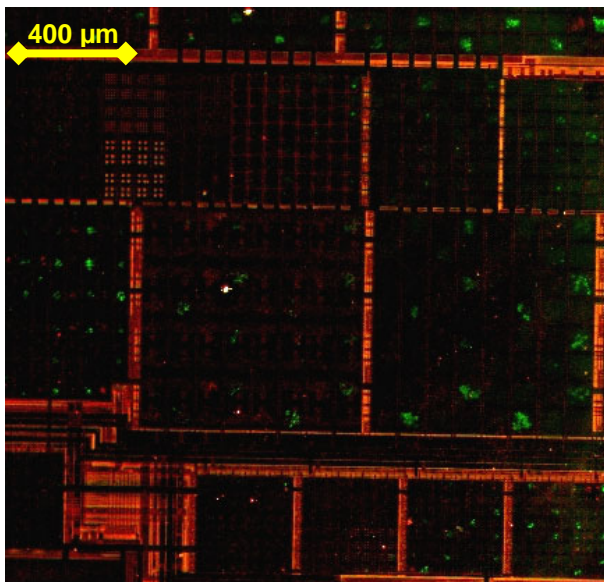


Fig. 7.10: Synthesis results for FLAG and HA epitopes after immunostaining. HA: red, FLAG: green. Autofluorescence of the chip is visible in the form of red lines co-located with parallel metal tracks inside the chip. Overlay image of two fluorescence scans, generated by scanner software.

7.2.4 Discussion

These results represent the first synthesis of a peptide epitope from amino acid particles on a CMOS chip. Strong signals were detected on some synthesis loci of the FLAG epitope after immunostaining with fluorescence labeled antibodies. Only low background on other pixels was observed. However, since the synthesis appears highly inhomogeneous, future experiments should aim at the improvement of deposition and synthesis quality. Double depositing and coupling steps for each amino acid before a complete washing and de-protecting cycle might help address inhomogeneities [MIR99].

Why neither HA nor c-myc were detected is hard to ascertain. For the synthesis of both of these epitopes, some amino acid particles that performed badly during deposition had to be employed. The corresponding batches were stored for several years prior to deposition, which might have led to decreased chargeability and degradation of amino acids, e.g. through humidity, which might have resulted in low peptide concentrations. Peptide concentrations might have been too low to detect a fluorescence signal of the labeled antibody. Therefore, particle batches with bad performance should be replaced by fresh batches prior to the next synthesis.

Biochemical reasons may also have caused the failure to monitor staining of HA. During application of Peptidchip 5, detection of the HA epitopes also failed employing the same anti-HA mouse antibody and corresponding secondary antibodies with red fluorophores.

Exchanging the fluorophores of the secondary anti-mouse and anti-rabbit antibodies gave the desired results (see 7.3.3).

Autofluorescence of the chips in wavelengths of fluorophores that are commonly used must be avoided in future chip generations. Routing supply and data metal tracks only underneath the potential areas or other covering top layer metal is a solution to prevent this effect.

Due to their tiny size, Peptidchip 3.1 chips were difficult to handle during synthesis and deposition. The PCB was unsuitable for detection, requiring the chip to be separated from the PCB and fixed into an appropriate holder for scanning. While small chips are sufficient for proof-of-principle particle transfer experiments, larger chips are preferable for synthesis experiments, as the handling of such chips can be improved (see 6.3.2 and 5.4.3).

7.3 Synthesis on Peptidchip 5

7.3.1 Objectives and Preparation

Peptidchip 5 is the first chip suitable for a fully combinatorial synthesis, with thousands of distinct peptide synthesis loci per chip. As the results from the previous synthesis on Peptidchip 3.1 had shown limitations in synthesis and deposition quality, the first synthesis on Peptidchip 5 was a simple synthesis of two peptides in a checkerboard pattern in order to implement improvements in deposition and synthesis. The FLAG and HA epitopes described in 7.2.1 were also chosen for this experiment [BLO09]. Focus of this synthesis was to obtain homogeneous peptide spots over the whole chip area in order to allow comparative studies (e.g. comparing the affinities of different antibody binding epitopes) in future experiments.

Particles from newly-made batches, which showed good deposition results in preliminary experiments, replaced batches that yielded strong contaminations in 7.2. Furthermore, each particle layer was double-deposited. In double-deposition, the amino acid particles of each layer are deposited and coupled as in the standard process, thereafter the remains of the particles, solid solvent and excess amino acids are washed away. However, the coupled amino acids are not de-protected at this stage. Particle deposition in the same pattern is then repeated. After coupling the amino acids from the second deposition, a full washing and de-protecting cycle is performed. This procedure improves synthesis yield by providing a greater excess of amino acids over amino groups available on the support.

Different chip surfaces and polymers were compared in this experiment. As shown in 6.5, chips with closed passivation only allow heteropolymers of 20% PEGMA, 80% MMA, while chips with passivation openings can be used with up to 100% PEGMA. Only PEGMA provides amino groups to start the synthesis, therefore higher PEGMA content in the polymer is expected to yield more peptides, and thus stronger signals. Polymer thickness may also affect signal intensity, as a thicker polymer contains a greater number of monomers, and thus amino groups. It was measured by ellipsometry on reference silicon wafers. Tab. 7.2 summarizes the chip and polymer variants used.

Variant ID	Chip variant	Polymer variant	Polymer thickness
A	passivation openings	100% PEGMA	ca. 98 μm
B	passivation openings	50% PEGMA, 50% MMA	ca. 61 μm
C	passivation openings	20% PEGMA, 80% MMA	ca. 73 μm
D	closed passivation	20% PEGMA, 80% MMA	ca. 73 μm

Tab. 7.2: List of chip and surface modification variants used for comparative synthesis on Peptidchip 5.

Prior experiments on peptide arrays generated on glass slides revealed that using three β -alanine groups instead of the C11-linker and one β -alanine group which were used in 7.2 improved accessibility of peptides for antibodies, resulting in increased signal intensity. After coupling of three β -alanine groups, the first amino acid of the epitopes (alanine) was also coupled from solution in order to receive peptides of equal length. Since the epitopes are embedded in longer sequences in nature, and the C terminus is known to be irrelevant to the recognition of the FLAG epitope via the corresponding anti-FLAG antibodies, no interference with detection was expected. Afterwards, particle deposition based peptide synthesis was performed resulting in the HA and FLAG epitopes shown in tab. 7.3.

Epitope name	Amino Acid Sequence										
HA	NH ₂	Tyr	Pro	Tyr	Asp	Val	Pro	Asp	Tyr	Ala	support
FLAG + Ala	NH ₂	Asp	Tyr	Lys	Asp	Asp	Asp	Asp	Lys	Ala	support

Tab. 7.3: List of synthesized peptide epitopes, which can be detected using specific antibodies. As the peptides are written in standard amino acid order, synthesis is performed from right to left, starting on the support. The first amino acid, alanine, (red) was added from solution.

During deposition and coupling, the chip covering (see 5.4.3.3) was removed. For washing and de-protecting, the covering was mounted on the chip, to protect the bound wires and the PCB from exposure to solutions and organic solvents. For all washing and de-protecting steps, each chip was placed in a synthesis chamber for protection (see 5.4.3.3) [BLO09].

7.3.2 Amino Acid Particle Deposition and Peptide Synthesis

The twelve chips used in this experiment were surface-modified, glued onto the PCB and bonded. 6 chips were fully operational, two chips were partially non-functional (pixels stuck off), but as on one chip, more than 95%, on the other chip more than 80% of all pixels were still functional, these chips were nevertheless used in the synthesis experiment. Due to the large area of the chips, such defects, caused e.g. by dust adsorption during deposition of metal layers in chip manufacturing, are not unexpected. The four remaining chips were found to be unusable in initial electric tests. One was both unresponsive to I²C access and showed random deposition after programming by direct control (see 5.4.2). Three chips, two of them variant D (closed passivation), had short circuits between high voltage or digital supply voltage and ground. The deposition and synthesis process was thus started with a total of three chips of variant B, two chips of variants A and C, and one chip of variant D.

After coupling the second layer, the remaining variant D chip experienced a short circuit, and was destroyed. Two variant B chips detached from the PCB before deposition of the fourth layer and could not be repaired.

In comparison to Peptidchip 3.1 the novel design of Peptidchip 5 as well as the corresponding washing chambers proved to be more failure resistant:

- During washing and de-protecting, the new cover with resistant o-ring on a dedicated area of the chip never leaked.
- The much shorter, flat bond wires proved more robust; thus no bond wires were damaged during this experiment.

Replacing some old batches of amino acid particles with new batches tested for less contamination and improved saturation of pixels with particles led to an increase in deposition quality for these amino acids. Typical examples of particle depositions are shown in fig. 7.11,

fig. 7.12, and fig. 7.13. The surface variants of the chips did not noticeably influence deposition quality. For deposition, a pixel voltage of 100 V and a grid voltage of 25 V were used.

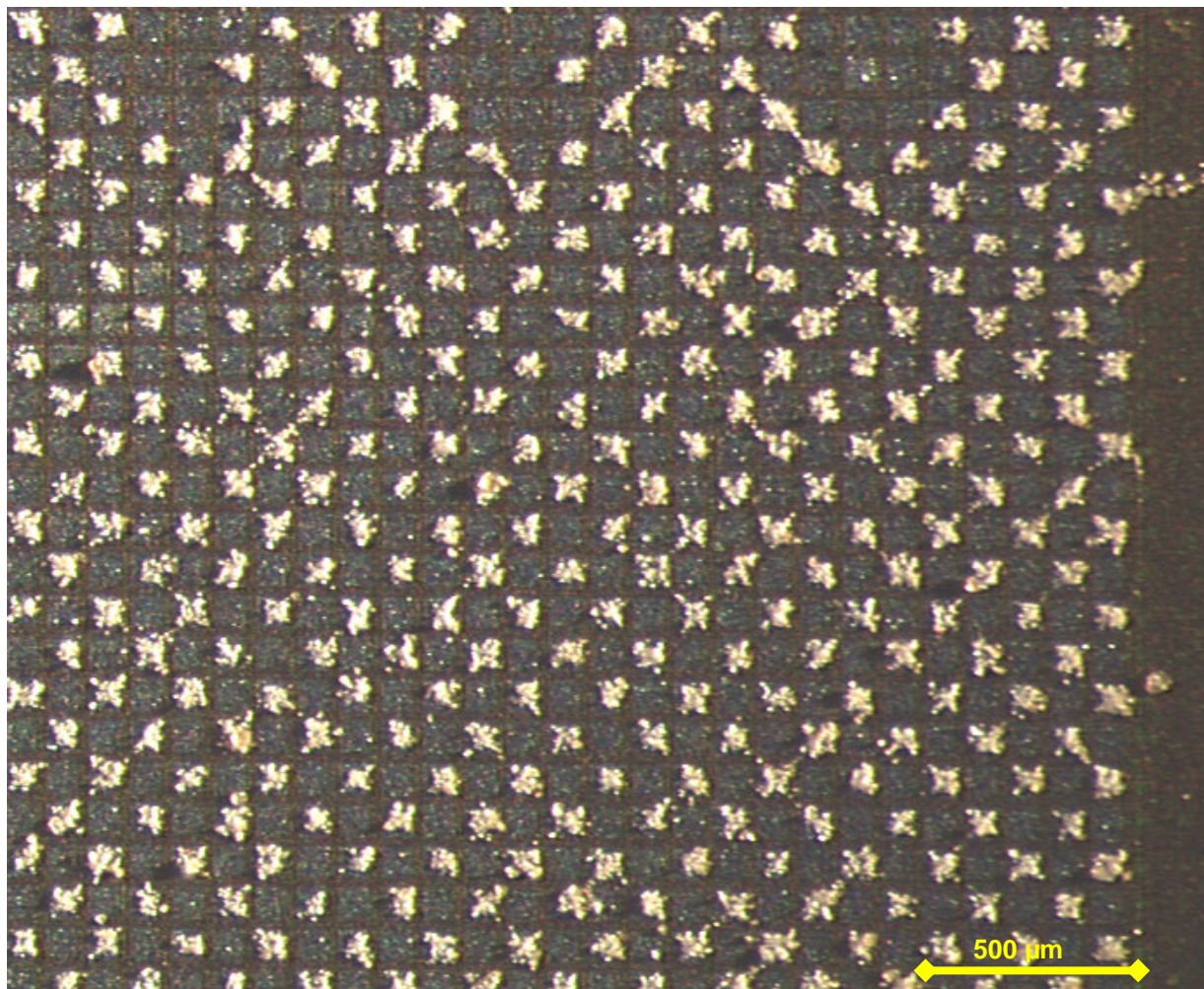


Fig. 7.11: Deposition result for lysine particles (15 μm average diameter), on chip with surface variant C (passivation openings).

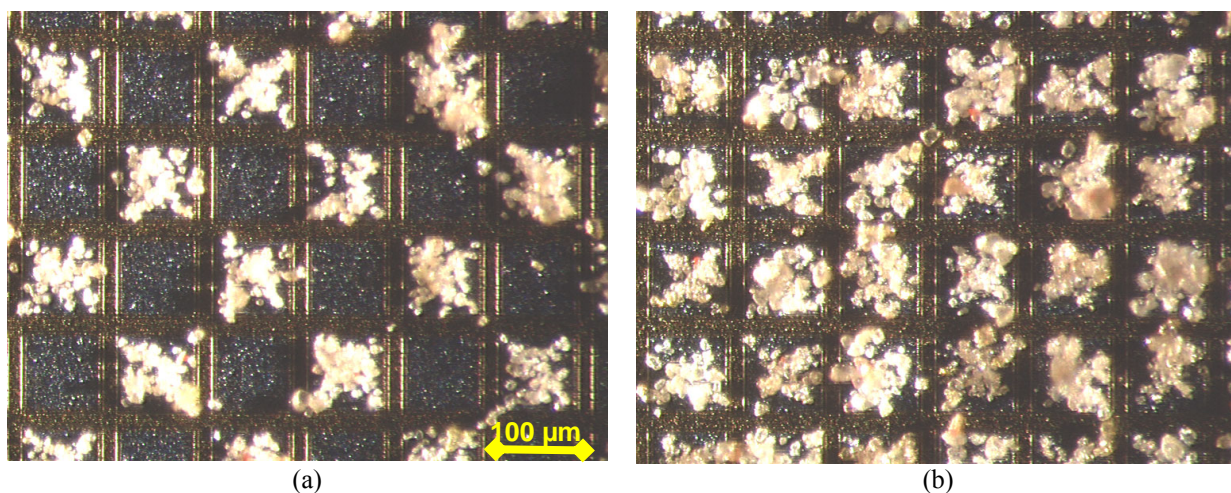


Fig. 7.12: Detail images of typical particle depositions. (a): Lys particles. (b): Lys particles (fused) and Tyr particles in a checkerboard pattern (top left pixel: Tyr). Average particle diameter for Lys: 15 μm, Tyr: 17 μm.

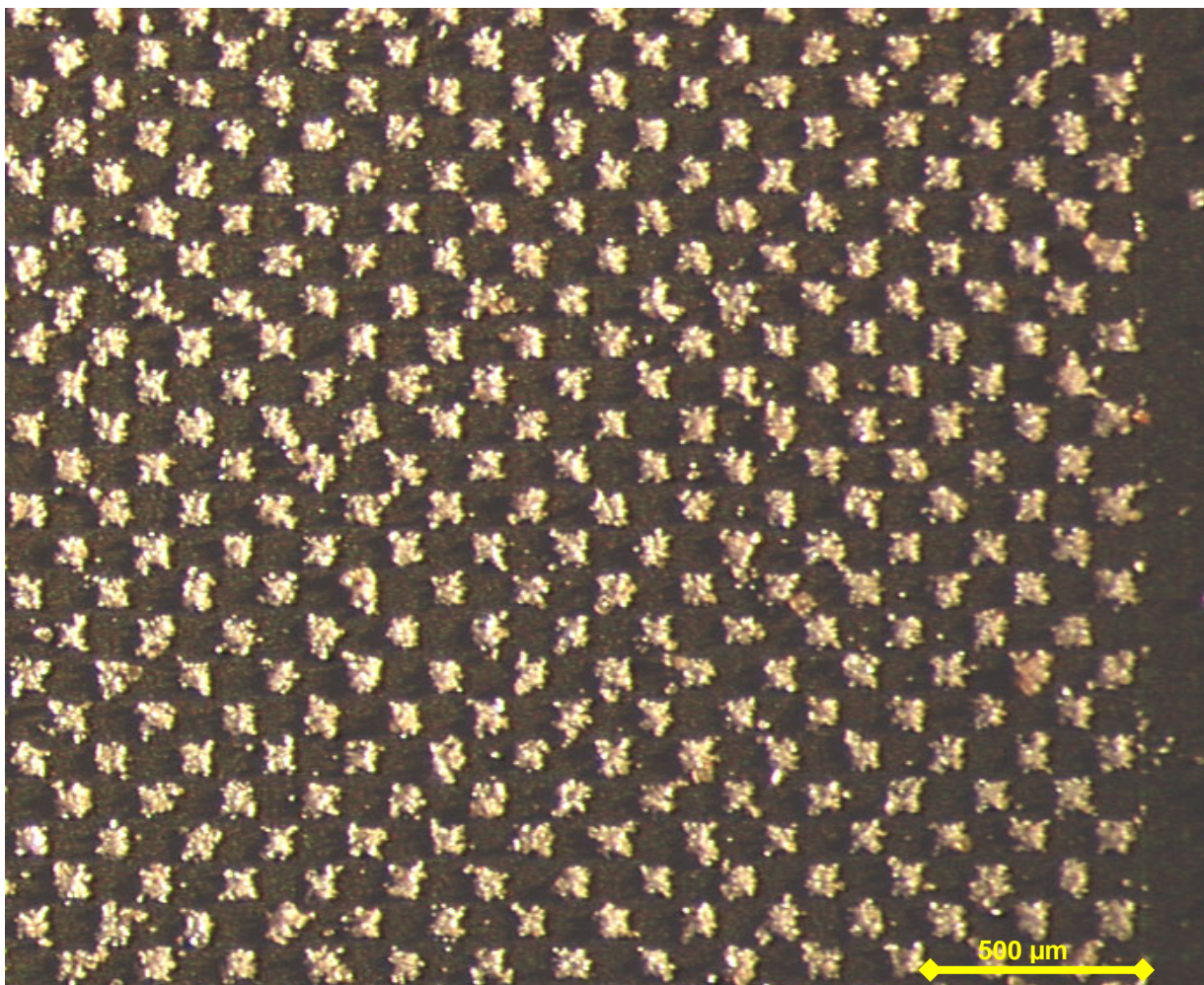


Fig. 7.13: Deposition result for lysine particles (15 μm average diameter), on chip with surface variant D (closed passivation).

The different surfaces of the Peptidchip 5 variants (tab. 7.2) were compared with regard to the spreading of the melted particle matrix during coupling. Even though the passivation is only between 0.5 μm and 1 μm thick, spreading of the particle melt is hindered by the passivation edge. In addition to the edge itself, the differences in surface properties of aluminum and silicon nitride may contribute to this effect. As shown in fig. 7.14 spreading to the grid electrode is rare on pixels with passivation openings. In comparison, fig. 7.15 shows the particle matrix after melting on a Peptidchip 5 with no passivation openings. The melts from neighboring pixels have spread beyond the target pixel areas and merged on the grid.

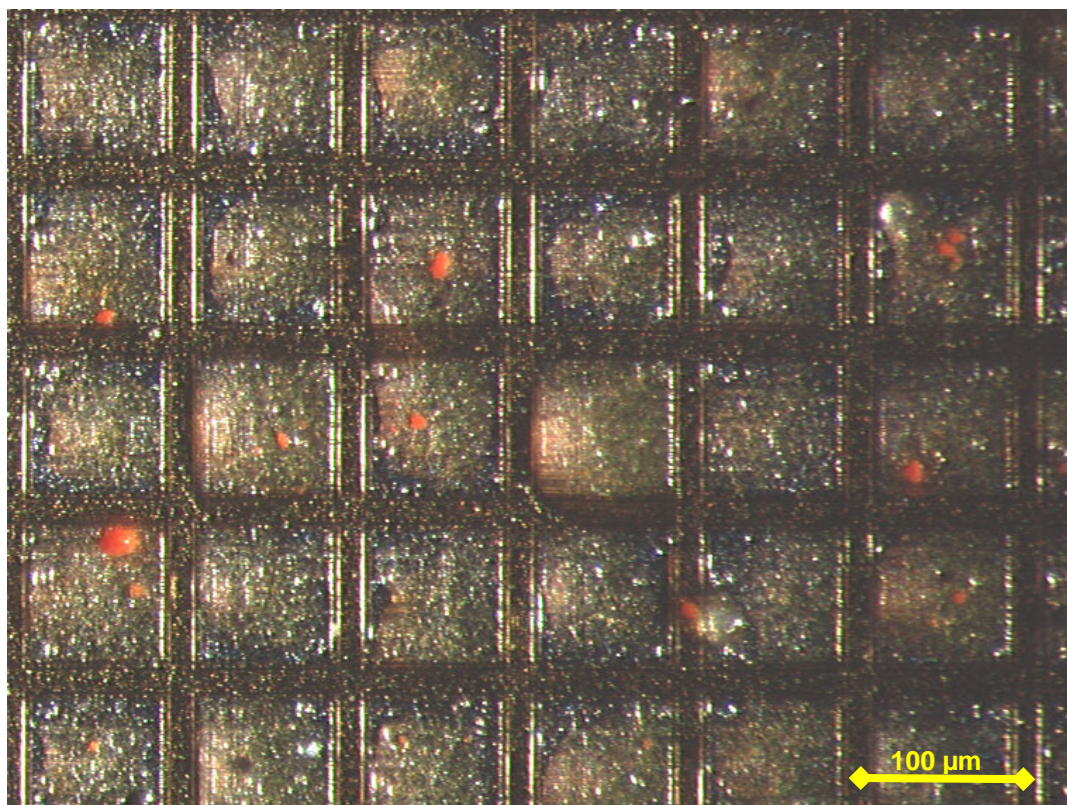


Fig. 7.14: Lys and Tyr particles after melting (yellow semitransparent elevations) on the surface of Peptidchip 5 with passivation openings after coupling, before washing.

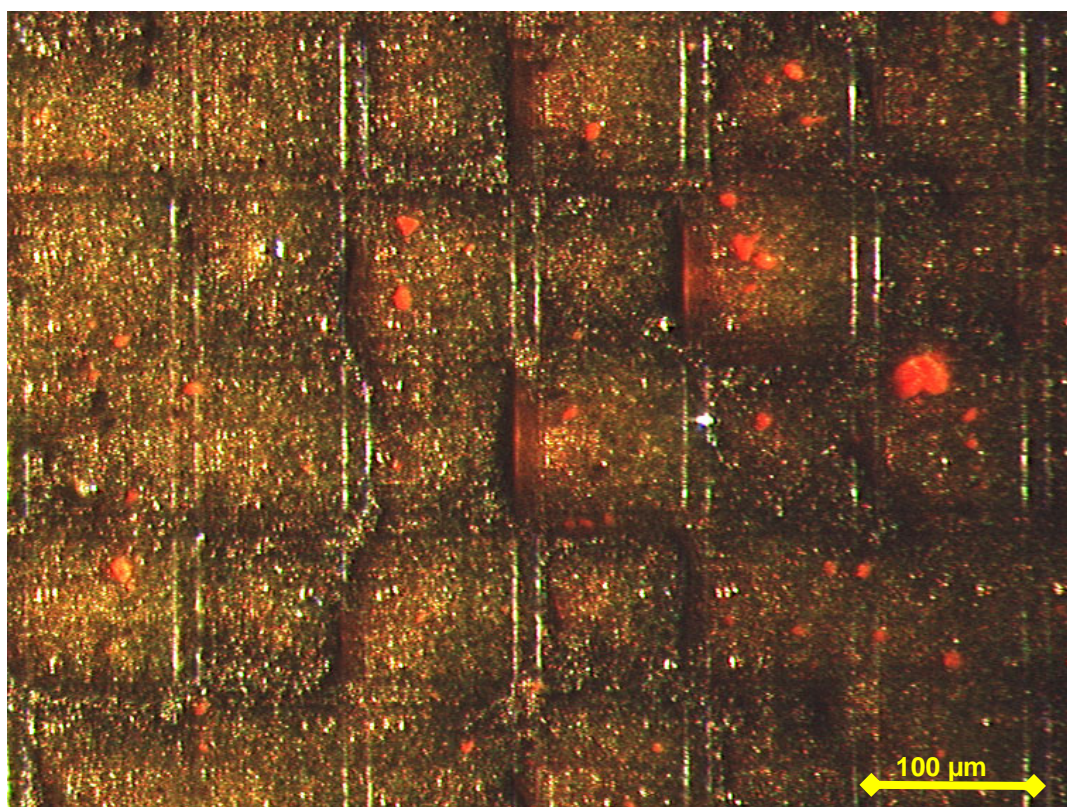


Fig. 7.15: Lys and Tyr particles after melting (yellow semitransparent elevations) on the surface of Peptidchip 5 with closed passivation after coupling, before washing.

7.3.3 Removing of Side-Chain Protection Groups, Staining and Detection of Epitopes

After synthesis, the side chain protecting groups were removed using TFA (trifluoroacetic acid). During TFA treatment, the 100% PEGMA polymer coating completely detached from both variant A chips. On the chip of surface variant B (50% PEGMA, 50% MMA), the polymer detached from the chip in the central part. On the two chips of surface variant C (20% PEGMA, 80% MMA), the polymer coating remained stably bound to the surface.

Initially, antibody staining was performed on one of the variant C chips with some dysfunctional pixels. While detection of FLAG epitopes with anti-flag rabbit antibodies and secondary anti-rabbit antibodies with green fluorophores succeeded, detection of HA epitopes using anti-HA mouse antibodies and anti-mouse secondary antibodies with red fluorophores failed (fig. 7.16), like in the previous experiment on Peptidchip 3.1.

Given the successful synthesis of FLAG epitopes, a complete failure of the HA synthesis was considered unlikely. However, incompatibilities of primary and secondary antibodies could be a reason for these results. Therefore, detection on the second chip of surface variant C was performed using a different set of antibodies, with the fluorophores of the secondary antibodies exchanged. This resulted in successful detection of both FLAG and HA epitopes. The improved protocol was applied to the remaining chips.

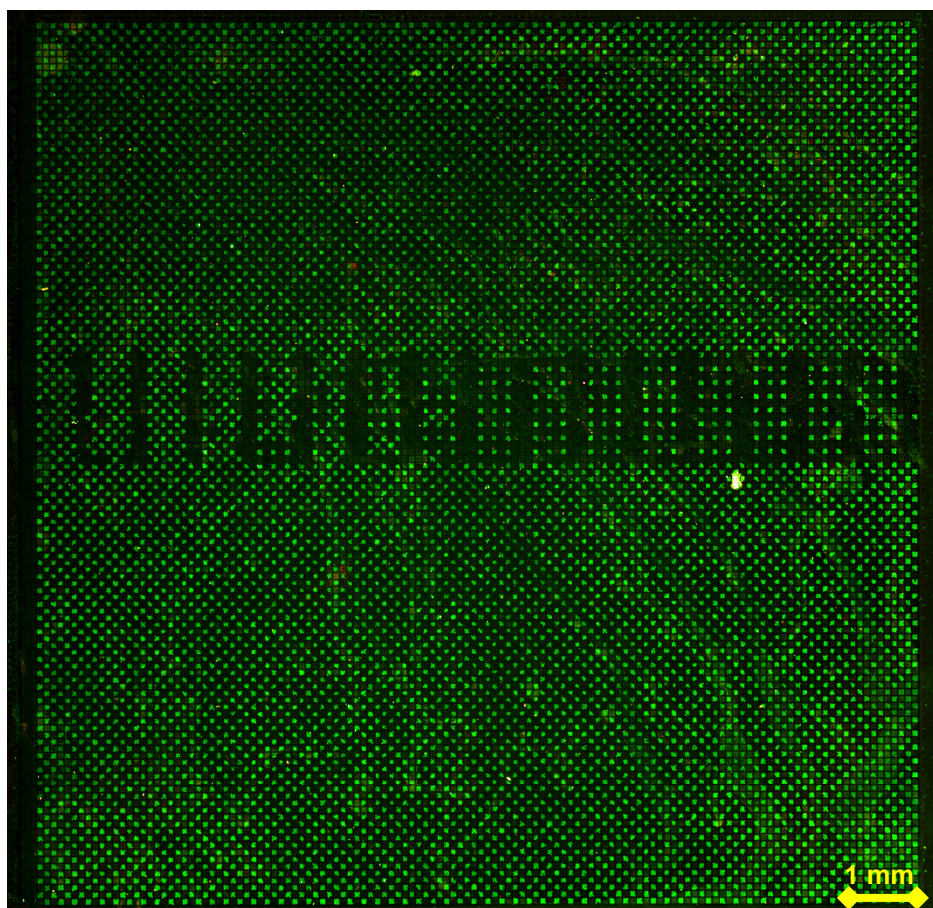


Fig. 7.16: Peptidchip 5 with surface variant C (20% PEGMA, 80% MMA), first chip, after immunostaining (green: FLAG, red: HA). While FLAG epitopes were detected using anti-FLAG rabbit antibodies and anti-rabbit secondary antibodies with green fluorophores, HA detection using anti-HA mouse antibodies and anti-mouse secondary antibodies with red fluorophores failed.

Immunostaining was performed on one variant A chip in spite of the damaged polymer. The checkerboard pattern of FLAG and HA epitopes was discernible over the whole chip (fig. 7.16), even though the polymer had largely detached. A more detailed view (fig. 7.17) shows quite regular signals on the pixel, especially in the pixel edges. Homogeneity over the area of pixels improved compared to 7.2.3. It appears that while most of the polymer layer separated from the chip, part of the polymer, with peptides attached, remained bound to the chip surface. Had the polymer detached completely, all peptides would have been removed and no specific signal could have been detected. The white spots that can be seen in the image are currently unexplained.

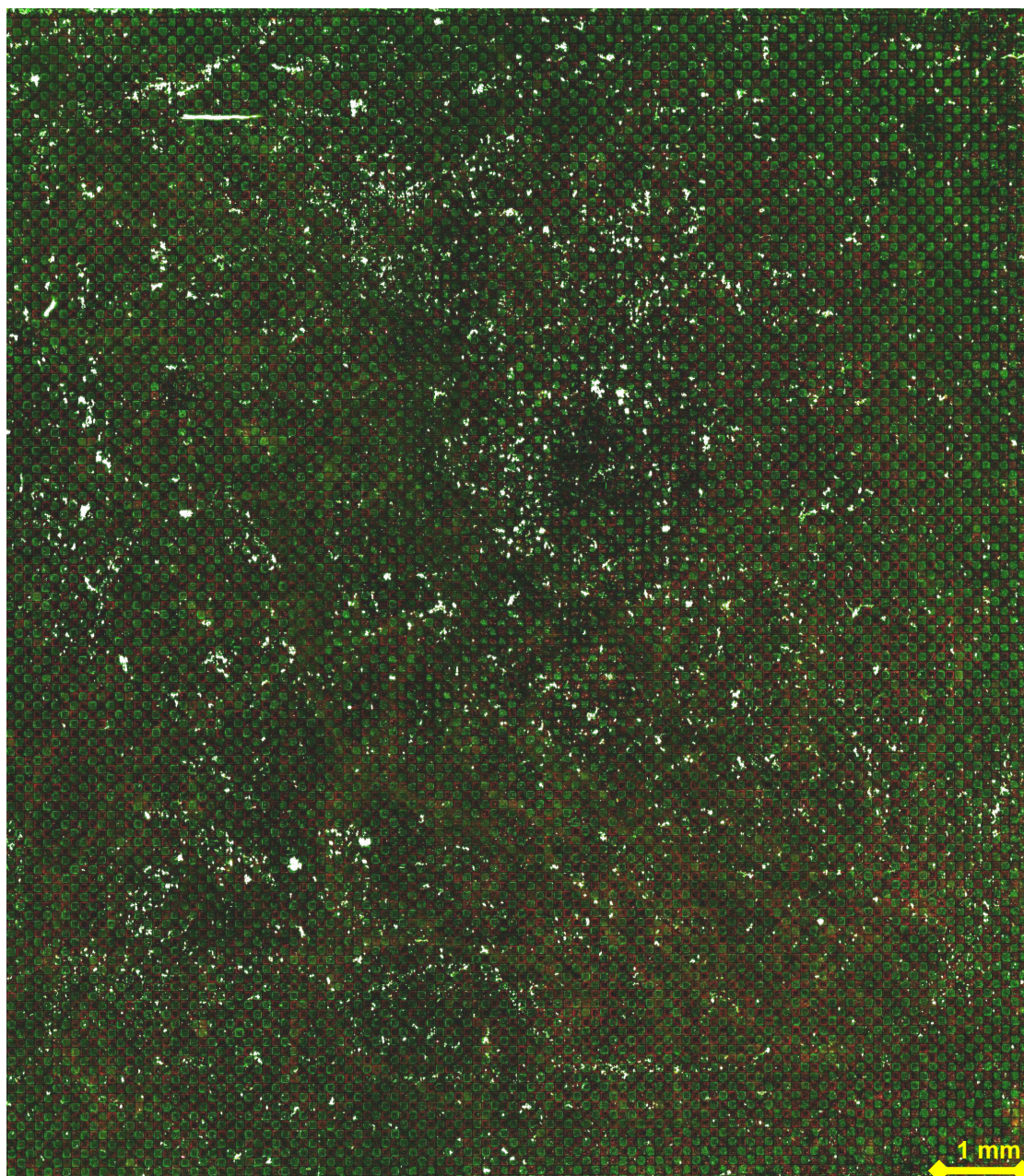


Fig. 7.16: Peptidchip 5 with surface variant A (100% PEGMA) after immunostaining. The PEGMA layer detached from the chip during removal of peptide side chain protection groups using TFA. Nevertheless, the synthesis pattern can be discerned on the chip (red: FLAG, green: HA). Overlay of two fluorescence images generated by scanner software.

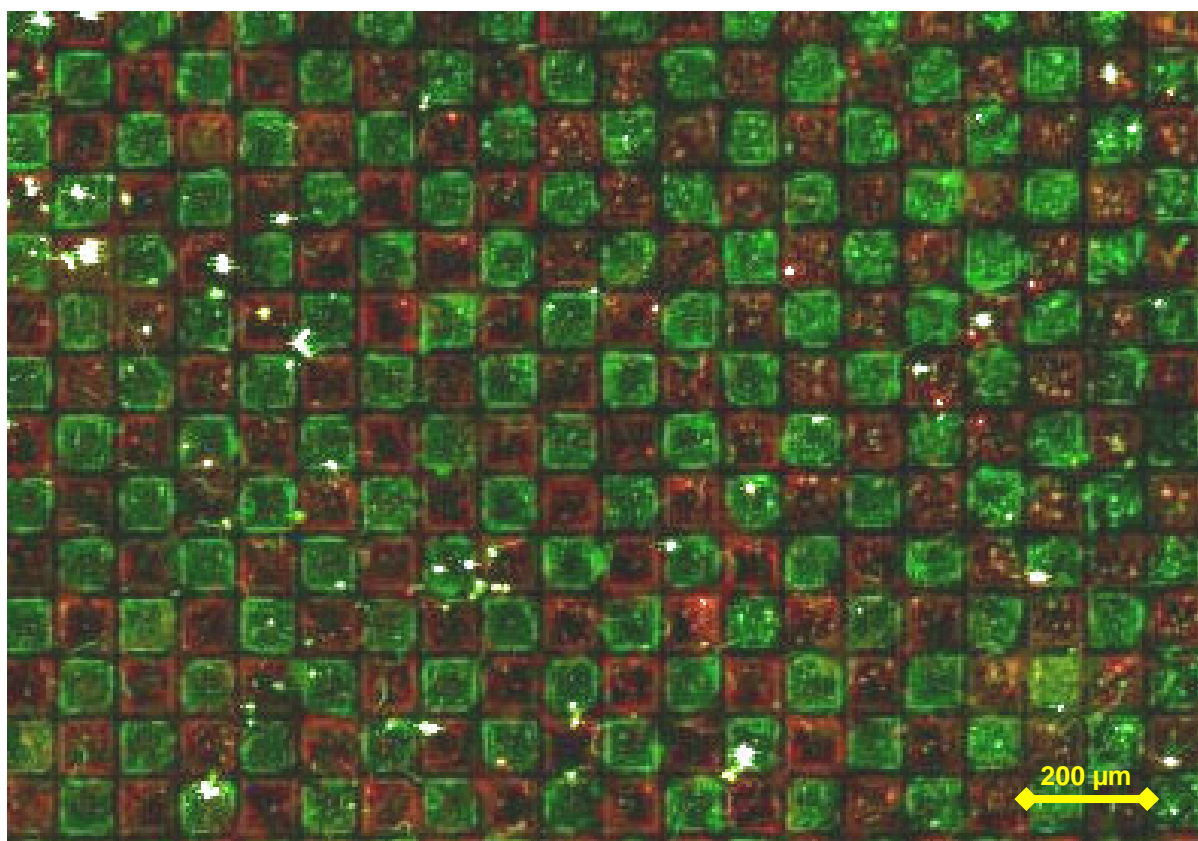


Fig. 7.17: Peptidchip 5 with surface variant A (100% PEGMA) after immunostaining, detail (red: FLAG, green: HA).

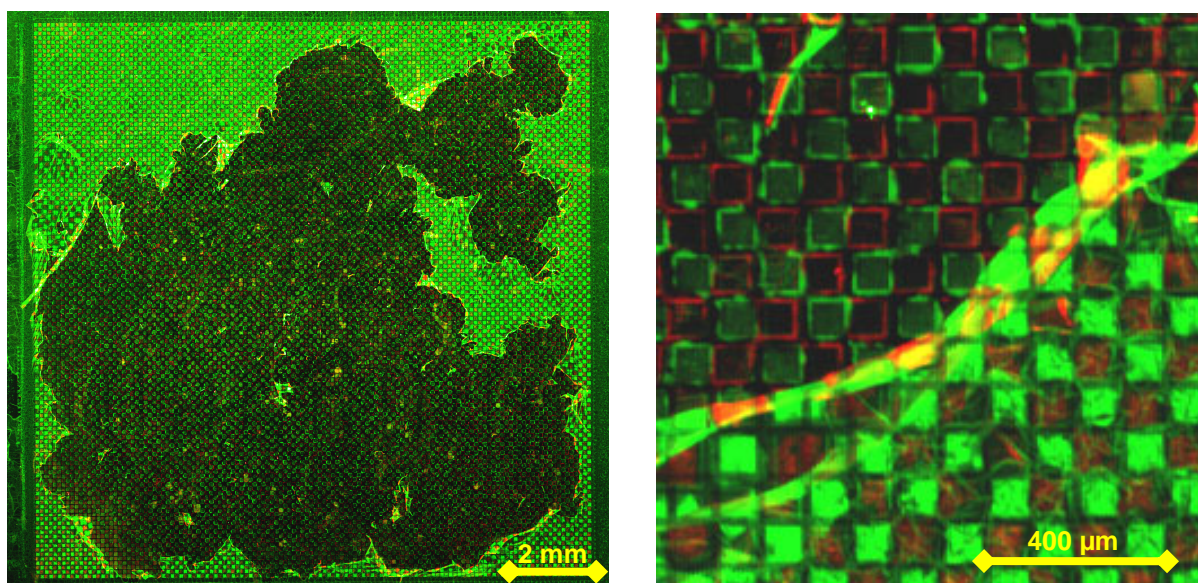


Fig. 7.18: Peptidchip 5 with surface variant B (50% PEGMA, 50% MMA) after immunostaining. The heteropolymer layer separated from the chip in the central area during TFA treatment. Nevertheless, the synthesis pattern can be discerned on the chip (red: FLAG, green: HA). Left: Complete Chip overview. Right: Detail of the edge of the separating film. Fluorescence signals can be seen from both the chip and the polymer, showing that most, but not all of the peptides and bound antibodies were removed along with the film. Overlay of two fluorescence images generated by scanner software.

The surface variant B chip was also immunostained (fig. 7.18). In the areas where the polymer had detached, results were similar to those on surface variant A in signal intensity. In the areas where the polymer was still in place, much stronger signals were obtained, and even though FLAG signals were detected only on the edges of the pixels, the signals were regular and homogeneous.

The results achieved with second chip of surface variant C are shown in fig. 7.19 and fig. 7.20. The detail images show high regularity of the fluorescence signals of each pixel, while the overview shows a good homogeneity over the whole chip area with minor gradients. Only a few small areas showed stronger signals than the rest of the chip.

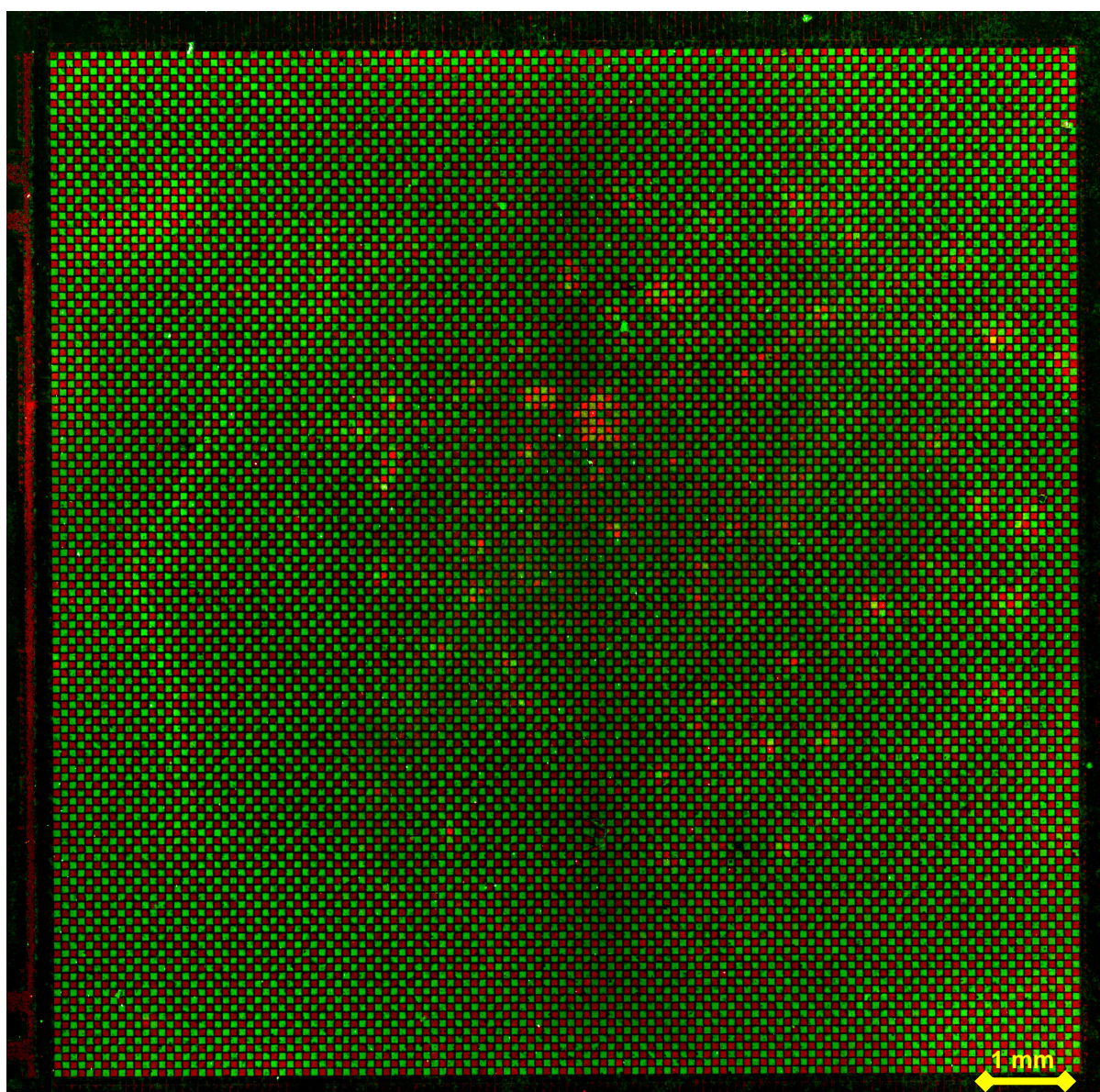


Fig. 7.19: Peptidchip 5 with surface variant C (20% PEGMA, 80% MMA), second chip, after immunostaining (red: FLAG, green: HA). Overlay of two fluorescence images generated by scanner software.

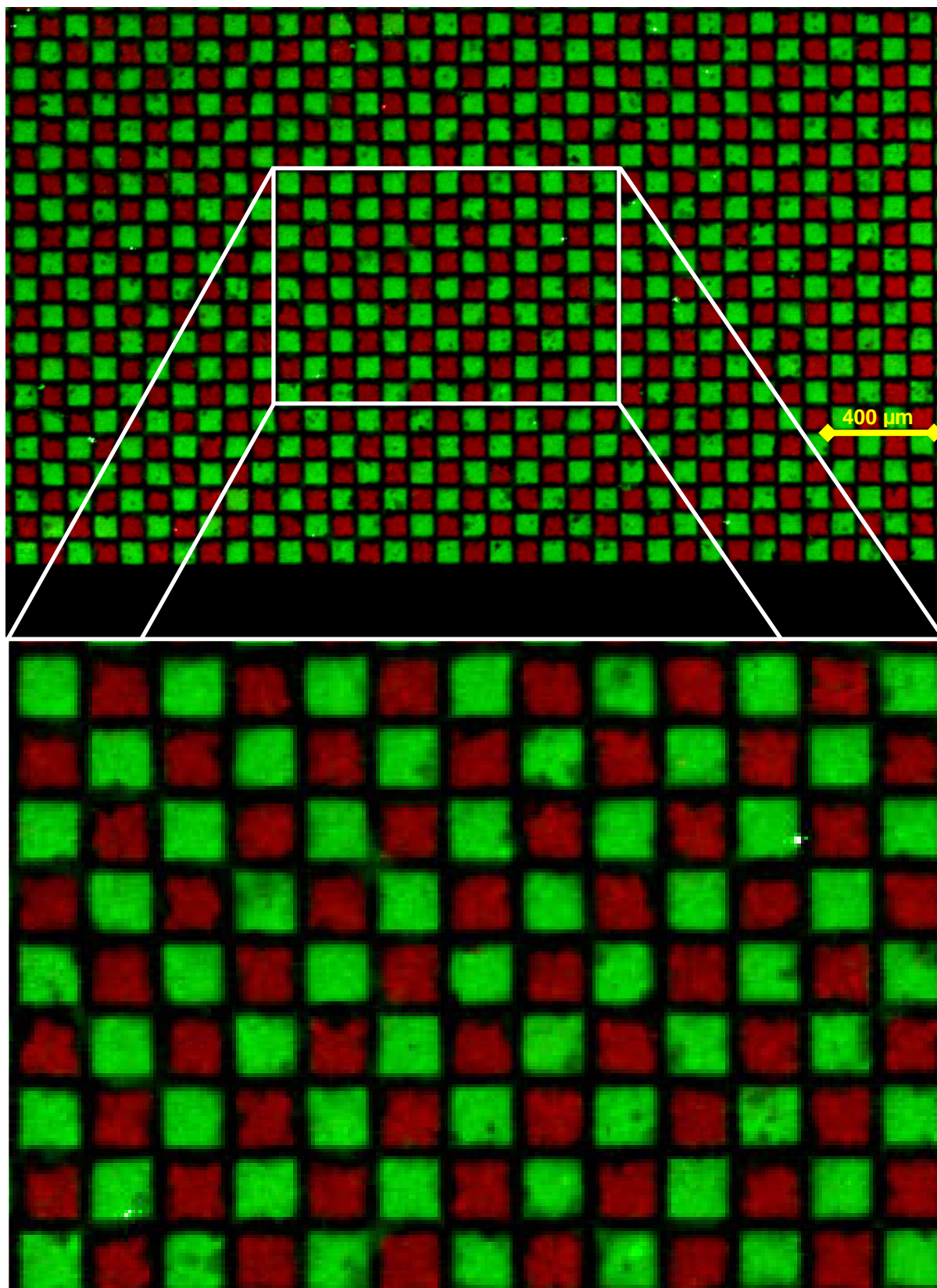


Fig. 7.20: Detail image of Peptidchip 5 with surface variant C (20% PEGMA, 80% MMA), second chip, after immunostaining (red: FLAG, green: HA).

Fig 7.19 also shows that autofluorescence of the chip still exists in areas of parallel metal tracks without top layer metal covering (left edge of the image, outside of the pixel area). However, as all such metal tracks in the pixel area are covered with top layer metal, autofluorescence was not noticeable in the pixel area, and thus does not interfere with the detection of binding signals (see also fig. 7.20).

7.3.4 Discussion

The synthesis experiment performed on Peptidchip 5 resulted in the successful synthesis of the FLAG and HA epitope in a checkerboard pattern with a density of 10,000 peptides per cm^2 . Comparable signal intensities were detected over the entire surface of the chip, indicating comparable peptide synthesis yield. Different antibodies were employed for HA detection, resulting in a final antibody selection for further tests being established. In future applications, it may be necessary to test the antibodies to be used for detection before synthesis. Using double deposition, more regular shape of spots and improved homogeneity of synthesis over the chip area in comparison to Peptidchip 3.1 have been achieved.

The results also indicate which surface modification should be given preference. While polymers with 50% and 100% PEGMA percentages were unstable in their bond to the chip surface when exposed to TFA for side-chain protection group removal, the heteropolymer of 20% PEGMA and 80% MMA was stably bound to the surface. Signal intensity was strong enough to be clearly discernible in the fluorescence scan even with this low PEGMA content.

Failure of all chips with closed passivation is surprising, as the passivation was expected to make these chips more robust to environmental influences. One possible explanation would be that these chips were already defective when received from the manufacturer, as there is currently no explanation that could be derived from differences in the design. As most particle transfer experiments were performed using chips with passivation openings, there is not enough statistical data for a yield analysis of these chips.

Chips with passivation openings proved to be robust during synthesis. The passivation openings prevent spreading and mixing of the molten particle matrix on top of the chip during coupling. On passivated chips, the same effect could be achieved by adding a grid-shaped pattern of elevations on top of the passivation, using a post-CMOS MEMS surface modification process for manufacture. Whether merging of particle melts actually causes incorrect peptides to be synthesized depends on the mobility of the amino acid molecules inside the melt, which is yet to be determined.

The issue of chip autofluorescence, as detected when using Peptidchip 3.1, was successfully circumvented by routing all metal tracks under covering top layer metal in the pixel area. The new chip covering prevented leakage of liquids past the seal. The layout of the PCB for Peptidchip 5, matching the dimensions of a microscope glass slide, proved suitable for inserting the chip directly into the array scanner.

Detachment of chips from the PCB is a mechanism of chip failure that was not observed before Peptidchip 5. As the PCB is flexible (woven glass laminated with epoxy resin), while the chip is rigid (single crystal silicon) and large compared to previous chips, bending the PCB may cause failure of the conductive epoxy glue fixing the chip to the PCB, and thus detachment of the chip from the PCB. Using the covering or at least the back-covering to stabilize the PCB should prevent this failure mechanism. Special care should be taken when installing or removing the covering to avoid bending the PCB.

With the given quality of spots, e.g. antibody affinities could be compared [STA08]. Gradients in intensity over the large chip area could be normalized using a repetitive pattern of pixels with reference epitope pixels spread over the chip. Proof-of-principle for a system for peptide synthesis and detection on Peptidchip 5 is achieved. Reproducing an experiment in which antibody affinities were compared for numerous different peptides using a different system (e.g. the peptide laser printer), and verifying the results obtained using Peptidchip 5 by comparison to the established data, could be the next step to establishing a system suitable for applications.

8. Conclusion and Outlook

8.1 Discussion of Results

8.1.1 Microelectronics and Materials

A high voltage CMOS chip for the study of electrostatic transfer of amino acid particles and chemical synthesis of peptides was built. This prototype chip was designed to allow studying particle transfer at voltages between 30 V and 100 V, for a pixel pitch between 100 μm and 45 μm . Proof-of-principle experiments performed with this chip resulted in the creation of large-area chips of 16,384 pixels for the combinatorial synthesis of 10,000 peptide spots per cm^2 . Supporting materials, such as PCBs, main boards, mechanic coverings and synthesis chambers were also designed and optimized. The final chips are easy to handle in synthesis and detection and were combined with the PCB such that the assembly matches the physical dimension of a standard microscope glass slide, making the system compatible to standard array scanners and microscopes. The large-area chip is useable in a setup for peptide library applications.

8.1.2 Particle Transfer

Particle transfer of amino acid particles was performed, in comparison to reference particles studied previously [KÖN05]. Patterns with a high density of active pixels (up to one in four active) could be deposited with a quality similar to the results achieved with the reference particles. Pixels to be deposited with particles were completely covered, while contaminations of other pixels were rare. However, the results diverged for patterns with few active pixels. Using the coarse particle fraction (average diameter around 10 μm), contaminating particles were observed for such patterns. The use of fine fraction particles, with an average diameter around 5 μm offers a solution [LOE].

Investigating particle transfer further allowed setting up a protocol for particle transfer, which was used in the successful syntheses described in chapter 7. Additionally, the weakness of the aerosol chamber concept was revealed, namely the inability to obtain stable aerosol conditions due to wall effects and irregular uptake of stored particles into the airstream. This can be circumvented in manual deposition, but is difficult to handle in an automated system. Consequently, development of a novel linear deposition system was started.

Compatibility of particle deposition to surface modifications for peptide synthesis was investigated, revealing incompatibilities between conducting surfaces including pure PEGMA layers and chips with closed passivation. Methods for achieving selective particle transfer onto chips with surface modifications for peptide synthesis were tested and confirmed: Both the use of chips with passivation openings and the use of heteropolymers of 20 % PEGMA and 80 % MMA instead of the PEGMA homopolymers used previously returned particle deposition quality to the level achieved without surface modifications, which is suitable for peptide synthesis.

8.1.3 Synthesis

Successful particle transfer on chips surface-modified with PEGMA homopolymers and heteropolymers enabled on-chip peptide synthesis. The system of on-chip synthesis was established in first experiments.

FLAG and HA epitopes (9- and 10-meric peptides) were synthesized and detected by immunostaining using fluorescence labeled antibodies in a sandwich assay. A first proof-of-principle synthesis on a prototype chip, surface-modified with 20% PEGMA, 80% MMA heteropolymer, was performed and resulted in discernible fluorescence signals. A synthesis on the full-scale application chip yielded much stronger signals from the entire spot areas, with only minor gradients in intensity over the whole chip with more than 16,000 synthesis loci.

Combining the results from the synthesis on Peptidchip 5 and advances in particle deposition, combinatorial synthesis on up to 16,384 distinct synthesis sites can be performed. Fine fraction particles in a linear deposition system allow sparse deposition patterns required for combinatorial synthesis, while 20% PEGMA, 80% MMA heteropolymers on CMOS chips with passivation openings are used as support. The spot density of 10,000 synthesis sites per cm^2 compares favorably to the state of the art in particle based synthesis using a laser printer of 400 spots per cm^2 . While the laser printer is a more mature technology, and laser printed arrays with 5,400 peptide spots per support on glass slides of the same size as the Peptidchip PCB are already commercially available, chip technology, promises unrivaled density of synthesis sites. Though increased material cost of CMOS chips over glass slides are a disadvantage, reduced amounts of reagents (and molecules of interest) required on the smaller substrate area economically favor the chip concept. A comprehensive comparison of cost-per-peptide for printer and chip technology is yet to be performed.

A more advanced antibody binding experiment using fine fraction particles is currently in progress [LOE]. In this experiment, both the FLAG and the HA epitope are permuted over all 20 standard amino acids on two positions, for a total of $20^2 = 400$ different peptides for each epitope. In addition, more than 1,000 different peptides are synthesized in a fully combinatorial way, varying each amino acid position with two to four different amino acids used per layer. In order to examine reproducibility, the fully combinatorial pattern is repeated four times over each chip, while the permutations are performed eight times per chip in parallel. This high level of redundancy will allow for additional investigations of reproducibility. Pixels where the FLAG epitope, the HA epitope and negative control pixels (an epitope anti-FLAG and anti-HA antibodies are known to have a very low affinity to) are synthesized are distributed over the chip in a regular pattern as a reference. If necessary, these reference pixels could be used to compensate for intensity gradients over the chip.

Following this fully combinatorial synthesis, the Peptidchip system could be used for real applications, e.g. antibody binding studies of epitopes not previously tested on other platforms. Preliminary tests to screen for antibodies in serum could also be performed.

8.2 From Prototype to Application

Already being successfully used for syntheses under the care of experienced operators, the current on-chip peptide synthesis system forms the foundation for a volume production system of on-chip peptide arrays for customers. The chip itself is fully usable without further improvements, but automation of the entire synthesis system has to be addressed in future works.

Both deposition and washing cannot reasonably be performed manually in syntheses with dozens of couplings and hundreds of depositions per chip due to the associated experimenters' workload. Reproducibility might also benefit from automation. In a first step, both a chip washing machine and a particle transfer machine could be built, with the operator verifying the results, performing the coupling of the amino acids by melting the particles and moving the chip between the machines. In the end, however, a fully integrated machine that produces completely synthesized peptide arrays from surface-modified chips and deposition pattern files is required for volume production. Due to the large amount of spots, software to design the peptide array is required as well. The array generation machine must be programmed through a user-friendly interface, and the analysis of the synthesis results obtained, i.e. with a fluorescence scanner, must be supported.

In such a system, quality control can no longer be performed manually, either. Besides the obvious biological controls distributed on the array, safeguards against malfunctions of the transfer system must be integrated already at particle deposition. Image processing methods used to analyze the deposition results of all or part of the chip could warn of bad depositions before coupling, allow for repeating a failed deposition instead of losing chips, or even delivering a chip with bad peptides to the customer [WAG10].

8.3 Future Chip Generations

Once automated creation of peptide arrays on chip is established, the system can be developed further. Higher spot densities are limited by the dimensions of the semiconductor process used, especially the minimum dimensions of the HV devices. Using Peptidchip 3.1, the potential for higher densities has been shown with depositions of coarse fraction particles on pixels down to 45 μm pitch. These experiments have to be repeated using fine fraction particles. Tab. 8.1 shows the minimum pixel sizes for the given HV devices in the AMIS I2T100 process currently used. In this process, if reliable particle transfer at 30 V can be established for arbitrary patterns, a spot density of almost 50.000 synthesis sites per cm^2 can be achieved. Currently, DNA arrays with a spot size of 60 μm are commercially available [AGI]. Particle-based synthesis could therefore, with current chip technology, close the gap in spot density between DNA and peptide arrays on a chip based on an advanced variant of the current Peptidchip 5 (5.2.3.4).

min. pixel pitch / μm	max HV voltage / V	spots / cm^2
80	100	15.625
60	60	27.777
45	30	49.382

Tab. 8.1: Minimum pixel sizes, corresponding spot densities and maximum HV voltages in the AMIS I2T100 process [AMI].

Further miniaturization might be possible in other semiconductor processes, especially processes that offer HV devices with trench insulation for higher integration densities, even though particles would to be tested at such dimensions. Fluorescence scanners are readily available down to a resolution of 2 μm [AGI]. Assuming that 50 scanner pixels per fluorescence spot are needed for evaluation of spot, current scanners could process pixels down to 7 μm in pixel size, which might result in a pixel pitch of less than 20 μm .

Integrating photodiodes for fluorescence detection is another option for future chip generations, though this limits maximum spot density due to the photodiodes' need for silicon

area. Retaining 100 μm pixel pitch with integrated detection might be feasible, especially if the HV can be reduced to 30 V. The spectral range of incident and fluorescent light would be limited as well, depending on the chosen strategy for filtering incident light; therefore not all fluorophores would be compatible with such a system.

The process currently used is not an optoelectronic process specified for integrating photodiodes. Therefore, it is likely that another prototype chip, possibly in a different semiconductor process (see 2.2.4), would be required to obtain an optical detection system suitable for the detection of fluorescence light. All strategies proposed for separating incident light from fluorescent light on chip still require further testing and optimization, especially if the chip is to accept arbitrary fluorescence wavelengths, as it is desirable from the users' point of view. Therefore, the use of fluorescence scanners for detection of binding events might be preferable for standard laboratory use. If the need for a highly compact device for detection of binding events warrants the development effort, however, integrated detection might be a decisive advantage.

The chips developed in this work are in no way limited to the synthesis of standard peptides. Advanced techniques, such as synthesis of D-peptides, peptides from β -amino acids or non-natural amino acids are possible in this system with little additional effort. These techniques are of special interest in pharmacological applications, as they prevent e.g. peptidic drug molecules from being rapidly destroyed by peptidases in the human body. Peptides including post-translational modifications present in proteins and peptides present in organisms could also be mimicked this way, allowing biologists to study their effects.

While called "Peptidchip", synthesis of DNA, RNA or PNA could be performed on the chips described as well, provided suitable particles and surface modifications are developed. Indeed, any kind of combinatorial synthesis for which suitable particles and synthesis chemistry can be found could be transferred to this chip-based system.

References

- [AGI] www.chem.agilent.com
- [ALB99] Alberts B, Bray D, Johnson A, Lewis J, Raff M, Roberts K, Walter P. *Lehrbuch der molekularen Zellbiologie*. Wiley VCH; 1999.
- [ALB08] Albert T, Egler C, Jakushev S, Schuldenzucker U, Schmitt A, Brokemper O, Zabe-Kühn M, Hoffmann D, Oldenburg J, Schwaab R. *The B-cell epitope of the monoclonal anti-factorVIII antibody ESH8 characterized by peptide array analysis*. *Thrombosis and Haemostasis*, vol 99; 2008. pp 634-637.
- [ALI98] Aliotta F, Di Marco G, Fontanella ME, Lanza M. *Structural relaxation processes in poly(ethylene glycol) methacrylate macromonomers*. *Journal of Physics: Condensed Matter*, vol 10; 1998. pp 545-556.
- [AMI] www.onsemi.com
- [AMS] www.austriamicrosystems.com
- [AXO] www.moleculardevices.com
- [BAL99] Ballan H, Declercq M. *High Voltage Devices and Circuits in Standard CMOS Technologies*. Kluwer Academic Publishers, 1999.
- [BEN06] Benoiton NL. *Chemistry of Peptide Synthesis*. Taylor & Francis, Boca Raton, 2006.
- [BEY05] Beyer M. *Doctoral Thesis: Entwicklung und Anwendung neuartiger Trägeroberflächen zur kombinatorischen Peptidsynthese mit Aminosäure-Tonerpartikeln*. Universität Heidelberg; 2005.
- [BEY07] Beyer M, Nesterov A, Block I, König K, Felgenhauer T, Fernandez S, Leibe K, Torralba G, Hausmann M, Trunk U, Lindenstruth V, Bischoff FR, Breitling F, Stadler V. *Combinatorial synthesis of peptide arrays onto a microchip*. *Science*, vol 318; 2007. p 1888.
- [BIA03] Bialek K, Swistowski A, Frank R. *Epitope-targeted proteome analysis: towards a large-scale automated protein-protein-interaction mapping utilizing synthetic peptide arrays*. *Analytical and Bioanalytical Chemistry*, vol 376; 2003. pp 1006-1013.
- [BLI81] Blicher A. *Field-Effect and Bipolar Power Transistor Physics*. Academic Press; 1981.
- [BLO09] Block I. *Doctoral Thesis: Herstellung und Anwendung von hochkomplexen Peptidbibliotheken*. Universität Heidelberg, 2009.
- [BRA98] Branden C, Tooze J. *Introduction to Protein Structure*. Garland Publishing, New York, 1998.

- [BRE10] Breitling F, Löffler F, Schirwitz F, Cheng Y-C, Märkle F, König K, Felgenhauer T, Dörsam E, Bischoff FR, Nesterov-Müller A. *Alternative Setups for Automated Peptide Synthesis*. Mini Reviews in Organic Chemistry, in press.
- [BRU05] Brunekreef B, Forsberg B. *Epidemiological evidence of effects of coarse airborne particles on health*. European Respiratory Journal, vol 26; 2005. pp 309-318.
- [CHA00] Chan WC, White PD. *Fmoc-Solid Phase Peptide Synthesis - A Practical Approach*. Oxford University Press, Oxford, 2000.
- [CHE] Cheng Y-C. *Doctoral Thesis*. Technical University of Darmstadt, in preparation.
- [COI07] Coin I, Beyermann M, Bienert M. *Solid-phase peptide synthesis: from standard procedures to the synthesis of difficult sequences*. Nature Protocols, vol 2; 2007. pp 3247-3256.
- [DAS55] Dash WC, Newman R. *Intrinsic optical absorption in single-crystal germanium and silicon at 77K and 300K*. Physical Review, vol 99; 1955. pp 1151-1155.
- [EIC04] Eichler J. *Rational and random strategies for the mimicry of discontinuous protein binding sites*. Protein and Peptide Letters, vol 11; 2004. pp 281-290.
- [EIC05] Eichler J. *Synthetic Peptide Arrays and Peptide Combinatorial Libraries for the Exploration of Protein-Ligand Interactions and the Design of Protein Inhibitors*. Combinatorial Chemistry & High Throughput Screening, vol 8; 2005. pp 135-143.
- [EUR] www.europractice-ic.com
- [FED05] Fedder GK, Chae J, Kulah H, Najafi K, Denison T, Kuang J, Lewis S. *Monolithically Integrated Inertial Sensors* in Baltes H, Brand O, Fedder GK, Hierold C, Tabata O. *CMOS - MEMS*. Wiley-VCH; 2005.
- [FOD91] Fodor SPA, Read JL, Pirrung MC, Stryer L, Lu AT, Solas D. *Light-directed, Spatially Addressable Parallel Chemical Synthesis*. Science, vol 251; 1991. pp 767-773.
- [FRA92] Frank R. *Spot-Synthesis. An Easy Technique for the Positionally Addressable, Parallel Chemical Synthesis on a Membrane Support*. Tetrahedron, vol 48; 1992. pp 9217-9232.
- [FRO08] Fromherz P. *Joining microelectronics and microionics: Nerve cells and brain tissue on semiconductor chips*. Solid-State Electronics, vol 52; 2008. pp 1364-1373.
- [GAI05] Gail R, Frank R, Wittinghofer A. *Systematic peptide array-based delineation of the differential beta-catenin interaction with Tcf4, E-cadherin, and adenomatous polyposis coli*. Journal of Biological Chemistry, vol 280; 2005. pp 7107-7117.
- [GAO03] Gao XL, Zhou XC, Gulari E. *Light directed massively parallel on-chip synthesis of peptide arrays with t-Boc chemistry*. Proteomics, vol 3; 2003. pp 2135-2141.

- [GRA09] Graf H-G, Harendt C, Engelhardt T, Scherjon C, Warkentin K, Richter H, Burghartz JN. *High Dynamic Range CMOS Imager Technologies for Biomedical Applications*. IEEE Journal of Solid-State Circuits, vol 44; 2009. pp 281-289.
- [HE08] He M, Stoevesandt O, Taussig MJ. *In situ synthesis of protein arrays*. Current Opinion in Biotechnology, vol 19; 2008. pp 4-9.
- [HIE05] Hierlemann A. *CMOS-based Chemical Sensors* in Baltes H, Brand O, Fedder GK, Hierold C, Tabata O. *CMOS - MEMS*. Wiley-VCH; 2005.
- [HOS06] Hoshuyama H. *Color separation device of solid-state image sensor*. United States Patent 7,138,663. 2006.
- [HOU91] Houghten RA, Pinilla C, Blondelle SE, Appel JR, Dooley CT, Cuervo JH. *Generation and use of synthetic peptide combinatorial libraries for basic research and drug discovery*. Nature, vol 354; 1991. pp 84-86.
- [IMS] www.ims-chips.de
- [IPA] The International Platinum Group Metals Association. <http://www.ipa-news.com/pgm/palladium/properties.htm>
- [ISI09] Isidro-Llobet A, Álvarez M, Albericio F. *Amino Acid Protecting Groups*. Chemical Reviews, vol 109; 2009. pp2455-2504
- [JAC02] Jacobs HO, Campbell SA, Steward MG. *Approaching nanoxerography: The use of electrostatic forces to position nanoparticles with 100 nm scale resolution*. Advanced Materials, vol 12; 2002. pp 1553-1557.
- [JPT] www.jpt.com
- [KAL94] Kal S. *Isolation Technology in Monolithic integrated-circuits – an overview*. IETE Technical Review, vol 11; 1994. pp 91-103.
- [KNO99] Knoblauch NTM, Rüdiger S, Schönfeld HJ, Driessen AJM, Schneider-Mergener J, Bukau B. *Substrate specificity of the SecB chaperone*. Journal of Biological Chemistry, vol 274; 1999. pp 34219-34225.
- [KÖN05] König K. *Diploma Thesis: Entwicklung eines ASICs in Hochspannungstechnologie zur kombinatorischen Microarray – Peptidsynthese*. University of Heidelberg; 2005.
- [KÖN10] König K, Block I, Nesterov A, Torralba G, Fernandez S, Felgenhauer T, Leibe K, Schirwitz C, Löffler F, Painke F, Wagner J, Trunk U, Bischoff FR, Breitling F, Stadler V, Hausmann M, Lindenstruth V. *Programmable high voltage CMOS chips for particle-based high-density combinatorial peptide synthesis*. Sensors and Actuators B: Chemical, in press, doi:10.1016/j.snb.2009.12.039.
- [LAM91] Lam KS, Salmon SE, Hersh EM, Hruby VJ, Kazmierski WM, Knapp RJ. *A new type of synthetic peptide library for identifying ligand-binding activity*. Nature, vol 354; 1991. pp 82-84.

- [LEE00] Lee HK, Fang YK, Lee WJ, Ho JJ, Chen KH, Liao KC. *Novel electrochemic devices (ECD) of tungsten oxide (WO₃) thin film integrated with amorphous silicon germanium photodetector for hydrogen sensor*. Sensors and Actuators B, vol 69; 2000. S 96-99.
- [LOE] Löffler F. *Doctoral Thesis*. University of Heidelberg, in preparation.
- [LOE01] Loeliger T. *Doctoral Thesis: Large-Area Photosensing in CMOS*. Swiss Federal Institute of Technology Zürich; 2001.
- [LOE09] Löffler F. *Diploma Thesis: Physikalische Charakterisierung von Biopartikeln und deren Ablagerungsverhalten auf CMOS-Chips*. University of Heidelberg; 2009.
- [LOO96] Loose M. *Diploma Thesis: Layout und Test eines Systems adaptiver Photorezeptoren in analoger CMOS-Technologie*. Heidelberg University; 1996.
- [LUL00] Lulé T, Benthien S, Keller H, Mutze F, Rieve P, Seibel K, Sommer M, Bohm M. *Sensitivity of CMOS Based Imagers and Scaling Perspectives*. IEEE Transactions on Electron Devices, vol 47; 2000. pp 2110-2122.
- [MAC90] Machold HT. *Organische Pigmente für Photokopierer und Laserdrucker*. Chemie in unserer Zeit, vol 4; 1990. pp 176-181.
- [MER63] Merrifield RB. *Solid Phase Peptide Synthesis. The Synthesis of a Tetrapeptide*. Journal of the American Chemical Society, vol 85; 1963. pp 2149-2154.
- [MER64-1] Merrifield RB. *Solid Phase Peptide Synthesis II. The Synthesis of Bradykinin*. Journal of the American Chemical Society, vol 86; 1964. p 304.
- [MER64-2] Merrifield RB. *Solid Phase Peptide Synthesis III. An Improved Synthesis of Bradykinin*. Biochemistry, vol 3; 1964. pp 1385-1390.
- [MER99] Merrill RB. *Color separation in an active pixel cell imaging array using a triple-well structure*. United States Patent 5,965,875. 1999.
- [MIR99] Miranda LP, Alewood PF. *Accelerated chemical synthesis of peptides and small proteins*. Proceedings of the National Academy of Sciences of the United States of America, vol 96; 1999. pp 1181-1186.
- [MOO65] Moore GE. *Cramming more components onto integrated circuits*. Electronics, vol 38; 1965.
- [MÜL04] Müller H-J, Röder T. *Der Experimentator Microarrays*. Elsevier Spektrum Akademischer Verlag, Heidelberg, 2004.
- [NAK03] Nakagawa H, Yamamoto N, Okazaki S, Chinzei T, Asakura S. *A room temperature operated hydrogen leak sensor*. Sensors and Actuators B, vol 93; 2003. pp 468-474.
- [NES06] Nesterov-Müller A. *Doctoral Thesis: Ortsgenaue Ablagerung von Aminosäurepartikeln für die kombinatorische Synthese von Peptidarrays auf einem Chip*. University of Heidelberg; 2006.

- [NES07] Nesterov A, Löffler F, König K, Trunk U, Leibe K, Felgenhauer T, Stadler V, Bischoff R, Breitling F, Lindenstruth V, Hausmann M. *Noncontact charge measurement of moving microparticles contacting dielectric surfaces*. Review of Scientific Instruments, vol 78; 2007.
- [NES07-2] Nesterov A, Löffler F, König K, Trunk U, Leibe K, Felgenhauer T, Bischoff R, Breitling F, Lindenstruth V, Stadler V, Hausmann M. *Measurement of triboelectric charging of moving micro particles by means of an inductive cylindrical probe*. Journal of Physics D: Applied Physics, vol 40; 2007. pp 6115-6120.
- [NES08] Nesterov-Müller A. *Habilitational Thesis: Physical Aspects of Combinatorial Fabrication and Processing of Microchip-Based Peptide Libraries*. University of Heidelberg; 2008.
- [NES09] Nestor JJ. *The Medicinal Chemistry of Peptides*. Current Medicinal Chemistry, vol 16; 2009. pp 4399-4418.
- [NES10] Nesterov A, Löffler F, Cheng YC, Torralba G, König K, Hausmann M, Lindenstruth V, Stadler V, Bischoff FR, Breitling F. *Characterization of Triboelectrically Charged Particles Deposited on Dielectric Surfaces*. Journal of Physics D: Applied Physics, vol 43; 2010.
- [OKI] www.oki.com
- [OTV08] Otvos L. *Peptide-Based Drug Design: Here and Now*. Methods in Molecular Biology, vol 494; 2008. pp 1-8.
- [PAI10] Painke F. *Doctoral Thesis*. University of Heidelberg, in preparation.
- [PEL02] Pellois JP, Zhou XC, Srivannavit O, Zhou TC, Gulari E, Gao XL. *Individually addressable parallel peptide synthesis on microchips*. Nature Biotechnology, vol 20; 2002. pp 922-926.
- [PET09] Petrone J. *Germany's PepPerPrint Designing Next-Gen Peptide Array Printer; Plans Year-End Debut*. BioArray News; May 26, 2009.
- [PHI00] Philips Semiconductors. *The I²C Bus Specification Version 2.1*. Philips Semiconductors; 2000. document order number: 9398 393 40011. www.semiconductors.philips.com
- [POR08] Porcheddu A, Giacomelli G, Piredda I, Carta M, Nieddu G. *A Practical and Efficient Approach to PNA Monomers Compatible with Fmoc-Mediated Solid-Phase Synthesis Protocols*. European Journal of Organic Chemistry, vol 34; 2008. pp 5786-5797.
- [QAD10] Qadir MI, Malik SA. *HIV fusion inhibitors*. Reviews in Medical Virology, vol 20; 2010. pp 23-33.
- [RAU09] Raucher D, Moktan S, Massodi I, Bidwell GL. *Therapeutic peptides for cancer therapy. Part II - cell cycle inhibitory peptides and apoptosis-inducing peptides*. Expert Opinion on Drug Delivery, vol 6; 2009. pp 1049-1064.
- [REI02] Reineke U, Ivascu C, Schlieff M, Landgraf C, Gericke S, Zahn G, Herzel H, Volkmer-Engerdt R, Schneider-Mergener J. *Identification of distinct antibody epitopes and mimotopes from a peptide array of 5520 randomly generated sequences*. Journal of Immunological Methods, vol 267; 2002. pp 37-51.

- [REV07] Revell JD, Wennemers H. *Identification of Catalysts in Combinatorial Libraries*. Topics in Current Chemistry, Creative Chemical Sensor Systems. Springer Berlin / Heidelberg, 2007.
- [SBS04] *ANSI/SBS 1-2004 Microplates - Footprint Dimensions and ANSI/SBS 2-2004: Microplates - Height Dimensions and ANSI/SBS 3-2004: Microplates - Bottom Outside Flange Dimensions and ANSI/SBS 4-2004: Microplates - Well Positions*. American National Standards Institute and Society for Biomolecular Sciences, 2004.
- [SCH76] Schüttler A, Meltzow W, Föhles J, Zahn H. *Aminolysis and racemization of activated esters with the use of high temperatures*. Hoppe-Seyler's Zeitschrift für Physiologische Chemie, vol 357; 1976. pp 741-744.
- [SCH90] Schulz M, Zinkernagel RM, Hengartner H. *Peptide-induced antiviral protection by cytotoxic T cells*. Proceedings of the National Academy of Sciences of the United States of America, vol 88; 1990. pp 991-993.
- [SCH08] Schirwitz C, Block I, König K, Nesterov A, Fernandez S, Felgenhauer T, Leibe K, Torralba G, Hausmann M, Lindenstruth V, Stadler V, Breitling F, Bischoff F. *Combinatorial Peptide Synthesis on a Microchip*. Current Protocols, Wiley Interscience, 2008.
- [SEK00] Sekimoto S, Yamamoto N, Okazaki S, Fukuda K, Asakura S, Shigemori T, Takahashi S. *A fiber-optic evanescent-wave hydrogen gas sensor using palladium-supported tungsten oxide*. Sensors and Actuators B, vol 66; 2000. pp 142-145.
- [SHR09] Shrivastava A, Nunn AD, Tweedle MF. *Designer Peptides: Learning from Nature*. Current Pharmaceutical Design, vol 15; 2009. pp 675-681.
- [STA07] Stadler V, Beyer M, König K, Nesterov A, Torralba G, Lindenstruth V, Hausmann M, Bischoff FR, Breitling F. *Multifunctional CMOS Microchip Coatings for Protein and Peptide Arrays*. Journal of Protein Research, vol 6; 2007. pp 3197-3202.
- [STA08] Stadler V, Felgenhauer T, Beyer M, Fernandez S, Leibe K, Güttler S, Gröning M, König K, Torralba G, Hausmann M, Lindenstruth V, Nesterov A, Block I, Pipkorn R, Poustka A, Bischoff FR, Breitling F. *Combinatorial synthesis of peptide arrays with a laser printer*. Angewandte Chemie – International Edition, vol 47; 2008. pp 7132-7135.
- [STA08-2] Stadler V, Kirmse R, Beyer M, Breitling F, Ludwig T, Bischoff FR. *PEGMA/MMA Copolymer Graftings: Generation, Protein Resistance, and a Hydrophobic Domain*. Langmuir, vol 24; 2008. pp 8151-8157.
- [STI97] Stieß M. *Mechanische Verfahrenstechnik 2*. Springer, Berlin; 1997.
- [STI09] Stieß M. *Mechanische Verfahrenstechnik – Partikeltechnologie 1*. Springer, Berlin; 2009.
- [SZE07] Sze SM, Ng KK. *Physics of Semiconductor Devices*. John Wiley & Sons; 2007.
- [SZE07-1] Sze SM, Ng KK. *Physics of Semiconductor Devices. Appendix H*. John Wiley & Sons; 2007. p 791.

- [TRI99] Tritthart U. *Doctoral Thesis: Hydrogen doped tungstenoxide-films (WO₃): Properties of electrical transport - metal insulator transition*. Technical University Braunschweig; 1999.
- [TOR] Torralba G. *Project Notes and Personal Communications*.
- [TRO79] Troutnab RR. *VLSI Limitations from Drain-Induced Barrier Lowering*. IEEE Transactions on Electron Devices, vol ED-26; 1979. pp 461-469.
- [TUD] www.ihm.to-dresden.de
- [UTT08] Uttamchandani M, Yao SQ. *Peptide Microarrays: Next Generation Biochips for Detection, Diagnostics and High-Throughput Screening*. Current Pharmaceutical Design, vol 14; 2008. pp 2428-2438.
- [VLI10] Vlieghe P, Lisowski V, Martinez J, Khrestchatisky M. *Synthetic therapeutic peptides: science and market*. Drug Discovery Today, vol 15; 2010. pp 40-56.
- [VOE92] Voet D, Voet JG. *Biochemie*. VCH, Weinheim, 1992.
- [VOL09] Volkmer R. *Synthesis and Application of Peptide Arrays: Quo Vadis SPOT Technology*. ChemBioChem, vol 10; 2009. pp 1431-1442.
- [WAG10] Wagner J, Löffler F, König K, Fernandez S, Bischoff FR, Nesterov A, Breitling F, Hausmann M, Lindenstruth V. *Quality Analysis of Selective Micro-particle Depositions on Electrically Programmable Surfaces*. In preparation.
- [WAN03] Wang SQ, Humphreys ES, Chung SY, Delduco DF, Lustig SR, Wang H, Parker KN, Rizzo NW, Subramoney S, Chiang YM, Jagota A. *Peptides with selective affinity for carbon nanotubes*. Nature Materials, vol 2; 2003. pp 196-200.
- [WAN06] Wang L, Xie J, Schultz PG. *Expanding the genetic code*. Annual Review of Biophysics and Biomolecular Structure, vol 35; 2006. pp 225-249.
- [WIL05] Williams T. *The Circuit Designer's Companion*. Elsevier, 2005.
- [XFA] www.xfab.com
- [ZHA06] Zhang Y. *Diploma Thesis: A CMOS Optical Sensor for the Identification of the Fluorescence Labeled Peptides*. University of Heidelberg, 2006.
- [ZHA10] Zhang P, Zheng Y, Shi J, Zhang YX, Liu SL, Liu YX, Zheng DX. *Targeting a Novel N-terminal Epitope of Death Receptor 5 Triggers Tumor Cell Death*. Journal of Biological Chemistry, vol 285; 2010. pp 8953-8966.

Acknowledgements

I am very grateful to Prof. Dr. Volker Lindenstruth for his lectures that sparked my interest in microelectronics, for offering me the opportunity to work on this project, and for his encouraging and supportive supervision of this thesis.

I am equally grateful for PD. Dr. F. Ralf Bischoff for supervising this thesis, for his support, and for most interesting interdisciplinary discussions.

I am indebted to Prof. Dr. Michael Hausmann, who was very helpful and supportive in the completion of this thesis, for his advice and encouragement.

I am very thankful to Dr. Volker Stadler for the opportunity to work on this project, an excellent interdisciplinary working environment and for his support. My thanks also go to PD. Dr. Frank Breitling for his support and encouragement and most interesting discussions.

PD. Dr. Alexander Nesterov has my gratitude for his works on particle properties and transfer, works on fixed-pattern chips, encouraging discussions, and for his general support.

I am indebted to Dr. Ulrich Trunk for his aid and expert advice especially in matters of electronics and physics.

Dr. Ines Block never tired of increasing my understanding of chemistry and biology. For this, and for the excellent interdisciplinary collaboration especially regarding the on-chip peptide syntheses, I am very thankful. Christopher Schirwitz also has by thanks for excellent interdisciplinary collaboration.

To Dr. Simon Fernandez go my thanks for his works in particle production, and for his advice and excellent collaboration in particle deposition.

I am thankful to Klaus Leibe for his advice and aid in mechanical and engineering matters, especially concerning the aerosol chambers. I am also thankful to Dr. Thomas Felgenhauer and Dr. Mario Beyer for their work on surface modifications, particles and synthesis.

I thank Dr. Gloria Torralba and Yipin Zhang for good collaboration in the field of microelectronics and on-chip optical detection. Dr. Gloria Torralba also has my thanks for her work on pattern generation software.

Felix Löffler has my thanks for the excellent collaboration in aerosol and particle transfer matters. Frieder Märkle, Florian Painke and Yun-Chien Cheng also have my thanks for excellent collaboration

Thorsten Kühlwein and Daniela Rambow have my thanks for their work in particle manufacture, chip surface modifications and array synthesis.

I am very thankful to Ralf Achenbach for his support in bonding and measurement issues, and to Markus Dorn for his support in using and installing the CADENCE software and the AMIS I2T100 design kit.

My thanks go to Volker Kiworra for his support in designing the PCBs used in this project. Also, my thanks go to the members of the mechanical workshop of the Kirchhoff-Institute for Physics for building the numerous mechanical components that were required in this work.

My gratitude also goes to all my other colleagues at the DKFZ Junior Research Group “Chip-based Peptide Libraries” and the Kirchhoff-Institute for Physics, with whom it was a pleasure to work.

I would like to thank Jenny Wagner, Dr. Ines Block, Dr. Ulrich Trunk and Dr. Dieter Koch for their efforts in proofreading this thesis manuscript.

I am grateful to the DKFZ PhD program for financial support.

My best thanks also go to my family for the support I was given during my studies. I am also very grateful to my girlfriend and to my friends for their continued support and encouragement.

APPENDICES

A1. Introduction to Amino Acids, Peptides and Proteins

A1.1 Biochemical Classification

Amino acids and their polymers, *peptides* and *proteins*, are essential components of all known living organisms. The chemical bond between amino acids is called a peptide bond, and a polymer of multiple amino acids is called a peptide. Long peptides of 30 to over 10,000 (typically several hundred) amino acids are called proteins, and they are one of the most versatile classes of molecules. In organisms, the functions of proteins are, among others [ALB99]:

- to catalyze and regulate chemical reactions as *enzymes*,
- signal transduction (e.g. sensor proteins like rhodopsin),
- to provide form or structure (e.g. tubulin, actin, keratin),
- to exert physical force or cause motion using chemical energy (e.g. myosin, kinein),
- to transport molecules through membranes (pores and channels) or in fluids (e.g. haemoglobin, serumalbumin),
- to emit fluorescent light (e.g. green fluorescent protein),
- amino acid storage (e.g. casein, ovalbumin).

Two properties of proteins enable this diversity. First, they are capable of highly selective non-covalent binding to other molecules. Second, their polymer chains fold into distinct *conformations*, from globular to fibrous, which can either be fixed or have two or more possible states of local energy minima. Conformational changes can be effected, facilitated or hindered by environmental conditions (e.g. temperature, pH, electrical field). Binding affinities to substrates often depend on conformation, and vice versa. These effects can be used in living cells, e.g. to convert solar energy to storable chemical energy, to use chemical energy to cause motion, or to separate electrical charges through active transport of ions through the cellular membrane.

Shorter peptides (less than 30 amino acids) may lack the conformational stability of proteins. Yet, they still can be very selective binders, and can be used in organisms, e.g. as chemical messengers like *signal peptides*.

A1.2 Amino Acids and the Peptide Bond

A1.2.1 The Peptide Backbone

To understand the versatility of proteins, it is helpful to first look at their chemical structure, starting with their monomers and the way these monomers are linked to each other [ALB99, VOE92, BRA98].

Proteins are *linear heteropolymers*, that is polymers consisting of different parts (monomers) linked in a distinct, non-branched sequence. In this, they are alike to DNA and RNA, which are also linear heteropolymers (but composed of nucleic acids). They differ from many synthetic polymers like polyethylene or polypropylene, which are *nonlinear homopolymers* with a mesh-like structure of equal monomers.

Amino acids are the monomers of proteins. There are 20 different amino acids, called *standard proteinogenic amino acids*, generally used in organisms for the purpose of protein synthesis. They have the same chemical structure, but differ in their *side-chains*. Fig. A1.1 shows the basic structure of the α -amino-acids¹ used for protein synthesis in organisms. *Non-standard proteinogenic amino acids* also exist, and may be integrated into proteins after ribosomal synthesis of the peptide chains in a process called *post-translational modification*. Shorter peptides naturally occurring in organisms can contain an even larger assortment of amino acids, while biochemists today experiment with integrating synthetic amino acids into *in vitro* and *in vivo* peptide synthesis [WAN06].

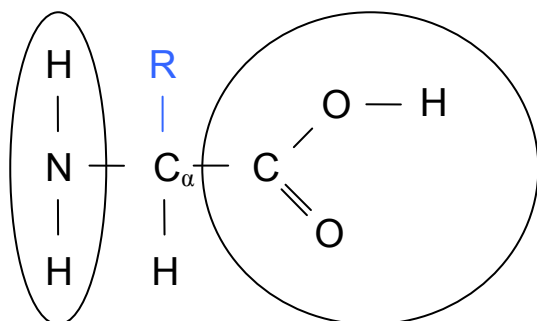


Fig. A1.1: Nominal structure of amino acids. Left: amine group; right: carboxyl group. The central carbon atom, which links the amine group, the carboxyl group, and the side-chain (denoted 'R') is called the C_α carbon atom.

Fig. A1.1 depicts the nominal structure of an amino acid, containing one *amine group* which is basic (can accept a third H^+ -ion), and one *carboxylic acid group* (or *carboxyl group*) which is acidic (can donate its H^+ -ion), and a side chain. The four possible states of the molecule are shown in fig. A1.2.

The tendency of an acidic or basic group to donate or accept protons is described by its *dissociation constant* K , which is defined by

$$K = [H^+] \cdot [A^-] / [HA], \quad (\text{Eq. A1.1})$$

assuming the substance HA is dissolved in pure water, where $[H^+]$ denotes the concentration of hydrogen ions in the solution. (This includes these H^+ -ions that are actually bound to water and are present in the form of H_3O^+ ions. In aqueous solution, practically all H^+ ions are bound in this way.) $[A^-]$ is the concentration of dissociated ions of the acid A, and $[HA]$ the concentration of the acid in the form where it retains its proton. The equation is invariant to a shift in the charges of A and HA. For example, considering a base B, the dissociation constant would be $K = [H^+] \cdot [B] / [HB^+]$.

¹ The carbon atoms in amino acids are labeled in ascending order with Greek letters, starting from the carbon atom closest to the amine group. The amino acid is then named after the carbon atom linked to the carboxyl group. In an α -amino-acid, if present, the C_β and all higher order carbon atoms would be in the side-chain. In a β -amino acid, the carboxy group would be bound to the second carbon atom, counting from the amine group. Some β - and γ -amino acids exist naturally, but are not used in protein biosynthesis.

Values of K range over several decades. Therefore, it is useful to transform eq. A1.1 to

$$-\lg [H^+] = -\lg K + \lg ([A^-] / [HA]). \quad (\text{Eq. A1.2})$$

Using the definition of the pH -value of a solution

$$pH = -\lg [H^+] \quad (\text{Eq. A1.3})$$

and defining the pK of a substance

$$pK = -\lg K \quad (\text{Eq. A1.4})$$

we get the *Henderson-Hasselbalch-Equation*:

$$pH = pK + \lg ([A^-] / [HA]) \quad (\text{Eq. A1.5})$$

From this equation, we see an alternative definition of the pK : The pK of a substance is equal to the pH of a solution in which the concentration of the protonated substance equals that of the deprotonated substance.

Some substances, including amino acids, have multiple groups that can accept or donate protons. In this case, the pK s are enumerated, starting with the most acidic group, and assuming that the groups deprotonate in order.

Both the pK_1 of the carboxyl group and the pK_2 of the amine group of a peptide are influenced by the side-chain. For the 20 standard proteinogenic amino acids, pK_1 is between 1.80 and 2.43, and pK_2 is between 8.84 and 10.78. Therefore, dissolved in water under physiological conditions of $pH \approx 7$, practically all amine groups of amino acids are present as *ammonium ions*, and practically all carboxyl groups are present as *carboxylate ions*. This is the state depicted in the lower right drawing of Fig. A1.2. Such a molecule with both positive and negative ion groups is called *zwitterion*.

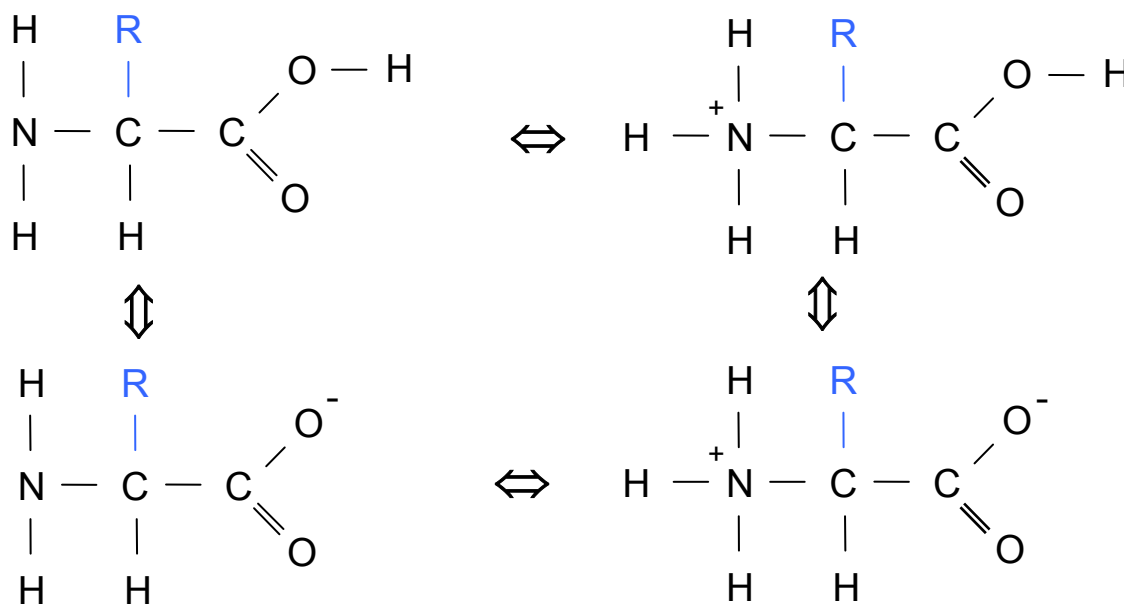


Fig. A1.2: The four protonization states of amino acids. In solution, any amino acid molecule can donate or accept H^+ -ions (e.g. from or to water molecules, from hydronium or to hydroxyl ions) and thus change between these states as indicated by the arrows. The ratio between these four states strongly depends on the number of H^+ -ions in the solution (its pH). The lower right state is dominant under physiological conditions.

Under adequate conditions (see A1.4 and 1.1), amino acids polymerize to peptides, forming a peptide bond between two *amino acid residues*, as shown in fig. A1.3. This structure forms the *backbone* of a peptide chain or protein structure.

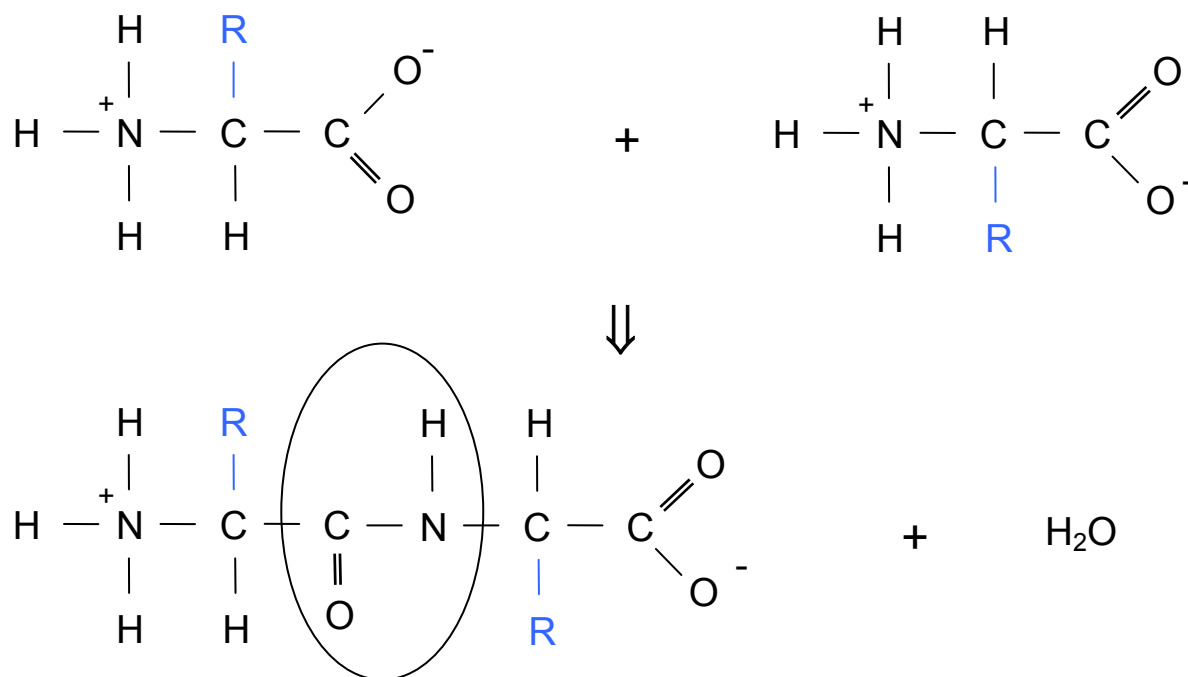


Fig. A1.3: Chemical bonding of two amino acids, forming a peptide. The peptide bond is encircled.

Looking at the structure of the peptide backbone, we see only single bonds, and may be led to believe that free rotation around these bonds might be possible. In reality, however, only rotation around the bonds that involve the C_α -atom is possible, while the peptide bond is fixed. This is due to the fact that the peptide bond is actually a partial double bond, which cannot rotate freely (fig. A1.4). Therefore, the four atoms of the peptide bond (OCNH) and both adjacent C_α s are located in a single plane. In most cases, the oxygen atom and the hydrogen atom of the peptide bond are located on opposite sides of the backbone as a *trans-peptide*. *Cis-peptides*, with oxygen and hydrogen on the same side of the backbone, are rare for energetic reasons, and almost always involve a residue of the amino acid proline [VOE92].

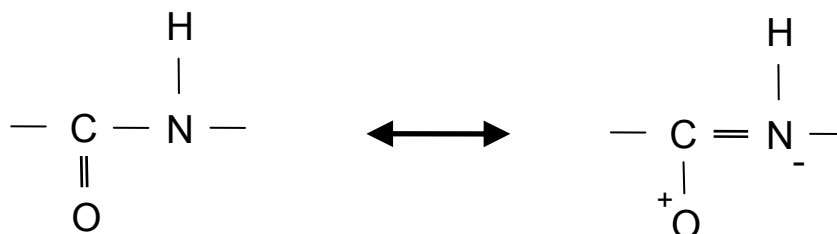


Fig. A1.4: Resonance stabilization of the peptide bond. It should be noted that in spite of this notation, the atom does not “switch” between two states, but exists in a stable intermediate state with the electrons in a quantum superposition of both states.

Fig. A1.5 shows fixed and flexible bonds in a peptide chain. Rotation is possible around both of the bonds involving the C_α -atom. For each residue, the three-dimensional orientation of the peptide backbone can be described using two angles per residue, called Φ and Ψ .

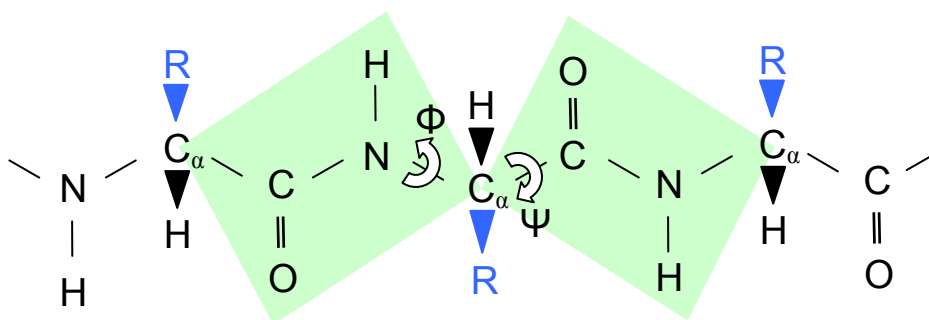


Fig. A1.5: Flexibility of the polypeptide chain. The peptide bond planes can rotate freely around their bonds to the C_α -atoms, giving Φ and Ψ is sufficient to describe its orientation relative to its neighbors in the polypeptide backbone.

Even though steric interactions between atoms further away from each bond, both in the backbone and in the side-chain, restrict the possible (or at least likely) combinations of angles, the ability to rotate around two bonds per amino acid gives the polymer chain of a polypeptide some freedom of conformations. This even includes the possibility of a reverse turn of the polypeptide chain over only two residues in a *hairpin loop* structure. Detailed biophysical considerations of allowed angles can be found in the literature [BRA98, VOE92].

However, this ability to rotate freely does not allow the individual atoms to swap their locations in three-dimensional space. Looking down at the plane of the C_α from the point of view of the adjacent hydrogen atom, counting clockwise, and starting with the side group, two sequences of chemical groups are possible: side group – carboxyl – amine, or side group – amine – carboxyl (fig. A1.6). These forms are mirror images of one another and cannot be matched by rotations. Therefore, they are indeed different molecules, *chiral isomers* of one another. While chiral isomers are undistinguishable in many “simple” chemical reactions, more complex interactions common in organisms depend on matching of the shape of the molecule to a receptor and only work with molecules of adequate chirality. All proteinogenic amino acids are of the same type, called *left-handed* or *L-amino-acids* [VOE92]. Conversion between chirality states (*racemization*) is rare in organisms because of the energy barrier between these states. It requires high temperatures to occur at significant rates [SCH76, STA08].



Fig. A1.6: Structure of L- and D- amino acids, looking “down” from the position of the hydrogen atom onto the carbon atom “in the middle” and the other chemical groups on the plane “below” (the structure is tetrahedral). Note their chirality: Even though the same groups are bound to the central carbon atom in the molecule on the left and on the right, they are not equal, as they cannot be transformed into one another using only rotational transformations: They are mirror images of each other. The amino acid on the left is called left-handed, or L-amino acid, the one on the right is a right-handed D-amino acid. All proteinogenic amino acids are L-amino acids.

A1.2.2 Side Groups of Amino Acids and Peptides

Along the backbone of a peptide, each amino acid contributes not only two half peptide bonds, but also one side-chain attached to its C_{α} . The side-chains of the 20 standard proteinogenic amino acids contain one to about 20 atoms, and vary widely in their size, polarity and charge. This diversity is one essential distinguishing feature of polypeptides compared to other types of biopolymers. For example, polar amino acids may bind ions or other charged molecules, or reinforce the protein structure, by ionic bonds or hydrogen bonds. Non-polar amino acids tend to be located inside a folded protein, as they are hydrophobic. In membrane-bound proteins, they may contact the non-polar inside of the membrane. Two cysteine groups can form a disulfide bond, which is covalent and thus strong. Glycine enables hairpins in the peptide backbone. Notably, one of the twenty proteinogenic amino acids, Proline, differs from the basic structure described above insofar that the side-chain links back to the backbone at the nitrogen atom of the amine group, forming a ring, thus limiting the torsional angles of proline more strictly than those of other amino acids. Despite the differences, its amino group functions like the amino group of the other amino acids in the formation of a peptide bond. Fig. A1.7 shows the side-chains of all standard proteinogenic amino acids and their one-letter and three-letter codes.

Amino acid side-chains also have a direct influence on peptide and protein synthesis. Fig. A1.2 is deceptive in so far as, due to the planarised drawing style, it suggests that the side-chains are irrelevant to the formation of the peptide bond. In reality, however, certain “bulky” side-chains sterically interfere with each other. Especially *in vitro*, without the aid of the *ribosome* (the enzyme that catalyzes protein synthesis) and other proteins involved in protein synthesis, certain sequences are inefficient to synthesize, with synthesis efficiency reduced and special techniques required for synthesis [COI07].

A1.3 Protein Structure

Comparing the peptide backbone to the nucleic acid backbones, we note that the DNA backbone has a strong tendency to form a double-helical structure, while in polypeptides, this tendency to form a fixed three-dimensional structure is weaker. Nevertheless, certain frequent structures, like α -*helices*, and parallel or antiparallel strands, like β -*sheets*, which are both stabilized by hydrogen bonds within the peptide backbone, are common *motifs* [ALB99].

Protein structure is generally described in four layers:

- The *primary structure* simply lists the amino acid sequence of the polypeptide.
- The *secondary structure* describes frequent elements such as α -helices or β -sheets and their position in the amino acid sequence.
- *Tertiary structure* is the actual three-dimensional *conformation* of a polypeptide chain
- The *quarternary structure* describes the structure of the whole functional protein, including its polypeptide chains, incorporated ions and other components and their three-dimensional arrangement.

Many proteins consist of several peptide chains covalently or non-covalently linked. They may also incorporate other substances besides peptide chains, such as specialized small molecules and ions, but also other biopolymers such as RNAs and polysaccharides.

Modification of the side-chains of a peptide, e.g. selenoylation, methylation, or hydroxylation by special enzymes during or after synthesis is also frequent [ALB99].

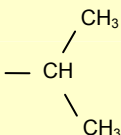
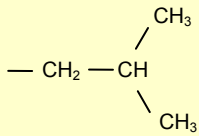
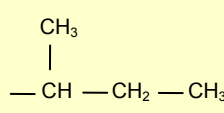
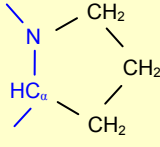
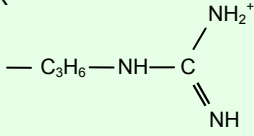
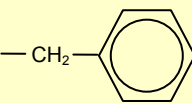
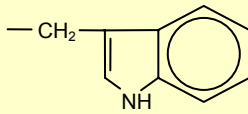
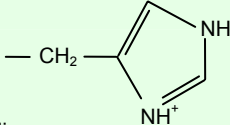
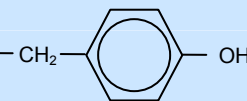
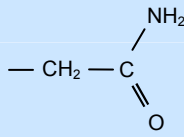
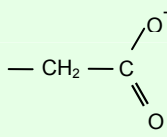
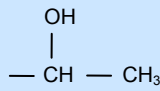
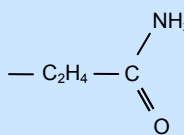
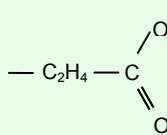
G — H Gly Glycine	A — CH ₃ Ala Alanine	V  Val Valine	K — C ₄ H ₉ — NH ₃ ⁺ Lys Lysine
L  Leu Leucine	I  Ile Isoleucine	P  Pro Proline	R  Arg Arginine
M — C ₂ H ₄ — S — CH ₃ Met Methionine	F  Phe Phenylalanine	W  Trp Tryptophan	H  His Histidine
C — CH ₂ — SH Cys Cysteine	Y  Tyr Tyrosine	N  Asn Asparagine	D  Asp Aspartic Acid
S — CH ₂ — OH Ser Serine	T  Thr Threonine	Q  Gln Glutamine	E  Glu Glutamic Acid

Fig. A1.7: The chemical structures of the side groups of the 20 standard proteinogenic amino acids. The dominant forms at pH 7.0 are shown. Three-letter and one-letter codes are given. The peptide backbone has been omitted, except for proline where it is marked in blue. The amino acids are grouped and color-coded according to their chemical properties under physiological conditions: Charged polar amino acids are on green background, non-charged polar amino acids on blue background, and non-polar amino acids are on yellow background. Glycine is special, as it is the amino acid with the lowest possible molecular weight and greatest flexibility in binding angles in a peptide chain.

A1.4 Protein biosynthesis

In living organisms, proteins are synthesized as described by “blueprints” provided by the genetic code. The double-stranded DNA molecule is well-suited for storage of the genetic information, being stable and suitable for reproduction.

However, the DNA molecule is not suitable for directly synthesizing proteins from it. For this purpose, a “working copy” in the form of *messenger RNA (mRNA)* is *transcribed* from the DNA by *RNA polymerase* enzymes. *Ribosomes* can then bind to the mRNA, and *translate* the RNA into a polypeptide chain, using *tRNAs (transfer RNA)* providing the amino acids. Each mRNA may be translated by several ribosomes at once. During all of these steps, regulatory systems may promote, modify or prevent synthesis of specific proteins, allowing eukaryotic cells to *differentiate* e.g. into neural, muscle or epidermal cells, and to react to environmental changes. In the cell, mRNA is much less stable than DNA. It has to be constantly re-transcribed if continued production of a protein is desired.

DNA and RNA are translated into proteins in groups of three base pairs per amino acid. This allows for 64 different *codons*, some of which translate to the same amino acid. The exact *codon use*, that is which nucleic acid code is used for which amino acid, varies slightly between different organisms.

Protein biosynthesis has a remarkably low rate of error around the order of one faulty amino acid in 10.000 amino acids, depending on the organism and the sequence. This is achieved by “error correction mechanisms” integrated into the protein biosynthesis system.

A2. Bond Pad Lists and Bond Diagrams

A2.1 Peptidchip 3.1

The dimensions of all bond pads on Peptidchip 3.1 are $76 \times 76 \mu\text{m}^2$. The bond pads are located on the left edge of the die in two staggered rows, and on the top and bottom near the left edge in a single row. Bond pad locations (fig. A2.1), a list of bond pads with their positions on the connector (tab. A2.1), and bond diagrams (fig. A2.2 and fig. A2.3) are shown below. For most purposes, the reduced bond plan is recommended, as it provides sufficient connections, is easier to bond, and has a reduced risk of bond failure or bond wires contacting one another.

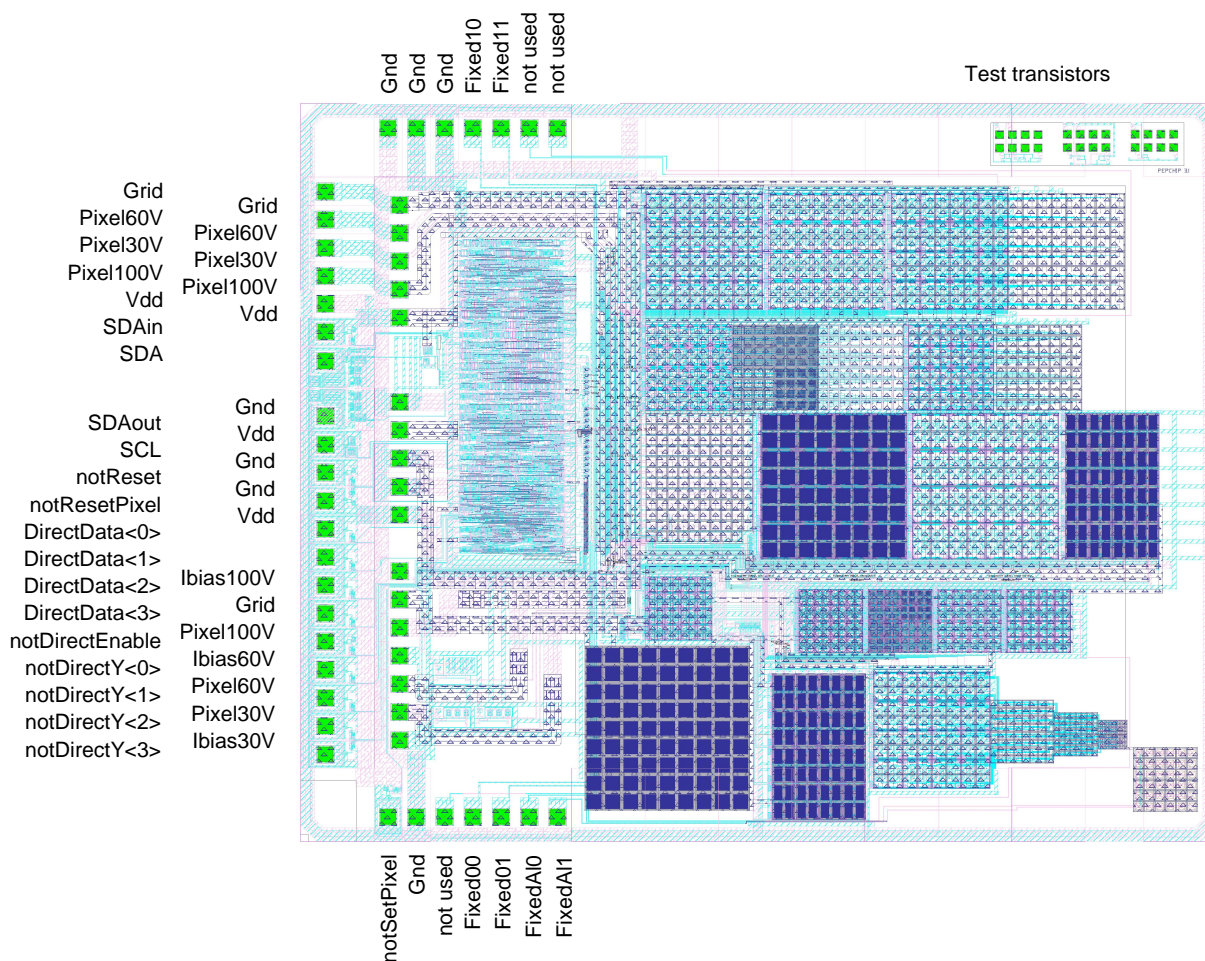


Fig. A2.1: Peptidchip 3.1 bond pad locations (green) on the die.

Position on Chip	Position on Connector	Function Pep3.1	Function Pep3.0
top 1 (starting right)	24	not used	MultipolY3
top 2	22	not used	MultipolY2
top 3	20	Fixed11	MultipolY1
top 4	18	Fixed10	MultipolY0
top 5..7	1,3,5,7	Gnd	PhotoPad5..2
left & inner 1 (starting top)	9	Grid	=
left & inner 2	11	Pixel60V	=
left & inner 3	13	Pixel30V	=
left & inner 4	15	Pixel100V	=
left & inner 5	23, 25	Vdd	=
left 6	10	SDAin	=
left 7	8	SDA	=
inner 8	1,3,5,7	Gnd	PhotoPad5..2
left 9	6	SDAout	=
inner 9	23, 25	Vdd	
left 10	4	SCL	=
inner 10	1,3,5,7	Gnd	PhotoPad5..2
left 11	2	notReset	=
inner 11 (don't bond!)	1,3,5,7	Gnd	PhotoPad5..2
left 12	38	notResetPixel	=
inner 12	23, 25	Vdd	=
left 13	40	DirectData<0>	=
left 14	42	DirectData<1>	=
inner 14	29	Ibias100V	=
left 15	44	DirectData<2>	=
inner 15	31	Grid	=
left 16	46	DirectData<3>	=
inner 16	33	Pixel100V	=
left 17	48	notDirectEnable	=
inner 17	35	Ibias60V	=
left 18	49	notDirectY3	=
inner 18	37	Pixel60V	=
left 19	47	notDirectY2	=
inner 19	39	Pixel30V	=
left 20	45	notDirectY1	=
inner 20	41	Ibias30V	=
left 21	43	notDirectY0	=
bottom 1 (starting left)	36	notSetPixel	=
bottom 2	1,3,5,7	Gnd	PhotoPad5..2
bottom 3	34	not used	MultipolGitter
bottom 4	32	Fixed00	MultipolX0
bottom 5	30	Fixed01	MultipolX1
bottom 6	28	FixedAL0	MultipolX2
bottom 7	27	FixedAL1	Iphotobias (needs main PCB change)

Tab. A2.1: List of Peptidchip 3.1 bond pads, the corresponding position on the connector on the Peptidchip 3.1 support PCB, and function of this connector pin on Peptidchip 3. ‘=’ signifies equal function on both chips.

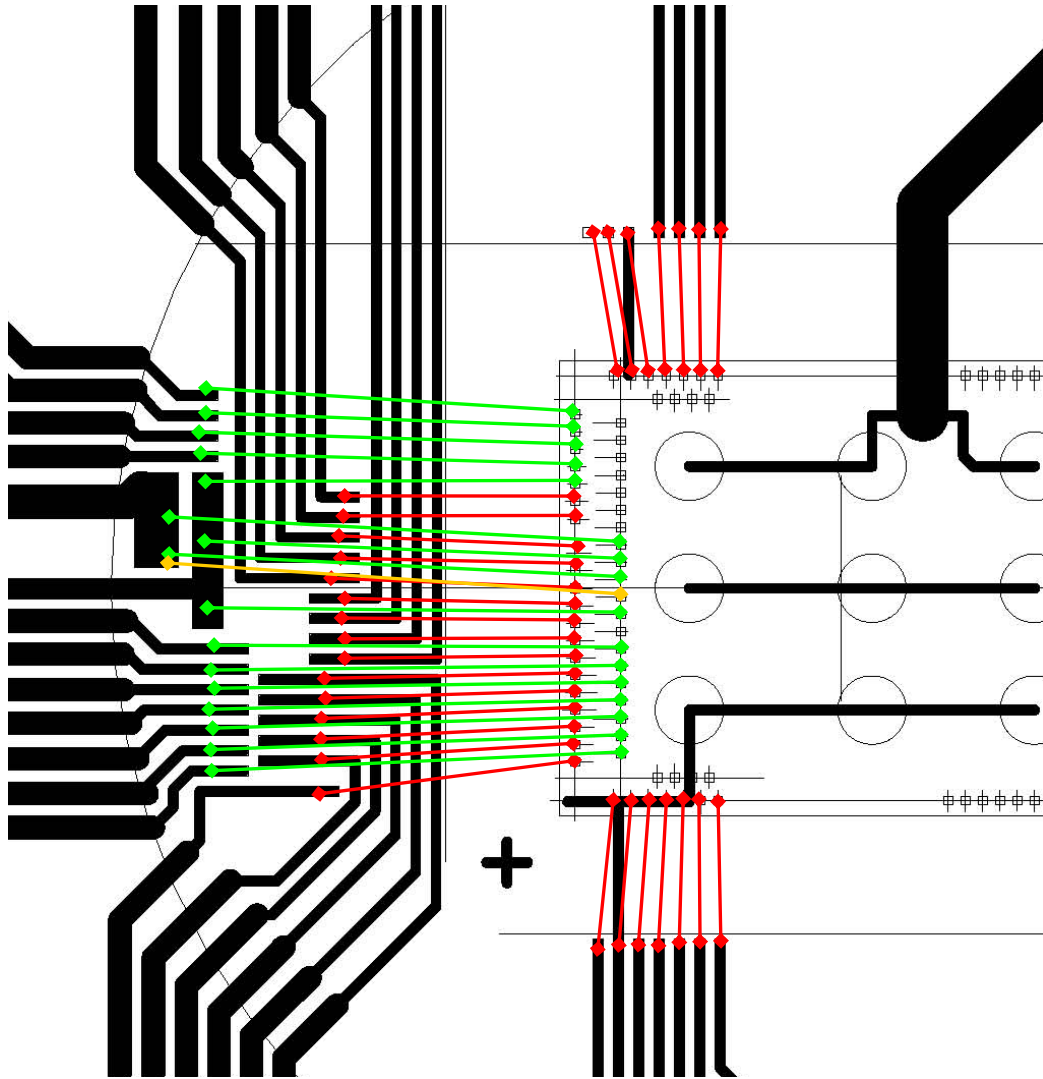


Fig. A2.2: Bond plan for Peptidchip 3.1. Second row bonds in green. The yellow bond is commonly omitted, as it is redundant and difficult to bond.

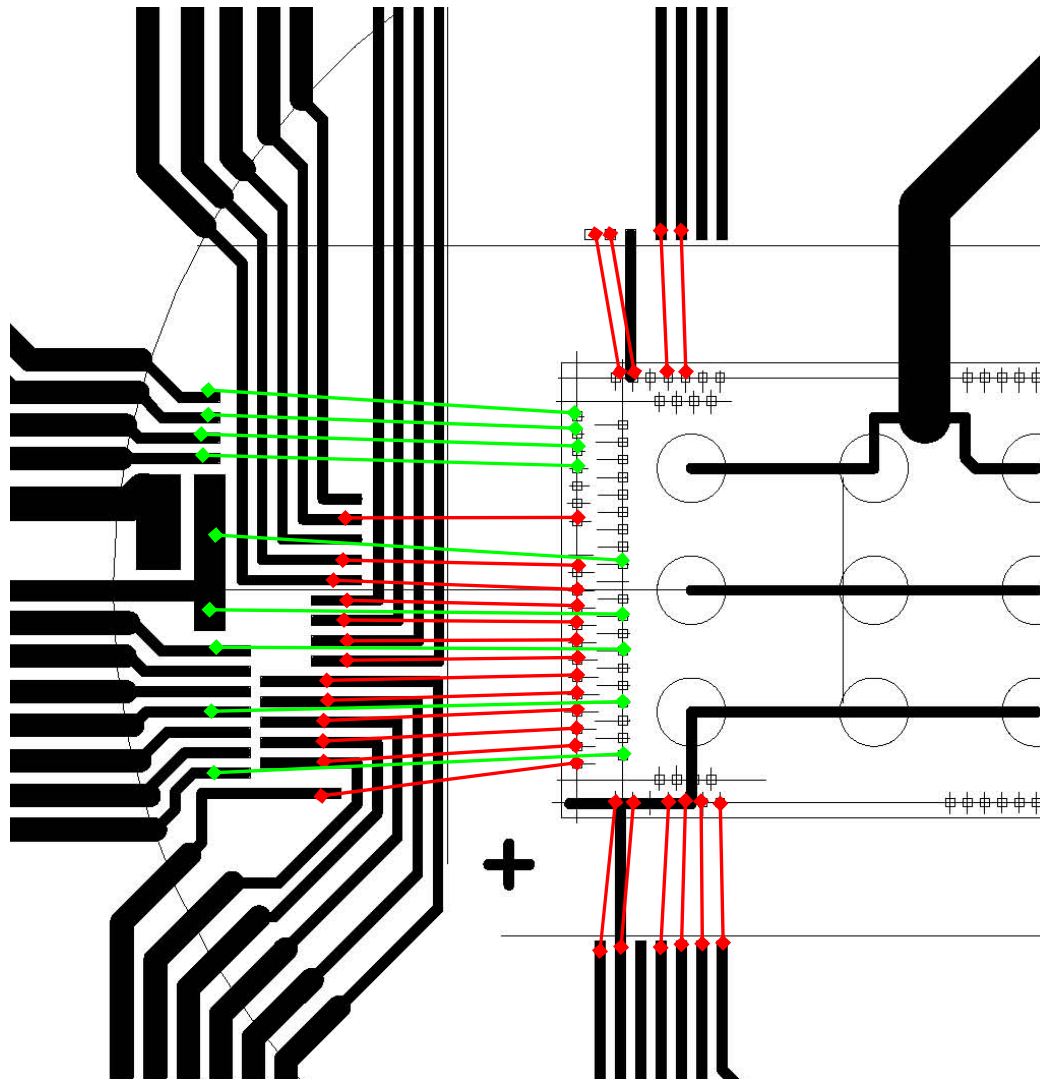


Fig. A2.3: Reduced bond plan for Peptidchip 3.1. Second row bonds in green. This reduced bond plan offers less redundant connections, but due to the reduced number of long wires also less risk of wire rupture under mechanical stress.

A2.2 Peptidchip 5

As sufficient space is available, all bond pads on Peptidchip 5 are well-spaced and of large size, allowing for multiple wire bonds or alternative contacting methods. Except for the pads required solely for the direct interface, which is only to be used for first tests, all bond pads are at least $280\ \mu\text{m} \times 280\ \mu\text{m}$ in passivation opening size. Tab. A2.2 lists the bond pads and the corresponding positions on the connector.

Position on chip (top to bottom)	Position on connector	Function	Size [$\mu\text{m} \times \mu\text{m}$]
1	back 1	contact detection 1	580 × 280
2	back 2	grid electrode	580 × 280
3	back 3	Gnd	580 × 280
4	back 4	Ibias	580 × 280
5	back 4	Ibias	280 × 280
6	back 5	Vdd100V	580 × 280
7	back 5	Vdd100V	580 × 280
8	back 3	Gnd	580 × 280
9	back 6	Vdd	580 × 280
10	back 7	notReset	280 × 280
11	back 8	SDA	280 × 280
12	back 9	SCL	280 × 280
13	front 1	notResetPixel	76 × 280
14	front 2	notSetPixel	76 × 280
15	front 3	DirectData0	76 × 280
16	front 4	DirectData1	76 × 280
17	front 5	DirectData2	76 × 280
18	front 6	DirectData3	76 × 280
19	front 7	notDirectEnable	76 × 280
20	front 8	notDirectY0	76 × 280
21	front 9	notDirectY1	76 × 280
22	front 10	notDirectY2	76 × 280
23	front 11	notDirectY3	76 × 280
24	back 6	Vdd	580 × 280
25	back 3	Gnd	580 × 280
26	back 3	Gnd	580 × 280
27	back 5	Vdd100V	580 × 280
28	back 5	Vdd100V	580 × 280
29	back 3	Gnd	580 × 280
30	back 2	grid electrode	580 × 280
31	back 10	contact detection 2	580 × 280
32	back 11	contact detection 3	580 × 280

Tab. A2.2: List of Peptidchip 5 bond pads, their positions on the connector, function and size. Bonds required only for optional direct control in green, bonds for optional contact detection in blue.

A3. Pressure Tolerance of Peptidchip 3.1

As described in 5.3.3.2, the Teflon covering is pressed onto the chip on top of metal and semiconductor structures of pixel areas with enough force that the thin Teflon lid exhibits plastic flow. The pressure applied by fastening the template holder screws is insufficient to achieve a liquid-tight sealing. However, liquid tight sealing can be achieved by installing the chip and covering into the synthesis chamber, which uniformly transfers pressure onto the covering.

On the other hand, pressure on the chip is not uniform, but only applied in the small area of the Teflon lid edge. As the chip is not planarized, pressure might be even higher in slightly elevated areas such as over metal tracks. Pressure might also vary locally due to irregularities in the Teflon covering. During experiments in the synthesis chamber using the covering at pressures sufficient to complete the seal, an increase in electric chip failures (mainly “dead chips” and shorts, even on previously functioning chips) compared to experiments without the covering in place was observed. In these experiments, the chip was pressed into the chamber by a Teflon plate on the backside of the back-covering, with four screws on the corners of the plate being tightened in order to build up the required pressure. These screws were tightened by hand, and though care was taken to tighten them about evenly, the maximum torque, and thus maximum pressure, varied.

In order to determine whether the increased number of chip failures was caused by the pressure applied by the lid or by other reasons (such as exposure to chemicals), it was tested whether chips can be destroyed by applying force onto the Teflon lid without chemicals present. The setup described above was used, but the screws were tightened using a torque-limiting ratchet spanner in order to determine the conditions of failure and set a maximum torque for future use of the synthesis chamber.

Only two Peptidchip 3.1 chips were tested, as these measurements are destructive. Both chips were tested in the aerosol after mounting the covering, and then after exposure to pressure from 2 cN m to 10 cN m in increments of 2 cN m, and from 10 cN m to 30 cN m in increments of 5 cN m. For the first chip, the pressure was applied for 5 minutes each pressure step, while the second chip was exposed to each pressure step for 4 hours.

The first chip showed no defects up to 20 cN m, while at 25 cN m all fixed-pattern pixels and all 30 V and 60 V maximum voltage pixels failed. During the final test after exposure to 30 cN m, the chip was destroyed by a massive short-circuit which melted bond wires and metal tracks on the chip.

The second chip showed defects of the 50 μm fixed-pattern pixels already after exposure to 6 cN m, with the rest of the chip still functional. After being exposed to 10 cN m, the 30 V pixels failed as well, with the 60 V pixels failing at the subsequent test at 15 cN m. The remaining pixels continued to function up to 25 cN m, while after the stress of 30 cN m, the chip was destroyed by a massive short-circuit.

Even though there is not enough data for more specific claims, the chips are indeed sensitive to the forces applied on the covering for sealing. The failure of entire regions of pixels,

including the fixed-pattern pixels, points at breakage of metal tracks as the primary cause of chip failure.

As a fix for Peptidchip 3.1, use of the torque-limiting ratchet spanner to tighten the screws was implemented. It was found that a maximum torque of 6 cN m is sufficient to regularly achieve a tight seal, and using this protocol, the number of chips destroyed after chemical processing reduced noticeably. For future chips, however, the use of an o-ring seal which more evenly distributes the forces on the chip surface while providing a more reliable seal is preferable. On the chip, a seal area is to be designated, in which only a minimal number of metal tracks of increased width with neither vias nor corners may be routed. This has been implemented in Peptidchip 5, and resulted in improved reliability.

A4. Peptidchip 5 Main PCB Schematics

This appendix contains the schematics of the main PCB described in 5.4.3.5 (fig. A4.1 - 6). High-voltage wires are marked in violet; for these signals, HV components and connectors must be used. Contact pins for probing have been included for all relevant signals.

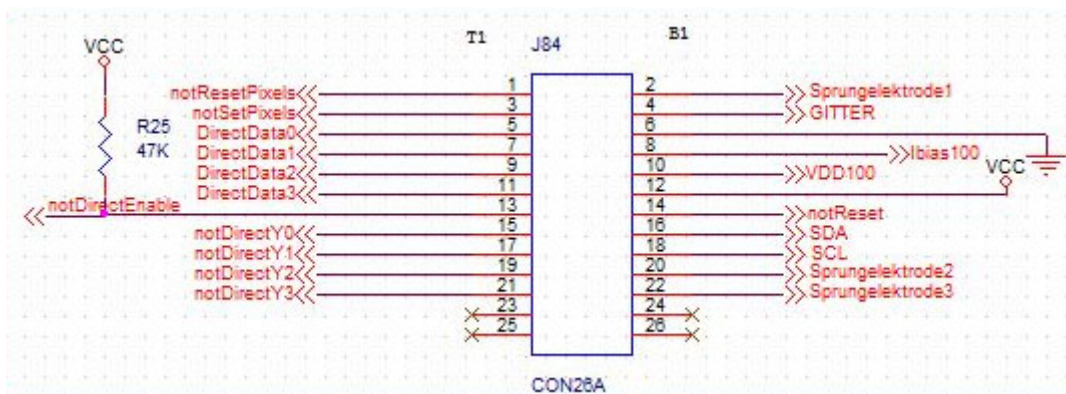


Fig. A4.1: Chip connector, into which the ribbon cable to the chip is plugged. Odd pin numbers are required for direct control only, which was used for initial tests. They may be omitted in a PCB for use in a synthesis machine. “Sprungelektrode” signals are the contacts for the contact detection pads (5.4.2.4) and can be omitted if a non-contact particle transfer method is used.

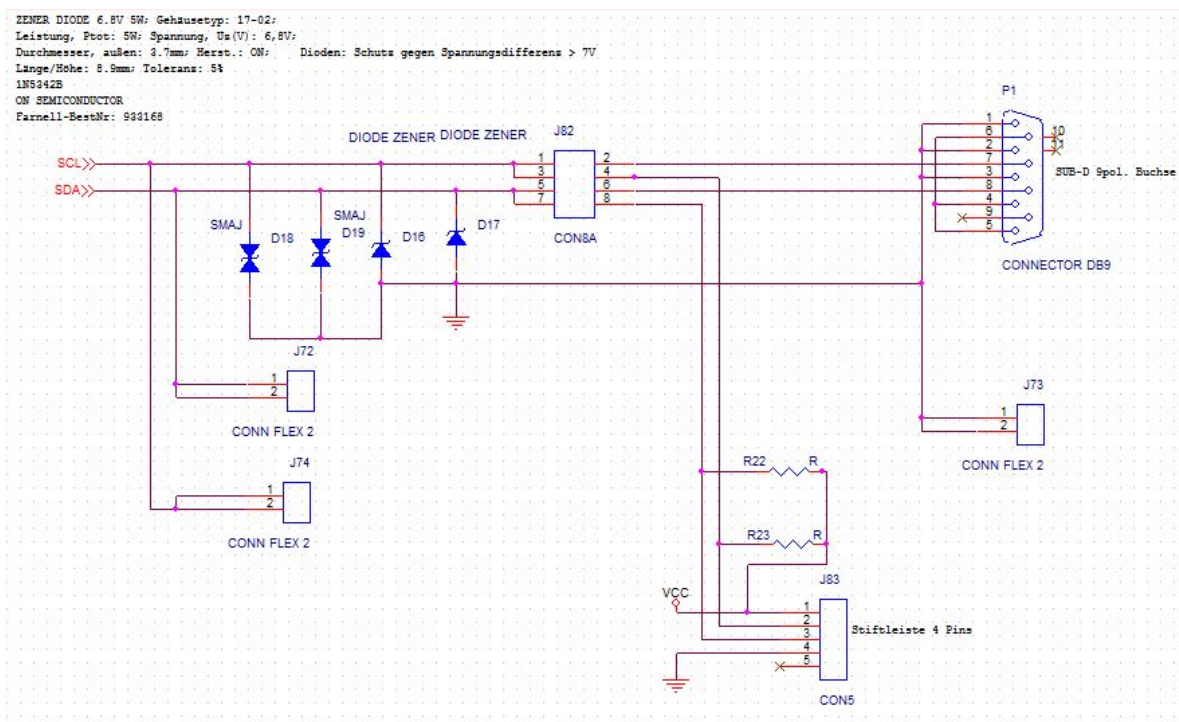


Fig. A4.2: I²C connectors including overvoltage protection diodes.

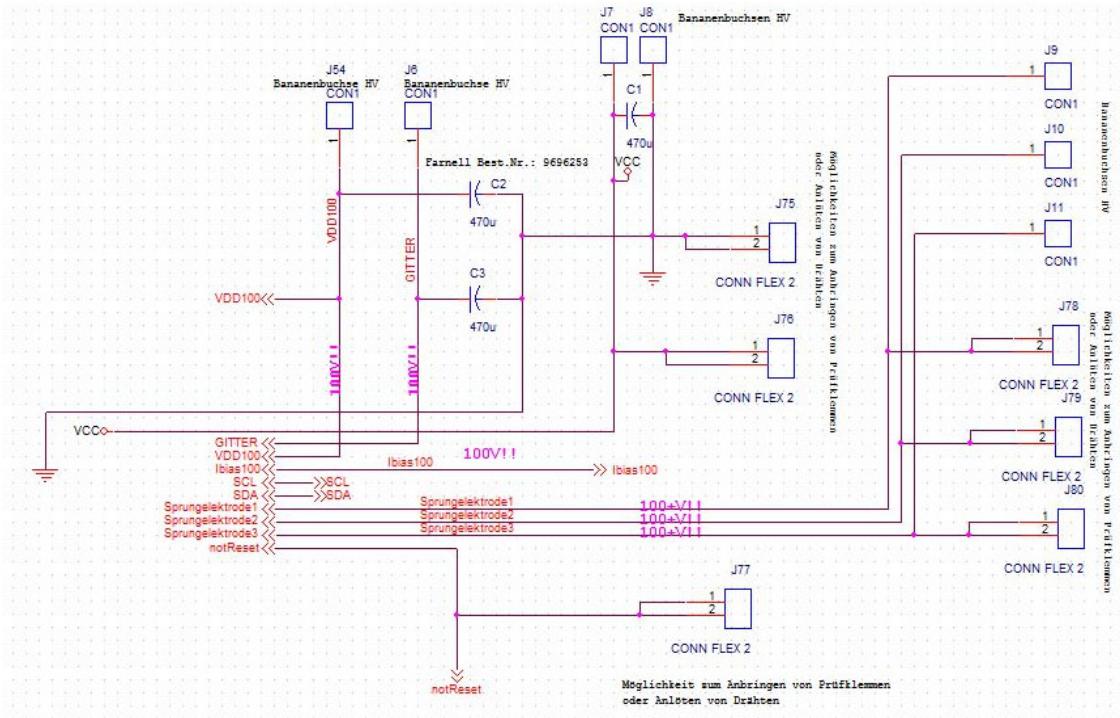


Fig. A4.3: Power supply connectors and filtering capacitances. Use HV banana jacks for HV signals. “Sprungelektrode” signals can be omitted if a non-contact particle transfer method is used.

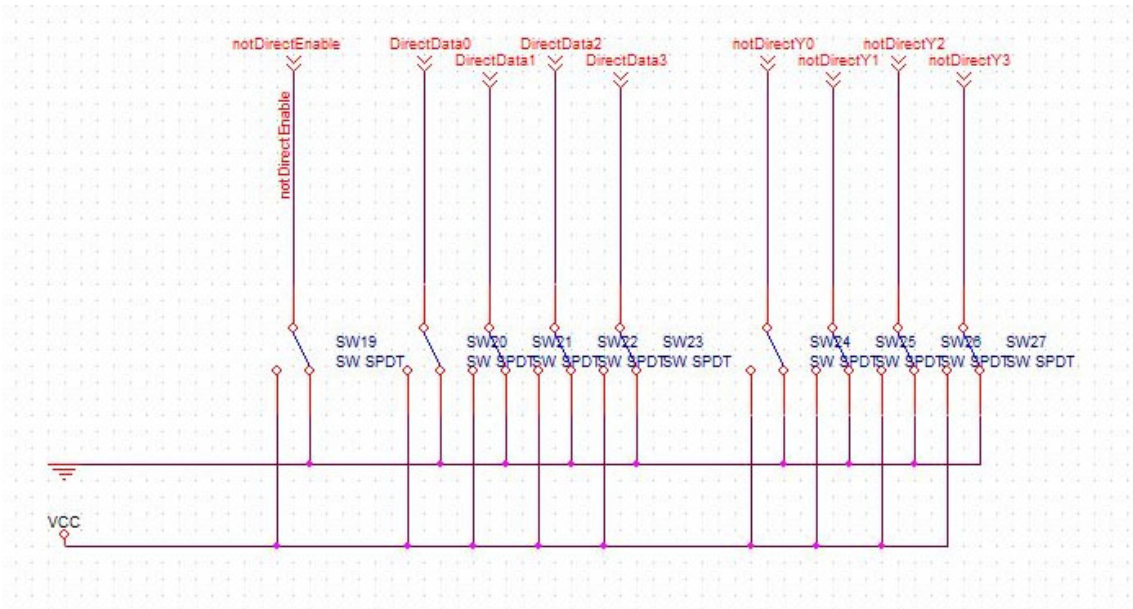


Fig. A4.4: Switches for direct control (for initial testing), may be omitted in a PCB for use in a synthesis machine.

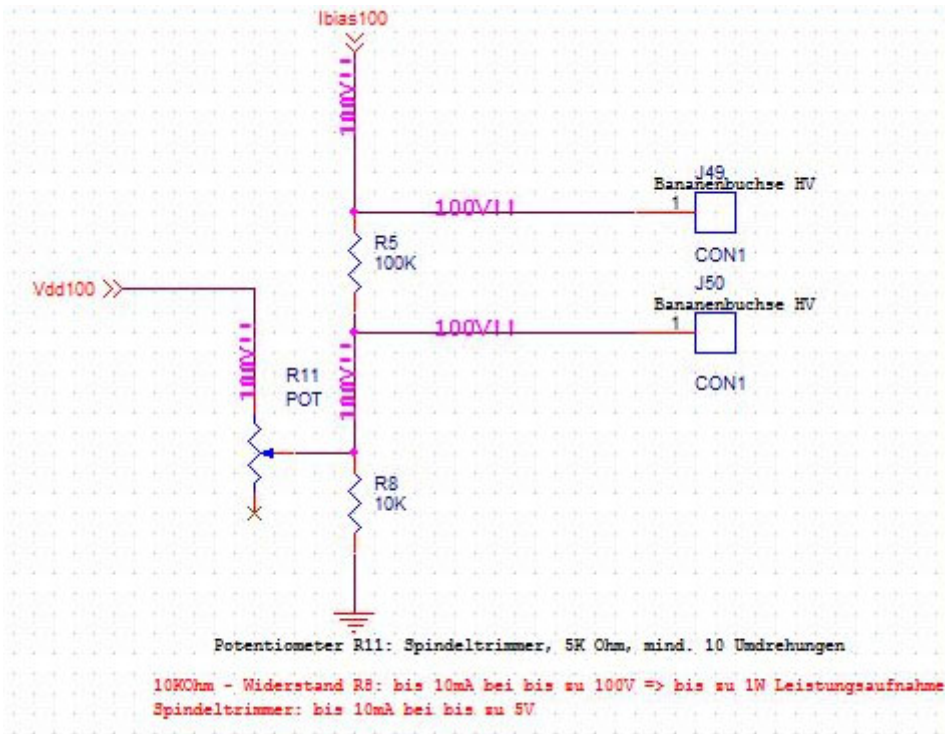


Fig. A4.5: Bias current generation and measurement. Use 5 k Ω potentiometer, at least 10 turns, up to 10 mA at 5 V. R8 must be capable of handling at least 10 mA at 100 V.

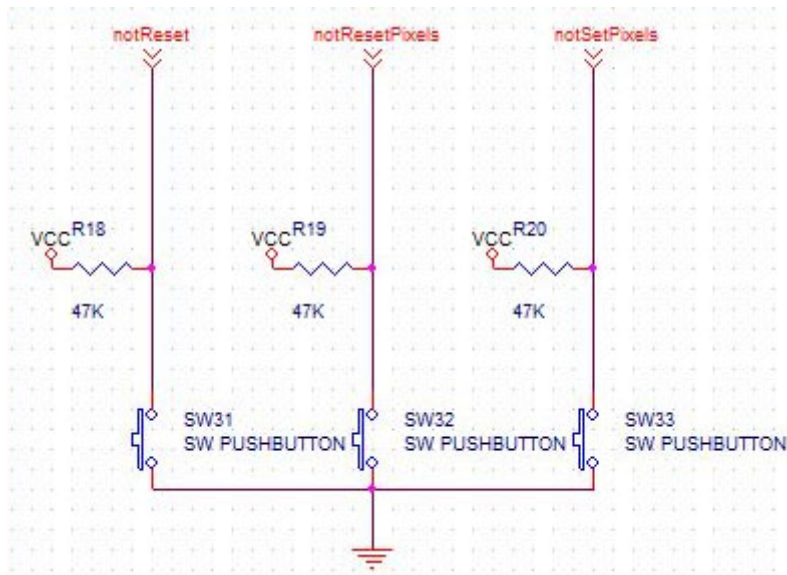


Fig. A4.6: Reset buttons. NOTSETPIXELS and NOTRESETPIXELS may be omitted in a PCB for use in a synthesis machine.